Alma Mater Studiorum – Università di Bologna
Facoltà di Ingegneria

***

D.I.S.T.A.R.T.
SEDE DI SCIENZA DELLE COSTRUZIONI

Dottorato di Ricerca in Meccanica delle Strutture
XXII ciclo

Coordinatore

Chiar.mo Prof. Ing. Erasmo Viola

Mixed Mode Fracture Behaviour
of Piezoelectric Materials

Tesi di Dottorato di

Claudia Boldrini

Relatore

Prof. Ing. Erasmo Viola

S.S.D. ICAR 08

A.A. 2009-2010

PRESENTAZIONE DELLA TESI DI DOTTORATO

di CLAUDIA BOLDRINI

Lo studio presentato in questa Tesi di Dottorato si inserisce nell'ambito della trattazione analitica della Meccanica della Frattura.

Il tema principale del lavoro svolto è la risposta elettro-elasto-statica alla frattura di un mezzo piezoelettrico fessurato, in regime di carico tensionale ed elettrico biassiale all'infinito.

Per la trattazione analitica è stato adattato al caso piezoelettrico un formalismo, analogo a quello di Stroh, che era precedentemente stato utilizzato per il più semplice caso dei materiali ortotropi [Piva, 1987; Piva e Viola, 1988]. Questo metodo, attraverso l'applicazione del teorema spettrale dell'algebra sulla matrice fondamentale, permette di esprimere le equazioni governanti il problema elastico mediante dei potenziali complessi. In seguito, con l'imposizione delle condizioni al contorno (meccaniche ed elettriche) sui bordi del crack, ci si riconduce a un problema di Hilbert, la cui soluzione è nota.

Un primo aspetto, ampiamente discusso in letteratura, che è stato affrontato in questa ricerca è stato la definizione delle opportune condizioni al contorno elettriche da imporre ai bordi della discontinuità (fessura). In questa tesi sono state analizzate le soluzioni per tre diversi modelli di fessura (crack permeabile, impermeabile e semi-permeabile al campo elettrico), ed i risultati ottenuti sono stati confrontati per cercare di quantificare quale sia l'importanza della corretta scelta del modello da applicare, verificando che in molti casi questo è un aspetto tutt'altro che trascurabile.

Un altro aspetto analizzato con attenzione è stato l'influenza dell'applicazione di un carico biassiale, ed in particolare l'effetto del carico collineare alla direzione del

crack. Mentre il caso di un carico biassiale è stato ampiamente trattato in letteratura per quanto riguarda il caso dei materiali isotropi [ad esempio Carpinteri et al., 1979; Eftis et al., 1990] od ortotropi [ad esempio Lim et al., 2001; Carloni et al., 2003], esso non è stato quasi mai considerato per la frattura nei materiali piezoelettrici. Il carico collineare compare solo nell'espressione dei termini non singolari della soluzione del problema elettroelastico. La tendenza prevalente è di considerare solo la parte asintotica della soluzione nell'analisi del campo tensionale nell'intorno della fessura, dal momento che questa è inversamente proporzionale alla distanza r dal tip del crack e quindi predominante nelle sue immediate vicinanze. L'eliminazione dei termini non singolari dalla soluzione implica però il trascurare la possibilità che anche una forza parallela alla direzione del crack possa esercitare un'influenza sul campo elettroelastico riscontrato nei pressi della discontinuità. Nella nostra analisi i termini non singolari sono stati ritenuti, ed attraverso una simulazione numerica del comportamento di diverse ceramiche piezoelettriche i risultati così ottenuti sono stati confrontati con quelli asintotici. Per valutare la possibile propagazione della fessura all'interno del materiale sono stati utilizzati due diversi criteri: il criterio della massima tensione circonferenziale [Erdogan e Sih, 1963], ed il criterio della minima densità di energia di deformazione [Sih, 1973]. Un interessante risultato ottenuto è la dimostrazione che la presenza di un carico collineare può avere conseguenze macroscopiche per quanto riguarda lo studio dell'angolo di diramazione della fessura. Infatti, secondo entrambi i criteri suddetti, l'applicazione di un carico sufficientemente elevato parallelo al crack provoca una brusca diversione dall'orizzontale della direzione di estensione della lesione, pur in condizioni di carico simmetrico (cioè in assenza di forze tangenziali applicate). Dallo studio analitico si evince quindi che l'effetto della biassialità del carico non è assolutamente trascurabile nello studio dei problemi di frattura; sarebbe importante avvalorare i risultati analitici con prove sperimentali.

Nella seconda parte di questa tesi sono riportati i risultati di una ricerca sperimentale a cui ho collaborato durante un periodo di soggiorno come Visiting

Researcher presso il Department of Mechanical Engineering, The City College of New York, nell'A.A. 2008/09.

L'obiettivo del progetto di ricerca (tuttora in corso) è la validazione di una tecnica self-sensing per la rilevazione di danni da delaminazione in elementi strutturali laminati compositi. La tecnica utilizza la resistenza elettrica trasversale di un laminato composito come principale parametro per l'individuazione della presenza e propagazione di un crack interlaminare. Il principio alla base è che la presenza o la propagazione di un crack di delaminazione ingeneri una diminuzione della conduttività elettrica trasversale nella zona in prossimità del danno, con conseguente aumento della resistenza.

La tecnica tradizionale prevede sensori a due terminali, che sono utilizzati sia per applicare la corrente elettrica, sia per misurare la differenza di potenziale e conseguentemente la resistenza. Il limite di questo metodo è che la resistenza così misurata non è solo quella del materiale che si vuole testare, ma anche quella del filo attraverso cui viene fatta passare la corrente e dell'elettrodo stesso. In particolare nel caso di una non perfetta connessione dell'elettrodo al materiale, l'errore così introdotto può non essere trascurabile. Per ovviare a questo problema è stata proposta una seconda tecnica a quattro elettrodi, dove i primi due sono utilizzati per il passaggio della corrente ed i secondi due, posti nelle immediate vicinanze, per la misurazione della resistenza, permettendo di eliminare dalla misura l'impedenza dei cavi.

La ricerca ha lo scopo principale di capire i limiti di applicazione e la potenzialità del metodo e di esplorarne le possibilità di utilizzo industriale. Una tecnica di self-sensing potrebbe ridurre o eliminare l'utilizzo di sensori quali MEMS o piezoelettrici, correntemente utilizzati nel monitoraggio automatico dell'integrità strutturale. I dati ricavati dimostrano quasi sempre che all'avanzare della delaminazione lungo il provino corrisponde un aumento del valore registrato della resistenza, indicando che la tecnica self-sensing può essere una promettente metodologia di diagnostica strutturale.

Tutti i test sono stati effettuati presso il Laboratorio di Meccanica dei Materiali del City College of New York. Alcuni dei risultati dei test sono stati presentati al convegno International Conference on Integrity, Reliability and Failure, tenutosi a Porto, 20-24 Luglio 2009.

CONTENTS

PART 2

Outline

Piezoelectrics present an interactive electromechanical behaviour that, especially in recent years, has generated much interest since it renders these materials adapt for use in a variety of electronic and industrial applications like sensors, actuators, transducers, smart structures. Both mechanical and electric loads are generally applied on these devices and can cause high concentrations of stress, particularly in proximity of defects or inhomogeneities, such as flaws, cavities or included particles. A thorough understanding of their fracture behaviour is crucial in order to improve their performances and avoid unexpected failures. Therefore, a considerable number of research works have addressed this topic in the last decades.

Most of the theoretical studies on this subject find their analytical background in the complex variable formulation of plane anisotropic elasticity. This theoretical approach bases its main origins in the pioneering works of Muskelishvili and Lekhnitskii who obtained the solution of the elastic problem in terms of independent analytic functions of complex variables.

In the present work, the expressions of stresses and elastic and electric displacements are obtained as functions of complex potentials through an analytical formulation which is the application to the piezoelectric static case of an approach introduced for orthotropic materials to solve elastodynamics problems. This method can be considered an alternative to other formalisms currently used, like the Stroh's formalism. The equilibrium equations are reduced to a first order system involving a six-dimensional vector field. After that, a similarity transformation is induced to reach three independent Cauchy-Riemann systems, so justifying the introduction of the complex variable notation. Closed form expressions of near tip stress and displacement fields are therefore obtained.

In the theoretical study of cracked piezoelectric bodies, the issue of assigning consistent electric boundary conditions on the crack faces is of central importance and has been addressed by many researchers. Three different boundary conditions are commonly accepted in literature: the permeable, the impermeable and the semipermeable ("exact") crack model. This thesis takes into considerations all the

three models, comparing the results obtained and analysing the effects of the boundary condition choice on the solution.

The influence of load biaxiality and of the application of a remote electric field has been studied, pointing out that both can affect to a various extent the stress fields and the angle of initial crack extension, especially when non-singular terms are retained in the expressions of the electro-elastic solution.

Furthermore, two different fracture criteria are applied to the piezoelectric case, and their outcomes are compared and discussed.

The work is organized as follows:

Chapter 1 briefly introduces the fundamental concepts of Fracture Mechanics.

Chapter 2 describes plane elasticity formalisms for an anisotropic continuum (Eshelby-Read-Shockley and Stroh) and introduces for the simplified orthotropic case the alternative formalism we want to propose.

Chapter 3 outlines the Linear Theory of Piezoelectricity, its basic relations and electro-elastic equations.

Chapter 4 introduces the proposed method for obtaining the expressions of stresses and elastic and electric displacements, given as functions of complex potentials. The solution is obtained in close form and non-singular terms are retained as well.

Chapter 5 presents several numerical applications aimed at estimating the effect of load biaxiality, electric field, considered permittivity of the crack. Through the application of fracture criteria the influence of the above listed conditions on the response of the system and in particular on the direction of crack branching is thoroughly discussed.

Finally, Appendix A lists a few mathematical definitions and concepts useful for understanding some algebraic steps of the analysis, and Appendix B reports the explicit form of the fundamental matrix of the electro-elastic problem.

NOMENCLATURE

a	Griffith crack semilength
B	Biot's generalized free energy
c_{ijks}	elastic constants of material
C_v	specific heat per unit mass
D_i, D_i^∞	components of electric displacement and of electric displacement applied at infinity
D_y^0	electric displacement at the crack surfaces
e_{sij}	piezoelectric constants of material
E_s, E_s^∞	components of electric field and of electric field applied at infinity
f_{bi}	body force
$g_j^{(k)}$, $h_j^{(k)}$	real and imaginary parts of element $f_j^{(k)}$ of eigenvector $\mathbf{f}^{(k)}$
g	Gibbs function
G	Energy Release Rate
K_I, K_{II}, K_D	stress intensity factors (Mode I, Mode II and electric)
p_k, q_k	real and imaginary parts of eigenvalues λ_k
q_b	electric charge density
r/a	ratio of distance from crack tip on crack semilength
s	entropy density
$s_1 = \sigma_{xx}^\infty / \sigma_{yy}^\infty$	ratio of collinear on perpendicular remote loads
$s_2 = \sigma_{xy}^\infty / \sigma_{yy}^\infty$	ratio of tangential on perpendicular remote loads
S	Sih's Energy Density
T^a	absolute temperature
u, v	elastic displacement components
χ_m	pyroelectric coefficients
γ_{ks}	strain tensor components
ε_{is}	dielectric constants of material
ε_c	permittivity of the medium inside the crack
λ_k	eigenvalues
φ	electric potential
ρ	mass density

$\sigma_{ij}, \sigma_{ij}^{\infty}$	components of stress tensor and of mechanical loading applied at infinity
$\sigma_{\theta\theta}$	hoop stress
$\Omega_k(z_k)$	complex potentials $(k=1,2,3)$
$\mathbf{a}_\alpha, \mathbf{b}_\alpha$	Stroh's eigenvectors
$\mathbf{f}^{(1)}, \mathbf{f}^{(2)}, \mathbf{f}^{(3)}$	eigenvectors corresponding to eigenvalues $\lambda_1, \lambda_2, \lambda_3$
$\mathbf{t}_1, \mathbf{t}_2$	generalized stress vectors
$\mathbf{t}_1^{\infty}, \mathbf{t}_2^{\infty}$	remote loading vectors
$\mathbf{\Gamma}^{(1)}, \mathbf{\Gamma}^{(2)}$	generalized strain vectors
$\mathbf{\Lambda}(z)$	analytic vector null at infinity
$\mathbf{U}$	generalized displacement vector
U	Airy's stress function
(r, θ)	polar coordinates originating at the crack tip

CHAPTER 1

BASIC CONCEPTS OF FRACTURE MECHANICS

1.1   Introduction

It is common knowledge learned from experience that cracks can be very detrimental to strength, even when small. Cracks running rapidly through hard structural materials (metal, rocks, concrete) are also within common experience. The cracking or complete fracture is often so rapid that it is difficult to detect with eyes the sudden extension from some small initial defect, notch hole or other irregularities. Such irregularities are extremely important because they modify the state of stress in their immediate neighbourhood, usually introducing a local intensification.

Until the material in question does not fail, the calculation of the fields of stress and strain around the crack can be carried out by solving a boundary value problem in some kind of idealized body. The calculation of stress and strain in the vicinity of a crack in the process of extending requires consideration of a sequence of ordinary boundary value problems, as well as of some additional conditions in order to know when the boundary undergoes a change.

The two basic problems in Fracture Mechanics are therefore the evaluation of stress and strain fields around the crack tip and the knowledge of the conditions under which a crack can extend into a medium [1].

1.2   Modes of fracture and stress intensity factors

Some basic definitions of Fracture Mechanics are now introduced, referring for simplicity to an isotropic material, and along with Williams's method [2,3], that sought the solution of the fracture problem expressing it in terms of Airy's bi-

harmonic stress function. For brevity we will report the results only, referring to the work in bibliography for further details.

Consider first a crack of length $2a$, embedded in an isotropic elastic continuum plate subjected at infinity to biaxial load (Fig. 1.1). A plane state of strain is considered.
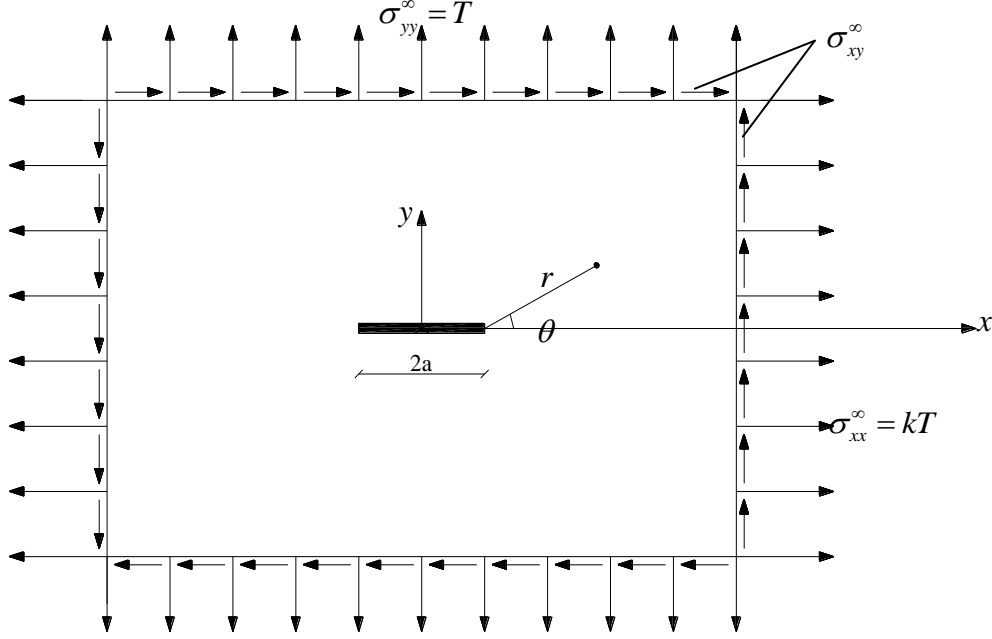
Fig. 1.1 – Geometry of the crack problem

It can be useful to consider also a polar coordinate system centred in the right tip of the crack. We will also suppose the crack faces to be free from applied stresses, which means applying the boundary conditions:

$$\sigma_\theta\left(r,\pm\pi\right)=\sigma_{r\theta}\left(r,\pm\pi\right)=0 \tag{1.1}$$

The general loading condition illustrated in Figure 1.1 can be decomposed into the sum of a symmetric (Figure 1.2) and an anti-symmetric (Figure 1.3) load, which yield symmetry and anti-symmetry conditions on the stresses as well.

1.2.1. Symmetric plane problem (Mode I)

Stress components must comply to the symmetry conditions:

$$\begin{aligned}
\sigma_r\left(r,\theta\right)&=\sigma_r\left(r,-\theta\right)\\
\sigma_\theta\left(r,\theta\right)&=\sigma_\theta\left(r,-\theta\right)\\
\sigma_{r\theta}\left(r,\theta\right)&=-\sigma_{r\theta}\left(r,-\theta\right)
\end{aligned} \tag{1.2}$$

The general solution of the differential system is a linear combination of the particular solutions:

$$U(r,\theta) = \sum_{n=1}^{\infty} r^{\lambda_n + 1} f_n(\theta) \qquad (1.3)$$

where $U(r,\theta)$ is Airy's stress function. This yields the following expressions for the stress components:

$$\sigma_r = \sum_{n=1}^{\infty} r^{\frac{n}{2}-1} \left[f_n''(\theta) + \left(\frac{n}{2}+1\right) f_n(\theta) \right]$$

$$\sigma_\theta = \sum_{n=1}^{\infty} r^{\frac{n}{2}-1} \left[\frac{n}{2}\left(\frac{n}{2}+1\right) f_n(\theta) \right] \qquad (1.4)$$

$$\sigma_{r\theta} = -\sum_{n=1}^{\infty} r^{\frac{n}{2}-1} \left[\frac{n}{2} f_n'(\theta) \right]$$

Fig. 1.2 – Symmetric problem

Equations (1.4) show that the first terms of the series (for $n=1$) present an inverse square root singularity of the radial distance from the crack tip. In the vicinity of the crack tip, for $r \ll 1$, the asymptotic representations of stress fields, in Cartesian coordinates, are therefore [4,5,6]:

$$\sigma_{xx} \simeq \frac{K_I}{\sqrt{2\pi r}} \cos\frac{\theta}{2}\left(1 - \sin\frac{\theta}{2}\sin\frac{3\theta}{2}\right)$$

$$\sigma_{yy} \simeq \frac{K_I}{\sqrt{2\pi r}} \cos\frac{\theta}{2}\left(1 + \sin\frac{\theta}{2}\sin\frac{3\theta}{2}\right) \qquad (1.5)$$

$$\sigma_{xy} \simeq \frac{K_I}{\sqrt{2\pi r}} \sin\frac{\theta}{2}\cos\frac{\theta}{2}\cos\frac{3\theta}{2}$$

where the relations between Cartesian and polar coordinates:

$$\sigma_{xx} = \sigma_r\cos^2\theta + \sigma_\theta\sin^2\theta - \tau_{r\theta}\sin 2\theta$$
$$\sigma_{yy} = \sigma_r\sin^2\theta + \sigma_\theta\cos^2\theta + \tau_{r\theta}\sin 2\theta \quad (1.6)$$
$$\sigma_{xy} = \frac{\sigma_r - \sigma_\theta}{2}\sin 2\theta + \sigma_{r\theta}\left(\cos^2\theta - \sin^2\theta\right)$$

have been used, and where K_I is a constant. From equation (1.5)-2, for $\theta = 0$ and switching to the variable $\xi(x) = x - a$, one obtains the definition of K_I:

$$K_I = \lim_{r\to 0}\sqrt{2\pi r}\,\sigma_{yy}\left(r,0\right) = \lim_{x\to a}\sqrt{2\pi r(x-a)}\,\sigma_{yy}\left(\xi,0\right) \quad (1.7)$$

which is called *stress intensity factor* for the first (opening) mode.

It is to be noted that the applied collinear load σ_{xx}^∞ does not appear in the asymptotic representations of the stress fields (1.5).

1.2.2. Anti-symmetric plane problem (Mode II)

For the anti-symmetric problem, symmetry conditions for the stress components are:

$$\sigma_r\left(r,\theta\right) = -\sigma_r\left(r,-\theta\right)$$
$$\sigma_\theta\left(r,\theta\right) = -\sigma_\theta\left(r,-\theta\right) \quad (1.8)$$
$$\sigma_{r\theta}\left(r,\theta\right) = \sigma_{r\theta}\left(r,-\theta\right)$$

Fig. 1.3 – **Anti-symmetric problem**

Through the boundary conditions (1.8) and (1.1), superposing the particular solutions and considering only the first terms of the series, that present inverse square root singularities of r, one gets for the stress components, in Cartesian coordinates:

$$\sigma_{xx} \simeq -\frac{K_{II}}{\sqrt{2\pi r}} \sin\frac{\theta}{2}\left(2 + \cos\frac{\theta}{2}\cos\frac{3\theta}{2}\right)$$

$$\sigma_{yy} \simeq \frac{K_{II}}{\sqrt{2\pi r}} \cos\frac{\theta}{2}\sin\frac{\theta}{2}\cos\frac{3\theta}{2} \qquad (1.9)$$

$$\sigma_{xy} \simeq \frac{K_{II}}{\sqrt{2\pi r}} \cos\frac{\theta}{2}\left(1 - \sin\frac{\theta}{2}\sin\frac{3\theta}{2}\right)$$

where K_{II} is a constant. From equation (1.9)-3, for $\theta = 0$ and switching to the variable $\xi(x) = x - a$, one obtains the definition of K_{II}:

$$K_{II} = \lim_{r \to 0}\sqrt{2\pi r}\,\sigma_{xy}(r,0) = \lim_{x \to a}\sqrt{2\pi r(x-a)}\,\sigma_{xy}(\xi,0) \qquad (1.10)$$

which is called *stress intensity factor* for the second (sliding) mode.

1.2.3. Anti-plane problem (Mode III)

There is a third basic fracture mechanism, characterised by the presence of only two stress components:

$$\sigma_{xx} = \sigma_{yy} = \sigma_{zz} = \sigma_{xy} = 0 \qquad \tau_{zx} = \tau_{zx}(x,y), \qquad \tau_{zy} = \tau_{zy}(x,y) \qquad (1.11)$$

For this mechanism, caused by out-of-plane shear, Williams obtained:

$$\sigma_{rz} = \frac{K_{III}}{\sqrt{2\pi r}}\sin\frac{\theta}{2}$$

$$\sigma_{\theta z} = \frac{K_{III}}{\sqrt{2\pi r}} \qquad (1.12)$$

where:

$$K_{III} = \lim_{x \to a}\sqrt{2\pi r(x-a)}\,\sigma_{\theta z}(\xi,0) \qquad (1.13)$$

is called *stress intensity factor* for the third (tearing) mode.

The superposition of the three modes describes the general case of fracture.

In particular for the plane case, of major concern in this study, we have [7]:

$$\sigma_{ij} = \frac{K_I}{\sqrt{2\pi r}} f_{ij}^{I}(\theta) + \frac{K_{II}}{\sqrt{2\pi r}} f_{ij}^{II}(\theta) \qquad (1.14)$$

The whole (asymptotic) stress field at the crack tip is known when the stress intensity factors are evaluated [7]. This asymptotic representation gives a sufficiently accurate description of the problem in the vicinity of the crack, although some authors [8-14] have noted that retaining the second terms of the series can be extremely important to study the effect of biaxial load.

The stress components are proportional to the external load, they vary with the square root of the crack size and tend to infinity at the crack tip.

Analogous expressions for displacement components can be deduced.

The elastic solution does not prohibit that the stresses become infinite at the crack tip. In the reality this does not occur: plastic deformation takes place. An evaluation of the size of the crack tip plastic zone can be obtained using the yield criterion [15,16].

It should be noted that in this work attention will be focused on the elastic behaviour of a cracked plate, thus, outside the plastic zone.

1.3   Fracture criteria for crack initiation

A fracture criterion is a constitutive equation stating the critical condition of a crack on the verge of branching. Among the local criteria generally used to predict the critical stress conditions and the angle of incipient fracture, the Maximum Normal Stress Criterion [17,18] and the Strain Energy Density Theory [15,16,19,20] will be discussed.

Note that the abovementioned criteria refer to the study of crack initiation. This means that the attention is focused on the incipient crack propagation.

In what follows the fracture criteria are applied to isotropic materials.

1.3.1 Maximum Circumferential Tensile Stress Theory

For isotropic materials, the circumferential stress σ_θ, defined as:

$$\sigma_\theta = \sigma_{11} \sin^2 \theta + \sigma_{22} \cos^2 \theta - \sigma_{12} \sin 2\theta \qquad (1.15)$$

can be studied to analyse the crack extension angle, for plane problems.

According to this criterion, crack extension occurs in the direction of the maximum circumferential stress σ_θ evaluated at a small distance r_0 from the crack tip, sufficient to be outside the plastic zone [16]. Designating the polar angle that defines the direction of extension as θ_0, the following conditions must be satisfied for the circumferential stress to be maximized:

$$\sigma_\theta \big|_{\theta=\theta_0} > 0 \qquad (1.16)$$

$$\frac{\partial}{\partial \theta}(\sigma_\theta)\big|_{\theta=\theta_0} = 0 \qquad (1.17)$$

$$\frac{\partial^2}{\partial \theta^2}(\sigma_\theta)\big|_{\theta=\theta_0} < 0 \qquad (1.18)$$

The crack extension begins as soon as the following situation is reached:

$$\sigma_\theta \big|_{\theta=\theta_0} = \frac{K_{IC}}{\sqrt{2\pi r_0}} \qquad (1.19)$$

12

where K_{IC} is the critical value of the stress intensity factor K_I which is defined at the onset of crack initiation. This is a material parameter and is also referred to as the *fracture toughness* of the material.

1.3.2 Strain Energy Density Theory

Referring to the problems of fracture mechanics, the strain energy per unit of volume can be expressed as [15,16,19,20]:

$$\frac{\mathrm{d}W}{\mathrm{d}V} = \frac{S}{r} \tag{1.20}$$

S is the *strain energy density factor* and it is related to the stress intensity factors as follows:

$$S = a_{11}K_I^2 + 2a_{12}K_I K_{II} + a_{22}K_{II}^2 \tag{1.21}$$

where the coefficients a_{ij} are defined by:

$$a_{11} = \frac{1}{16\pi\mu}\left[(3-4\nu-\cos\theta)(1+\cos\theta)\right] \tag{1.22}$$

$$a_{12} = \frac{1}{16\pi\mu}(2\sin\theta)\left[\cos\theta-(1-2\nu)\right] \tag{1.23}$$

$$a_{22} = \frac{1}{16\pi\mu}\left[4(1-\nu)(1-\cos\theta)+(1+\cos\theta)(3\cos\theta-1)\right] \tag{1.24}$$

and μ is the second Lamé constant of elasticity.

Note that the strain energy density criterion allows to consider all the three modes of fracture together [15], and so it can be used to predict crack initiation in spatial problems, despite of the first criterion.

The fundamental hypotheses of crack extension according to the Strain Energy Density Theory can be summarized as follows. The crack will spread in the direction of the minimum strain energy density, and the critical value of S (say, S_{cr}) governs the onset of the crack propagation. Summarizing, the crack begins to propagate in the θ_0 direction when the following conditions are satisfied:

$$\frac{\partial}{\partial\theta}(S)\Big|_{\theta=\theta_0} = 0 \tag{1.25}$$

$$\frac{\partial^2}{\partial\theta^2}(S)\Big|_{\theta=\theta_0} > 0 \tag{1.26}$$

$$S\Big|_{\theta=\theta_0} \geq S_{cr} \tag{1.27}$$

The critical value of S is a material parameter and for the isotropic case it is related to K_{IC}.

References

[1]   Liebowitz H., (edited by) *Fracture: An advanced treatise* (Vol.II), Academic Press, New York, 1968.

[2]   Williams M.L., *On the stress distribution at the base of a stationary crack*, J. Appl. Mech. 24, Trans. ASME, vol. 79 (1957), 109-114.

[3]   Irwin G. R., *Fracture*, in: «Handbuch der Physik», vol. 6, Springer, Berlin (1958), 551-590.

[4]   Broek D., *Elementary Engineering Fracture Mechanics*, Noordhoff International Publishing, Leyden, The Netherlands, 1974.

[5]   Viola E., *In tema di sviluppi asintotici all'apice di una fessura rettilinea*, Nota Tecnica 128, Università di Bologna, Facoltà di Ingegneria, DISTART, A.A. 1991-92

[6]   Viola E., *Deduzione non tradizionale del metodo di Westergaard per problemi di meccanica della frattura*, Nota Tecnica 129, Università di Bologna, Facoltà di Ingegneria, DISTART, A.A. 1991-92

[7]   Sih G.C., *Handbook of stress intensity factors,* Institute of Fracture and Solid Mechanics, Bethlehem, Pennsylvania, 1973.

[8]   Eftis J., Subramonian N., Liebowitz H., *Biaxial load effect on the crack border elastic strain energy and strain energy rate,* Engng. Fract. Mech. (1977); 9: 753-764.

[9]   Eftis J., Subramonian N., Liebowitz H., *Crack Border Stress and Displacement Equations Revisited,* Engng. Fract. Mech. (1977); 9: 189-210.

[10]   Eftis J., Subramonian N., *The inclined crack under Biaxial Load,* Engng. Fract. Mech. (1978); 10: 43-67.

[11]   Liebowitz H., Lee J.D., Eftis J., *Biaxial Load Effects in Fracture Mechanics,* Engng. Fract. Mech. (1978); 10: 315-335.

[12]   Liebowitz H., Lee J.D., Subramonian N., *Theoretical and experimental biaxial studies*, Proc. Int. Symp. Fract. Mech., George Washington University (1978); 593-628.

[13] Viola E., *Influenza delle tensioni non singolari sulla direzione di diramazione di un crack dominante in regime biassiale,* Giornale del Genio Civile, Fasc. I, II, III, 1979.

[14] Viola E., *Non-singular stress effects on two interacting equal collinear cracks,* Engng. Fract. Mech. (1977); 18: 801-814.

[15] Sih G.C., *A special theory of crack propagation: methods of analysis and solutions of crack problems,* Mechanics of Fracture I, Noordhoff, Leyden, The Netherlands, 1973.

[16] Sih G.C., *Mechanics of Fracture initiation and propagation*, Kluwer Academic Publisher, 1991.

[17] Erdogan F., Sih G.C., *On the crack extension in plates under plane loading and transverse shear,* J. Basic Engng. (1963); 85: 519-527.

[18] Di Tommaso A., Nobile L., Viola E., *Diramazione di un crack dominante in un solido a regime de formativo biassiale*, Atti del III Congresso Nazionale dell'Associazione Italiana di Meccanica Teorica e Applicata, Cagliari, 1976.

[19] Sih G.C., *Cracks in composite materials,* Mechanics of Fracture VI, Noordhoff, Leyden, The Netherlands, 1981.

[20] Sih G.C., *Strain density factor applied to mixed mode crack problems,* Int. J. Fract. (1974); 10:305-321.

CHAPTER 2

PLANE ELASTICITY FORMALISMS FOR ANISOTROPIC MATERIALS

2.1 Introduction

In this chapter, the displacement components u_i and the generalized stress vectors $\mathbf{t}_1$ and $\mathbf{t}_2$ for anisotropic materials in plane deformation conditions are defined through Stroh's formalism [1-3]. The Stroh's formalism can be traced to the work of Eshelby-Read-Shockley (1953) [4], which therefore will be presented first. Furthermore, in the simplified case of an orthotropic material, an alternative formalism is introduced, and the relations between this last formulation and Stroh's one are outlined.

2.2 Eshelby-Read-Shockley's formalism

In a Cartesian coordinate system $\left(x_1, x_2, x_3\right)$ let u_i and σ_{ij} $\left(i, j = 1, 2, 3\right)$ be the displacement and stress components in an anisotropic elastic material, respectively.

Hooke's law and the equilibrium condition can be expressed in index form as:

$$\sigma_{ij} = c_{ijks} u_{k,s} = c_{ijks} \frac{\partial u_k}{\partial x_s} \tag{2.1}$$

and:

$$\sigma_{ij,j} = c_{ijks} u_{k,sj} = c_{ijks} \frac{\partial^2 u_k}{\partial x_s \partial x_j} = 0 \tag{2.2}$$

where addition on repeated index is implicit, and where the stiffness tensor components c_{ijks} satisfy the symmetry conditions:

$$c_{ijks} = c_{jiks} , \; c_{ijks} = c_{jisk} , \; c_{ijks} = c_{ksij} \tag{2.3}$$

For two-dimensional deformations where u_i $(i=1,2,3)$ only depend on (x_1, x_2), a general solution for the homogeneous second-order differential equation system (2.2) is a function of one composite variable which is a linear combination of variables x_1 and x_2.

Let us assume:

$$u_i = u_i (x_1, x_2) = a_i f(z), \qquad z = x_1 + p x_2, \qquad i = 1,2,3 \tag{2.4}$$

where f is an arbitrary function of z, p and a_i are constants to be determined, and the coefficient for x_1 in the linear combination was chosen to be unity. In matrix form:

$$\mathbf{u} = \mathbf{a} f(z) \tag{2.5}$$

Differentiation of in x_1 and x_2 yields:

$$\frac{\partial u_k}{\partial x_1} = a_k f'(z), \quad \frac{\partial u_k}{\partial x_2} = p a_k f'(z) \tag{2.6}$$

or:

$$\frac{\partial u_k}{\partial x_s} = (\delta_{s1} + p \delta_{s2}) a_k f'(z) \tag{2.7}$$

where δ_{si} is the Kronecker Delta. From (2.7):

$$\frac{\partial^2 u_k}{\partial x_j \partial x_s} = (\delta_{j1} + p \delta_{j2})(\delta_{s1} + p \delta_{s2}) a_k f''(z) \tag{2.8}$$

and so equilibrium is satisfied when:

$$\left[c_{ijks} (\delta_{j1} + p \delta_{j2})(\delta_{s1} + p \delta_{s2}) \right] a_k = 0 \tag{2.9}$$

where sum is implicit on repeated indexes. Expliciting (2.9):

$$\sum_{j=1}^{3} \sum_{s=1}^{2} \left[c_{ijks} (\delta_{j1} + p \delta_{j2})(\delta_{s1} + p \delta_{s2}) \right] a_k = 0$$

$$: \sum_{j=1}^{3} \left[c_{ijk1} (\delta_{j1} + p \delta_{j2}) + c_{ijk2} (p \delta_{j1} + p^2 \delta_{j2}) \right] a_k = 0$$

$$: \left[c_{i1k1} + \left(c_{i2k1} + c_{i1k2} \right) p + c_{i2k2} p^2 \right] a_k = 0 \tag{2.10}$$

and passing to the matrix form:

$$\left[\mathbf{Q} + \left(\mathbf{R} + \mathbf{R}^T \right) p + \mathbf{T} p^2 \right] \mathbf{a} = \mathbf{0} \tag{2.11}$$

where the elements of the three 3x3 matrices are defined as follows:

$$Q_{ik} = c_{i1k1}, \quad R_{ik} = c_{i1k2}, \quad T_{ik} = c_{i2k2} \tag{2.12}$$

One can verify that matrices $\mathbf{Q}$ and $\mathbf{T}$ are symmetric, as the equalities $c_{i1k1} = c_{k1i1}$ and $c_{i2k2} = c_{k2i2}$ hold, and positive-definite, in order for the energy of elastic deformation to be positive. For the homogeneous system (2.11) to admit solutions different from the trivial one, it must be:

$$\det \left[\mathbf{Q} + \left(\mathbf{R} + \mathbf{R}^T \right) p + \mathbf{T} p^2 \right] = 0 \tag{2.13}$$

which is a sixth-grade equation in the eigenvalue p and yields three pairs of complex conjugate roots. Being p_α, $\mathbf{a}_\alpha$ $(\alpha = 1, 2, ..., 6)$ the eigenvalues and the correspondent eigenvectors solutions of the 6-grade equation, one can assume:

$$\text{Im } p_\alpha > 0 \quad \text{for } \alpha = 1, 2, 3 \tag{2.14}$$

$$p_{\alpha+3} = \overline{p}_\alpha \quad \mathbf{a}_{\alpha+3} = \overline{\mathbf{a}}_\alpha \quad \alpha = 1, 2, 3 \tag{2.15}$$

where the overbar denotes the complex conjugate.

The components of the stress vector can be obtained through (2.1); one gets:

$$\sigma_{i1} = c_{i1k1} a_k f'(z) + c_{i1k2} p a_k f'(z) = \left(Q_{ik} + p R_{ik} \right) a_k f'(z) \quad i = 1, 2, 3 \tag{2.16}$$

and:

$$\sigma_{i2} = c_{i2k1} a_k f'(z) + c_{i2k2} p a_k f'(z) = \left(R_{ki} + p T_{ik} \right) a_k f'(z) \quad i = 1, 2, 3 \tag{2.17}$$

One can define the generalized stress vectors as:

$$\mathbf{t}_1 = \left(\sigma_{11} \quad \sigma_{21} \quad \sigma_{31} \right)^T = \left(\mathbf{Q} + p \mathbf{R} \right) \mathbf{a} f'(z) \tag{2.18}$$

$$\mathbf{t}_2 = \left(\sigma_{12} \quad \sigma_{22} \quad \sigma_{32} \right)^T = \left(\mathbf{R}^T + p \mathbf{T} \right) \mathbf{a} f'(z) \tag{2.19}$$

The components of the displacement vector can be obtained through (2.5) by superposing six solutions. With the assumption that the six eigenvalues, and consequently the six eigenvectors, are distinct, and from (2.14) one gets:

$$\mathbf{u}_\alpha = \mathbf{a}_\alpha f_\alpha \left(z_\alpha \right) \quad \mathbf{u}_{\alpha+3} = \overline{\mathbf{a}}_\alpha f_{\alpha+3} \left(\overline{z_\alpha} \right) \quad \alpha = 1, 2, 3 \tag{2.20}$$

The general solution is obtained through superposition of (2.20):

$$\mathbf{u} = \sum_{\alpha=1}^{6} \mathbf{u}_\alpha = \sum_{\alpha=1}^{3} \left[\mathbf{a}_\alpha f_\alpha \left(z_\alpha \right) + \bar{\mathbf{a}}_\alpha f_{\alpha+3} \left(\overline{z_\alpha} \right) \right] \tag{2.21}$$

Likewise, the general solutions for the stresses can be written as:

$$\mathbf{t}_1 = \sum_{\alpha=1}^{3} \left[\left(\mathbf{Q} + p_\alpha \mathbf{R} \right) \mathbf{a}_\alpha f_\alpha {}'\left(z_\alpha \right) + \left(\mathbf{Q} + \overline{p}_\alpha \mathbf{R} \right) \bar{\mathbf{a}}_\alpha f {}'_{\alpha+3} \left(\overline{z_\alpha} \right) \right] \tag{2.22}$$

$$\mathbf{t}_2 = \sum_{\alpha=1}^{3} \left[\left(\mathbf{R}^T + p_\alpha \mathbf{T} \right) \mathbf{a}_\alpha f_\alpha {}'\left(z_\alpha \right) + \left(\mathbf{R}^T + \overline{p}_\alpha \mathbf{T} \right) \bar{\mathbf{a}}_\alpha f {}'_{\alpha+3} \left(\overline{z_\alpha} \right) \right] \tag{2.23}$$

2.3   Stroh's Formalism

From equation (2.11) one obtains:

$$\left(\mathbf{R}^T + \mathbf{T}p \right) p \mathbf{a} = -\left(\mathbf{Q} + \mathbf{R}p \right) \mathbf{a} \tag{2.24}$$

One can define a vector $\mathbf{b}$ such as:

$$\mathbf{b} = \left(\mathbf{R}^T + \mathbf{T}p \right) \mathbf{a} = -\frac{1}{p} \left(\mathbf{Q} + \mathbf{R}p \right) \mathbf{a} \tag{2.25}$$

whose components are:

$$b_i = \left(R_{ki} + p T_{ik} \right) a_k = -\frac{1}{p} \left(Q_{ik} + p R_{ik} \right) a_k \tag{2.26}$$

where the sum on index $k = 1, 2, 3$ is implicit. The components of the stress vectors can now be expressed as:

$$\sigma_{i1} = -p b_i f {}'\left(z \right) \qquad \sigma_{i2} = b_i f {}'\left(z \right) \qquad i = 1, 2, 3 \tag{2.27}$$

Introducing the stress functions:

$$\phi_i = b_i f \left(z \right) \tag{2.28}$$

expressions (2.27) can be written as:

$$\sigma_{i1} = -\phi_{i,2} = -\frac{\partial}{\partial x_2} \left[b_i f \left(x_1 + p x_2 \right) \right] \qquad \sigma_{i2} = \phi_{i,1} = \frac{\partial}{\partial x_1} \left[b_i f \left(x_1 + p x_2 \right) \right] \tag{2.29}$$

It is sufficient therefore to consider the stress functions ϕ_i, because stresses can be obtained by differentiation. Since $\sigma_{21} = \sigma_{12}$, we have:

$$\phi_{1,1} + \phi_{2,2} = 0 \tag{2.30}$$

and so, from (2.28):

$$b_1 + p b_2 = 0 \tag{2.31}$$

20

Vectors $\mathbf{b}_\alpha$ are correlated to vectors $\mathbf{a}_\alpha$ via the relation (2.25), so for them as well the position $\mathbf{b}_{\alpha+3} = \overline{\mathbf{b}}_\alpha$ with $\alpha = 1, 2, 3$ holds. The general solution of the plane problem can be obtained through superposition of the six particular solutions associated to the six eigenvalues p_α, in the form:

$$\mathbf{u} = \sum_{\alpha=1}^{3} \left[\mathbf{a}_\alpha f_\alpha \left(z_\alpha \right) + \overline{\mathbf{a}}_\alpha f_{\alpha+3} \left(\overline{z}_\alpha \right) \right] \tag{2.32}$$

$$\mathbf{\Phi} = \sum_{\alpha=1}^{3} \left[\mathbf{b}_\alpha f_\alpha \left(z_\alpha \right) + \overline{\mathbf{b}}_\alpha f_{\alpha+3} \left(\overline{z}_\alpha \right) \right] \tag{2.33}$$

Relations (2.32) and (2.33) express the *Stroh's Formalism*, and vectors $\mathbf{a}_\alpha$ and $\mathbf{b}_\alpha$ are called *Stroh's eigenvectors*. The stress vectors can be obtained by differentiation of (2.33). The only stress component missing is σ_{33}, which can be determined in terms of other stress components using the condition for $\varepsilon_{33} = 0$.

In many plane problems the arbitrary functions f_α have the same shape. We may therefore assume:

$$f_\alpha \left(z_\alpha \right) = f \left(z_\alpha \right) q_\alpha, \quad f_{\alpha+3} \left(\overline{z}_\alpha \right) = \overline{f} \left(\overline{z}_\alpha \right) \overline{q}_\alpha \qquad \alpha = 1, 2, 3 \tag{2.34}$$

where q_α are arbitrary complex constants. The second equation is necessary for obtaining real form solutions for $\mathbf{u}$ and $\mathbf{\Phi}$, when superposing f_α. Expression (2.32) becomes:

$$\mathbf{u} = \sum_{\alpha=1}^{3} \left[\mathbf{a}_\alpha f \left(z_\alpha \right) q_\alpha + \overline{\mathbf{a}}_\alpha \overline{f} \left(\overline{z}_\alpha \right) \overline{q}_\alpha \right] =$$

$$= \begin{pmatrix} a_{11} \\ a_{12} \\ a_{13} \end{pmatrix} f \left(z_1 \right) q_1 + \begin{pmatrix} a_{21} \\ a_{22} \\ a_{23} \end{pmatrix} f \left(z_2 \right) q_2 + \begin{pmatrix} a_{31} \\ a_{32} \\ a_{33} \end{pmatrix} f \left(z_3 \right) q_3 + \left(\text{conjugate terms} \right) =$$

$$= \begin{pmatrix} a_{11} & a_{21} & a_{31} \\ a_{12} & a_{22} & a_{32} \\ a_{13} & a_{23} & a_{33} \end{pmatrix} \begin{pmatrix} f \left(z_1 \right) & 0 & 0 \\ 0 & f \left(z_2 \right) & 0 \\ 0 & 0 & f \left(z_3 \right) \end{pmatrix} \begin{pmatrix} q_1 \\ q_2 \\ q_3 \end{pmatrix} + \left(\text{conjugate terms} \right)$$

$$\tag{2.35}$$

and in matrix form:

$$\mathbf{u} = 2 \operatorname{Re} \left[\mathbf{A} \mathrm{diag} \left[f \left(z_k \right) \right] \mathbf{q} \right] \tag{2.36}$$

where $\mathbf{A}$ is the 3x3 matrix whose columns are eigenvectors $\mathbf{a}_\alpha$. Analogously (2.33) becomes:

$$\mathbf{\Phi} = 2\operatorname{Re}\left[\mathbf{B}\operatorname{diag}\left[f\left(z_{k}\right)\right]\mathbf{q}\right] \tag{2.37}$$

where $\mathbf{B}$ is the 3x3 matrix whose columns are eigenvectors $\mathbf{b}_{\alpha}$.

For a given problem it is necessary to determine the unknown function $f\left(z_{k}\right)$ and the complex vector $\mathbf{q}$.

The eigenvalues p_{α} and the eigenvectors $\mathbf{a}_{\alpha}$ and $\mathbf{b}_{\alpha}$ depend on the elastic stiffnesses c_{ijks} only. Therefore, p_{α}, $\mathbf{a}_{\alpha}$ and $\mathbf{b}_{\alpha}$ can be regarded as material constants even though they are complex-valued.

2.4   Ortogonality and closure relations

What distinguishes the Stroh's formalism from others is that the vectors $\mathbf{a}_{\alpha}$ and $\mathbf{b}_{\alpha}$ for different α are related. The complex matrices $\mathbf{A}$ and $\mathbf{B}$ possess some peculiar properties [5,6].

From equations (2.24) and (2.25) one gets:

$$-\mathbf{Q}\mathbf{a} = p\mathbf{R}\mathbf{a} + \mathbf{b} \tag{2.38}$$

$$-\mathbf{R}^{T}\mathbf{a} + \mathbf{b} = p\mathbf{T}\mathbf{a} \tag{2.39}$$

which in matrix notation become:

$$\begin{pmatrix} -\mathbf{Q} & \mathbf{0} \\ -\mathbf{R}^{T} & \mathbf{I} \end{pmatrix}\begin{pmatrix} \mathbf{a} \\ \mathbf{b} \end{pmatrix} = p\begin{pmatrix} \mathbf{R} & \mathbf{I} \\ \mathbf{T} & \mathbf{0} \end{pmatrix}\begin{pmatrix} \mathbf{a} \\ \mathbf{b} \end{pmatrix} \tag{2.40}$$

where $\mathbf{I}$ is the 3x3 identity matrix. On the basis that $\mathbf{T}$ is positive definite and therefore $\mathbf{T}^{-1}$ exists, it can be demonstrated that:

$$\begin{pmatrix} \mathbf{0} & \mathbf{T}^{-1} \\ \mathbf{I} & -\mathbf{R}\mathbf{T}^{-1} \end{pmatrix}\begin{pmatrix} \mathbf{R} & \mathbf{I} \\ \mathbf{T} & \mathbf{0} \end{pmatrix} = \begin{pmatrix} \mathbf{I} & \mathbf{0} \\ \mathbf{0} & \mathbf{I} \end{pmatrix} \tag{2.41}$$

Pre-multiplying both sides of (2.40) by the first matrix on the left of (2.41) gets:

$$\begin{pmatrix} \mathbf{0} & \mathbf{T}^{-1} \\ \mathbf{1} & -\mathbf{R}\mathbf{T}^{-1} \end{pmatrix}\begin{pmatrix} -\mathbf{Q} & \mathbf{0} \\ -\mathbf{R}^{T} & \mathbf{1} \end{pmatrix}\begin{pmatrix} \mathbf{a} \\ \mathbf{b} \end{pmatrix} = p\begin{pmatrix} \mathbf{0} & \mathbf{T}^{-1} \\ \mathbf{1} & -\mathbf{R}\mathbf{T}^{-1} \end{pmatrix}\begin{pmatrix} \mathbf{R} & \mathbf{1} \\ \mathbf{T} & \mathbf{0} \end{pmatrix}\begin{pmatrix} \mathbf{a} \\ \mathbf{b} \end{pmatrix}$$

$$\therefore \quad \begin{pmatrix} \mathbf{0} & \mathbf{T}^{-1} \\ \mathbf{1} & -\mathbf{R}\mathbf{T}^{-1} \end{pmatrix}\begin{pmatrix} -\mathbf{Q}\,\mathbf{a} \\ -\mathbf{R}^{T}\mathbf{a} + \mathbf{b} \end{pmatrix} = p\begin{pmatrix} \mathbf{0} & \mathbf{T}^{-1} \\ \mathbf{1} & -\mathbf{R}\mathbf{T}^{-1} \end{pmatrix}\begin{pmatrix} \mathbf{R}\,\mathbf{a} + \mathbf{b} \\ \mathbf{T}\,\mathbf{a} \end{pmatrix}$$

$$\therefore \quad \begin{pmatrix} \mathbf{T}^{-1}(-\mathbf{R}^{T}\mathbf{a} + \mathbf{b}) \\ -\mathbf{Q}\,\mathbf{a} - \mathbf{R}\mathbf{T}^{-1}(-\mathbf{R}^{T}\mathbf{a} + \mathbf{b}) \end{pmatrix} = p\begin{pmatrix} \mathbf{a} \\ \mathbf{b} \end{pmatrix}$$

$$: \begin{pmatrix} -\mathbf{T}^{-1}\mathbf{R}^T & \mathbf{T}^{-1} \\ \mathbf{R}\mathbf{T}^{-1}\mathbf{R}^T - \mathbf{Q} & -\mathbf{R}\mathbf{T}^{-1} \end{pmatrix}\begin{pmatrix} \mathbf{a} \\ \mathbf{b} \end{pmatrix} = p\begin{pmatrix} \mathbf{a} \\ \mathbf{b} \end{pmatrix} \tag{2.42}$$

Defining:

$$\mathbf{N}_1 = -\mathbf{T}^{-1}\mathbf{R}^{\mathrm{T}} \; , \;\; \mathbf{N}_2 = \mathbf{T}^{-1} \; , \;\; \mathbf{N}_3 = \mathbf{R}\mathbf{T}^{-1}\mathbf{R}^{\mathrm{T}} - \mathbf{Q}$$

(2.43)

and:

$$\mathbf{N} = \begin{pmatrix} \mathbf{N}_1 & \mathbf{N}_2 \\ \mathbf{N}_3 & \mathbf{N}_1^{\mathrm{T}} \end{pmatrix} \tag{2.44}$$

the following standard eigenrelation is obtained:

$$\mathbf{N}\,\xi = p\,\xi \;, \qquad \xi = \begin{pmatrix} \mathbf{a} \\ \mathbf{b} \end{pmatrix} \tag{2.45}$$

The 6x6 matrix $\mathbf{N}$ is called the fundamental elasticity matrix. Since $\mathbf{N}$ is not symmetric, ξ is a right eigenvector. Denoting by η the left eigenvector, the following eigenrelation holds:

$$\mathbf{N}^T\eta = p\eta \tag{2.46}$$

Introducing the 6x6 constant matrix:

$$\hat{\mathbf{I}} = \begin{pmatrix} \mathbf{0} & \mathbf{I} \\ \mathbf{I} & \mathbf{0} \end{pmatrix} \;, \quad \hat{\mathbf{I}} = \hat{\mathbf{I}}^{\mathrm{T}} = \hat{\mathbf{I}}^{-1} \tag{2.47}$$

it can be shown that $\hat{\mathbf{I}}\mathbf{N}$ is symmetric, or:

$$\hat{\mathbf{I}}\mathbf{N} = (\hat{\mathbf{I}}\mathbf{N})^{\mathrm{T}} = \mathbf{N}^{\mathrm{T}}\hat{\mathbf{I}} \tag{2.48}$$

From (2.45) we have:

$$\hat{\mathbf{I}}\mathbf{N}\xi = p\hat{\mathbf{I}}\xi \tag{2.49}$$

and by (2.48):

$$\mathbf{N}^T(\hat{\mathbf{I}}\xi) = p(\hat{\mathbf{I}}\xi) \tag{2.50}$$

The left eigenvector has therefore the form:

$$\eta = \hat{\mathbf{I}}\xi = \begin{pmatrix} \mathbf{b} \\ \mathbf{a} \end{pmatrix} \tag{2.51}$$

It is known that the right and left eigenvectors corresponding to different eigenvalues are orthogonal to each other, i.e. for $p_\alpha \neq p_\beta$ the following relation holds:

$$\boldsymbol{\eta}_\alpha \cdot \boldsymbol{\xi}_\beta = 0 \tag{2.52}$$

The vector $\boldsymbol{\xi}$, and hence the vector $\boldsymbol{\eta}$, are unique up to an arbitrary multiplier. It is convenient to normalize them such that:

$$\boldsymbol{\eta}_\alpha \cdot \boldsymbol{\xi}_\beta = \delta_{\alpha\beta} \ , \quad \alpha, \beta = 1, 2, ..., 6 \tag{2.53}$$

or:

$$(\eta_{\alpha 1}, \quad \eta_{\alpha 2}, \quad ..., \quad \eta_{\alpha 6}) \begin{pmatrix} \xi_{\beta 1} \\ \xi_{\beta 2} \\ \vdots \\ \xi_{\beta 6} \end{pmatrix} = \boldsymbol{\eta}_\alpha^T \boldsymbol{\xi}_\beta = \delta_{\alpha\beta} \tag{2.54}$$

where $\delta_{\alpha\beta}$ is the Kronecker delta. This condition yields:

$$\boldsymbol{\eta}_1^T \boldsymbol{\xi}_1 = \boldsymbol{\eta}_2^T \boldsymbol{\xi}_2 = \boldsymbol{\eta}_3^T \boldsymbol{\xi}_3 = \overline{\boldsymbol{\eta}}_1^T \overline{\boldsymbol{\xi}}_1 = \overline{\boldsymbol{\eta}}_2^T \overline{\boldsymbol{\xi}}_2 = \overline{\boldsymbol{\eta}}_3^T \overline{\boldsymbol{\xi}}_3 = 1 \tag{2.55}$$

and all other products equal to zero. Introducing two 6x6 matrices such as:

$$\mathbf{U} = (\boldsymbol{\xi}_1, \boldsymbol{\xi}_2, \boldsymbol{\xi}_3, \overline{\boldsymbol{\xi}}_1, \overline{\boldsymbol{\xi}}_2, \overline{\boldsymbol{\xi}}_3) \tag{2.56}$$

$$\mathbf{V} = (\boldsymbol{\eta}_1, \boldsymbol{\eta}_2, \boldsymbol{\eta}_3, \overline{\boldsymbol{\eta}}_1, \overline{\boldsymbol{\eta}}_2, \overline{\boldsymbol{\eta}}_3) = \hat{\mathbf{1}} \mathbf{U} \tag{2.57}$$

one can express the orthonormality conditions (2.54) as:

$$\mathbf{V}^T \mathbf{U} = \mathbf{I} \tag{2.58}$$

Now, since;

$$\boldsymbol{\xi}_\alpha = \begin{pmatrix} \mathbf{a}_\alpha \\ \mathbf{b}_\alpha \end{pmatrix} = \begin{pmatrix} a_{\alpha 1} \\ a_{\alpha 2} \\ a_{\alpha 3} \\ b_{\alpha 1} \\ b_{\alpha 2} \\ b_{\alpha 3} \end{pmatrix} = \begin{pmatrix} \xi_{\alpha 1} \\ \xi_{\alpha 2} \\ \xi_{\alpha 3} \\ \xi_{\alpha 4} \\ \xi_{\alpha 5} \\ \xi_{\alpha 6} \end{pmatrix}, \qquad \boldsymbol{\eta}_\beta = \begin{pmatrix} \mathbf{b}_\beta \\ \mathbf{a}_\beta \end{pmatrix} = \begin{pmatrix} b_{\beta 1} \\ b_{\beta 2} \\ b_{\beta 3} \\ a_{\beta 1} \\ a_{\beta 2} \\ a_{\beta 3} \end{pmatrix} = \begin{pmatrix} \eta_{\beta 1} \\ \eta_{\beta 2} \\ \eta_{\beta 3} \\ \eta_{\beta 4} \\ \eta_{\beta 5} \\ \eta_{\beta 6} \end{pmatrix} \tag{2.59}$$

matrix $\mathbf{U}$ gets the shape:

$$\mathbf{U} = \left(\begin{pmatrix} \mathbf{a}_1 \\ \mathbf{b}_1 \end{pmatrix}, \ \begin{pmatrix} \mathbf{a}_2 \\ \mathbf{b}_2 \end{pmatrix}, \ \begin{pmatrix} \mathbf{a}_3 \\ \mathbf{b}_3 \end{pmatrix}, \ \begin{pmatrix} \overline{\mathbf{a}}_1 \\ \overline{\mathbf{b}}_1 \end{pmatrix}, \ \begin{pmatrix} \overline{\mathbf{a}}_2 \\ \overline{\mathbf{b}}_2 \end{pmatrix}, \ \begin{pmatrix} \overline{\mathbf{a}}_3 \\ \overline{\mathbf{b}}_3 \end{pmatrix} \right) =$$

$$= \begin{pmatrix} a_{11} & \dots & a_{31} & \overline{a}_{11} & \dots & \overline{a}_{31} \\ \vdots & & \vdots & \vdots & & \vdots \\ a_{13} & \dots & a_{33} & \overline{a}_{13} & \dots & \overline{a}_{33} \\ \vdots & & \vdots & \vdots & & \vdots \\ b_{13} & \dots & b_{33} & \overline{b}_{13} & \dots & \overline{b}_{33} \end{pmatrix} = \begin{pmatrix} \mathbf{A} & \overline{\mathbf{A}} \\ \mathbf{B} & \overline{\mathbf{B}} \end{pmatrix} \tag{2.60}$$

and analogously matrix $\mathbf{V}$:

24

$$\mathbf{V} = \left(\begin{pmatrix} \mathbf{b}_1 \\ \mathbf{a}_1 \end{pmatrix}, \begin{pmatrix} \mathbf{b}_2 \\ \mathbf{a}_2 \end{pmatrix}, \begin{pmatrix} \mathbf{b}_3 \\ \mathbf{a}_3 \end{pmatrix}, \begin{pmatrix} \overline{\mathbf{b}}_1 \\ \overline{\mathbf{a}}_1 \end{pmatrix}, \begin{pmatrix} \overline{\mathbf{b}}_2 \\ \overline{\mathbf{a}}_2 \end{pmatrix}, \begin{pmatrix} \overline{\mathbf{b}}_3 \\ \overline{\mathbf{a}}_3 \end{pmatrix} \right) = \begin{pmatrix} \mathbf{B} & \overline{\mathbf{B}} \\ \mathbf{A} & \overline{\mathbf{A}} \end{pmatrix} \qquad (2.61)$$

and thus:

$$\mathbf{V}^{\mathrm{T}} = \begin{pmatrix} \mathbf{B}^{\mathrm{T}} & \mathbf{A}^{\mathrm{T}} \\ \overline{\mathbf{B}}^{\mathrm{T}} & \overline{\mathbf{A}}^{\mathrm{T}} \end{pmatrix} \qquad (2.62)$$

The orthogonality relations (2.58) assume the aspect:

$$\mathbf{V}^{\mathrm{T}}\mathbf{U} = \begin{pmatrix} \mathbf{B}^{\mathrm{T}} & \mathbf{A}^{\mathrm{T}} \\ \overline{\mathbf{B}}^{\mathrm{T}} & \overline{\mathbf{A}}^{\mathrm{T}} \end{pmatrix} \begin{pmatrix} \mathbf{A} & \overline{\mathbf{A}} \\ \mathbf{B} & \overline{\mathbf{B}} \end{pmatrix} = \begin{pmatrix} \mathbf{I} & \mathbf{0} \\ \mathbf{0} & \mathbf{I} \end{pmatrix} \qquad (2.63)$$

or:

$$\begin{aligned} \mathbf{B}^{\mathrm{T}}\mathbf{A} + \mathbf{A}^{\mathrm{T}}\mathbf{B} = \mathbf{I} = \overline{\mathbf{B}}^{\mathrm{T}}\overline{\mathbf{A}} + \overline{\mathbf{A}}^{\mathrm{T}}\overline{\mathbf{B}} \\ \mathbf{B}^{\mathrm{T}}\overline{\mathbf{A}} + \mathbf{A}^{\mathrm{T}}\overline{\mathbf{B}} = \mathbf{0} = \overline{\mathbf{B}}^{\mathrm{T}}\mathbf{A} + \overline{\mathbf{A}}^{\mathrm{T}}\mathbf{B} \end{aligned} \qquad (2.64)$$

From (2.63) one can deduce that matrices $\mathbf{U}$ and $\mathbf{V}$ are the inverses of each other, and hence their product commute:

$$\mathbf{V}^{\mathrm{T}}\mathbf{U} = \mathbf{U}\mathbf{V}^{\mathrm{T}} = \begin{pmatrix} \mathbf{A} & \overline{\mathbf{A}} \\ \mathbf{B} & \overline{\mathbf{B}} \end{pmatrix} \begin{pmatrix} \mathbf{B}^{\mathrm{T}} & \mathbf{A}^{\mathrm{T}} \\ \overline{\mathbf{B}}^{\mathrm{T}} & \overline{\mathbf{A}}^{\mathrm{T}} \end{pmatrix} = \begin{pmatrix} \mathbf{I} & \mathbf{0} \\ \mathbf{0} & \mathbf{I} \end{pmatrix} \qquad (2.65)$$

from which we obtain the relations:

$$\begin{aligned} \mathbf{A}\,\mathbf{B}^{\mathrm{T}} + \overline{\mathbf{A}}\,\overline{\mathbf{B}}^{\mathrm{T}} = \mathbf{I} = \mathbf{B}\,\mathbf{A}^{\mathrm{T}} + \overline{\mathbf{B}}\,\overline{\mathbf{A}}^{\mathrm{T}} \\ \mathbf{A}\,\mathbf{A}^{\mathrm{T}} + \overline{\mathbf{A}}\,\overline{\mathbf{A}}^{\mathrm{T}} = \mathbf{0} = \mathbf{B}\,\mathbf{B}^{\mathrm{T}} + \overline{\mathbf{B}}\,\overline{\mathbf{B}}^{\mathrm{T}} \end{aligned} \qquad (2.66)$$

that are the closure relations. Equations (2.66) imply that the real part of $\mathbf{AB}^{\mathrm{T}}$ is $\mathbf{I}/2$, while $\mathbf{AA}^{\mathrm{T}}$ and $\mathbf{BB}^{\mathrm{T}}$ are purely imaginary. The eigenrelation (2.45) can be written as:

$$\mathbf{N}(\xi_1, \xi_2, \xi_3, \overline{\xi}_1, \overline{\xi}_2, \overline{\xi}_3) = (\xi_1, \xi_2, \xi_3, \overline{\xi}_1, \overline{\xi}_2, \overline{\xi}_3)\mathbf{P} \qquad (2.67)$$

where:

$$\mathbf{P} = \mathbf{diag}(p_1, p_2, p_3, \overline{p}_1, \overline{p}_2, \overline{p}_3) \qquad (2.68)$$

We get:

$$\mathbf{N}\,\mathbf{U} = \mathbf{U}\,\mathbf{P} \qquad (2.69)$$

that through (2.65) can be diagonalized as:

$$\mathbf{N} = \mathbf{U}\,\mathbf{P}\,\mathbf{V}^{\mathrm{T}} \qquad (2.70)$$

The derivations presented so far assume that the eigenvalues p_α are distinct, or that anyway six independent eigenvectors ξ_α exist.

25

2.5   The case of orthotropic materials

In the case of an orthotropic material, and for a plane problem, the matrix of elastic constants is simplified as follows:

$$\mathbf{C} = \begin{pmatrix} c_{11} & c_{12} & 0 & 0 & 0 \\ c_{12} & c_{22} & 0 & 0 & 0 \\ 0 & 0 & c_{44} & 0 & 0 \\ 0 & 0 & 0 & c_{55} & 0 \\ 0 & 0 & 0 & 0 & c_{66} \end{pmatrix} \tag{2.71}$$

Consequently, matrices $\mathbf{Q}$, $\mathbf{R}$ and $\mathbf{T}$ defined in the Stroh's formalism become:

$$\mathbf{Q} = \begin{pmatrix} c_{11} & 0 & 0 \\ 0 & c_{66} & 0 \\ 0 & 0 & c_{55} \end{pmatrix}, \qquad \mathbf{R} = \begin{pmatrix} 0 & c_{12} & 0 \\ c_{66} & 0 & 0 \\ 0 & 0 & 0 \end{pmatrix}, \qquad \mathbf{T} = \begin{pmatrix} c_{66} & 0 & 0 \\ 0 & c_{22} & 0 \\ 0 & 0 & c_{44} \end{pmatrix} \tag{2.72}$$

and:

$$\mathbf{Q} + \left(\mathbf{R} + \mathbf{R}^T\right) p + \mathbf{T} p^2 = \begin{pmatrix} c_{11} + p^2 c_{66} & (c_{12} + c_{66}) p & 0 \\ (c_{12} + c_{66}) p & c_{66} + p^2 c_{22} & 0 \\ 0 & 0 & c_{55} + p^2 c_{44} \end{pmatrix} \tag{2.73}$$

The characteristic equation is:

$$\left(c_{55} + p^2 c_{44}\right)\left[\left(c_{66} + p^2 c_{22}\right)\left(c_{11} + p^2 c_{66}\right) - \left(c_{12} + c_{66}\right)^2 p^2\right] = 0 \tag{2.74}$$

Posing

$$p^2 = \frac{1}{\lambda^2} \tag{2.75}$$

yields:

$$\begin{cases} c_{44} + \lambda^2 c_{55} = 0 \\ c_{11} c_{66} \lambda^4 + \left[c_{66}^2 + c_{11} c_{22} - \left(c_{12} + c_{66}\right)^2\right] \lambda^2 + c_{22} c_{66} = 0 \end{cases} \tag{2.76}$$

Dividing the second equation by $c_{11} c_{66}$ and with the positions:

$$\alpha = \frac{c_{66}}{c_{11}}, \quad \alpha_1 = \frac{c_{22}}{c_{66}}, \quad 2\beta = \frac{c_{12} + c_{66}}{c_{11}}, \quad 2\beta_1 = \frac{c_{12} + c_{66}}{c_{66}}, \quad 2a_1 = \alpha + \alpha_1 - 4\beta\beta_1, \quad a_2 = \alpha\alpha_1$$

$$\tag{2.77}$$

equation (2.76)-2 becomes:

$$\lambda^4 + 2a_1 \lambda^2 + a_2 = 0 \tag{2.78}$$

Equation (2.78) has no real solution. It is necessary to distinguish two cases: the four eigenvalues are imaginary or complex conjugate.

2.5.1. Imaginary Eigenvalues

This case happens when:

$$a_1^{\,2} - a_2 > 0, \qquad a_1 > 0 \tag{2.79}$$

The four imaginary eigenvalues are:

$$\lambda_1 = \mathrm{i}k_1, \qquad \lambda_2 = \mathrm{i}k_2, \qquad \lambda_3 = \overline{\lambda}_1, \qquad \lambda_4 = \overline{\lambda}_2 \tag{2.80}$$

with

$$k_1 = \left(a_1 - \sqrt{a_1^{\,2} - a_2} \right)^{1/2}, \qquad k_2 = \left(a_1 + \sqrt{a_1^{\,2} - a_2} \right)^{1/2} \tag{2.81}$$

positive constants.

2.5.2. Complex conjugate eigenvalues

This case happens when:

$$a_1^{\,2} - a_2 < 0 \tag{2.82}$$

One gets:

$$\lambda_1^{\,2} = -a_1 \pm \mathrm{i}\sqrt{a_2 - a_1^{\,2}} \tag{2.83}$$

$$\lambda_1^{\,2} = -a_1 \mp \mathrm{i}\sqrt{a_2 - a_1^{\,2}} \tag{2.84}$$

and the two pairs of conjugate roots are:

$$
\begin{aligned}
\lambda_{1,1} &= \sqrt{-a_1 + \mathrm{i}\sqrt{a_2 - a_1^{\,2}}}, & \lambda_{1,2} &= \sqrt{-a_1 - \mathrm{i}\sqrt{a_2 - a_1^{\,2}}}, \\
\lambda_{2,1} &= \lambda_{1,2} = \sqrt{-a_1 - \mathrm{i}\sqrt{a_2 - a_1^{\,2}}}, & \lambda_{2,2} &= \lambda_{1,1} = \sqrt{-a_1 + \mathrm{i}\sqrt{a_2 - a_1^{\,2}}}
\end{aligned}
\tag{2.85}
$$

If we impose $-a_1 + \mathrm{i}\sqrt{a_2 - a_1^{\,2}} = \sqrt{a_2}\,\mathrm{e}^{\mathrm{i}\varphi}$ and $-a_1 - \mathrm{i}\sqrt{a_2 - a_1^{\,2}} = \sqrt{a_2}\,\mathrm{e}^{-\mathrm{i}\varphi}$ we can obtain:

$$\lambda_1 = \sqrt[4]{a_2}\,\mathrm{e}^{\mathrm{i}\frac{\varphi}{2}} = \sqrt[4]{a_2}\left(\cos\frac{\varphi}{2} + i\sin\frac{\varphi}{2} \right) = \gamma_1 + i\gamma_2$$

$$\lambda_2 = -\sqrt[4]{a_2}\,\mathrm{e}^{-\mathrm{i}\frac{\varphi}{2}} = -\sqrt[4]{a_2}\left(\cos\frac{\varphi}{2} - i\sin\frac{\varphi}{2} \right) = -\gamma_1 + i\gamma_2 \tag{2.86}$$

$$\lambda_3 = \overline{\lambda}_1, \qquad \lambda_4 = \overline{\lambda}_2$$

where:

$$\gamma_1 = \sqrt[4]{a_2}\cos\frac{\varphi}{2} = \left(\frac{\sqrt{a_2}-a_1}{2}\right)^{1/2}, \qquad \gamma_2 = \sqrt[4]{a_2}\sin\frac{\varphi}{2} = \left(\frac{\sqrt{a_2}+a_1}{2}\right)^{1/2} \quad (2.87)$$

Furthermore, the first equation of (2.76) yields:

$$\lambda = \pm ik_3, \qquad k_3 = \sqrt{\frac{c_{44}}{c_{55}}} \tag{2.88}$$

From the system (2.73), six eigenvalues (either imaginary or complex conjugate) have been found; these can now be ordered considering first those with positive imaginary part:

Case 1)

$$p_1 = \frac{i}{k_1}, \qquad p_2 = \frac{i}{k_2}, \qquad p_3 = \frac{i}{k_3}, \qquad p_4 = \overline{p_1}, \qquad p_5 = \overline{p_2}, \qquad p_6 = \overline{p_3} \quad (2.89)$$

Case 2)

$$p_1 = \frac{1}{\sqrt[4]{a_2}}e^{i\frac{\varphi}{2}}, \qquad p_2 = -\frac{1}{\sqrt[4]{a_2}}e^{-i\frac{\varphi}{2}}, \qquad p_3 = \frac{i}{k_3}, \qquad p_4 = \overline{p_1}, \qquad p_5 = \overline{p_2}, \qquad p_6 = \overline{p_3}$$

$$(2.90)$$

We now consider for the sake of simplicity the first case only, and proceed with the calculations of the correspondent eigenvectors. Through equations (2.74) for $j = 1, 2$:

$$\begin{bmatrix} c_{11} + p_j^2 c_{66} & \left(c_{12} + c_{66}\right)p_j & 0 \\ \left(c_{12} + c_{66}\right)p_j & c_{66} + p_j^2 c_{22} & 0 \\ 0 & 0 & c_{55} + p_j^2 c_{44} \end{bmatrix} \begin{pmatrix} a_{j1} \\ a_{j2} \\ a_{j3} \end{pmatrix} = 0 \tag{2.91}$$

From the third equation, being $\left(c_{55} + p_j^2 c_{44}\right) \neq 0$ for $j = 1, 2$, it is obviously yielded $a_{j3} = 0$. The first and the second equation can be outlined in the shape:

$$\begin{aligned} \left(1 + \alpha p_j^2\right)a_{j1} + 2\beta p_j a_{j2} &= 0 \\ 2\beta_1 p_j a_{j1} + \left(1 + \alpha_1 p_j^2\right)a_{j2} &= 0 \end{aligned} \tag{2.92}$$

so we can set:

$$\mathbf{a}_j = \begin{pmatrix} \rho_j\left(1 + \alpha_1 p_j^2\right) \\ -\rho_j 2\beta_1 p_j \\ 0 \end{pmatrix}, \qquad j = 1, 2 \tag{2.93}$$

and then choose the arbitrary factor $\rho_j = -1$. With this position the first equation becomes the characteristic one and the second is always satisfied. For $j = 3$ the system is:

$$
\begin{bmatrix}
c_{11} + p_3^2 c_{66} & (c_{12} + c_{66}) p_3 & 0 \\
(c_{12} + c_{66}) p_3 & c_{66} + p_3^2 c_{22} & 0 \\
0 & 0 & c_{55} + p_3^2 c_{44}
\end{bmatrix}
\begin{pmatrix}
a_{31} \\
a_{32} \\
a_{33}
\end{pmatrix}
= 0
\qquad (2.94)
$$

whose solution is $a_{31} = a_{32} = 0$, $a_{33} = \rho_3$ with ρ_3 arbitrarily chosen constant. Stroh's matrix $\mathbf{A}$ is then:

$$
\mathbf{A} = \begin{bmatrix} \mathbf{a}_1 & \mathbf{a}_2 & \mathbf{a}_3 \end{bmatrix} = \begin{bmatrix}
-(1 + \alpha_1 p_1^2) & -(1 + \alpha_1 p_2^2) & 0 \\
2\beta_1 p_1 & 2\beta_1 p_2 & 0 \\
0 & 0 & \rho_3
\end{bmatrix}
\qquad (2.95)
$$

From the definition of vectors $\mathbf{b}_j$ one gets:

$$
\mathbf{b} = (\mathbf{R}^T + \mathbf{T}p)\mathbf{a} = \begin{bmatrix}
c_{66} p_j & c_{66} & 0 \\
c_{12} & c_{22} p_j & 0 \\
0 & 0 & c_{44} p_j
\end{bmatrix}
\begin{pmatrix}
a_{j1} \\
a_{j2} \\
a_{j3}
\end{pmatrix}
\qquad (2.96)
$$

thus Stroh's matrix $\mathbf{B}$ can be written as:

$$
\mathbf{B} = \begin{bmatrix} \mathbf{b}_1 & \mathbf{b}_2 & \mathbf{b}_3 \end{bmatrix} = \begin{bmatrix}
c_{66}(p_1 a_{11} + a_{12}) & c_{66}(p_2 a_{21} + a_{22}) & 0 \\
c_{12} a_{11} + c_{22} p_1 a_{12} & c_{12} a_{21} + c_{22} p_2 a_{22} & 0 \\
0 & 0 & c_{44} p_3 a_{33}
\end{bmatrix}
\qquad (2.97)
$$

or, by setting the arbitrary factor $\rho_3 = \dfrac{1}{c_{44} p_3}$:

$$
\mathbf{B} = \begin{bmatrix} \mathbf{b}_1 & \mathbf{b}_2 & \mathbf{b}_3 \end{bmatrix} = \begin{bmatrix}
c_{66}(p_1 a_{11} + a_{12}) & c_{66}(p_2 a_{21} + a_{22}) & 0 \\
c_{12} a_{11} + c_{22} p_1 a_{12} & c_{12} a_{21} + c_{22} p_2 a_{22} & 0 \\
0 & 0 & 1
\end{bmatrix}
\qquad (2.98)
$$

From Stroh's matrices $\mathbf{A}$ and $\mathbf{B}$, through relations (2.36) and (2.37) it is possible to calculate the displacement vector $\mathbf{u}$ and the generalized potential vector $\mathbf{\Phi}$, and from this through relation (2.29) one gets the stress components.

2.6 Alternative formalism

A formalism alternative to the Stroh's one for the orthotropic case is now outlined [7-9]. We can define two vectors of generalized strain components:

$$\mathbf{\Gamma}^{(1)} = \left(\frac{\partial \mathbf{u}}{\partial x_1}\right) = \left(\frac{\partial u_1}{\partial x_1} \quad \frac{\partial u_2}{\partial x_1} \quad \frac{\partial u_3}{\partial x_1}\right)^T \tag{2.99}$$

$$\mathbf{\Gamma}^{(2)} = \left(\frac{\partial \mathbf{u}}{\partial x_2}\right) = \left(\frac{\partial u_1}{\partial x_2} \quad \frac{\partial u_2}{\partial x_2} \quad \frac{\partial u_3}{\partial x_2}\right)^T \tag{2.100}$$

and express the stress vectors in the form:

$$\mathbf{t}_1 = \left(\sigma_{11} \quad \sigma_{21} \quad \sigma_{31}\right)^T = \mathbf{Q}\mathbf{\Gamma}^{(1)} + \mathbf{R}\mathbf{\Gamma}^{(2)} \tag{2.101}$$

$$\mathbf{t}_2 = \left(\sigma_{12} \quad \sigma_{22} \quad \sigma_{32}\right)^T = \mathbf{R}^T\mathbf{\Gamma}^{(1)} + \mathbf{T}\mathbf{\Gamma}^{(2)} \tag{2.102}$$

For the equilibrium to be satisfied it must be:

$$\frac{\partial \mathbf{t}_1}{\partial x_1} + \frac{\partial \mathbf{t}_2}{\partial x_2} = \mathbf{0} \tag{2.103}$$

or:

$$\begin{cases} \mathbf{Q}\dfrac{\partial \mathbf{\Gamma}^{(1)}}{\partial x_1} + \mathbf{R}\dfrac{\partial \mathbf{\Gamma}^{(2)}}{\partial x_1} + \mathbf{R}^T\dfrac{\partial \mathbf{\Gamma}^{(1)}}{\partial x_2} + \mathbf{T}\dfrac{\partial \mathbf{\Gamma}^{(2)}}{\partial x_2} = \mathbf{0} \\[2mm] \dfrac{\partial \mathbf{\Gamma}^{(2)}}{\partial x_1} - \dfrac{\partial \mathbf{\Gamma}^{(1)}}{\partial x_2} = \mathbf{0} \end{cases} \tag{2.104}$$

where the second equation is the condition of equality of crossed derivatives (Schwartz condition).

The system of equations obtained can be written in matricial form as:

$$\frac{\partial}{\partial x_1}\begin{pmatrix} \mathbf{\Gamma}^{(1)} \\ \mathbf{\Gamma}^{(2)} \end{pmatrix} + \begin{bmatrix} \mathbf{Q}^{-1}\left(\mathbf{R}+\mathbf{R}^T\right) & \mathbf{Q}^{-1}\mathbf{T} \\ \mathbf{-1} & \mathbf{0} \end{bmatrix}\frac{\partial}{\partial x_2}\begin{pmatrix} \mathbf{\Gamma}^{(1)} \\ \mathbf{\Gamma}^{(2)} \end{pmatrix} = \mathbf{0} \tag{2.105}$$

If we define the vector $\mathbf{\Phi} = \left(\phi_1, \phi_2, \phi_3, \phi_4, \phi_5, \phi_6\right)^T = \left(\mathbf{\Gamma}^{(1)}, \mathbf{\Gamma}^{(2)}\right)^T$, the system (2.105) can be written as:

$$\frac{\partial \mathbf{\Phi}}{\partial x_1} + \mathbf{D}\frac{\partial \mathbf{\Phi}}{\partial x_2} = \mathbf{0} \tag{2.106}$$

with:

$$\mathbf{D} = \begin{pmatrix} 0 & 2\beta & 0 & \alpha & 0 & 0 \\ 2\beta_1 & 0 & 0 & 0 & \alpha_1 & 0 \\ 0 & 0 & 0 & 0 & 0 & \gamma \\ -1 & 0 & 0 & 0 & 0 & 0 \\ 0 & -1 & 0 & 0 & 0 & 0 \\ 0 & 0 & -1 & 0 & 0 & 0 \end{pmatrix} \qquad (2.107)$$

where:

$$\alpha = \frac{c_{66}}{c_{11}}, \qquad \alpha_1 = \frac{c_{22}}{c_{66}}, \qquad 2\beta = \frac{c_{12}+c_{66}}{c_{11}}, \qquad 2\beta_1 = \frac{c_{12}+c_{66}}{c_{66}}, \qquad \gamma = \frac{c_{44}}{c_{55}} \quad (2.108)$$

In fact, remembering the definition of matrices $\mathbf{Q}$, $\mathbf{R}$ and $\mathbf{T}$, we have:

$$\mathbf{Q}^{-1}\left(\mathbf{R}+\mathbf{R}^T\right) = \begin{pmatrix} \dfrac{1}{c_{11}} & 0 & 0 \\ 0 & \dfrac{1}{c_{66}} & 0 \\ 0 & 0 & \dfrac{1}{c_{55}} \end{pmatrix} \begin{pmatrix} 0 & c_{12}+c_{66} & 0 \\ c_{12}+c_{66} & 0 & 0 \\ 0 & 0 & 0 \end{pmatrix} = \begin{pmatrix} 0 & \dfrac{c_{12}+c_{66}}{c_{11}} & 0 \\ \dfrac{c_{12}+c_{66}}{c_{66}} & 0 & 0 \\ 0 & 0 & 0 \end{pmatrix}$$

$$(2.109)$$

and

$$\mathbf{Q}^{-1}\mathbf{T} = \begin{pmatrix} \dfrac{1}{c_{11}} & 0 & 0 \\ 0 & \dfrac{1}{c_{66}} & 0 \\ 0 & 0 & \dfrac{1}{c_{55}} \end{pmatrix} \begin{pmatrix} c_{66} & 0 & 0 \\ 0 & c_{22} & 0 \\ 0 & 0 & c_{44} \end{pmatrix} = \begin{pmatrix} \dfrac{c_{66}}{c_{11}} & 0 & 0 \\ 0 & \dfrac{c_{22}}{c_{66}} & 0 \\ 0 & 0 & \dfrac{c_{44}}{c_{55}} \end{pmatrix} \qquad (2.110)$$

Developing the system (2.106) one gets the three differential equations governing the elastic problem in the case of orthotropic materials:

$$\begin{cases} \dfrac{\partial^2 u_1}{\partial x_1^2} + 2\beta \dfrac{\partial^2 u_2}{\partial x_1 \partial x_2} + \alpha \dfrac{\partial^2 u_1}{\partial x_2^2} = 0 \\[2mm] \dfrac{\partial^2 u_1}{\partial x_1^2} + 2\beta_1 \dfrac{\partial^2 u_1}{\partial x_1 \partial x_2} + \alpha_1 \dfrac{\partial^2 u_2}{\partial x_2^2} = 0 \\[2mm] \dfrac{\partial^2 u_3}{\partial x_1^2} + \gamma \dfrac{\partial^2 u_3}{\partial x_2^2} = 0 \end{cases} \qquad (2.111)$$

and the three conditions of equality of crossed derivatives:

$$\frac{\partial^2 u_1}{\partial x_1 \partial x_2} - \frac{\partial^2 u_1}{\partial x_2 \partial x_1} = 0, \qquad \frac{\partial^2 u_2}{\partial x_1 \partial x_2} - \frac{\partial^2 u_2}{\partial x_2 \partial x_1} = 0, \qquad \frac{\partial^2 u_3}{\partial x_1 \partial x_2} - \frac{\partial^2 u_3}{\partial x_2 \partial x_1} = 0 \quad (2.112)$$

Developing the algebraic calculations for the characteristic equation of the system

$$\det\left(\mathbf{D}-\lambda\mathbf{I}\right)=0 \tag{2.113}$$

the following equation is found:

$$\left(\lambda^4 + 2a_1\lambda^2 + a_2\right)\left(\lambda^2 + \gamma\right) = 0 \tag{2.114}$$

where

$$2a_1 = \alpha + \alpha_1 - 4\beta\beta_1, \qquad a_2 = \alpha\alpha_1 \tag{2.115}$$

Equation (2.114) yields six complex roots. Considering the simpler case for which the first part of the equation has four imaginary roots, the eigenvalues can be ordered considering those with positive imaginary part first, in this way:

$$\lambda_1 = ik_1, \quad \lambda_2 = ik_2, \quad \lambda_3 = ik_3, \quad \lambda_4 = \overline{\lambda_1}, \quad \lambda_5 = \overline{\lambda_2}, \quad \lambda_6 = \overline{\lambda_3} \tag{2.116}$$

with $k_3 = \sqrt{\gamma} = \sqrt{\dfrac{c_{44}}{c_{55}}}$.

The six relative eigenvectors are

$$\mathbf{V}^{(j)} = \left(ik_j\left(\alpha_1 - k_j^2\right) \quad -2\beta_1 k_j^2 \quad 0 \quad \left(k_j^2 - \alpha_1\right) \quad -2i\beta_1 k_j \quad 0\right)^T, \quad j = 1,2$$
$$\mathbf{V}^{(3)} = \left(0 \quad 0 \quad -ik_3 \quad 0 \quad 0 \quad -1\right)^T$$
$$\tag{2.117}$$

and the correspondent conjugates. Considering the first three eigenvectors, it is possible to build the matrix:

$$\mathbf{W} = \left(\operatorname{Im}\mathbf{V}^{(1)} \quad \operatorname{Re}\mathbf{V}^{(1)} \quad \operatorname{Im}\mathbf{V}^{(2)} \quad \operatorname{Re}\mathbf{V}^{(2)} \quad \operatorname{Im}\mathbf{V}^{(3)} \quad \operatorname{Re}\mathbf{V}^{(3)}\right) \tag{2.118}$$

that induces the trasformation (spectral theorem):

$$\mathbf{W}^{-1}\mathbf{D}\mathbf{W} = \mathbf{E} = \begin{pmatrix} 0 & -k_1 & 0 & 0 & 0 & 0 \\ k_1 & 0 & 0 & 0 & 0 & 0 \\ 0 & 0 & 0 & k_2 & 0 & 0 \\ 0 & 0 & -k_2 & 0 & 0 & 0 \\ 0 & 0 & 0 & 0 & 0 & -k_3 \\ 0 & 0 & 0 & 0 & k_3 & 0 \end{pmatrix} \tag{2.119}$$

Pre-multiplying (2.106) by $\mathbf{W}^{-1}$ and considering that $\mathbf{W}^{-1}\mathbf{D} = \mathbf{E}\mathbf{W}^{-1}$, the system becomes:

$$\frac{\partial\mathbf{\Psi}}{\partial x_1} + \mathbf{E}\frac{\partial\mathbf{\Psi}}{\partial x_2} = \mathbf{0} \tag{2.120}$$

32

where:

$$\Psi = \mathbf{W}^{-1}\Phi \tag{2.121}$$

Now, defining the vectors:

$$\Psi^{(1)} = \begin{pmatrix} \Psi_1 & \Psi_2 \end{pmatrix}^T, \qquad \Psi^{(2)} = \begin{pmatrix} \Psi_3 & \Psi_4 \end{pmatrix}^T, \qquad \Psi^{(3)} = \begin{pmatrix} \Psi_5 & \Psi_6 \end{pmatrix}^T \tag{2.122}$$

the system (2.120) can be split into three sub-systems:

$$\frac{\partial \Psi^{(j)}}{\partial x_1} + \mathbf{K}_j \frac{\partial \Psi^{(j)}}{\partial x_2} = \mathbf{0}, \quad j = 1, 2, 3 \tag{2.123}$$

where:

$$\mathbf{K}_j = \begin{pmatrix} 0 & -k_j \\ k_j & 0 \end{pmatrix} = k_j \begin{pmatrix} 0 & -1 \\ 1 & 0 \end{pmatrix}, \quad j = 1, 2, 3 \tag{2.124}$$

With the change of variable $y_j = \dfrac{x_2}{k_j}$, the sub-systems can be reformulated in the shape:

$$\frac{\partial \Psi^{(j)}}{\partial x_1} + \mathbf{S}\frac{\partial \Psi^{(j)}}{\partial y_j} = \mathbf{0}, \quad \mathbf{S} = \begin{pmatrix} 0 & -1 \\ 1 & 0 \end{pmatrix}, \quad j = 1, 2, 3 \tag{2.125}$$

which are the Cauchy-Riemann conditions for complex potentials of the type:

$$\Omega_j(z_j) = \Psi_1^{(j)}(x_1, y_j) + i\Psi_2^{(j)}(x_1, y_j), \quad j = 1, 2, 3 \tag{2.126}$$

of the complex variables:

$$z_j = x_1 + iy_j = x_1 + p_j x_2, \qquad p_j = \frac{1}{k_j} \tag{2.127}$$

From equation (2.121) we obtain the elements of vector Φ in the following shape:

$$\Phi_i = \sum_{k=1}^{6} W_{ik}\Psi_k, \qquad i = 1, 2, ..., 6 \tag{2.128}$$

If one writes the eigenvectors as $\mathbf{V}^{(j)} = \mathbf{g}^{(j)} + i\mathbf{h}^{(j)}$ for $j = 1, 2, 3$, then gets $W_{i1} = h_i^{(1)}$, $W_{i2} = g_i^{(1)}$, $W_{i3} = h_i^{(2)}$, $W_{i4} = g_i^{(2)}$, $W_{i5} = h_i^{(3)}$, $W_{i6} = g_i^{(3)}$, and:

$$\Phi_i = h_i^{(1)}\Psi_1 + g_i^{(1)}\Psi_2 + h_i^{(2)}\Psi_3 + g_i^{(2)}\Psi_4 + h_i^{(3)}\Psi_5 + g_i^{(3)}\Psi_6 =$$
$$= h_i^{(1)}\operatorname{Re}\Omega_1 + g_i^{(1)}\operatorname{Im}\Omega_1 + h_i^{(2)}\operatorname{Re}\Omega_2 + g_i^{(2)}\operatorname{Im}\Omega_2 + h_i^{(3)}\operatorname{Re}\Omega_3 + g_i^{(3)}\operatorname{Im}\Omega_3$$

$$(2.129)$$

In compact form $(i \to j)$:

$$\Phi_j = \sum_{k=1}^{3}\left[h_j^{(k)}\operatorname{Re}\Omega_k(z_k) + g_j^{(k)}\operatorname{Im}\Omega_k(z_k) \right] = \operatorname{Im}\sum_{k=1}^{3}\left[V_j^{(k)}\Omega_k(z_k) \right] \tag{2.130}$$

and developing the calculations for the elements of vector $\boldsymbol{\Phi}$:

$$
\begin{cases}
\Phi_1 = k_1\left(a_1 - k_1^2\right)\Psi_1 + k_2\left(a_1 - k_2^2\right)\Psi_3 = k_1\left(a_1 - k_1^2\right)\mathrm{Re}\,\Omega_1 + k_2\left(a_1 - k_2^2\right)\mathrm{Re}\,\Omega_2 \\
\Phi_2 = -2\beta_1\left(k_1^2\Psi_2 + k_2^2\Psi_4\right) = -2\beta_1\left(k_1^2\,\mathrm{Im}\,\Omega_1 + k_2^2\,\mathrm{Im}\,\Omega_2\right) \\
\Phi_3 = -k_3\Psi_5 = -k_3\,\mathrm{Re}\,\Omega_3 \\
\Phi_4 = \left(k_1^2 - a_1\right)\Psi_2 + \left(k_2^2 - a_1\right)\Psi_4 = \left(k_1^2 - a_1\right)\mathrm{Im}\,\Omega_1 + \left(k_2^2 - a_1\right)\mathrm{Im}\,\Omega_2 \\
\Phi_5 = -2\beta_1\left(k_1\,\Psi_1 + k_2\,\Psi_3\right) = -2\beta_1\left(k_1\,\mathrm{Re}\,\Omega_1 + k_2\,\mathrm{Re}\,\Omega_2\right) \\
\Phi_6 = \Psi_6 = \mathrm{Im}\,\Omega_3
\end{cases}
\tag{2.131}
$$

Through the relation (2.130) one obtains:

$$
\boldsymbol{\Gamma}^{(1)} = \left(\Phi_1 \quad \Phi_2 \quad \Phi_3\right)^T = \frac{1}{2i}\left[\mathbf{F}_1\boldsymbol{\Omega}(z) - \overline{\mathbf{F}}_1\overline{\boldsymbol{\Omega}(z)}\right]
\tag{2.132}
$$

$$
\boldsymbol{\Gamma}^{(2)} = \left(\Phi_4 \quad \Phi_5 \quad \Phi_6\right)^T = \frac{1}{2i}\left[\mathbf{F}_2\boldsymbol{\Omega}(z) - \overline{\mathbf{F}}_2\overline{\boldsymbol{\Omega}(z)}\right]
\tag{2.133}
$$

with:

$$
\mathbf{F}_1 = \begin{pmatrix} V_1^{(1)} & V_1^{(2)} & V_1^{(3)} \\ V_2^{(1)} & V_2^{(2)} & V_2^{(3)} \\ V_3^{(1)} & V_3^{(2)} & V_3^{(3)} \end{pmatrix} = \begin{pmatrix} ik_1\left(\alpha_1 - k_1^2\right) & ik_2\left(\alpha_1 - k_2^2\right) & 0 \\ -2\beta_1 k_1^2 & -2\beta_1 k_2^2 & 0 \\ 0 & 0 & -ik_3 \end{pmatrix}
\tag{2.134}
$$

$$
\mathbf{F}_2 = \begin{pmatrix} V_4^{(1)} & V_4^{(2)} & V_4^{(3)} \\ V_5^{(1)} & V_5^{(2)} & V_5^{(3)} \\ V_6^{(1)} & V_6^{(2)} & V_6^{(3)} \end{pmatrix} = \begin{pmatrix} \left(k_1^2 - \alpha_1\right) & \left(k_2^2 - \alpha_1\right) & 0 \\ -2i\beta_1 k_1 & -2i\beta_1 k_2 & 0 \\ 0 & 0 & -1 \end{pmatrix}
\tag{2.135}
$$

Considering that matrices $\mathbf{Q}$, $\mathbf{R}$ and $\mathbf{T}$ are real, the generalized stress vectors are expressed as:

$$
\begin{aligned}
\mathbf{t}_1 &= \left(\sigma_{11} \quad \sigma_{21} \quad \sigma_{31}\right)^T = \mathbf{Q}\boldsymbol{\Gamma}^{(1)} + \mathbf{R}\boldsymbol{\Gamma}^{(2)} = \\
&= \frac{1}{2i}\left[\mathbf{Q}\mathbf{F}_1\boldsymbol{\Omega}(z) - \mathbf{Q}\overline{\mathbf{F}}_1\overline{\boldsymbol{\Omega}(z)}\right] + \frac{1}{2i}\left[\mathbf{R}\mathbf{F}_2\boldsymbol{\Omega}(z) - \mathbf{R}\overline{\mathbf{F}}_2\overline{\boldsymbol{\Omega}(z)}\right] = \\
&= \frac{1}{2i}\left\{\left[\mathbf{Q}\mathbf{F}_1 + \mathbf{R}\mathbf{F}_2\right]\boldsymbol{\Omega}(z) - \left[\mathbf{Q}\overline{\mathbf{F}}_1 + \mathbf{R}\overline{\mathbf{F}}_2\right]\overline{\boldsymbol{\Omega}(z)}\right\} = \\
&= \frac{1}{2i}\left[\mathbf{G}_1\boldsymbol{\Omega}(z) - \overline{\mathbf{G}}_1\overline{\boldsymbol{\Omega}(z)}\right] = \mathrm{Im}\left[\mathbf{G}_1\boldsymbol{\Omega}(z)\right]
\end{aligned}
\tag{2.136}
$$

and analogally:

$$
\mathbf{t}_2 = \left(\sigma_{12} \quad \sigma_{22} \quad \sigma_{32}\right)^T = \mathbf{R}^T\boldsymbol{\Gamma}^{(1)} + \mathbf{T}\boldsymbol{\Gamma}^{(2)} = \mathrm{Im}\left[\mathbf{G}_2\boldsymbol{\Omega}(z)\right]
\tag{2.137}
$$

where matrices $\mathbf{G}_1$ and $\mathbf{G}_2$ are defined:

$$\mathbf{G}_1 = \mathbf{QF}_1 + \mathbf{RF}_2, \qquad \mathbf{G}_2 = \mathbf{R}^T\mathbf{F}_1 + \mathbf{TF}_2 \qquad (2.138)$$

We have:

$$\text{Im}\left[\mathbf{G}_1\mathbf{\Omega}(z)\right] = \text{Im}\left[\left(\text{Re}\,\mathbf{G}_1 + i\,\text{Im}\,\mathbf{G}_1\right)\left(\text{Re}\,\mathbf{\Omega} + i\,\text{Im}\,\mathbf{\Omega}\right)\right] = \text{Re}\,\mathbf{G}_1\,\text{Im}\,\mathbf{\Omega} + \text{Im}\,\mathbf{G}_1\,\text{Re}\,\mathbf{\Omega}$$

$$(2.139)$$

The explicit forms of the stress components of vector $\mathbf{t}_1$ are then:

$$\begin{cases} \sigma_{11} = k_1\left[c_{11}\left(\alpha_1 - k_1^2\right) - 2\beta_1 c_{12}\right]\text{Re}\,\Omega_1(z_1) + k_2\left[c_{11}\left(\alpha_1 - k_2^2\right) - 2\beta_1 c_{12}\right]\text{Re}\,\Omega_2(z_2) \\ \sigma_{21} = c_{66}\left\{\left[-2\beta_1 k_1^2 + k_1^2 - \alpha_1\right]\text{Im}\,\Omega_1(z_1) + \left[-2\beta_1 k_2^2 + k_2^2 - \alpha_1\right]\text{Im}\,\Omega_2(z_2)\right\} \\ \sigma_{31} = -c_{55}k_3\,\text{Re}\,\Omega_3(z_3) \end{cases}$$

$$(2.140)$$

and analogally, for the stress components of vector $\mathbf{t}_2$:

$$\begin{cases} \sigma_{12} = c_{66}\left\{\left[-2\beta_1 k_1^2 + k_1^2 - \alpha_1\right]\text{Im}\,\Omega_1(z_1) + \left[-2\beta_1 k_2^2 + k_2^2 - \alpha_1\right]\text{Im}\,\Omega_2(z_2)\right\} \\ \sigma_{22} = k_1\left[c_{12}\left(\alpha_1 - k_1^2\right) - 2\beta_1 c_{22}\right]\text{Re}\,\Omega_1(z_1) + k_2\left[c_{12}\left(\alpha_1 - k_2^2\right) - 2\beta_1 c_{22}\right]\text{Re}\,\Omega_2(z_2) \\ \sigma_{32} = c_{44}\,\text{Im}\,\Omega_3(z_3) \end{cases}$$

$$(2.141)$$

The displacement components $\mathbf{u} = \left(u_1 \quad u_2 \quad u_3\right)^T$ can be obtained directly by integration in x_1 of the vector $\mathbf{\Gamma}^{(1)} = \left(\dfrac{\partial\mathbf{u}}{\partial x_1}\right)$. Neglecting a rigid displacement, and being $\mathbf{\omega}(z)$ the primitive of $\mathbf{\Omega}(z)$, we get:

$$\mathbf{u} = \frac{1}{2i}\left[\mathbf{F}_1\mathbf{\omega}(z) - \overline{\mathbf{F}}_1\overline{\mathbf{\omega}(z)}\right] = \text{Im}\left[\mathbf{F}_1\mathbf{\omega}(z)\right] \qquad (2.142)$$

Since:

$$\text{Im}\left[\mathbf{F}_1\mathbf{\omega}(z)\right] = \text{Re}\,\mathbf{F}_1\,\text{Im}\,\mathbf{\omega}(z) + \text{Im}\,\mathbf{F}_1\,\text{Re}\,\mathbf{\omega}(z) \qquad (2.143)$$

remembering the explicit form of matrix $\mathbf{F}_1$, the displacement components are:

$$\begin{cases} u_1 = k_1\left(\alpha_1 - k_1^2\right)\text{Re}\,\omega_1(z_1) + k_2\left(\alpha_1 - k_2^2\right)\text{Re}\,\omega_2(z_2) \\ u_2 = -2\beta_1\left[k_1^2\,\text{Im}\,\omega_1(z_1) + k_2^2\,\text{Im}\,\omega_2(z_2)\right] \\ u_3 = -k_3\,\text{Re}\,\omega_3(z_3) \end{cases} \qquad (2.144)$$

If the complex potentials are formally equals, or, in other words, they differ only by a (complex) multiplying factor r_i, then their expression can be simplified as:

$$\Omega_i(z_i) = r_i\Omega(z_i), \qquad i = 1,2,3, \qquad r_i \in \mathbb{C} \qquad (2.145)$$

and the expressions of the stress and displacement vectors become:

$$\mathbf{t}_1 = \mathrm{Im}\left\{\mathbf{G}_1 \mathbf{diag}\left[\Omega(z_i)\right]\mathbf{r}\right\} \tag{2.146}$$

$$\mathbf{t}_2 = \mathrm{Im}\left\{\mathbf{G}_2 \mathbf{diag}\left[\Omega(z_i)\right]\mathbf{r}\right\} \tag{2.147}$$

$$\mathbf{u} = \mathrm{Im}\left\{\mathbf{F}_1 \mathbf{diag}\left[\omega(z_i)\right]\mathbf{r}\right\} \tag{2.148}$$

2.7   Relations with Stroh's formalism

The relations (2.146), (2.147), (2.148) defining stress and displacement components through the alternative formalism are compared in this paragraph with Stroh's relations (2.36) and (2.37).

The shape of Stroh's first matrix $\mathbf{A}$ is:

$$\begin{cases} a_{j1} = \rho_j\left(1+\alpha_1 p_j^2\right) \\ a_{j2} = -2\rho_j\beta_1 p_j \end{cases}, \quad j=1,2, \qquad \mathbf{a}_j = \begin{pmatrix} 0 \\ 0 \\ \rho_j \end{pmatrix}, \quad j=3 \tag{2.149}$$

Given the arbitrariness of ρ_j we set:

$$\rho_j = -k_j^3 = -\frac{i}{p_j^3} \qquad j=1,2$$
$$\rho_3 = -k_3 \tag{2.150}$$

so that the matrix is:

$$\mathbf{A} = \begin{bmatrix} \mathbf{a}_1 & \mathbf{a}_2 & \mathbf{a}_3 \end{bmatrix} = \begin{bmatrix} k_1\left(\alpha_1-k_1^2\right) & k_2\left(\alpha_1-k_2^2\right) & 0 \\ 2i\beta_1 k_1^2 & 2i\beta_1 k_2^2 & 0 \\ 0 & 0 & -k_3 \end{bmatrix} \tag{2.151}$$

and from a comparison with (2.134) one gets:

$$\mathbf{A} = -i\mathbf{F}_1 \tag{2.152}$$

or:

$$\mathrm{Re}\,\mathbf{A} = \mathrm{Im}\,\mathbf{F}_1 \tag{2.153}$$

Regarding the stress components, let's consider matrices $\mathbf{G}_1$ and $\mathbf{G}_2$, whose explicit forms are:

36

$$\mathbf{G}_1 = \mathbf{Q}\mathbf{F}_1 + \mathbf{R}\mathbf{F}_2 = \begin{bmatrix} ik_1\left[c_{11}\left(\alpha_1 - k_1^2\right) - 2\beta_1 c_{12}\right] & ik_2\left[c_{11}\left(\alpha_1 - k_2^2\right) - 2\beta_1 c_{12}\right] & 0 \\ c_{66}\left[-2\beta_1 k_1^2 + \left(k_1^2 - \alpha_1\right)\right] & c_{66}\left[-2\beta_1 k_2^2 + \left(k_2^2 - \alpha_1\right)\right] & 0 \\ 0 & 0 & -ic_{55}k_3 \end{bmatrix}$$

$$(2.154)$$

$$\mathbf{G}_2 = \mathbf{R}^T\mathbf{F}_1 + \mathbf{T}\mathbf{F}_2 = \begin{bmatrix} -c_{66}\left[2\beta_1 k_1^2 - \left(k_1^2 - \alpha_1\right)\right] & -c_{66}\left[2\beta_1 k_2^2 - \left(k_2^2 - \alpha_1\right)\right] & 0 \\ -ik_1\left[c_{12}\left(k_1^2 - \alpha_1\right) + 2i\beta_1 c_{22}\right] & -ik_2\left[c_{12}\left(k_2^2 - \alpha_1\right) + 2i\beta_1 c_{22}\right] & 0 \\ 0 & 0 & c_{44} \end{bmatrix}$$

$$(2.155)$$

Taking into account the positions (2.89) matrix $\mathbf{B}$, explicited in (2.97), becomes:

$$\mathbf{B} = \begin{bmatrix} ic_{66}\left[2\beta_1 k_1^2 - \left(k_1^2 - \alpha_1\right)\right] & ic_{66}\left[2\beta_1 k_2^2 - \left(k_2^2 - \alpha_1\right)\right] & 0 \\ -k_1\left[c_{12}\left(k_1^2 - \alpha_1\right) + 2i\beta_1 c_{22}\right] & -k_2\left[c_{12}\left(k_2^2 - \alpha_1\right) + 2i\beta_1 c_{22}\right] & 0 \\ 0 & 0 & -ic_{44} \end{bmatrix} = -i\mathbf{G}_2 \quad (2.156)$$

thus it is again:

$$\mathrm{Re}\,\mathbf{B} = \mathrm{Im}\,\mathbf{G}_2 \tag{2.157}$$

Vectors $\mathbf{b}_j$ can also be obtained through:

$$\mathbf{b}_j = -\frac{1}{p_j}\left(\mathbf{Q} + p_j\mathbf{R}\right)\mathbf{a}_j \tag{2.158}$$

and remembering the relation $-\dfrac{1}{p_j} = ik_j$ matrix $\mathbf{B}$ is explicited in the form:

$$\mathbf{B} = \begin{bmatrix} ik_1^2\left[c_{11}\left(\alpha_1 - k_1^2\right) - 2c_{12}\beta_1\right] & ik_2^2\left[c_{11}\left(\alpha_1 - k_2^2\right) - 2c_{12}\beta_1\right] & 0 \\ -c_{66}k_1\left[\left(\alpha_1 - k_1^2\right) + 2k_1^2\beta_1\right] & -c_{66}k_2\left[\left(\alpha_1 - k_2^2\right) + 2k_2^2\beta_1\right] & 0 \\ 0 & 0 & -ic_{55}k_3^2 \end{bmatrix} \tag{2.159}$$

From relation (2.29) the first generalized stress vector is obtained as:

$$\mathbf{t}_1 = -\frac{\partial\varphi}{\partial x_2} = -\frac{\partial}{\partial x_2}\left\{2\,\mathrm{Re}\left[\mathbf{B}\,\mathbf{diag}\left[f\left(z_j\right)\right]\mathbf{q}\right]\right\} \tag{2.160}$$

where the complex variable is:

$$z_j = x_1 + iy_j = x_1 + \frac{i}{k_j}x_2 \tag{2.161}$$

Then:

$$\mathbf{t}_1 = -2\operatorname{Re}\left[\mathbf{Bdiag}\left[\frac{i}{k_j}f(z_j)\right]\mathbf{q}\right] = 2\operatorname{Im}\left[\mathbf{Bdiag}\left[\frac{i}{k_j}\right]\mathbf{diag}\left[f(z_j)\right]\mathbf{q}\right] \qquad (2.162)$$

and one can immediately see:

$$\mathbf{Bdiag}\left[\frac{i}{k_j}\right] = \begin{bmatrix} ik_1\left[c_{11}\left(\alpha_1-k_1^2\right)-2\beta_1 c_{12}\right] & ik_2\left[c_{11}\left(\alpha_1-k_2^2\right)-2\beta_1 c_{12}\right] & 0 \\ c_{66}\left[-2\beta_1 k_1^2+\left(k_1^2-\alpha_1\right)\right] & c_{66}\left[-2\beta_1 k_2^2+\left(k_2^2-\alpha_1\right)\right] & 0 \\ 0 & 0 & -ic_{55}k_3 \end{bmatrix} = \mathbf{G}_1$$

$$(2.163)$$

It is demonstrated that Stroh's formalism and the alternative formalism are formally equivalent. Both theoretical approaches find their main origins in the fundamental works of Muskelishvili [10] and Lekhnitskii [11], who introduced formulations of plane elasticity in terms of functions of complex variables.

References

[21] Stroh A.N., *Dislocations and cracks in anisotropic elasticity*, Philos. Mag. (1958); 3: 625-646.

[22] Stroh A.N., *Steady state problems in anisotropic elasticity*, J. Math. Phys. (1962); 41: 77-103.

[23] Ting T.C.T., *Anisotropic Elasticity, Theory and Applications*, Oxford University Press, N.Y. (1996).

[24] Eshelby J.D., Read W.T., Shockley W., *Anisotropic elasticity with applications to dislocation theory*, Acta Metallurgica (1953); 1: 251-259.

[25] Barnett D.M., Lothe J., *Synthesis of the sextic and the integral formalism for dislocations, Green's function and surface waves in anisotropic elastic solids*, Phys. Norv. (1973); 7: 13-19.

[26] Chadwick P., Smith G.D., *Foundations of the theory of surface waves in anisotropic elastic materials*, Adv. Appl. Mech. (1977); 17: 303-376.

[27] Piva A., *An alternative approach to elastodynamic crack problems in an orthotropic medium*, Quart Appl Maths. (1987); 45:97-104.

[28] Piva A., Viola E., *Crack propagation in an orthotropic medium*, Engng Fract Mech. (1988); 29:535-548.

[29] Viola E., Piva A., Radi E., *Crack propagation in an orthotropic medium under general loading*, Engng Fract Mech. (1989); 34:1155-1174.

[30] Muskhelishvili N.I., *Some basic problems of the mathematical theory of elasticity*, Noordhoof, Groningen (1952).

[31] Lekhnitskii S.G., *Theory of Elasticity of an Anisotropic Body*, Mir Publishers, Moscow (1977).

CHAPTER 3

LINEAR THEORY OF PIEZOELECTRICITY

3.1   Introduction

Piezoelectric material is such that when it is subjected to a mechanical load it generates an electric charge. This effect is usually called the "piezoelectric effect". Conversely, when piezoelectric material is stressed electrically by a voltage, its dimensions change. This phenomenon is known as the "inverse piezoelectric effect".

The piezoelectric effect was first discovered more than one century ago by Pierre and Jacques Curie [1], who found that certain crystalline materials generated an electric charge proportional to the mechanical stress in their experiments to demonstrate a connection between macroscopic piezoelectric phenomena and crystallographic structure. The experiment consisted of a conclusive measurement of surface charges appearing on specially prepared crystals (tourmaline, quartz, topaz, cane sugar and Rochelle salt among them) which were subjected to mechanical stress. Pierre and Jacques Curie presented papers on this discovery [1] at the Meeting of Société Mineralogique de France on 8 April 1880 and at the Académie des Sciences during the meeting of 24 August 1880. In the scientific circles of the day, this effect was considered quite a discovery, and was quickly dubbed "piezoelectricity" in order to distinguish it from other areas of scientific phenomenological experience such as pyroelectricity (electricity generated from

crystals by heating). The Curies asserted that there was a one-to-one correspondence between the electrical effects of temperature change and mechanical stress in a given crystal, and that they had used this correspondence not only to select the crystals for the experiment, but also to determine the cuts of those crystals. To them, their demonstration was a confirmation of predictions which followed naturally from their understanding of the microscopic crystallographic origins of pyroelectricity. The Curies did not, however, predict that crystals exhibiting the direct piezoelectric effect (electricity from applied stress) would also exhibit the inverse piezoelectric effect (stress in response to applied electric field). One year later this property was theoretically predicted on the basis of thermodynamic consideration by Lippmann [2], who proposed that converse effects must exist for piezoelectricity, pyroelectricity etc. Subsequently, the inverse piezoelectric effect was confirmed experimentally by the Curies [3], who proceeded to obtain quantitative proof of the complete reversibility of electromechanical deformations in piezoelectric crystals.

Other papers by Pierre and Jacques Curie [3-6] reported a series of results from experiments on quartz and tourmaline, and suggested some laboratory experiments that could use the piezoelectric effect for measuring forces or pressures and high voltages by means of a "manomètre à quartz" and an "electromètre à quartz". The most famous device was the "quartz piezoélectrique" utilized to produce known electric charges for the measurement of voltages, currents, capacitances, etc. This piezo-quartz instrument played an important role in Marie Curie's later work on radioactivity.

These events and publications might be viewed as the beginning of the history of piezoelectricity. Based on them, Woldemar Voigt [7] developed the first complete and rigorous formulation of piezoelectricity in 1890. Since then, several other books on the phenomenon and theory of piezoelectricity have been written. Among the books are the references by Cady [8] and Parton and Kudryavtsev [9]. The first of these [8] treated the physical properties of piezoelectric crystals as

well as their practical applications, and the second [9] gave a more detailed description of the physical properties of piezoelectricity.

During the past half-century, piezoelectric device development has made significant progress. In 1951, several Japanese companies and universities formed a "competitively cooperative" association, established as the Barium Titanate Application Research Committee. This association set an organizational precedent for successfully surmounting not only technical challenges and manufacturing hurdles, but also defining new market areas.

Persistent efforts in material research created new piezoceramic families. The most common industrially produced piezoelectric materials are lead zirconate titanate (PZT).

A piezoelectric ceramic has a crystal structure generally composed of a small tetravalent metallic ion (most commonly Titanium or Zirconium) in a lattice of bivalent metallic ions (Lead, or Barium) and Oxygen ions. Above a critical temperature (said Curie temperature) every crystal exhibits cubic symmetry with no dipole moment, while below that temperature, the crystals present a tetragonal or rhombohedric symmetry producing a dipole moment. Adjacent dipoles form domains of local polarization, whose random directions however tend to nullify their macroscopic effect.

If the material is subjected to an electric field strong enough, with a temperature slightly below the critical one, poled domains align with the applied field, and they tend to maintain this alignment even after the removal of the electric stimulus. This procedure is called permanent polarization treatment (Figure 3.1).

When a poled ceramic is mechanically stressed, the dipole moment is modified and generates an electric potential difference (mechanical energy is converted into electrical energy). In particular, a stress of compression applied along the polarization direction generates a voltage with same polarity, whereas a tension returns a voltage with opposite polarity (Figure 3.2).
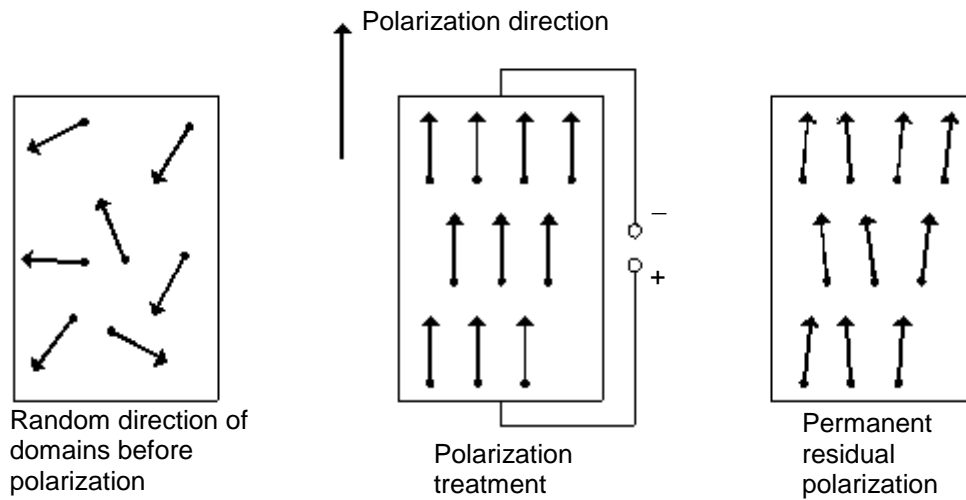
Fig. 3.1 – Polarization treatment of a piezoelectric ceramic
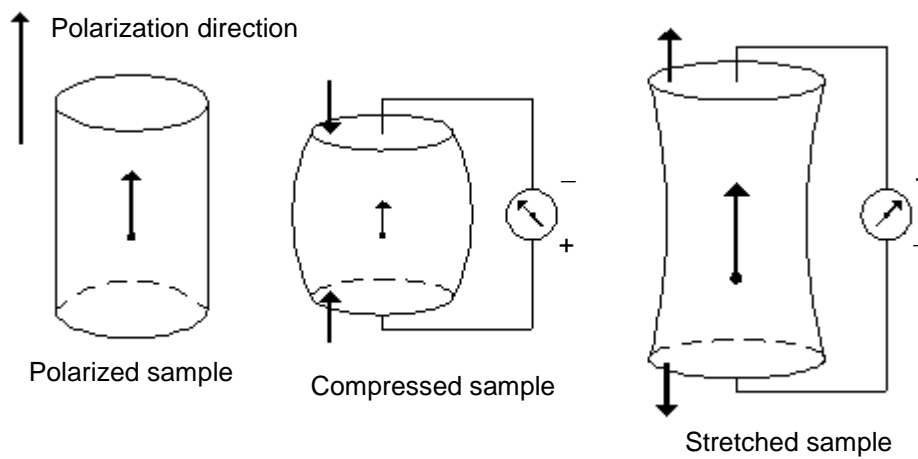
Fig. 3.2 – Direct piezoelectric effect

For the inverse effect, depicted in Figure 3.3, a same-polarity voltage applied along the polarization direction causes a stretch, and an opposite-polarity voltage causes a contraction (electrical energy turned into mechanical energy).

A cyclic application of stress or difference of potential gives a cyclic response.

Polarization direction

Same-polarity
applied voltage

Opposite-polarity
applied voltage
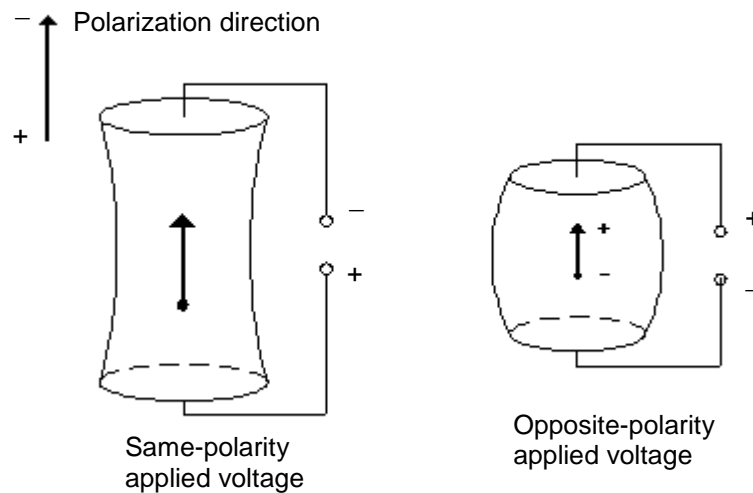
Fig. 3.3 – Inverse piezoelectric effect

With these materials available, Japanese manufacturers quickly developed several types of piezoelectric signal filters, which addressed needs arising in television, radio and communication equipment markets; and piezoelectric igniters for natural gas/butane appliances. As time progressed, the markets for these products continued to grow, and then similarly valuable ones were found. Most notable were audio buzzers (smoke alarms), air ultrasonic transducers (television remote controls and intrusion alarms) and devices employing surface acoustic wave effects to achieve high frequency signal filtering.

The commercial success of the Japanese efforts attracted the attention of industry in many other countries and spurred new efforts to develop successful piezoelectric products. There has been a large increase in publication rate in China, India, Russia and the USA. The search for perfect piezo product opportunities is still in progress. Judging by the increase in worldwide activity focusing on using a large number of very precise piezoelectric sensors and actuators for active control in communications, navigation and packaging systems, and from the successes encountered in the last fifty years, it is expected that piezoelectricity will enjoy a continuing role in both fundamental and technical applications in the future.

As with most ceramics, a significant disadvantage of these materials is their brittleness. Stress concentration in proximity of defects or inhomogeneities, such as flaws, cavities or included particles, can contribute to critical crack growth and subsequent mechanical failure or dielectric breakdown. Their performances can be significantly improved getting a complete understanding of their damage process: a thorough understanding of their fracture behaviour is crucial in order to improve their performances and avoid unexpected failures. Therefore, a considerable number of research works have addressed this topic in the last decades.

Application of the concepts of fracture mechanics to the failure of cracked piezoelectric ceramics is found in several papers [10-16], and a thorough review of the literature can be found in [17].

In this chapter, the linearized piezoelectricity formulations described in [8-9] which will be needed in later chapters, are briefly summarized. The basic equations of linear electroelasticity are first reviewed, followed by a brief discussion on the physical constants. An analytical solution procedure in anisotropic electro-elasticity is considered. Then the properties of transversely isotropic piezoelectric materials are described. Finally, some boundary conditions in electroelasticity theory are outlined.

3.2   Basic equations of Linear Thermopiezoelectricity

Of concern in this work is the study of the elastostatic fracture response of a cracked piezoelectric body.

In this section we recall briefly the three-dimensional formulation of linear piezoelectricity that appeared in [8-9]. Here, a three-dimensional Cartesian coordinate system is adopted where the position vector is denoted by $\mathbf{x}$ (or x_i). In this thesis, both conventional indicial notation x_i and traditional Cartesian

notation (x, y, z) are utilized. In the case of indicial notation we invoke the summation convention over repeated Latin indices, which can be of two types with different ranges: $i, j, k = 1, 2, 3$ for lower-case letters and $M, N = 1, 2, 3, 4$ for upper-case letters. Moreover, vectors, tensors and their matrix representations are denoted by bold-face letters. The three-dimensional constitutive equations for linear piezoelectricity can be derived by considering the full Gibbs function per unit volume, g, defined as [9]:

$$g = U - E_m D_m - T^a s \tag{3.1}$$

where U, s, D_m and E_m are the internal energy density, entropy density, electric displacement and electric field, respectively, $T^a = T_0 + T$ is the absolute temperature, where T_0 is reference temperature and T a small temperature change: $|T| \ll T_0$. E_i is defined by

$$E_i = -\varphi_{,i} \tag{3.2}$$

in which φ is the electric potential, and a comma followed by arguments denotes partial differentiation with respect to the arguments. From the exact differential

$$dg = \sigma_{ij} d\gamma_{ij} - D_m dE_m - s dT \tag{3.3}$$

where σ_{ij} and γ_{ij} are respectively stress and strain, while γ_{ij} is defined by

$$\gamma_{ij} = \frac{1}{2} \left(u_{i,j} + u_{j,i} \right) \tag{3.4}$$

in which u_i is the elastic displacement, we obtain:

$$s = -\left[\frac{\partial g}{\partial T} \right]_{\gamma, E}, \quad \sigma_{ij} = \left[\frac{\partial g}{\partial \gamma_{ij}} \right]_{T, E}, \quad D_m = -\left[\frac{\partial g}{\partial E_m} \right]_{\gamma, T}. \tag{3.5}$$

When the function g is expanded with respect to T, γ_{ij} and E_m within the scope of linear interaction, we have:

$$g = \frac{1}{2} \left(T \frac{\partial}{\partial T} + \gamma_{ij} \frac{\partial}{\partial \gamma_{ij}} + E_m \frac{\partial}{\partial E_m} \right) \left(T \frac{\partial}{\partial T} + \gamma_{kl} \frac{\partial}{\partial \gamma_{kl}} + E_n \frac{\partial}{\partial E_n} \right) \tag{3.6}$$

The following constants can then be defined:

$$c_{ijkl}^{(T,E)} = \left[\frac{\partial^2 g}{\partial \gamma_{ij} \partial \gamma_{kl}}\right]_{T,E}, \quad \varepsilon_{nm}^{(\gamma,T)} = -\left[\frac{\partial^2 g}{\partial E_n \partial E_m}\right]_{\gamma,T}, \quad \frac{\rho C_v^{(\gamma,E)}}{T_0} = -\left[\frac{\partial^2 g}{\partial T^2}\right]_{\gamma,E},$$

$$e_{mij}^{(T)} = -\left[\frac{\partial^2 g}{\partial \gamma_{ij} \partial E_m}\right]_T, \quad \lambda_{ij}^{(E)} = -\left[\frac{\partial^2 g}{\partial \gamma_{ij} \partial T}\right]_E, \quad \chi_m^{(\gamma)} = -\left[\frac{\partial^2 g}{\partial T \partial E_m}\right]_\gamma,$$

(3.7)

where $c_{ijkl}^{(T,E)}$ are the elastic moduli measured at constant electric field and temperature, $\varepsilon_{nm}^{(\gamma,T)}$ the dielectric constants measured at constant strain and temperature, ρ is the mass density, $C_v^{(\gamma,E)}$ is the specific heat per unit mass, $e_{mij}^{(T)}$ the piezoelectric coefficients measured at constant temperature, $\lambda_{ij}^{(E)}$ the thermal-stress coefficients measured at constant electric field, and $\chi_m^{(\gamma)}$ the pyroelectric coefficients measured at a constant strain.

When the function g is differentiated according to equation (3.3), and the above constants are used, we find

$$s = \frac{\rho C_v}{T_0} T + \lambda_{ij} \gamma_{ij} + \chi_m E_m,$$

$$\sigma_{ij} = -\lambda_{ij} T + c_{ijkl} \gamma_{kl} - e_{mij} E_m,$$

(3.8)

$$D_n = \chi_n T + e_{nij} \gamma_{ij} + \varepsilon_{nm} E_m.$$

A set of these three equations is the constitutive relation in the coupled system. It should be noted that the superscripts appearing in equations (3.7) have been dropped here. To simplify the subsequent writing they will be omitted in the remaining part of this work. Using the notation defined above, the Gibbs function per unit volume can now be expressed as:

$$g = \frac{1}{2} c_{ijkl} \gamma_{ij} \gamma_{kl} - \frac{1}{2} \varepsilon_{ij} E_i E_j - \frac{\rho C_v}{2T_0} T^2 - e_{ijk} E_i \gamma_{jk} - \chi_m T E_m - \lambda_{ij} T \gamma_{ij}$$

(3.9)

Having defined the material constants, the related divergence equations and boundary conditions can be derived by considering the modified Biot's variational principle [18]:

$$\delta \int_V (B + 2F) dV - \int_V (f_{bi} \delta u_i - q_b \delta\phi) dV - \int_S \left(T_i \delta u_i - q_s \delta\phi - h_n \frac{\delta T}{T_0}\right) dS = 0 \quad (3.10)$$

where V and S are the domain and boundary of the material, f_{bi} and q_b are the body force per unit volume and electric charge density, T_i, q_s and h_n are the

applied surface traction, charge, and prescribed surface heat flow, respectively, B and F are Biot's generalized free energy density and the dissipation function, which are defined by [18]:

$$B = U - T_0 s = g + E_i D_i + Ts, \qquad F = \frac{1}{2T_0} k_{ij} T_{,i} T_{,j} \qquad (3.11)$$

in which k_{ij} is the heat conduction coefficient.

The variational equation (3.10) provides the following results:

$$\sigma_{ij} + f_{bi} = 0, \qquad D_{i,i} = q_b, \qquad h_{i,i} = -T_0 \Delta s, \qquad (3.12)$$

$$\sigma_{ij} n_j = T_i, \qquad D_i n_i = -q_s, \qquad h_i n_i = h_n \qquad (3.13)$$

where n_i is the outer unit normal vector to S, and h_i is heat flow. Equations (3.12) are the elastic equilibrium equations, Gauss's law of electrostatics, and heat conduction equation, respectively, and equations (3.13) are boundary conditions.

3.3 Fundamental electroelastic relations

In order to identify directions in a piezoelectric element, three axes are used. These axes, termed 1, 2 and 3, are analogous to X, Y and Z of the classical orthogonal set of axes. The polar axis, or axis 3, is taken parallel to the direction of polarization within the ceramic. This direction is established during manufacturing by a high DC voltage that is applied between a pair of electrode faces to activate the material

The discussion is now focused on an electromechanically coupled system. In the preceding section was showed how the thermal system, as a third system, affects to a greater or lesser degree the elastic, dielectric, and piezoelectric constants. It is therefore necessary to specify the thermal condition, i.e. whether it is isothermal or adiabatic. Since most electromechanical measurements are made under an alternating field or stress, the observed constants are adiabatic. On the other hand, discussion of phase transformation in solid-state physics requires

knowledge of isothermal constants. In fact, the distinction is rarely mentioned because electric-to-thermal and mechanical-to-thermal couplings are rather weak, except in a few special cases.

At constant temperature, equations (3.8) are reduced to:

$$\sigma_{ij} = c_{ijkl}\gamma_{kl} - e_{mij}E_m \tag{3.14}$$

$$D_n = e_{nij}\gamma_{ij} + \varepsilon_{nm}E_m \tag{3.15}$$

In this thesis it was chosen to use equations (3.14) and (3.15) to describe the coupled interaction between elastic and electric variables. Nonetheless, there are four equivalent constitutive representations commonly used in the stationary theory of linear piezoelectricity. Each type has its own different set of independent variables and corresponds to a different thermodynamic function, as listed in Table 3.1. While all equations are actually tensorial, the indices have been omitted for brevity. It should be pointed out that an alternative derivation of formulae is merely a transformation from one type of relation to another. Some relationships between various constants occurring in the four types are given as follows [19]:

$$\beta_{np}\varepsilon_{pm} = \delta_{nm}, \qquad \beta_{nm}^{\gamma} - \beta_{nm}^{\sigma} = g_{nkl}h_{nkl}, \qquad \varepsilon_{nm}^{\sigma} - \varepsilon_{nm}^{\gamma} = g_{nkl}h_{mkl},$$

$$c_{ijkl}^{D} - c_{ijkl}^{E} = e_{mij}h_{mkl}, \qquad f_{ijkl}^{E} - f_{ijkl}^{D} = d_{mij}g_{mkl}, \qquad d_{nij} = \varepsilon_{nm}^{\sigma}g_{mij} = e_{nkl}f_{klij}^{E},$$

$$e_{nij} = \varepsilon_{nm}^{\gamma}h_{mij} = d_{nkl}c_{klij}^{E}, \qquad g_{nij} = \beta_{nm}^{\sigma}d_{mij} = h_{nkl}f_{klij}^{D}, \qquad h_{nij} = \beta_{nm}^{\gamma}e_{mij} = g_{nkl}c_{klij}^{D}.$$

$$\tag{3.16}$$

The material constants can be reduced by the following consideration. According to definition (3.4) we may write $\gamma_{ij} = \gamma_{ji}$. It follows that:

$$c_{ijkm} = c_{ijmk} \tag{3.17}$$

Further, from $\sigma_{ij} = \sigma_{ji}$ we have:

$$c_{ijkm} = c_{jimk}, \quad e_{kij} = e_{kji}. \tag{3.18}$$

Table 3.1. Types of fundamental electroelastic relations.

Independent variable	Piezoelectric relation	Thermodynamic function
$\boldsymbol{\gamma}, \mathbf{E}$	$\begin{cases} \boldsymbol{\sigma} = \mathbf{c}^E \boldsymbol{\gamma} - \mathbf{e}\mathbf{E} \\ \mathbf{D} = \mathbf{e}\boldsymbol{\gamma} + \boldsymbol{\varepsilon}^\gamma \mathbf{E} \end{cases}$	Electric Gibbs energy $$g_0 = \frac{1}{2}\boldsymbol{\gamma}^T \mathbf{c}^E \boldsymbol{\gamma} - \frac{1}{2}\mathbf{E}^T \boldsymbol{\varepsilon}^\gamma \mathbf{E} - \mathbf{e}\boldsymbol{\gamma}\mathbf{E}$$
$\boldsymbol{\gamma}, \mathbf{D}$	$\begin{cases} \boldsymbol{\sigma} = \mathbf{c}^D \boldsymbol{\gamma} - \mathbf{h}\mathbf{D} \\ \mathbf{E} = -\mathbf{h}\boldsymbol{\gamma} + \boldsymbol{\beta}^\sigma \mathbf{D} \end{cases}$	Helmholtz free energy $$g_1 = g_0 + \mathbf{E}\mathbf{D}$$
$\boldsymbol{\sigma}, \mathbf{E}$	$\begin{cases} \boldsymbol{\gamma} = \mathbf{f}^E \boldsymbol{\sigma} - \mathbf{d}\mathbf{E} \\ \mathbf{D} = \mathbf{e}\boldsymbol{\sigma} + \boldsymbol{\varepsilon}^\sigma \mathbf{E} \end{cases}$	Gibbs free energy $$g_2 = g_0 - \boldsymbol{\sigma}\boldsymbol{\gamma}$$
$\boldsymbol{\sigma}, \mathbf{D}$	$\begin{cases} \boldsymbol{\gamma} = \mathbf{f}^D \boldsymbol{\sigma} - \mathbf{g}\mathbf{D} \\ \mathbf{E} = -\mathbf{g}\boldsymbol{\sigma} + \boldsymbol{\beta}^\sigma \mathbf{D} \end{cases}$	Elastic Gibbs energy $$g_3 = g_0 + \mathbf{E}\mathbf{D} - \boldsymbol{\sigma}\boldsymbol{\gamma}$$

3.4   Stroh's Formalism in the piezoelectric case

For two-dimensional deformations in a general anisotropic piezoelectric material, one of the most used solution procedure in the literature is the Stroh's formalism [20]. We will start the outline of the method by noting that posing $\varphi = U_4$, equations (3.14) and (3.15) can be re-written as follows:

$$\sigma_{ij} = c_{ijks}U_{k,s} + e_{sij}U_{4,s} \tag{3.19}$$

$$D_i = e_{iks}U_{k,s} - \varepsilon_{is}U_{4,s} \tag{3.20}$$

The analysis will be limited to the bi-dimensional (plane) problem, for which:

$$U_j = U_j\left(x_1, x_2\right) \qquad j = 1, 2, 3, 4 \tag{3.21}$$

and we will consider volume forces and free charges to be absent.

Let us assume:

$$U_j = a_j f\left(z\right) \tag{3.22}$$

or, in matrix notation:

$$\mathbf{U} = \mathbf{a}f\left(z\right) \qquad z = x_1 + px_2 \tag{3.23}$$

where f is an arbitrary function of z and p and a_j are constants to be determined. The following relations can be obtained differentiating once and twice the displacement components:

$$U_{k,s} = (\delta_{s1} + p\delta_{s2})a_k f'(z) \tag{3.24}$$

$$U_{k,js} = (\delta_{j1} + p\delta_{j2})(\delta_{s1} + p\delta_{s2})a_k f''(z) = U_{k,sj} \tag{3.25}$$

where δ_{sj} is the Kronecker delta.

Through (3.24) and (3.25), and given the arbitrariness of f, the constitutive relations (3.19) and (3.20) become:

$$\sigma_{ij} = (c_{ijks}a_k + e_{sij}a_4)(\delta_{s1} + p\delta_{s2})f'(z) \tag{3.26}$$

$$D_i = (e_{iks}a_k - \varepsilon_{is}a_4)(\delta_{s1} + p\delta_{s2})f'(z) \tag{3.27}$$

and the equilibrium and Maxwell equations:

$$\sigma_{ij,j} = c_{ijks}U_{k,sj} + e_{sij}U_{4,sj} = 0 \tag{3.28}$$

$$D_{i,i} = e_{iks}U_{k,si} - \varepsilon_{is}U_{4,si} = 0 \tag{3.29}$$

can be written:

$$(c_{ijks}a_k + e_{sij}a_4)(\delta_{j1} + p\delta_{j2})(\delta_{s1} + p\delta_{s2}) = 0 \tag{3.30}$$

$$(e_{iks}a_k - \varepsilon_{is}a_4)(\delta_{i1} + p\delta_{i2})(\delta_{s1} + p\delta_{s2}) = 0 \tag{3.31}$$

Expliciting in (3.30) the sums on indexes s and j respectively, we get:

$$(c_{ijk1}a_k + e_{1ij}a_4)(\delta_{j1} + p\delta_{j2}) + (c_{ijk2}a_k + e_{2ij}a_4)(p\delta_{j1} + p^2\delta_{j2}) = 0 \tag{3.32}$$

and:

$$(c_{i1k1}a_k + e_{1i1}a_4) + p(c_{i2k1}a_k + e_{1i2}a_4) + (c_{i1k2}a_k + e_{2i1}a_4)p + p^2(c_{i2k2}a_k + e_{2i2}a_4) = 0 \tag{3.33}$$

and gathering a_k and a_4:

$$\left[c_{i1k1} + p(c_{i2k1} + c_{i1k2}) + p^2 c_{i2k2}\right]a_k + \left[e_{1i1} + p(e_{1i2} + e_{2i1}) + p^2 e_{2i2}\right]a_4 = 0 \tag{3.34}$$

Indexes i and k assume the values 1, 2, 3.

If now we introduce the three-dimensional vectors:

$$\mathbf{e}_{ij} = \begin{pmatrix} e_{ij1} \\ e_{ij2} \\ e_{ij3} \end{pmatrix} = \begin{pmatrix} e_{i1j} \\ e_{i2j} \\ e_{i3j} \end{pmatrix} \tag{3.35}$$

52

equation (3.34) can be expressed in compact form as:

$$\left[\mathbf{Q}^e + p\left(\mathbf{R}^e + \mathbf{R}^{eT}\right) + p^2\mathbf{T}^e\right]\mathbf{a}^e + \left[\mathbf{e}_{11} + p\left(\mathbf{e}_{12} + \mathbf{e}_{21}\right) + p^2\mathbf{e}_{22}\right]a_4 = 0 \qquad (3.36)$$

where $\mathbf{a}^e = \left(a_1, \quad a_2, \quad a_3\right)^T$ and:

$$Q_{ik}^e = c_{i1k1}, \qquad\qquad R_{ik}^e = c_{i1k2}, \qquad\qquad T_{ik}^e = c_{i2k2} \qquad (3.37)$$

Matrices $\mathbf{Q}^e$ and $\mathbf{T}^e$ are symmetric and positive definite.

Now, expliciting in (3.31) the sums on indexes i and s respectively, we get:

$$e_{1ks}a_k\left(\delta_{s1} + p\delta_{s2}\right) + e_{2ks}a_k\left(p\delta_{s1} + p^2\delta_{s2}\right) - \varepsilon_{1s}a_4\left(\delta_{s1} + p\delta_{s2}\right) - \varepsilon_{2s}a_4\left(p\delta_{s1} + p^2\delta_{s2}\right) = 0$$

$$(3.38)$$

$$e_{1k1}a_k + e_{1k2}a_k p + e_{2k1}a_k p + e_{2k2}a_k p^2 - \varepsilon_{11}a_4 - \varepsilon_{12}a_4 p - \varepsilon_{21}a_4 p - \varepsilon_{22}a_4 p^2 = 0 \qquad (3.39)$$

and summing in k as well:

$$e_{111}a_1 + e_{112}a_2 + e_{113}a_3 + p\left(e_{121}a_1 + e_{122}a_2 + e_{123}a_3 + e_{211}a_1 + e_{212}a_2 + e_{213}a_3\right) + $$
$$+ p^2\left(e_{221}a_1 + e_{222}a_2 + e_{223}a_3\right) - \left[\varepsilon_{11} + p\left(\varepsilon_{12} + \varepsilon_{21}\right) + p^2\varepsilon_{22}\right]a_4 = 0 \qquad (3.40)$$

or:

$$\left[\mathbf{e}_{11}^T + p\left(\mathbf{e}_{12}^T + \mathbf{e}_{21}^T\right) + p^2\mathbf{e}_{22}^T\right]\mathbf{a}^e - \left[\varepsilon_{11} + p\left(\varepsilon_{12} + \varepsilon_{21}\right) + p^2\varepsilon_{22}\right]a_4 = 0 \qquad (3.41)$$

On the basis that $\mathbf{Q}^e$, $\mathbf{R}^e$ and $\mathbf{T}^e$ are all 3x3 matrices, relations (3.39) and (3.41) can be compacted into:

$$\left[\mathbf{Q} + p\left(\mathbf{R} + \mathbf{R}^T\right) + p^2\mathbf{T}\right]\mathbf{a} = 0 \qquad (3.42)$$

where $\mathbf{a} = \left(\mathbf{a}^e \quad a_4\right)^T = \left(a_1 \quad a_2 \quad a_3 \quad a_4\right)^T$ and:

$$\mathbf{Q} = \begin{pmatrix} \mathbf{Q}^e & \mathbf{e}_{11} \\ \mathbf{e}_{11}^T & -\varepsilon_{11} \end{pmatrix}, \qquad \mathbf{R} = \begin{pmatrix} \mathbf{R}^e & \mathbf{e}_{12} \\ \mathbf{e}_{12}^T & -\varepsilon_{12} \end{pmatrix}, \qquad \mathbf{T} = \begin{pmatrix} \mathbf{T}^e & \mathbf{e}_{22} \\ \mathbf{e}_{22}^T & -\varepsilon_{22} \end{pmatrix} \qquad (3.43)$$

4x4 matrices.

Now we can define vector $\mathbf{b}$ as:

$$\mathbf{b} = \left(\mathbf{R}^T + p\mathbf{T}\right)\mathbf{a} = -\frac{1}{p}\left(\mathbf{Q} + p\mathbf{R}\right)\mathbf{a} \qquad (3.44)$$

and the generalized potential:

$$\mathbf{\Phi} = \left(\phi_1, \phi_2, \phi_3, \phi_4\right)^T = \mathbf{b}f\left(z\right) \qquad (3.45)$$

Equations (3.26) and (3.27) assume the shape:

$$\sigma_{i1} = -\phi_{i,2} \qquad \sigma_{i2} = \phi_{i,1} \qquad D_1 = -\phi_{4,2} \qquad D_2 = \phi_{4,1} \qquad i = 1,2,3 \qquad (3.46)$$

It suffices therefore to consider the functions ϕ because the stresses σ_{ij} and the electric displacements D_i can be obtained by differentiation.

From equations (3.46) the following relations can be introduced:

$$\mathbf{t}_1 = \left(\sigma_{i1}, D_1\right)^T = \left(\sigma_{11}, \sigma_{21}, \sigma_{31}, D_1\right)^T = -\mathbf{\Phi}_{,2}$$
$$\mathbf{t}_2 = \left(\sigma_{i2}, D_2\right)^T = \left(\sigma_{12}, \sigma_{22}, \sigma_{32}, D_2\right)^T = \mathbf{\Phi}_{,1} \tag{3.47}$$

and since $\sigma_{21} = \sigma_{12}$ we get:

$$\phi_{1,1} + \phi_{2,2} = 0 \tag{3.48}$$

As in the case of anisotropic materials, eigenvalues p_α cannot be real. The four pairs of complex conjugates, and the associated eigenvectors, can be ordered as follows:

$$\operatorname{Im} p_\alpha > 0, \qquad p_{\alpha+4} = \overline{p}_\alpha \qquad \alpha = 1,..,4$$
$$\mathbf{a}_\alpha = (\, a_{\alpha 1} \,, a_{\alpha 2} \,, a_{\alpha 3} \,, a_{\alpha 4} \,)^T, \qquad \mathbf{a}_{\alpha+4} = \overline{\mathbf{a}}_\alpha \qquad \alpha = 1,..,4 \tag{3.49}$$

Assuming for vectors $\mathbf{b}_\alpha$ as well the position:

$$\mathbf{b}_{\alpha+4} = \overline{\mathbf{b}}_\alpha \qquad \alpha = 1,..,4 \tag{3.50}$$

the general solutions for $\mathbf{U}$ and $\mathbf{\Phi}$ are obtained by superposing the eight solutions in the form of equations (3.23) and (3.45):

$$\mathbf{U} = \sum_{\alpha=1}^{8} \mathbf{a}_\alpha f_\alpha\left(z_\alpha\right) = \sum_{\alpha=1}^{4}\left[\mathbf{a}_\alpha f_\alpha\left(z_\alpha\right) + \overline{\mathbf{a}}_\alpha f_{\alpha+4}\left(\overline{z}_\alpha\right)\right] \tag{3.51}$$

$$\mathbf{\Phi} = \sum_{\alpha=1}^{4}\left[\mathbf{b}_\alpha f_\alpha\left(z_\alpha\right) + \overline{\mathbf{b}}_\alpha f_{\alpha+4}\left(\overline{z}_\alpha\right)\right] \tag{3.52}$$

In most applications f_α assume the same functional form, so that we may write:

$$f_\alpha\left(z_\alpha\right) = f\left(z_\alpha\right) q_\alpha, \qquad f_{\alpha+4}\left(\overline{z}_\alpha\right) = \overline{f}\left(\overline{z}_\alpha\right)\overline{q}_\alpha \tag{3.53}$$

where q_α are complex constants to be determined. The second equation is for obtaining real solutions for $\mathbf{U}$ and $\mathbf{\Phi}$. Expressions (3.51) and (3.52) can then be compacted as:

$$\mathbf{U} = 2\operatorname{Re}\left[\mathbf{A}\operatorname{diag}\left[f\left(z_\alpha\right)\right]\mathbf{q}\right]$$
$$\mathbf{\Phi} = 2\operatorname{Re}\left[\mathbf{B}\operatorname{diag}\left[f\left(z_\alpha\right)\right]\mathbf{q}\right] \tag{3.54}$$

where:

$$\mathbf{A} = \left(\mathbf{a}_1 \quad \mathbf{a}_2 \quad \mathbf{a}_3 \quad \mathbf{a}_4\right), \qquad\qquad \mathbf{B} = \left(\mathbf{b}_1 \quad \mathbf{b}_2 \quad \mathbf{b}_3 \quad \mathbf{b}_4\right) \tag{3.55}$$

Eigenvalues p_α and eigenvectors $\mathbf{a}_\alpha$ and $\mathbf{b}_\alpha$ are called Stroh's eigenvalues and eigenvectors. Through (3.47) we also get:

$$\begin{aligned} \mathbf{t}_1 &= -2\mathrm{Re}\left[\mathbf{B}\,\mathbf{diag}\left[p_\alpha f'(z_\alpha)\right]\mathbf{q}\right] \\ \mathbf{t}_2 &= 2\mathrm{Re}\left[\mathbf{B}\,\mathbf{diag}\left[p_\alpha f'(z_\alpha)\right]\mathbf{q}\right] \end{aligned} \tag{3.56}$$

In order to conclude the extension of Stroh's formalism to the piezoelectric case, it can be said that, although from (3.43)-3 it is clear that matrix $\mathbf{T}$ is symmetric but not positive definite (for the presence of the element $-\varepsilon_{22}$), it is easy to demonstrate that it is still non-singular, so that $\mathbf{T}^{-1}$ exists. Following the same algebraic procedure outlined for anisotropic materials, relation (3.44) can then be reduced to:

$$\mathbf{N}\boldsymbol{\xi} = p\boldsymbol{\xi}, \qquad \boldsymbol{\xi} = \begin{pmatrix} \mathbf{a} & \mathbf{b} \end{pmatrix}^T \tag{3.57}$$

where $\mathbf{N}$ is a matrix whose elements are still matrices defined as:

$$\mathbf{N}_{11} \equiv \mathbf{N}_1 = -\mathbf{T}^{-1}\mathbf{R}^{\mathrm{T}}, \quad \mathbf{N}_{12} \equiv \mathbf{N}_2 = \mathbf{T}^{-1}, \quad \mathbf{N}_{21} \equiv \mathbf{N}_3 = \mathbf{R}\mathbf{T}^{-1}-\mathbf{R}^{\mathrm{T}}-\mathbf{Q}, \quad \mathbf{N}_{22} \equiv \mathbf{N}_4 = \mathbf{N}_1^{\mathrm{T}}$$

$$\tag{3.58}$$

Relation (3.57) outlines the 8-dimensional Stroh's formalism for piezoelectric materials. Orthogonality and closure relations formally equal to those for anisotropic materials can be obtained.

3.5   Transversely isotropic piezoelectric materials

Polarized piezoelectric materials (like PZT ceramics) are generally transversely isotropic.

For their representation, it is useful to introduce the so-called two-index notation or compressed matrix notation [21]. Two-index notation consists of replacing ij or km by p or q, where i,j,k,m take the values 1-3, and p,q assume the values 1-6 according to the following replacements: $11\to1$, $22\to2$, $33\to3$, 23 or $32\to4$, 13 or $31\to5$, 12 or $21\to6$. Relations (3.14) and (3.15) then become:

$$\sigma_p = c_{pq}\gamma_q - e_{kp}E_k \tag{3.59}$$

$$D_i = e_{iq}\gamma_q + \varepsilon_{ik}E_k \tag{3.60}$$

in which:

$$\gamma_p = \begin{cases} \gamma_{ij}, & \text{when } i = j, \\ 2\gamma_{ij}, & \text{when } i \neq j. \end{cases} \tag{3.61}$$

For a transversely isotropic material with x_3 in the poling direction, the related material matrices are:

$$\mathbf{c} = \begin{bmatrix} c_{11} & c_{12} & c_{13} & 0 & 0 & 0 \\ c_{12} & c_{11} & c_{13} & 0 & 0 & 0 \\ c_{13} & c_{13} & c_{33} & 0 & 0 & 0 \\ 0 & 0 & 0 & c_{44} & 0 & 0 \\ 0 & 0 & 0 & 0 & c_{44} & 0 \\ 0 & 0 & 0 & 0 & 0 & c_{66} \end{bmatrix} \tag{3.62}$$

$$\mathbf{e} = \begin{bmatrix} 0 & 0 & 0 & 0 & e_{15} & 0 \\ 0 & 0 & 0 & e_{15} & 0 & 0 \\ e_{31} & e_{31} & e_{33} & 0 & 0 & 0 \end{bmatrix} \tag{3.63}$$

$$\boldsymbol{\varepsilon} = \begin{bmatrix} \varepsilon_{11} & 0 & 0 \\ 0 & \varepsilon_{11} & 0 \\ 0 & 0 & \varepsilon_{33} \end{bmatrix} \tag{3.64}$$

with $c_{66} = (c_{11} - c_{12})/2$.

It is clear that a material with this type of symmetry is described by 10 independent material constants.

In the MKS system the constants and variables mentioned above are measured in the following units: $[c_{ij}] = \mathrm{Nm}^{-2}$, $[e_{ij}] = \mathrm{N(Vm)}^{-1} = \mathrm{Cm}^{-2}$, $[\varepsilon_{ij}] = \mathrm{C^2N^{-1}m^{-2}} = \mathrm{NV}^{-2}$. For poled barium-titanate $(\mathrm{BaTiO_3})$ and lead-zirconate-titanate (PZT), these physical constants are of the orders: $c_{ij} \sim 10^{11}\mathrm{Nm}^{-2}$, $e_{ij} \sim 10\mathrm{Cm}^{-2}$, $\varepsilon_{ij} \sim 10^{-8}\mathrm{NV}^{-2}$.

Substitution of equations (3.2) and (3.4) into (3.59) and (3.60), and later into (3.12), results in:

$$c_{11}\frac{\partial^2 u_1}{\partial x_1^2} + c_{66}\frac{\partial^2 u_1}{\partial x_2^2} + c_{44}\frac{\partial^2 u_1}{\partial x_3^2} + (c_{12} + c_{66})\frac{\partial^2 u_2}{\partial x_1 \partial x_2} + (c_{13} + c_{44})\frac{\partial^2 u_3}{\partial x_1 \partial x_3} + (e_{31} + e_{15})\frac{\partial^2 \varphi}{\partial x_1 \partial x_3} + f_{b1} = 0$$

$$c_{66}\frac{\partial^2 u_2}{\partial x_1^2} + c_{11}\frac{\partial^2 u_2}{\partial x_2^2} + c_{44}\frac{\partial^2 u_2}{\partial x_3^2} + (c_{12} + c_{66})\frac{\partial^2 u_1}{\partial x_1 \partial x_2} + (c_{13} + c_{44})\frac{\partial^2 u_3}{\partial x_2 \partial x_3} + (e_{31} + e_{15})\frac{\partial^2 \varphi}{\partial x_2 \partial x_3} + f_{b2} = 0$$

$$c_{44}\frac{\partial^2 u_3}{\partial x_1^2}+c_{44}\frac{\partial^2 u_3}{\partial x_2^2}+c_{33}\frac{\partial^2 u_3}{\partial x_3^2}+\left(c_{13}+c_{44}\right)\frac{\partial^2 u_1}{\partial x_1\partial x_3}+\left(c_{13}+c_{44}\right)\frac{\partial^2 u_2}{\partial x_2\partial x_3}+e_{15}\frac{\partial^2\varphi}{\partial x_1^2}+e_{15}\frac{\partial^2\varphi}{\partial x_2^2}+e_{33}\frac{\partial^2\varphi}{\partial x_3^2}+f_{b3}=0$$

$$e_{15}\frac{\partial^2 u_3}{\partial x_1^2}+e_{15}\frac{\partial^2 u_3}{\partial x_2^2}+e_{33}\frac{\partial^2 u_3}{\partial x_3^2}+\left(e_{15}+e_{31}\right)\frac{\partial^2 u_1}{\partial x_1\partial x_3}+\left(e_{15}+e_{31}\right)\frac{\partial^2 u_2}{\partial x_2\partial x_3}-\varepsilon_{11}\frac{\partial^2\varphi}{\partial x_1^2}-\varepsilon_{11}\frac{\partial^2\varphi}{\partial x_2^2}-\varepsilon_{33}\frac{\partial^2\varphi}{\partial x_3^2}=q_b$$

$$(3.65)$$

for transversely isotropic materials. This type of material will be adopted in the remaining chapters.

Besides these equations, Maxwell's equations of electrostatics also hold. These, in absence of free charges, are:

$$E_i=-\varphi_{,i}\qquad D_{i,i}=0 \qquad\qquad (3.66)$$

where φ is the electric potential.

3.6   Two-dimensional problems

3.6.1. Plane problem

According to matrices (3.62), (3.63) and (3.64), the x_1-x_2 plane is the isotropic plane, and one can employ either the x_1-x_3 or x_2-x_3 plane for the study of the plane electromechanical problem. Choosing the former, we have:

$$\begin{Bmatrix}\sigma_1\\\sigma_3\\\sigma_5\\D_1\\D_3\end{Bmatrix}=\begin{bmatrix}c_{11}&c_{13}&0&0&e_{31}\\c_{13}&c_{33}&0&0&e_{33}\\0&0&c_{44}&e_{15}&0\\0&0&e_{15}&-\varepsilon_{11}&0\\e_{31}&e_{33}&0&0&-\varepsilon_{33}\end{bmatrix}\begin{Bmatrix}\gamma_1\\\gamma_3\\\gamma_5\\-E_1\\-E_3\end{Bmatrix} \qquad (3.67)$$

or inversely:

$$\begin{Bmatrix}\gamma_1\\\gamma_3\\\gamma_5\\-E_1\\-E_3\end{Bmatrix}=\begin{bmatrix}f_{11}&f_{13}&0&0&g_{31}\\f_{13}&f_{33}&0&0&g_{33}\\0&0&f_{44}&g_{15}&0\\0&0&g_{15}&-\beta_{11}&0\\g_{31}&g_{33}&0&0&-\beta_{33}\end{bmatrix}\begin{Bmatrix}\sigma_1\\\sigma_3\\\sigma_5\\D_1\\D_3\end{Bmatrix} \qquad (3.68)$$

in which f_{ij} is the elastic compliance tensor of the material, g_{ij} is the piezoelectric tensor and β_{ij} is the dielectric impermeability tensor. When the constitutive equations (3.67) are substituted into equations (3.12) one obtains:

$$c_{11}\frac{\partial^2 u_1}{\partial x_1^2}+c_{44}\frac{\partial^2 u_1}{\partial x_3^2}+\left(c_{13}+c_{44}\right)\frac{\partial^2 u_3}{\partial x_1 \partial x_3}+\left(e_{31}+e_{15}\right)\frac{\partial^2 \varphi}{\partial x_1 \partial x_3}+f_{b1}=0$$

$$c_{44}\frac{\partial^2 u_3}{\partial x_1^2}+c_{33}\frac{\partial^2 u_3}{\partial x_3^2}+\left(c_{13}+c_{44}\right)\frac{\partial^2 u_1}{\partial x_1 \partial x_3}+e_{15}\frac{\partial^2 \varphi}{\partial x_1^2}+e_{33}\frac{\partial^2 \varphi}{\partial x_3^2}+f_{b3}=0 \qquad (3.69)$$

$$e_{15}\frac{\partial^2 u_3}{\partial x_1^2}+e_{33}\frac{\partial^2 u_3}{\partial x_3^2}+\left(e_{15}+e_{31}\right)\frac{\partial^2 u_1}{\partial x_1 \partial x_3}-\varepsilon_{11}\frac{\partial^2 \varphi}{\partial x_1^2}-\varepsilon_{33}\frac{\partial^2 \varphi}{\partial x_3^2}=q_b$$

3.6.2. Antiplane problem

In this case only the out-of-plane elastic displacement u_3 and the in-plane electric fields are non-zero:

$$u_1 = u_2 = 0, \qquad u_3 = u_3\left(x_1, x_2\right) \qquad (3.70)$$

$$E_1 = E_1\left(x_1, x_2\right), \qquad E_2 = E_2\left(x_1, x_2\right), \qquad E_3 = 0 \qquad (3.71)$$

Thus, the constitutive equations (3.59) and (3.60) simplify to:

$$\begin{Bmatrix} \sigma_4 \\ \sigma_5 \\ D_1 \\ D_2 \end{Bmatrix} = \begin{bmatrix} c_{44} & 0 & 0 & e_{15} \\ 0 & c_{44} & e_{15} & 0 \\ 0 & e_{15} & -\varepsilon_{11} & 0 \\ e_{15} & 0 & 0 & -\varepsilon_{11} \end{bmatrix} \begin{Bmatrix} \gamma_4 \\ \gamma_5 \\ -E_1 \\ -E_2 \end{Bmatrix} \qquad (3.72)$$

The governing equations (3.65) become:

$$c_{44}\frac{\partial^2 u_3}{\partial x_1^2}+c_{44}\frac{\partial^2 u_3}{\partial x_2^2}+e_{15}\frac{\partial^2 \varphi}{\partial x_1^2}+e_{15}\frac{\partial^2 \varphi}{\partial x_2^2}+f_{b3}=0$$

$$e_{15}\frac{\partial^2 u_3}{\partial x_1^2}+e_{15}\frac{\partial^2 u_3}{\partial x_2^2}-\varepsilon_{11}\frac{\partial^2 \varphi}{\partial x_1^2}-\varepsilon_{11}\frac{\partial^2 \varphi}{\partial x_2^2}=q_b \qquad (3.73)$$

or:

$$c_{44}\nabla^2 u_3 + e_{15}\nabla^2 \varphi + f_{b3} = 0$$

$$e_{15}\nabla^2 u_3 - \varepsilon_{11}\nabla^2 \varphi = q_b \qquad (3.74)$$

where $\nabla^2 = (\ )_{,11}+(\ )_{,22}$ is the two-dimensional Laplacian operator.

3.7   Electric boundary conditions

In the theoretical study of cracked piezoelectric bodies, the issue of assigning consistent electric boundary conditions on the crack faces is of central importance and has been addressed by many researchers. Three different boundary conditions

are commonly accepted in literature: the permeable crack model proposed by Parton [22], the impermeable crack model assumed by Deeg [23], Suo et al. [10] and Pak [24], and the semipermeable ("exact") model, presented by Hao and Shen [25]. Under Parton's condition, the electric potential and the normal component of the electric displacement are continuous across the traction-free crack:

$$\varphi^+ = \varphi^-, \qquad D_n^+ = D_n^-, \tag{3.75}$$

where the superscripts "+" and "-" denote the upper and the lower side of the crack surface, respectively, and the subscript "n" indicates the component normal to the crack surface. This model was used for example in [26-27].

The impermeable condition was introduced on the basis that relations (3.75) can be acceptable for very slender slits for which the width of the flaw is negligible, whereas when a cracked body is subjected to traction the crack opens and generally some type of fluid (air) or vacuum fill the void, and therefore there will clearly be a potential drop across the lower capacitance crack. Since the dielectric constant of air or vacuum is some orders of magnitude lower than that of the ceramic, it can be approximated to zero, and the normal component of the electric displacement vanishes across the cavity:

$$D_n^+ = D_n^- = 0 \tag{3.76}$$

This model was adopted by Sosa [10], Zuo and Sih [28], among others.

The third condition takes a finite value of the permittivity of the medium inside the crack into account (ε_c) and considers the crack opening displacement:

$$D_n^+ = D_n^-, \qquad D_n^+ \left(u_n^+ - u_n^- \right) = -\varepsilon_c \left(\varphi^+ - \varphi^- \right) \tag{3.77}$$

This situation extrapolates between the impermeable and the permeable cases, reducing to the one or the other if the permittivity of the medium or the gap between the slit faces are assumed to be zero, respectively.

Several researchers adopted the exact boundary conditions in their analysis (McMeeking [29], Landis [30], Ou and Chen [31], Wippler et al. [32] and others). Furthermore, many interesting works compared the effect of the various

boundary conditions on the crack behaviour: Dunn [33] and Zhang et al. [34] considered elliptical flaws under different conditions, Xu and Rajapakse [35] regarded arbitrarily oriented elliptical voids and linear cracks, Wang and Mai [36] and Wu and Wu [37] carried out FEM analysis in order to verify the assumptions under consideration.

References

[1] Curie J., Curie P., *Dévéloppement par compression de l'électricité polaire dans les cristaux hémiédres à faces inclinées*, Bulletin n.4 de la Société Mineralogique de France (1880); 3: 90, and Comptes Rendus Acad. Sci. Paris (1880); 91: 294.

[2] Lippmann H.G., *Sur le principe de la conversion de l'électricité ou second principe de la theorie des phénomènes électriques*, Comptes Rendus Acad. Sci. Paris (1881); 92: 1049.

[3] Curie J., Curie P., *Contractions et dilatations productes par des tensions électriques dans les cristaux hémiédres à faces inclinées*, Comptes Rendus Acad. Sci. Paris (1884); 93: 1137.

[4] Curie J., Curie P., *Sur l'électricité polaire dans les cristaux hémiédres à faces inclinées*, Comptes Rendus Acad. Sci. Paris (1880); 91: 383.

[5] Curie J., Curie P., *Lois de dégagement d'électricité dans la tourmaline*, Comptes Rendus Acad. Sci. Paris (1881); 92: 186.

[6] Curie J., Curie P., *Les cristaux hémiédres à faces inclines comme sources constantes d'électricité*, Comptes Rendus Acad. Sci. Paris (1881); 93: 24.

[7] Voigt W., *General theory of the piezo and the pyroelectric properties of crystals*, Abh. Gott. (1890); 36: 1.

[8] Cady W.G., *Piezoelectricity Vols. 1 & 2*, Dover Publishers, New York, 1964.

[9] Parton V.Z., Kudryavtsev B.A., *Electromagnetoelasticity, Piezoelectrics and Electrically Conductive Solids*, Gordon and Breach Science Publishers, New York, 1988.

[10] Sosa H., *Plane problems in piezoelectric media with defects*, Int. J. Solids Struct. (1991); 28: 491-505.

[11] Pak Y.E., *Linear electro-elastic fracture mechanics of piezoelectric materials*, Int. J. Fract. (1992); 54: 79-100.

[12] Suo Z., Kuo C.M., Barnett D.M., Willis J.R. *Fracture mechanics for piezoelectric ceramics,* J. Mech. Phys. Solids (1992); 40: 739-765.

[13] Yang F., *Fracture mechanics for a Mode I crack in piezoelectric materials,* Int. J. Solids Struct. (2001); 38: 3813-3830.

[14] McMeeking R.M., *Towards a fracture mechanics for brittle piezoelectric and dielectric materials,* Int. J. Fract. (2001); 108: 25-41.

[15] Zhang T.Y., Liu G., Wang T., Tong P., *Application of the concepts of fracture mechanics to the failure of conductive cracks in piezoelectric ceramics,* Engng. Fract. Mech. (2007); 74: 1160-1173.

[16] Zhang T.Y., Gao C.F., *Fracture behaviors of piezoelectric materials,* J. Theor. Appl. Fract. Mech. (2004); 41: 339-379.

[17] Zhang T.Y., Zhao M., Tong P., *Fracture of piezoelectric ceramics,* Adv. Appl. Mech. (2001); 38: 147-288.

[18] Biot M.A., *Thermoelasticity and irreversible thermodynamics,* J. Appl. Phys. (1956); 27: 240-253.

[19] Qin Q.H., *Fracture Mechanics of Piezoelectric Materials,* Wit Press, Southampton, 2001.

[20] Stroh A.N., *Dislocations and cracks in anisotropic elasticity,* Philos. Mag. (1958); 3: 625-646.

[21] Nye J.F., *Physical properties of crystals,* Oxford University Press, 1957.

[22] Parton V.Z., *Fracture mechanics of piezoelectric materials,* Acta Astronautica (1976); 3: 671-683.

[23] Deeg W.F.J., *The analysis of dislocation, crack and inclusion problems in piezoelectric solids,* Ph.D. Thesis, Stanford University, 1980.

[24] Pak Y.E., *Crack extension force in a piezoelectric material.* J. Appl. Mech. (1990); 57: 647-653.

[25] Hao T.H., Shen Z.Y., *A new electric boundary condition of electric fracture mechanics and its applications,* Engng. Fract. Mech. (1994); 47: 793-802.

[26] Gao C.F., Wang M.Z., *Collinear permeable cracks between dissimilar piezoelectric materials,* Int. J. Solids Struct. (2000); 37:4969-4986.

[27] Zhou Z.G., Wang B., Cao M.S., *The behaviour of permeable multi-cracks in a piezoelectric material*, Mech. Res. Comm. (2003); 30:395-402.

[28] Zuo J.Z., Sih G.C., *Energy density theory formulation and interpretation of cracking behaviour for piezoelectric ceramics*, Theor. Appl. Fract. Mech. (2000); 34:17-33.

[29] McMeeking R.M., *Crack tip energy release rate for a piezoelectric compact tension specimen*, Engng. Fract. Mech. (1999); 64: 217-244.

[30] Landis C.M., *Energetically consistent boundary conditions for electro-mechanical fracture*, Int. J. Solids Struct. (2004); 41: 6291-6315.

[31] Ou Z.C., Chen Y.H., *On approach of crack tip energy release rate for a semi-permeable crack when electromechanical loads become very large*, Int. J. Fract. (2005); 133: 89-105.

[32] Wippler K., Ricoeur A., Kuna M., *Towards the computation of electrically permeable cracks in piezoelectrics*, Engng. Fract. Mech. (2004); 71: 2567-2587.

[33] Dunn M.L., *The effects of crack face boundary conditions on the fracture mechanics of piezoelectric solids*, Engng. Fract. Mech. (1994); 48: 25-39.

[34] Zhang T.Y., Qian C.F., Tong P., *Linear electro-elastic analysis of a cavity or a crack in a piezoelectric material*, Int. J. Solids Struct. (1998); 35:2121-2149.

[35] Xu X.L., Rajapakse R.K.N.D., *On a plane crack in piezoelectric solids*, Int. J. Solids Struct. (2001); 38: 7643-7658.

[36] Wang B.L., Mai Y.W., *On the electrical boundary conditions on the crack surfaces in piezoelectric ceramics*, Int. J. Engng. Science (2003); 41: 633-652.

[37] Wu D., Wu C.C., *Numerical analysis for piezoelectric crack under varied boundary conditions by optimized hybrid element method*, Engng. Fract. Mech. (2006); 73:649-670.

CHAPTER 4

ANALYTICAL SOLUTION FOR A CRACKED PIEZOELECTRIC BODY

4.1   Introduction

The most original contribution of this thesis to the fracture mechanics of piezoelectric materials is outlined in this chapter, which describes an analytical method for seeking the electro-elastic closed-form solution of the static problem of a crack in a piezoelectric plate subjected to biaxial loading at infinity, and in the next chapter, which reports several numerical applications and illustrates the results.

The novel procedure involves a transformation of similarity, induced by the fundamental matrix through the application of the spectral theorem of linear algebra, that enables to express the equations governing the problem in terms of Cauchy's complex potentials. The application of the mechanical boundary condition of stress-free crack and of one of the three considered electric boundary conditions (impermeable, permeable or semipermeable) leads then to the formulation of Hilbert problems whose solutions allow to obtain the generalized stress and displacement components.

The proposed analytical formulation is the application to the piezoelectric static case [1-3] of an approach introduced by Piva [4], Piva and Viola [5], Viola et al.

[6] in solving elastodynamic crack problems in orthotropic media. This method can be considered an alternative to other formalisms currently used, like the Stroh's formalism introduced in anisotropic elasticity [7-8], outlined in Chapter 2, and extended to piezoelectric media as illustrated in Chapter 3 [9]. Both theoretical approaches find their main origins in the fundamental works [10-11] where plane elasticity in terms of functions of complex variables was formulated. However, the present derivation of the basic equations does not require any "a priori" assumptions about the displacement vector as in Stroh's approach.

4.2   Alternative formalism applied to the piezoelectric case

In contract form, equations (3.59) and (3.60) become:

$$\boldsymbol{\sigma} = \mathbf{C}\boldsymbol{\gamma} - \mathbf{e}^T\mathbf{E} \qquad (4.1)$$

$$\mathbf{D} = \mathbf{e}\boldsymbol{\gamma} + \boldsymbol{\varepsilon}\mathbf{E} \qquad (4.2)$$

Considering generalized plane strain conditions $(\gamma_{22} = \gamma_{23} = \gamma_{12} = 0)$, the systems (4.1) and (4.2) can be reduced to:

$$\sigma_{11} = c_{11}\frac{\partial u_1}{\partial x_1} + c_{13}\frac{\partial u_3}{\partial x_3} + e_{31}\frac{\partial \varphi}{\partial x_3}$$

$$\sigma_{33} = c_{13}\frac{\partial u_1}{\partial x_1} + c_{33}\frac{\partial u_3}{\partial x_3} + e_{33}\frac{\partial \varphi}{\partial x_3} \qquad (4.3)$$

$$\sigma_{13} = c_{44}\left(\frac{\partial u_3}{\partial x_1} + \frac{\partial u_1}{\partial x_3}\right) + e_{15}\frac{\partial \varphi}{\partial x_1}$$

and:

$$D_1 = e_{15}\left(\frac{\partial u_3}{\partial x_1} + \frac{\partial u_1}{\partial x_3}\right) - \varepsilon_{11}\frac{\partial \varphi}{\partial x_1}$$

$$D_3 = e_{31}\frac{\partial u_1}{\partial x_1} + e_{33}\frac{\partial u_3}{\partial x_3} - \varepsilon_{33}\frac{\partial \varphi}{\partial x_3} \qquad (4.4)$$

With the substitutions $x_1 = x$, $x_3 = y$, $u_1 = u$, $u_3 = v$, and introducing the generalized strain vectors $\boldsymbol{\Gamma}^{(1)}$ and $\boldsymbol{\Gamma}^{(2)}$ defined as:

$$\mathbf{\Gamma}^{(1)} = \begin{bmatrix} \dfrac{\partial u}{\partial x} \\[2mm] \dfrac{\partial v}{\partial x} \\[2mm] \dfrac{\partial \varphi}{\partial x} \end{bmatrix} = \begin{bmatrix} \Gamma_1 \\ \Gamma_2 \\ \Gamma_3 \end{bmatrix}, \qquad \mathbf{\Gamma}^{(2)} = \begin{bmatrix} \dfrac{\partial u}{\partial y} \\[2mm] \dfrac{\partial v}{\partial y} \\[2mm] \dfrac{\partial \varphi}{\partial y} \end{bmatrix} = \begin{bmatrix} \Gamma_4 \\ \Gamma_5 \\ \Gamma_6 \end{bmatrix}, \tag{4.5}$$

and the generalized stress vectors $\mathbf{t}_1$ and $\mathbf{t}_2$ defined as:

$$\mathbf{t}_1 = \begin{bmatrix} \sigma_{xx} \\ \sigma_{xy} \\ D_x \end{bmatrix}, \qquad \mathbf{t}_2 = \begin{bmatrix} \sigma_{xy} \\ \sigma_{yy} \\ D_y \end{bmatrix}, \tag{4.6}$$

the constitutive equations can be expressed as:

$$\begin{bmatrix} \sigma_{xx} \\ \sigma_{xy} \\ D_x \end{bmatrix} = \begin{bmatrix} c_{11} & 0 & 0 \\ 0 & c_{44} & e_{15} \\ 0 & e_{15} & -\varepsilon_{11} \end{bmatrix} \begin{bmatrix} \Gamma_1 \\ \Gamma_2 \\ \Gamma_3 \end{bmatrix} + \begin{bmatrix} 0 & c_{13} & e_{31} \\ c_{44} & 0 & 0 \\ e_{15} & 0 & 0 \end{bmatrix} \begin{bmatrix} \Gamma_4 \\ \Gamma_5 \\ \Gamma_6 \end{bmatrix} \tag{4.7}$$

$$\begin{bmatrix} \sigma_{xy} \\ \sigma_{yy} \\ D_y \end{bmatrix} = \begin{bmatrix} 0 & c_{44} & e_{15} \\ c_{13} & 0 & 0 \\ e_{31} & 0 & 0 \end{bmatrix} \begin{bmatrix} \Gamma_1 \\ \Gamma_2 \\ \Gamma_3 \end{bmatrix} + \begin{bmatrix} c_{44} & 0 & 0 \\ 0 & c_{33} & e_{33} \\ 0 & e_{33} & -\varepsilon_{33} \end{bmatrix} \begin{bmatrix} \Gamma_4 \\ \Gamma_5 \\ \Gamma_6 \end{bmatrix} \tag{4.8}$$

or, in contract form:

$$\mathbf{t}_1 = \mathbf{A}\mathbf{\Gamma}^{(1)} + \mathbf{B}\mathbf{\Gamma}^{(2)} \tag{4.9}$$

$$\mathbf{t}_2 = \mathbf{B}^T\mathbf{\Gamma}^{(1)} + \mathbf{C}\mathbf{\Gamma}^{(2)} \tag{4.10}$$

The equilibrium equations for generalized plane strain conditions are:

$$\frac{\partial \sigma_{xx}}{\partial x} + \frac{\partial \sigma_{xy}}{\partial y} = 0$$

$$\frac{\partial \sigma_{xy}}{\partial x} + \frac{\partial \sigma_{yy}}{\partial y} = 0 \tag{4.11}$$

and the Maxwell equation for the electric displacement gives:

$$\frac{\partial D_x}{\partial x} + \frac{\partial D_y}{\partial y} = 0. \tag{4.12}$$

Introducing equations (4.7) and (4.8) into (4.11) and (4.12) one obtains the following relations:

$$c_{11}\frac{\partial^2 u}{\partial x^2}+\left(c_{13}+c_{44}\right)\frac{\partial^2 v}{\partial x\partial y}+\left(e_{31}+e_{15}\right)\frac{\partial^2 \varphi}{\partial x\partial y}+c_{44}\frac{\partial^2 u}{\partial y^2}=0$$

$$c_{44}\frac{\partial^2 v}{\partial x^2}+e_{15}\frac{\partial^2 \varphi}{\partial x^2}+\left(c_{13}+c_{44}\right)\frac{\partial^2 u}{\partial x\partial y}+c_{33}\frac{\partial^2 v}{\partial y^2}+e_{33}\frac{\partial^2 \varphi}{\partial y^2}=0 \qquad (4.13)$$

$$e_{15}\frac{\partial^2 v}{\partial x^2}-\varepsilon_{11}\frac{\partial^2 \varphi}{\partial x^2}+\left(e_{15}+e_{31}\right)\frac{\partial^2 u}{\partial x\partial y}+e_{33}\frac{\partial^2 v}{\partial y^2}-\varepsilon_{33}\frac{\partial^2 \varphi}{\partial y^2}=0$$

or, in contract form:

$$\mathbf{A}\boldsymbol{\Gamma}^{(1)}_{,1}+(\mathbf{B}+\mathbf{B}^T)\boldsymbol{\Gamma}^{(1)}_{,3}+\mathbf{C}\boldsymbol{\Gamma}^{(2)}_{,3}=\mathbf{0} \qquad (4.14)$$

in which the condition of equality of crossed derivatives (Schwartz equality) has been used:

$$\boldsymbol{\Gamma}^{(2)}_{,x}-\boldsymbol{\Gamma}^{(1)}_{,y}=0 \qquad (4.15)$$

The system constituted by equations (4.14) and (4.15) can be expressed with the fundamental relation:

$$\boldsymbol{\Gamma}_{,x}+\mathbf{D}\boldsymbol{\Gamma}_{,y}=\mathbf{0} \qquad (4.16)$$

where $\boldsymbol{\Gamma}=(\boldsymbol{\Gamma}^{(1)},\boldsymbol{\Gamma}^{(2)})^T$ and $\mathbf{D}=\begin{bmatrix} \mathbf{A}^{-1}\left(\mathbf{B}+\mathbf{B}^T\right) & \mathbf{A}^{-1}\mathbf{C} \\ \mathbf{-1} & \mathbf{0} \end{bmatrix}$ is a 6x6 matrix with the following explicit form:

$$\mathbf{D}=\begin{bmatrix} 0 & \alpha_1 & \alpha_2 & \alpha_3 & 0 & 0 \\ \beta_1 & 0 & 0 & 0 & \beta_2 & \beta_3 \\ \chi_1 & 0 & 0 & 0 & \chi_2 & \chi_3 \\ -1 & 0 & 0 & 0 & 0 & 0 \\ 0 & -1 & 0 & 0 & 0 & 0 \\ 0 & 0 & -1 & 0 & 0 & 0 \end{bmatrix} \qquad (4.17)$$

with entries given by:

$$\alpha_1=\frac{c_p}{c_{11}}, \qquad \alpha_2=\frac{e_p}{c_{11}}, \qquad \alpha_3=\frac{c_{44}}{c_{11}}, \qquad \beta_1=\frac{c_p}{c_{44}}-\frac{c_p e_{15}^2}{c_{44}\mu\varepsilon_{11}}+\frac{e_p e_{15}}{\mu\varepsilon_{11}},$$

$$\beta_2=\frac{c_{33}}{c_{44}}-\frac{c_{33}e_{15}^2}{c_{44}\mu\varepsilon_{11}}+\frac{e_{33}e_{15}}{\mu\varepsilon_{11}}, \qquad \beta_3=\frac{e_{33}}{c_{44}}-\frac{e_{33}e_{15}^2}{c_{44}\mu\varepsilon_{11}}+\frac{\varepsilon_{33}e_{15}}{\mu\varepsilon_{11}},$$

$$\chi_1=\frac{c_p e_{15}-e_p c_{44}}{\mu\varepsilon_{11}}, \qquad \chi_2=\frac{c_{33}e_{15}-e_{33}c_{44}}{\mu\varepsilon_{11}}, \qquad \chi_3=\frac{e_{33}e_{15}-\varepsilon_{33}c_{44}}{\mu\varepsilon_{11}}, \qquad (4.18)$$

$$c_p=c_{13}+c_{44}, \qquad e_p=e_{31}+e_{15}, \qquad \mu=c_{44}+\frac{e_{15}^2}{\varepsilon_{11}}.$$

The discussion of the system (4.16) is performed through the calculation of the

eigenvalues of $\mathbf{D}$. The characteristic equation, $\det(\mathbf{D} - \lambda\mathbf{I}) = 0$, gives:

$$\lambda^6 + p\lambda^4 + q\lambda^2 + r = 0 \qquad (4.19)$$

where:

$$
\begin{aligned}
p &= \beta_2 + \alpha_3 + \chi_3 - (\chi_1\alpha_2 + \alpha_1\beta_1), \\
q &= (\beta_2\chi_3 - \chi_2\beta_3) + \alpha_3(\beta_2 + \chi_3) + \chi_1(\alpha_1\beta_3 - \alpha_2\beta_2) - \beta_1(\alpha_1\chi_3 - \alpha_2\chi_2), \qquad (4.20) \\
r &= \alpha_3(\beta_2\chi_3 - \chi_2\beta_3).
\end{aligned}
$$

From equation (4.19) one obtains three pairs of complex conjugate eigenvalues, each corresponding to a six-dimensional eigenvector. Taking into account the three eigenvalues with positive imaginary part:

$$\lambda_k = p_k + iq_k, \qquad q_k > 0, \quad k = 1, 2, 3 \qquad (4.21)$$

it is possible to create a matrix $\mathbf{T}$ whose six columns are respectively the imaginary and real components of the three related eigenvectors $f_k = g^{(k)} + ih^{(k)} \ (k = 1, 2, 3)$:

$$
\mathbf{T} = \begin{bmatrix}
h_1^{(1)} & g_1^{(1)} & h_1^{(2)} & g_1^{(2)} & h_1^{(3)} & g_1^{(3)} \\
h_2^{(1)} & g_2^{(1)} & h_2^{(2)} & g_2^{(2)} & h_2^{(3)} & g_2^{(3)} \\
h_3^{(1)} & g_3^{(1)} & h_3^{(2)} & g_3^{(2)} & h_3^{(3)} & g_3^{(3)} \\
h_4^{(1)} & g_4^{(1)} & h_4^{(2)} & g_4^{(2)} & h_4^{(3)} & g_4^{(3)} \\
h_5^{(1)} & g_5^{(1)} & h_5^{(2)} & g_5^{(2)} & h_5^{(3)} & g_5^{(3)} \\
h_6^{(1)} & g_6^{(1)} & h_6^{(2)} & g_6^{(2)} & h_6^{(3)} & g_6^{(3)}
\end{bmatrix}. \qquad (4.22)
$$

The above matrix can induce a transformation of similarity on $\mathbf{D}$ such that:

$$
\mathbf{S} = \mathbf{T}^{-1}\mathbf{D}\mathbf{T} = \begin{bmatrix}
p_1 & -q_1 & 0 & 0 & 0 & 0 \\
q_1 & p_1 & 0 & 0 & 0 & 0 \\
0 & 0 & p_2 & -q_2 & 0 & 0 \\
0 & 0 & q_2 & p_2 & 0 & 0 \\
0 & 0 & 0 & 0 & p_3 & -q_3 \\
0 & 0 & 0 & 0 & q_3 & p_3
\end{bmatrix}. \qquad (4.23)
$$

Pre-multiplying equation (4.16) by $\mathbf{T}^{-1}$, with the position $\mathbf{T}^{-1}\mathbf{\Gamma} = \mathbf{\Psi}$, $\mathbf{\Psi} = \begin{bmatrix} \Psi_1 & \Psi_2 & \Psi_3 & \Psi_4 & \Psi_5 & \Psi_6 \end{bmatrix}^T$, the previous equation can be written as:

$$
\begin{bmatrix}
\dfrac{\partial \Psi_1}{\partial x} \\[2mm]
\dfrac{\partial \Psi_2}{\partial x} \\[2mm]
\dfrac{\partial \Psi_3}{\partial x} \\[2mm]
\dfrac{\partial \Psi_4}{\partial x} \\[2mm]
\dfrac{\partial \Psi_5}{\partial x} \\[2mm]
\dfrac{\partial \Psi_6}{\partial x}
\end{bmatrix}
+
\begin{bmatrix}
p_1 & -q_1 & 0 & 0 & 0 & 0 \\
q_1 & p_1 & 0 & 0 & 0 & 0 \\
0 & 0 & p_2 & -q_2 & 0 & 0 \\
0 & 0 & q_2 & p_2 & 0 & 0 \\
0 & 0 & 0 & 0 & p_3 & -q_3 \\
0 & 0 & 0 & 0 & q_3 & p_3
\end{bmatrix}
\begin{bmatrix}
\dfrac{\partial \Psi_1}{\partial y} \\[2mm]
\dfrac{\partial \Psi_2}{\partial y} \\[2mm]
\dfrac{\partial \Psi_3}{\partial y} \\[2mm]
\dfrac{\partial \Psi_4}{\partial y} \\[2mm]
\dfrac{\partial \Psi_5}{\partial y} \\[2mm]
\dfrac{\partial \Psi_6}{\partial y}
\end{bmatrix}
= \mathbf{0}
\tag{4.24}
$$

or, in contract form:

$$
\mathbf{\Psi}_{,x} + \mathbf{S}\mathbf{\Psi}_{,y} = \mathbf{0}
\tag{4.25}
$$

The above system can be split into three sub-systems:

$$
\begin{bmatrix}
\dfrac{\partial \Psi_1}{\partial x} \\[2mm]
\dfrac{\partial \Psi_2}{\partial x}
\end{bmatrix}
+
\begin{bmatrix}
p_1 & -q_1 \\
q_1 & p_1
\end{bmatrix}
\begin{bmatrix}
\dfrac{\partial \Psi_1}{\partial y} \\[2mm]
\dfrac{\partial \Psi_2}{\partial y}
\end{bmatrix}
= \mathbf{0}
\tag{4.26}
$$

$$
\begin{bmatrix}
\dfrac{\partial \Psi_3}{\partial x} \\[2mm]
\dfrac{\partial \Psi_4}{\partial x}
\end{bmatrix}
+
\begin{bmatrix}
p_2 & -q_2 \\
q_2 & p_2
\end{bmatrix}
\begin{bmatrix}
\dfrac{\partial \Psi_3}{\partial y} \\[2mm]
\dfrac{\partial \Psi_4}{\partial y}
\end{bmatrix}
= \mathbf{0}
\tag{4.27}
$$

$$
\begin{bmatrix}
\dfrac{\partial \Psi_5}{\partial x} \\[2mm]
\dfrac{\partial \Psi_6}{\partial x}
\end{bmatrix}
+
\begin{bmatrix}
p_3 & -q_3 \\
q_3 & p_3
\end{bmatrix}
\begin{bmatrix}
\dfrac{\partial \Psi_5}{\partial y} \\[2mm]
\dfrac{\partial \Psi_6}{\partial y}
\end{bmatrix}
= \mathbf{0}
\tag{4.28}
$$

Let's introduce now the following transformations:

$$
\begin{aligned}
\xi_1 &= x - \frac{p_1}{p_1^2 + q_1^2}\, y & \eta_1 &= \frac{q_1}{p_1^2 + q_1^2}\, y \\[2mm]
\xi_2 &= x - \frac{p_2}{p_2^2 + q_2^2}\, y \quad \text{and} \quad & \eta_2 &= \frac{q_2}{p_2^2 + q_2^2}\, y \\[2mm]
\xi_3 &= x - \frac{p_3}{p_3^2 + q_3^2}\, y & \eta_3 &= \frac{q_3}{p_3^2 + q_3^2}\, y
\end{aligned}
\tag{4.29}
$$

that in contract form become:

$$
\xi_j = x - \frac{p_j}{p_j^2 + q_j^2}\, y \quad \text{and} \quad \eta_j = \frac{q_j}{p_j^2 + q_j^2}\, y.
\tag{4.30}
$$

70

The functions Ψ_j are dependant on the variables (x, y). Operating a change of variables, we have:

$$\frac{\partial \Psi_1}{\partial x} = \frac{\partial \Psi_1}{\partial \xi_1} \frac{\partial \xi_1}{\partial x} + \frac{\partial \Psi_1}{\partial \eta_1} \frac{\partial \eta_1}{\partial x}$$

$$\frac{\partial \Psi_1}{\partial y} = \frac{\partial \Psi_1}{\partial \xi_1} \frac{\partial \xi_1}{\partial y} + \frac{\partial \Psi_1}{\partial \eta_1} \frac{\partial \eta_1}{\partial y} \qquad (4.31)$$

From relations (4.29):

$$\frac{\partial \xi_1}{\partial x} = 1, \qquad \frac{\partial \eta_1}{\partial x} = 0,$$

$$\frac{\partial \xi_1}{\partial y} = -\frac{p_1}{p_1^2 + q_1^2}, \qquad \frac{\partial \eta_1}{\partial y} = \frac{q_1}{p_1^2 + q_1^2}, \qquad (4.32)$$

and thus equations (4.31) become:

$$\frac{\partial \Psi_1}{\partial x} = \frac{\partial \Psi_1}{\partial \xi_1}$$

$$\frac{\partial \Psi_1}{\partial y} = -\frac{p_1}{p_1^2 + q_1^2} \frac{\partial \Psi_1}{\partial \xi_1} + \frac{q_1}{p_1^2 + q_1^2} \frac{\partial \Psi_1}{\partial \eta_1} \qquad (4.33)$$

leading to the system:

$$\frac{\partial \Psi_1}{\partial \xi_1} + p_1 \left(-\frac{p_1}{p_1^2 + q_1^2} \frac{\partial \Psi_1}{\partial \xi_1} + \frac{q_1}{p_1^2 + q_1^2} \frac{\partial \Psi_1}{\partial \eta_1} \right) - q_1 \left(-\frac{p_1}{p_1^2 + q_1^2} \frac{\partial \Psi_2}{\partial \xi_1} + \frac{q_1}{p_1^2 + q_1^2} \frac{\partial \Psi_2}{\partial \eta_1} \right) = 0$$

$$\frac{\partial \Psi_2}{\partial \xi_1} + q_1 \left(-\frac{p_1}{p_1^2 + q_1^2} \frac{\partial \Psi_1}{\partial \xi_1} + \frac{q_1}{p_1^2 + q_1^2} \frac{\partial \Psi_1}{\partial \eta_1} \right) + p_1 \left(-\frac{p_1}{p_1^2 + q_1^2} \frac{\partial \Psi_2}{\partial \xi_1} + \frac{q_1}{p_1^2 + q_1^2} \frac{\partial \Psi_2}{\partial \eta_1} \right) = 0$$

$$(4.34)$$

whose matrix form is:

$$\begin{bmatrix} 1 - \dfrac{p_1^2}{p_1^2 + q_1^2} & \dfrac{p_1 q_1}{p_1^2 + q_1^2} \\ -\dfrac{p_1 q_1}{p_1^2 + q_1^2} & 1 - \dfrac{p_1^2}{p_1^2 + q_1^2} \end{bmatrix} \begin{bmatrix} \dfrac{\partial \Psi_1}{\partial \xi_1} \\ \dfrac{\partial \Psi_2}{\partial \xi_1} \end{bmatrix} + \begin{bmatrix} \dfrac{p_1 q_1}{p_1^2 + q_1^2} & -\dfrac{q_1^2}{p_1^2 + q_1^2} \\ \dfrac{q_1^2}{p_1^2 + q_1^2} & \dfrac{p_1 q_1}{p_1^2 + q_1^2} \end{bmatrix} \begin{bmatrix} \dfrac{\partial \Psi_1}{\partial \eta_1} \\ \dfrac{\partial \Psi_2}{\partial \eta_1} \end{bmatrix} = \begin{bmatrix} 0 \\ 0 \end{bmatrix} \quad (4.35)$$

The inverse matrix of $\mathbf{K} = \begin{bmatrix} 1 - \dfrac{p_1^2}{p_1^2 + q_1^2} & \dfrac{p_1 q_1}{p_1^2 + q_1^2} \\ -\dfrac{p_1 q_1}{p_1^2 + q_1^2} & 1 - \dfrac{p_1^2}{p_1^2 + q_1^2} \end{bmatrix}$ is:

$$\mathbf{K}^{-1} = \frac{p_1^2 + q_1^2}{q_1^2} \begin{bmatrix} \dfrac{q_1^2}{p_1^2 + q_1^2} & -\dfrac{p_1 q_1}{p_1^2 + q_1^2} \\ \dfrac{p_1 q_1}{p_1^2 + q_1^2} & \dfrac{q_1^2}{p_1^2 + q_1^2} \end{bmatrix} = \begin{bmatrix} 1 & -\dfrac{p_1}{q_1} \\ \dfrac{p_1}{q_1} & 1 \end{bmatrix} \qquad (4.36)$$

Pre-multiplying equation (4.35) by $\mathbf{K}^{-1}$ one gets:

$$
\begin{bmatrix} \dfrac{\partial \Psi_1}{\partial \xi_1} \\[2ex] \dfrac{\partial \Psi_2}{\partial \xi_1} \end{bmatrix} + \begin{bmatrix} 0 & -1 \\ 1 & 0 \end{bmatrix} \begin{bmatrix} \dfrac{\partial \Psi_1}{\partial \eta_1} \\[2ex] \dfrac{\partial \Psi_2}{\partial \eta_1} \end{bmatrix} = \mathbf{0}
\tag{4.37}
$$

or:

$$
\begin{bmatrix} \dfrac{\partial \Psi_1}{\partial \xi_1} \\[2ex] \dfrac{\partial \Psi_2}{\partial \xi_1} \end{bmatrix} = \begin{bmatrix} 0 & 1 \\ -1 & 0 \end{bmatrix} \begin{bmatrix} \dfrac{\partial \Psi_1}{\partial \eta_1} \\[2ex] \dfrac{\partial \Psi_2}{\partial \eta_1} \end{bmatrix}
\tag{4.38}
$$

which are the Cauchy-Riemann conditions for complex potentials:

$$
\begin{aligned}
\frac{\partial \Psi_1}{\partial \xi_1} &= \frac{\partial \Psi_2}{\partial \eta_1} \\[2ex]
\frac{\partial \Psi_2}{\partial \xi_1} &= -\frac{\partial \Psi_1}{\partial \eta_1}
\end{aligned}
\tag{4.39}
$$

With the very same procedure one can obtain the Cauchy-Riemann conditions for the other sub-systems:

$$
\begin{bmatrix} \dfrac{\partial \Psi_3}{\partial \xi_2} \\[2ex] \dfrac{\partial \Psi_4}{\partial \xi_2} \end{bmatrix} = \begin{bmatrix} 0 & 1 \\ -1 & 0 \end{bmatrix} \begin{bmatrix} \dfrac{\partial \Psi_3}{\partial \eta_2} \\[2ex] \dfrac{\partial \Psi_4}{\partial \eta_2} \end{bmatrix}
\tag{4.40}
$$

$$
\begin{bmatrix} \dfrac{\partial \Psi_5}{\partial \xi_3} \\[2ex] \dfrac{\partial \Psi_6}{\partial \xi_3} \end{bmatrix} = \begin{bmatrix} 0 & 1 \\ -1 & 0 \end{bmatrix} \begin{bmatrix} \dfrac{\partial \Psi_5}{\partial \eta_3} \\[2ex] \dfrac{\partial \Psi_6}{\partial \eta_3} \end{bmatrix}
\tag{4.41}
$$

It can be demonstrated that the Cauchy-Riemann equations (4.38), (4.40) and (4.41) are valid for analytic functions like:

$$
\begin{aligned}
\Omega_1(z_1) &= \Psi_1(\xi_1, \eta_1) + i\Psi_2(\xi_1, \eta_1) \\
\Omega_2(z_2) &= \Psi_3(\xi_2, \eta_2) + i\Psi_4(\xi_2, \eta_2) \\
\Omega_3(z_3) &= \Psi_5(\xi_3, \eta_3) + i\Psi_6(\xi_3, \eta_3)
\end{aligned}
\tag{4.42}
$$

of the complex variables:

$$
z_j = \xi_j + i\eta_j = x + \left(\frac{-p_j + iq_j}{p_j^2 + q_j^2} \right) y, \qquad j = 1, 2, 3
\tag{4.43}
$$

The relation $\mathbf{T}^{-1}\boldsymbol{\Gamma} = \boldsymbol{\Psi}$ is equivalent to the relation $\boldsymbol{\Gamma} = \mathbf{T}\boldsymbol{\Psi}$, which is the contract form of the system:

$$
\begin{bmatrix} \Gamma_1 \\ \Gamma_2 \\ \Gamma_3 \\ \Gamma_4 \\ \Gamma_5 \\ \Gamma_6 \end{bmatrix} =
\begin{bmatrix}
h_1^{(1)} & g_1^{(1)} & h_1^{(2)} & g_1^{(2)} & h_1^{(3)} & g_1^{(3)} \\
h_2^{(1)} & g_2^{(1)} & h_2^{(2)} & g_2^{(2)} & h_2^{(3)} & g_2^{(3)} \\
h_3^{(1)} & g_3^{(1)} & h_3^{(2)} & g_3^{(2)} & h_3^{(3)} & g_3^{(3)} \\
h_4^{(1)} & g_4^{(1)} & h_4^{(2)} & g_4^{(2)} & h_4^{(3)} & g_4^{(3)} \\
h_5^{(1)} & g_5^{(1)} & h_5^{(2)} & g_5^{(2)} & h_5^{(3)} & g_5^{(3)} \\
h_6^{(1)} & g_6^{(1)} & h_6^{(2)} & g_6^{(2)} & h_6^{(3)} & g_6^{(3)}
\end{bmatrix}
\begin{bmatrix} \Psi_1 \\ \Psi_2 \\ \Psi_3 \\ \Psi_4 \\ \Psi_5 \\ \Psi_6 \end{bmatrix}
\tag{4.44}
$$

The introduction of the complex potentials (4.42) allows us to reformulate system (4.44) in the form:

$$
\begin{bmatrix} \Gamma_1 \\ \Gamma_2 \\ \Gamma_3 \\ \Gamma_4 \\ \Gamma_5 \\ \Gamma_6 \end{bmatrix} = \mathrm{Im} \left\{
\begin{bmatrix}
f_1^{(1)} & f_1^{(2)} & f_1^{(3)} \\
f_2^{(1)} & f_2^{(2)} & f_2^{(3)} \\
f_3^{(1)} & f_3^{(2)} & f_3^{(3)} \\
f_4^{(1)} & f_4^{(2)} & f_4^{(3)} \\
f_5^{(1)} & f_5^{(2)} & f_5^{(3)} \\
f_6^{(1)} & f_6^{(2)} & f_6^{(3)}
\end{bmatrix}
\begin{bmatrix} \Omega_1 \\ \Omega_2 \\ \Omega_3 \end{bmatrix}
\right\}
\tag{4.45}
$$

or:

$$
\Gamma_j = \mathrm{Im} \sum_{k=1}^{3} \left[f_j^{(k)} \Omega_k(z_k) \right], \qquad j = 1,2,3,4,5,6
\tag{4.46}
$$

where the definition of the eigenvectors of matrix $\mathbf{D}$, $f_j^{(k)} = g_j^{(k)} + i h_j^{(k)}$, has been used.

4.3 The problem of a static crack in a piezoelectric body

A Griffith crack in a piezoelectric medium, poled along the y axis, under the action of remote loading is considered. The crack is of length $2a$ and free from electro-mechanical loading, as represented in Fig. 4.1.

The loads applied at infinity are the following:

$$
\sigma_{xx}(\infty) = \sigma_{xx}^{\infty}, \qquad \sigma_{xy}(\infty) = \sigma_{xy}^{\infty}, \qquad \sigma_{yy}(\infty) = \sigma_{yy}^{\infty}, \qquad D_x(\infty) = D_x^{\infty}, \qquad D_y(\infty) = D_y^{\infty}
$$

The generalized stress vectors and the vectors of the loads at infinity are:

$$
\mathbf{t}_1 = (\sigma_{xx}, \sigma_{yx}, D_x)^T, \qquad \mathbf{t}_2 = (\sigma_{xy}, \sigma_{yy}, D_y)^T
\tag{4.47}
$$

$$\mathbf{t}_1^\infty = (\sigma_{xx}^\infty, \sigma_{yx}^\infty, D_x^\infty)^T, \qquad \mathbf{t}_2^\infty = (\sigma_{xy}^\infty, \sigma_{yy}^\infty, D_y^\infty)^T \qquad (4.48)$$
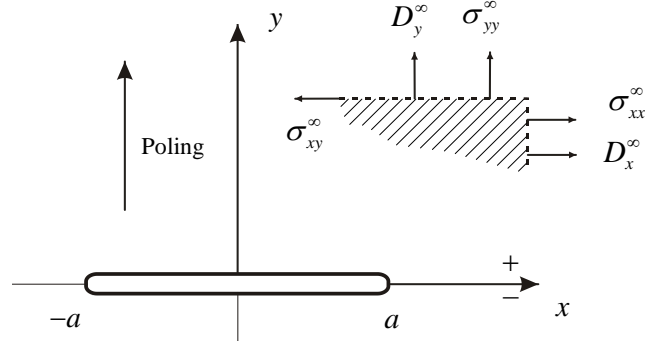
Fig. 4.1 – Griffith crack of length $2a$, free from applied loads, in a piezoelectric solid

One can represent the analytic potentials as the sum of two terms: one constant Ω_0 and another vanishing at infinity $\Lambda(z)$:

$$\Omega_k(z) = \Omega_{0k} + \Lambda_k(z), \qquad k = 1, 2, 3 \qquad (4.49)$$

This allows us to re-write the system (4.45) in the form:

$$
\begin{bmatrix} \Gamma_1 \\ \Gamma_2 \\ \Gamma_3 \\ \Gamma_4 \\ \Gamma_5 \\ \Gamma_6 \end{bmatrix} = \mathrm{Im} \left\{ \begin{bmatrix} f_1^{(1)} & f_1^{(2)} & f_1^{(3)} \\ f_2^{(1)} & f_2^{(2)} & f_2^{(3)} \\ f_3^{(1)} & f_3^{(2)} & f_3^{(3)} \\ f_4^{(1)} & f_4^{(2)} & f_4^{(3)} \\ f_5^{(1)} & f_5^{(2)} & f_5^{(3)} \\ f_6^{(1)} & f_6^{(2)} & f_6^{(3)} \end{bmatrix} \begin{bmatrix} \Omega_{01} + \Lambda_1(z) \\ \Omega_{02} + \Lambda_2(z) \\ \Omega_{03} + \Lambda_3(z) \end{bmatrix} \right\}. \qquad (4.50)
$$

System (4.50) can be splitted in two:

$$
\begin{bmatrix} \Gamma_1 \\ \Gamma_2 \\ \Gamma_3 \end{bmatrix} = \mathrm{Im} \left\{ \begin{bmatrix} f_1^{(1)} & f_1^{(2)} & f_1^{(3)} \\ f_2^{(1)} & f_2^{(2)} & f_2^{(3)} \\ f_3^{(1)} & f_3^{(2)} & f_3^{(3)} \end{bmatrix} \begin{bmatrix} \Omega_{01} + \Lambda_1(z) \\ \Omega_{02} + \Lambda_2(z) \\ \Omega_{03} + \Lambda_3(z) \end{bmatrix} \right\} = \mathrm{Im} \left[\mathbf{E}\Omega_0 + \mathbf{E}\Lambda(z) \right] \qquad (4.51)
$$

$$
\begin{bmatrix} \Gamma_4 \\ \Gamma_5 \\ \Gamma_6 \end{bmatrix} = \mathrm{Im} \left\{ \begin{bmatrix} f_4^{(1)} & f_4^{(2)} & f_4^{(3)} \\ f_5^{(1)} & f_5^{(2)} & f_5^{(3)} \\ f_6^{(1)} & f_6^{(2)} & f_6^{(3)} \end{bmatrix} \begin{bmatrix} \Omega_{01} + \Lambda_1(z) \\ \Omega_{02} + \Lambda_2(z) \\ \Omega_{03} + \Lambda_3(z) \end{bmatrix} \right\} = \mathrm{Im} \left[\mathbf{F}\Omega_0 + \mathbf{F}\Lambda(z) \right] \qquad (4.52)
$$

where $\mathbf{E} = \begin{bmatrix} f_1^{(1)} & f_1^{(2)} & f_1^{(3)} \\ f_2^{(1)} & f_2^{(2)} & f_2^{(3)} \\ f_3^{(1)} & f_3^{(2)} & f_3^{(3)} \end{bmatrix}$ and $\mathbf{F} = \begin{bmatrix} f_4^{(1)} & f_4^{(2)} & f_4^{(3)} \\ f_5^{(1)} & f_5^{(2)} & f_5^{(3)} \\ f_6^{(1)} & f_6^{(2)} & f_6^{(3)} \end{bmatrix}$. The two matrices are linked

by the relation $\mathbf{F} = \mathbf{E}\,diag(-1/\lambda_k)$.

Introducing these two systems into equations (4.9) and (4.10) gives:

$$\mathbf{t}_1 = \mathrm{Im}\big[\big(\mathbf{AE} + \mathbf{BF}\big)\mathbf{\Omega}_0\big] + \mathrm{Im}\big[\big(\mathbf{AE} + \mathbf{BF}\big)\mathbf{\Lambda}(z)\big] \qquad (4.53)$$

$$\mathbf{t}_2 = \mathrm{Im}\big[\big(\mathbf{B}^\mathrm{T}\mathbf{E} + \mathbf{CF}\big)\mathbf{\Omega}_0\big] + \mathrm{Im}\big[\big(\mathbf{B}^\mathrm{T}\mathbf{E} + \mathbf{CF}\big)\mathbf{\Lambda}(z)\big] \qquad (4.54)$$

and, with the positions:

$$\mathbf{G} = (\mathbf{AE} + \mathbf{BF}), \qquad \mathbf{H} = (\mathbf{B}^T\mathbf{E} + \mathbf{CF}), \qquad (4.55)$$

the two equations become:

$$\mathbf{t}_1 = \mathrm{Im}\big[\mathbf{G}\mathbf{\Omega}(z)\big] = \mathrm{Im}\big[\mathbf{G}\mathbf{\Omega}_0\big] + \mathrm{Im}\big[\mathbf{G}\mathbf{\Lambda}(z)\big] = \mathbf{t}_1^\infty + \mathrm{Im}\big[\mathbf{G}\mathbf{\Lambda}(z)\big] \qquad (4.56)$$

$$\mathbf{t}_2 = \mathrm{Im}\big[\mathbf{H}\mathbf{\Omega}(z)\big] = \mathrm{Im}\big[\mathbf{H}\mathbf{\Omega}_0\big] + \mathrm{Im}\big[\mathbf{H}\mathbf{\Lambda}(z)\big] = \mathbf{t}_2^\infty + \mathrm{Im}\big[\mathbf{H}\mathbf{\Lambda}(z)\big] \qquad (4.57)$$

The stress distribution will be known once determined the analytical functions $\mathbf{\Omega}_k(z) = \mathbf{\Omega}_{0k} + \mathbf{\Lambda}_k(z)$ in the particular conditions of the problem considered.

The generalized displacement vector can be obtained integrating, for example, equation (4.51); neglecting a rigid displacement one obtains:

$$\mathbf{U} = \begin{bmatrix} u \\ v \\ \varphi \end{bmatrix} = \mathrm{Im}\big[\mathbf{E}\boldsymbol{\omega}(z)\big] = \mathrm{Im}\big[\mathbf{E}\boldsymbol{\omega}_0(z)\big] + \mathrm{Im}\big[\mathbf{E}\boldsymbol{\lambda}(z)\big] = \mathbf{U}^\infty + \mathrm{Im}\big[\mathbf{E}\boldsymbol{\lambda}(z)\big] \qquad (4.58)$$

where $\omega_k(z)$ is the primitive of $\Omega_k(z)$:

$$\omega_k(z) = \int \Omega_k(z)dz = \Omega_{0k}z + \lambda_k(z) = \omega_{0k}(z) + \lambda_k(z). \qquad (4.59)$$

For the continuity of stress the static boundary condition on the x axis is:

$$\mathbf{t}_2^+(x,0) = \mathbf{t}_2^-(x,0) \qquad |x| < \infty \qquad (4.60)$$

that from equation (4.57) is equivalent to the relation:

$$\big[\mathbf{H}\mathbf{\Lambda}(x) - \overline{\mathbf{H}}\,\overline{\mathbf{\Lambda}(x)}\big]^+ = \big[\mathbf{H}\mathbf{\Lambda}(x) - \overline{\mathbf{H}}\,\overline{\mathbf{\Lambda}(x)}\big]^- \qquad |x| < \infty \qquad (4.61)$$

where the superscripts + and – denote the values of the stress components on the upper and lower edge of the x axis, that is, the limits for $z \to x$ and $y \to 0^\pm$.

By definition the following equality holds:

$$\overline{\mathbf{\Lambda}(z)} = \overline{\mathbf{\Lambda}(\bar{z})} \qquad (4.62)$$

moreover, since when the complex variable z tends to x_0 on the side $y > 0$, its conjugate $\bar{z}$ tends to x on the side $y < 0$ (and vice versa), like represented in Fig. 4.2, one can state:

$$\left[\overline{\Lambda(z)}\right]^{\pm} = \left[\overline{\Lambda(\bar{z})}\right]^{\mp} \tag{4.63}$$
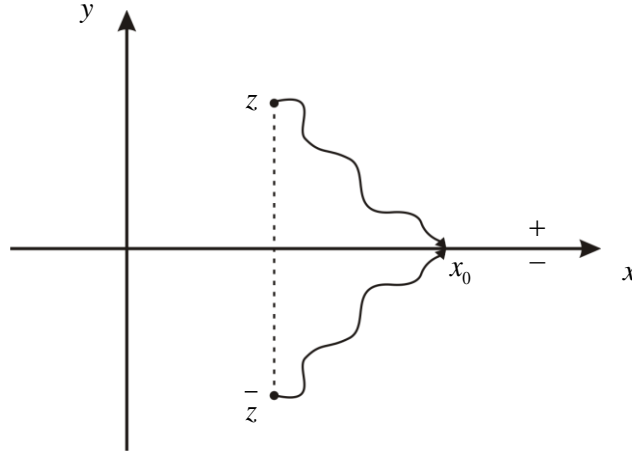
Fig. 4.2 – Representation of the complex variable z and of its conjugate $\bar{z}$

The previous relations lead to:

$$\left[\overline{\Lambda}(x)\right]^{\pm} = \left[\overline{\Lambda(x)}\right]^{\mp} \tag{4.64}$$

that modifies relation (4.61) into:

$$\left[\mathbf{H}\Lambda(x) + \overline{\mathbf{H}}\,\overline{\Lambda}(x)\right]^{+} = \left[\mathbf{H}\Lambda(x) - \overline{\mathbf{H}}\,\overline{\Lambda}(x)\right]^{-} \quad |x| < \infty \tag{4.65}$$

Keeping in mind the condition $\Lambda(\infty) = 0$, from Liouville's theorem, which states the constancy of an analytical function $f(z)$ limited for every $z \in C$, the following derives:

$$\mathbf{H}\Lambda(x) + \overline{\mathbf{H}}\,\overline{\Lambda}(x) = \mathbf{0}, \qquad |x| < \infty \tag{4.66}$$

or

$$\mathbf{H}\Lambda(x) = -\overline{\mathbf{H}}\,\overline{\Lambda}(x), \qquad |x| < \infty \tag{4.67}$$

holding for the three crack models (permeable semipermeable and impermeable to an electric field).

Now the solution can be sought and particularized in the three cases.

4.3.1. The impermeable crack

With this assumption the Griffith crack is considered to be electrically impermeable and so the electric field inside the crack is neglected. The boundary condition is:

76

$$D_y^+ = D_y^- = 0 \qquad |x| < a \tag{4.68}$$

Let's assume the crack to be traction free:

$$\sigma_{yy}^+(x,0) = \sigma_{yy}^-(x,0) = 0$$
$$\sigma_{xy}^+(x,0) = \sigma_{xy}^-(x,0) = 0 \qquad |x| < a \tag{4.69}$$

In contract form these conditions can be written as:

$$\mathbf{t}_2^+(x) = \mathbf{t}_2^-(x) = \mathbf{0} \qquad |x| < a \tag{4.70}$$

Through equation (4.57), the latter relation becomes:

$$\mathbf{t}_2^\infty + \frac{1}{2i}\left[\mathbf{H}\mathbf{\Lambda}^+(x) - \overline{\mathbf{H}}\overline{\mathbf{\Lambda}^+(x)} \right] = \mathbf{0} \qquad |x| < a$$
$$\mathbf{t}_2^\infty + \frac{1}{2i}\left[\mathbf{H}\mathbf{\Lambda}^-(x) - \overline{\mathbf{H}}\overline{\mathbf{\Lambda}^-(x)} \right] = \mathbf{0} \qquad |x| < a \tag{4.71}$$

From equations (4.64) and (4.67) one obtains:

$$\overline{\mathbf{H}}\overline{\mathbf{\Lambda}^+(x)} = \overline{\mathbf{H}}\overline{\mathbf{\Lambda}}^-(x) = -\mathbf{H}\mathbf{\Lambda}^-(x) \qquad |x| < \infty$$
$$\overline{\mathbf{H}}\overline{\mathbf{\Lambda}^-(x)} = \overline{\mathbf{H}}\overline{\mathbf{\Lambda}}^+(x) = -\mathbf{H}\mathbf{\Lambda}^+(x) \qquad |x| < \infty \tag{4.72}$$

and the introduction of relations (4.72) into equations (4.71) allows to express the condition of absence of stress on the crack boundary in the form of a Hilbert problem:

$$\mathbf{\Lambda}^+(x) + \mathbf{\Lambda}^-(x) = -2i\mathbf{H}^{-1}\mathbf{t}_2^\infty \qquad |x| < a \tag{4.73}$$

In terms of vector components, the problem (4.73) can be split into:

$$\Lambda_k^+(x) + \Lambda_k^-(x) = -2i\left[\mathbf{H}^{-1}\mathbf{t}_2^\infty \right]_k \qquad |x| < a \tag{4.74}$$

More precisely, equation (4.74) identify a Plemelj problem (APPENDIX A). The solution can be derived from the general relation [12]:

$$\Lambda_k(z) = \frac{X(z)}{2\pi i} \int_L \frac{g(x)dx}{X^+(x)(x-z)} + X(z)P(z) \tag{4.75}$$

where $X(z)$, the canonical function of the problem, in this specific case has the form:

$$X(z) = \frac{1}{\sqrt{z^2 - a^2}} \tag{4.76}$$

while its upper and lower limits on the x axis are:

$$X^+(z) = \frac{-i}{\sqrt{x^2 - a^2}} \tag{4.77}$$

$$X^{-}(z) = \frac{i}{\sqrt{x^2 - a^2}} \tag{4.78}$$

The solution of the problem assumes the following aspect:

$$\Lambda_k(z) = \frac{1}{2\pi i \sqrt{z^2 - a^2}} \int_L \left[-2i \left[\mathbf{H}^{-1}\mathbf{t}_2^\infty \right]_k \frac{-i\sqrt{a^2 - x^2}}{(x-z)} \right] dx + \frac{1}{\sqrt{z^2 - a^2}} P(z) \tag{4.79}$$

Since $\displaystyle\int_{-a}^{a} \frac{\sqrt{a^2 - x^2}}{(x-z)} dx = -\pi \left(z - \sqrt{z^2 - a^2} \right)$, $z \notin (-a, a)$ one obtains:

$$\Lambda_k(z) = i \left[\frac{z_k}{\sqrt{z_k^2 - a^2}} - 1 \right] \left(\mathbf{H}^{-1}\mathbf{t}_2^\infty \right)_k + \frac{1}{\sqrt{z^2 - a^2}} P(z) \tag{4.80}$$

For what concerns the polynomial $P(z)$, by definition $\Lambda(\infty) = 0$, or in other words $\Lambda(z) \in A_{-1}^\infty$, so $P(z)$ must inevitably reduce to a constant; it is furthermore demonstrable that for a tension free crack $P(z) = \text{cost} = 0$ holds. The solution to the Hilbert problem results to be:

$$\Lambda_k(z) = i \left[\frac{z_k}{\sqrt{z_k^2 - a^2}} - 1 \right] \left(\mathbf{H}^{-1}\mathbf{t}_2^\infty \right)_k \tag{4.81}$$

In matrix form equation (4.81) can be written as:

$$\Lambda(z) = i \left[\mathbf{diag}\left[\frac{z_k}{\sqrt{z_k^2 - a^2}} \right] - 1 \right] \mathbf{H}^{-1}\mathbf{t}_2^\infty \tag{4.82}$$

The introduction of the latter equation into the expression of the generalized stress vector (4.57) gives:

$$\mathbf{t}_2 = \mathbf{t}_2^\infty + \mathrm{Im}\left[\mathbf{H}\Lambda(z) \right] = \mathbf{t}_2^\infty + \mathrm{Re}\left\{ \mathbf{H} \left[\mathbf{diag}\left[\frac{z_k}{\sqrt{z_k^2 - a^2}} \right] - 1 \right] \mathbf{H}^{-1}\mathbf{t}_2^\infty \right\} =$$

$$= \mathrm{Re}\left\{ \mathbf{H} \left[\mathbf{diag}\left[\frac{z_k}{\sqrt{z_k^2 - a^2}} \right] \right] \mathbf{H}^{-1} \right\} \mathbf{t}_2^\infty \tag{4.83}$$

while the other generalized vector becomes:

$$\mathbf{t}_1 = \mathbf{t}_1^\infty + \mathrm{Im}\left[\mathbf{G}\Lambda(z) \right] = \mathbf{t}_1^\infty + \mathrm{Re}\left\{ \mathbf{G} \left[\mathbf{diag}\left[\frac{z_k}{\sqrt{z_k^2 - a^2}} \right] - 1 \right] \mathbf{H}^{-1}\mathbf{t}_2^\infty \right\} =$$

$$= \mathbf{t}_1^\infty - \mathrm{Re}\left[\mathbf{G}\mathbf{H}^{-1} \right] \mathbf{t}_2^\infty + \mathrm{Re}\left\{ \mathbf{G} \left[\mathbf{diag}\left[\frac{z_k}{\sqrt{z_k^2 - a^2}} \right] \right] \mathbf{H}^{-1} \right\} \mathbf{t}_2^\infty \tag{4.84}$$

One can verify that the solution is in compliance with the boundary condition (4.70), in fact with the position $f(z_k) = \dfrac{z_k}{\sqrt{z_k^2 - a^2}}$, from equation (4.83) it derives:

$$\mathbf{t}_2^{\pm}(x) = \text{Re}\left\{\mathbf{H}\text{diag}\left[f^{\pm}(x)\right]\mathbf{H}^{-1}\right\}\mathbf{t}_2^{\infty} = \frac{1}{2}\left\{\mathbf{H}\text{diag}\left[f^{\pm}(x)\right]\mathbf{H}^{-1} + \overline{\mathbf{H}}\text{diag}\left[\overline{f^{\pm}(x)}\right]\overline{\mathbf{H}}^{-1}\right\}\mathbf{t}_2^{\infty}$$

(4.85)

for $|x| < a$ one gets:

$$\overline{f^{\pm}(x)} = \pm\frac{ix}{\sqrt{a^2 - x^2}} = -f^{\pm}(x) \tag{4.86}$$

and therefore:

$$\mathbf{t}_2^{\pm}(x) = \frac{1}{2}f^{\pm}(x)\left[\mathbf{H}\mathbf{H}^{-1} - \overline{\mathbf{H}}\,\overline{\mathbf{H}}^{-1}\right]\mathbf{t}_2^{\infty} = \mathbf{0} \qquad |x| < a \tag{4.87}$$

as it was to be verified.

By means of integration of function (4.82) one obtains the primitive:

$$\boldsymbol{\lambda}(z) = i\left[\text{diag}\left[\sqrt{z_k^2 - a^2} - z_k\right]\mathbf{H}^{-1}\right]\mathbf{t}_2^{\infty} \tag{4.88}$$

and substituting $\boldsymbol{\lambda}(z)$ in the expression of the generalized displacement vector (4.58) gives:

$$\mathbf{U} = \mathbf{U}^{\infty} + \text{Im}\left[\mathbf{E}\boldsymbol{\lambda}(z)\right] = \mathbf{U}^{\infty} + \text{Re}\left\{\mathbf{E}\text{diag}\left[\sqrt{z_k^2 - a^2}\right]\mathbf{H}^{-1}\right\}\mathbf{t}_2^{\infty} - \text{Re}\left\{\mathbf{E}\text{diag}\left[z_k\right]\mathbf{H}^{-1}\right\}\mathbf{t}_2^{\infty}$$

(4.89)

Now it is possible to calculate the displacement discontinuity across the crack. With the position $h(z_k) = \sqrt{z_k^2 - a^2}$ one gets:

$$\mathbf{U}^+(x,0) = \mathbf{U}^{\infty} + \text{Re}\left\{\mathbf{E}\text{diag}\left[h^+(x)\right]\mathbf{H}^{-1}\right\}\mathbf{t}_2^{\infty} - \text{Re}\left\{x\mathbf{E}\mathbf{H}^{-1}\right\}\mathbf{t}_2^{\infty} \tag{4.90}$$

$$\mathbf{U}^-(x,0) = \mathbf{U}^{\infty} + \text{Re}\left\{\mathbf{E}\text{diag}\left[h^-(x)\right]\mathbf{H}^{-1}\right\}\mathbf{t}_2^{\infty} - \text{Re}\left\{x\mathbf{E}\mathbf{H}^{-1}\right\}\mathbf{t}_2^{\infty} \tag{4.91}$$

$$\Delta\mathbf{U}(x,0) = \mathbf{U}^+(x,0) - \mathbf{U}^-(x,0) = \text{Re}\left[\mathbf{E}\text{diag}\left[h^+(x) - h^-(x)\right]\mathbf{H}^{-1}\right]\mathbf{t}_2^{\infty} \tag{4.92}$$

Since:

$$h^+(x) = -h^-(x) = i\sqrt{a^2 - x^2} \qquad |x| < a \tag{4.93}$$

the discontinuity across the crack results:

$$\Delta\mathbf{U}(x) = -2\,\text{Im}(\mathbf{E}\mathbf{H}^{-1})\sqrt{a^2 - x^2}\,\mathbf{t}_2^{\infty} = 2\sqrt{a^2 - x^2}\,\mathbf{R}\mathbf{t}_2^{\infty} \tag{4.94}$$

where $\mathbf{R} = \text{Re}\left[i\mathbf{E}\mathbf{H}^{-1}\right]$.
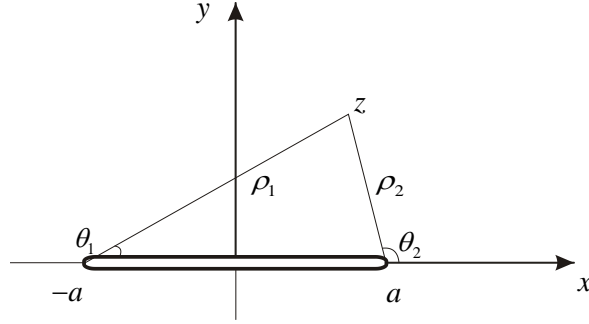
Fig. 4.3 – Polar coordinates originating at the crack tips for the complex variable z

With reference to Fig. 4.3, from the rules of vectorial sum:

$$z + a = \rho_1 e^{i\theta_1}, \qquad z - a = \rho_2 e^{i\theta_2} \tag{4.95}$$

and therefore:

$$h(z) = \sqrt{\rho_1 \rho_2}\, e^{i\left(\frac{\theta_1}{2} + \frac{\theta_2}{2}\right)} \tag{4.96}$$

Across the crack, that is for $|x| < a$, if $z \to x + i0^+$ then $\theta_1 = 0$ and $\theta_1 = \pi$, whereas if $z \to x + i0^-$ then $\theta_1 = 0$ and $\theta_1 = -\pi$, and the foregoing value of the discontinuity (4.94) derives. One can also notice that outside the crack width the function results to be continuous, in fact with the same arguments it is:

$$\begin{aligned} h^+(x) = h^-(x) = -\sqrt{x^2 - a^2} \qquad & x < -a \\ h^+(x) = h^-(x) = \sqrt{x^2 - a^2} \qquad & x > a \end{aligned} \tag{4.97}$$

The expression of the generalized stress allows to determine the stress intensity factor vector, defined by the relation:

$$\mathbf{K} = \lim_{x \to a} \sqrt{2\pi(x-a)}\, \mathbf{t}_2(x,0) \tag{4.98}$$

From equation (4.83), calculated at the vicinity of the right tip, on the x axis:

$$\mathbf{t}_2(x,0) = \frac{x}{\sqrt{x^2 - a^2}}\, \mathbf{t}_2^\infty \qquad x > a \tag{4.99}$$

Thus, the three dimensional vector $\mathbf{K}$ in the impermeable case assumes the aspect:

$$\mathbf{K}(a) = \sqrt{\pi a}\, \mathbf{t}_2^\infty \tag{4.100}$$

or, in explicit form:

$$\mathbf{K}_{\text{imp}}(a) = \begin{bmatrix} K_1(a) \\ K_2(a) \\ K_3(a) \end{bmatrix} = \begin{bmatrix} \sqrt{\pi a}\, \sigma_{xy}^{\infty} \\ \sqrt{\pi a}\, \sigma_{yy}^{\infty} \\ \sqrt{\pi a}\, D_y^{\infty} \end{bmatrix} = \begin{bmatrix} K_{II}^{(a)} \\ K_I^{(a)} \\ K_D^{(a)} \end{bmatrix} \tag{4.101}$$

where $K_{II}^{(a)}$ and $K_I^{(a)}$ are, respectively, the stress intensity factor for Sliding Mode and for Opening Mode, and $K_D^{(a)}$ is the intensity factor for Electric Displacement Mode, as introduced for analogy in [13].

4.3.2. The permeable crack

For a traction free, permeable crack, the following boundary conditions hold:

$$\begin{aligned} \sigma_{yy}^+(x,0) = \sigma_{yy}^-(x,0) = 0 \\ \sigma_{xy}^+(x,0) = \sigma_{xy}^-(x,0) = 0 \end{aligned} \qquad |x| < a \tag{4.102}$$

$$\begin{aligned} D_y^+(x,0) = D_y^-(x,0) \\ E_x^+(x,0) = E_x^-(x,0) \end{aligned} \qquad |x| < \infty \tag{4.103}$$

From equation (4.57) valued on the x axis it derives:

$$\begin{aligned} \mathbf{H}\boldsymbol{\Lambda}^+(x) - \overline{\mathbf{H}}\,\overline{\boldsymbol{\Lambda}^+(x)} = 2i\left[\mathbf{t}_2^+(x,0) - \mathbf{t}_2^{\infty} \right] \\ \mathbf{H}\boldsymbol{\Lambda}^-(x) - \overline{\mathbf{H}}\,\overline{\boldsymbol{\Lambda}^-(x)} = 2i\left[\mathbf{t}_2^-(x,0) - \mathbf{t}_2^{\infty} \right] \end{aligned} \qquad |x| < \infty \tag{4.104}$$

and inserting relation (4.64) produces:

$$\begin{aligned} \mathbf{H}\boldsymbol{\Lambda}^+(x) - \overline{\mathbf{H}}\,\overline{\boldsymbol{\Lambda}}^-(x) = 2i\left[\mathbf{t}_2^+(x,0) - \mathbf{t}_2^{\infty} \right] \\ \mathbf{H}\boldsymbol{\Lambda}^-(x) - \overline{\mathbf{H}}\,\overline{\boldsymbol{\Lambda}}^+(x) = 2i\left[\mathbf{t}_2^-(x,0) - \mathbf{t}_2^{\infty} \right] \end{aligned} \qquad |x| < \infty \tag{4.105}$$

Through relation (4.67), equations (4.105) lead to the condition:

$$\boldsymbol{\Lambda}^+(x) + \boldsymbol{\Lambda}^-(x) = 2i\mathbf{H}^{-1}\left[\mathbf{t}_2^{\pm}(x,0) - \mathbf{t}_2^{\infty} \right] \qquad |x| < \infty \tag{4.106}$$

From boundary conditions (4.102) and (4.103) it is evident that the only component of the generalized stress vector on the edges of the crack is the electric displacement D_y° (the others are null):

$$\mathbf{t}_2(x,0) = \begin{bmatrix} 0 \\ 0 \\ D_y^{\circ} \end{bmatrix} = D_y^{\circ}\begin{bmatrix} 0 \\ 0 \\ 1 \end{bmatrix} = D_y^{\circ}\mathbf{k} \qquad |x| < a \tag{4.107}$$

and so equation (4.106) can be written as:

$$\boldsymbol{\Lambda}^+(x) + \boldsymbol{\Lambda}^-(x) = -2i\mathbf{H}^{-1}\mathbf{J} \qquad |x| < a \tag{4.108}$$

where:

$$\mathbf{J} = \mathbf{t}_2^\infty - D_y^\circ \mathbf{k} \tag{4.109}$$

In analogy with the impermeable crack case, equation (4.108) is a Hilbert problem, whose solution is:

$$\mathbf{\Lambda}(z) = i\left[\mathbf{diag}\left[\frac{z_k}{\sqrt{z_k^2 - a^2}}\right] - \mathbf{1}\right]\mathbf{H}^{-1}\mathbf{J} = i\left[\mathbf{diag}\left[f(z_k)\right] - \mathbf{1}\right]\mathbf{H}^{-1}\mathbf{J} \tag{4.110}$$

where $f(z_k) = \dfrac{z_k}{\sqrt{z_k^2 - a^2}}$.

Substituting the solution of the Hilbert problem (4.110) into equations (4.57) and (4.56) respectively permits to find the expressions of the generalized stress vectors:

$$\mathbf{t}_2 = D_y^\circ \mathbf{k} + \mathrm{Re}\left[\mathbf{Hdiag}\left[f(z_k)\right]\mathbf{H}^{-1}\right]\mathbf{J} \tag{4.111}$$

$$\mathbf{t}_1 = \mathbf{t}_1^\infty - \mathrm{Re}\left[\mathbf{GH}^{-1}\right]\mathbf{J} + \mathrm{Re}\left[\mathbf{Gdiag}\left[f(z_k)\right]\mathbf{H}^{-1}\right]\mathbf{J} \tag{4.112}$$

The primitive of function (4.110) is:

$$\boldsymbol{\lambda}(z) = i\left[\mathbf{diag}\left[h(z_k)\right] - \mathbf{diag}\left[z_k\right]\right]\mathbf{H}^{-1}\mathbf{J} \tag{4.113}$$

where $h(z_k) = \sqrt{z_k^2 - a^2}$. Combining equation (4.113) with equation (4.58) produces:

$$\mathbf{U} = \mathbf{U}^\infty + \mathrm{Re}\left\{\mathbf{Ediag}\left[h(z_k) - z_k\right]\mathbf{H}^{-1}\mathbf{J}\right\} \tag{4.114}$$

The unknown electric displacement on the crack surface D_y° that appears in the vector $\mathbf{J}$ can be determined in relation to the applied loads. For this purpose, let's split the matrix relation (4.106) into three equations:

$$\begin{cases} \left[\mathbf{H}\right]_1 \left(\mathbf{\Lambda}^+ + \mathbf{\Lambda}^-\right) = -2i\sigma_{xy}^\infty \\ \left[\mathbf{H}\right]_2 \left(\mathbf{\Lambda}^+ + \mathbf{\Lambda}^-\right) = -2i\sigma_{yy}^\infty \\ \left[\mathbf{H}\right]_3 \left(\mathbf{\Lambda}^+ + \mathbf{\Lambda}^-\right) = 2i\left(D_y^\circ - D_y^\infty\right) \end{cases} \qquad |x| < a \tag{4.115}$$

where the notation $\left[\ \right]_k, k = 1, 2, 3$ indicates the k-th row of the matrix. It is now necessary to introduce the second of the boundary conditions (4.103):

$$E_x^+(x, 0) - E_x^-(x, 0) = \Delta\varphi_{,x}(x, 0) = 0 \qquad |x| < \infty \tag{4.116}$$

that since $\mathbf{\Gamma}^{(1)} = (\Gamma_1, \Gamma_2, \Gamma_3)^T = (U_{x,x}, U_{y,x}, \varphi_{,x})^T$ becomes:

$$\left[\Delta\mathbf{\Gamma}^{(1)}\right]_3 (x, 0) = \left[\mathbf{\Gamma}^{(1)}\right]_3^+ (x, 0) - \left[\mathbf{\Gamma}^{(1)}\right]_3^- (x, 0) = 0 \qquad |x| < \infty \tag{4.117}$$

From equations (4.51):

$$\mathbf{\Gamma}^{(1)+}(x) = \mathbf{\Gamma}_\infty^{(1)} + \frac{1}{2i}\left[\mathbf{E}\mathbf{\Lambda}^+(x) - \overline{\mathbf{E}}\overline{\mathbf{\Lambda}^+(x)}\right]$$

$$\mathbf{\Gamma}^{(1)-}(x) = \mathbf{\Gamma}_\infty^{(1)} + \frac{1}{2i}\left[\mathbf{E}\mathbf{\Lambda}^-(x) - \overline{\mathbf{E}}\overline{\mathbf{\Lambda}^-(x)}\right] \qquad |x| < \infty \qquad (4.118)$$

introducing relations (4.64) and (4.67):

$$\mathbf{\Gamma}^{(1)+}(x) = \mathbf{\Gamma}_\infty^{(1)} + \frac{1}{2i}\left[\mathbf{E}\mathbf{\Lambda}^+(x) + \overline{\mathbf{E}}\overline{\mathbf{H}}^{-1}\mathbf{H}\mathbf{\Lambda}^-\right]$$

$$\mathbf{\Gamma}^{(1)-}(x) = \mathbf{\Gamma}_\infty^{(1)} + \frac{1}{2i}\left[\mathbf{E}\mathbf{\Lambda}^-(x) + \overline{\mathbf{E}}\overline{\mathbf{H}}^{-1}\mathbf{H}\mathbf{\Lambda}^+\right] \qquad |x| < \infty \qquad (4.119)$$

and subtracting, one obtains:

$$\Delta\mathbf{\Gamma}^{(1)}(x) = \frac{1}{2i}\left[\left(\mathbf{E} - \overline{\mathbf{E}}\overline{\mathbf{H}}^{-1}\mathbf{H}\right)\left(\mathbf{\Lambda}^+ - \mathbf{\Lambda}^-\right)\right] \qquad |x| < \infty \qquad (4.120)$$

Since:

$$\mathbf{E} - \overline{\mathbf{E}}\overline{\mathbf{H}}^{-1}\mathbf{H} = \mathbf{E}\mathbf{H}^{-1}\mathbf{H} - \overline{\mathbf{E}}\overline{\mathbf{H}}^{-1}\mathbf{H} = \left(\mathbf{E}\mathbf{H}^{-1} - \overline{\mathbf{E}}\overline{\mathbf{H}}^{-1}\right)\mathbf{H} = 2i\,\mathrm{Im}\left(\mathbf{E}\mathbf{H}^{-1}\right)\mathbf{H} =$$

$$= -2i\,\mathrm{Re}\left(i\mathbf{E}\mathbf{H}^{-1}\right)\mathbf{H} = -2i\mathbf{R}\mathbf{H} \qquad (4.121)$$

where $\mathbf{R} = \mathrm{Re}(i\mathbf{E}\mathbf{H}^{-1})$, equation (4.120) becomes:

$$\Delta\mathbf{\Gamma}^{(1)}(x) = -\mathbf{R}\mathbf{H}\left(\mathbf{\Lambda}^+ - \mathbf{\Lambda}^-\right) \qquad |x| < \infty \qquad (4.122)$$

and (4.117) assumes the form:

$$\left[\mathbf{R}\mathbf{H}\left(\mathbf{\Lambda}^+ - \mathbf{\Lambda}^-\right)\right]_3(x,0) = \left[\mathbf{R}\right]_3\left(\mathbf{H}\left(\mathbf{\Lambda}^+ - \mathbf{\Lambda}^-\right)\right) = 0 \qquad |x| < \infty \qquad (4.123)$$

From the condition $\mathbf{\Lambda}(\infty) = \mathbf{0}$ it derives:

$$\left[\mathbf{R}\right]_3\left(\mathbf{H}\mathbf{\Lambda}(x)\right) = 0 \qquad |x| < \infty \qquad (4.124)$$

On the crack edges one gets:

$$\sum_{k=1}^{3} R_{3k}\left[\mathbf{H}\right]_k \mathbf{\Lambda}^+(x) = 0 \qquad |x| < a$$

$$\sum_{k=1}^{3} R_{3k}\left[\mathbf{H}\right]_k \mathbf{\Lambda}^-(x) = 0 \qquad |x| < a \qquad (4.125)$$

Adding the components of equations (4.125) leads to the expression:

$$\sum_{k=1}^{3} R_{3k}\left[\mathbf{H}\right]_k\left(\mathbf{\Lambda}^+(x) + \mathbf{\Lambda}^-(x)\right) = 0 \qquad |x| < a \qquad (4.126)$$

Through the combination of relations (4.126) and (4.115) one obtains the equation:

$$-2iR_{31}\sigma_{xy}^\infty - 2iR_{32}\sigma_{yy}^\infty + 2iR_{33}(D_y^\circ - D_y^\infty) = 0 \qquad (4.127)$$

83

thus, the expression of the electric displacement results:

$$D_y^\circ = D_y^\infty + \frac{R_{31}\sigma_{xy}^\infty + R_{32}\sigma_{yy}^\infty}{R_{33}} \qquad (4.128)$$

Now it is possible to determine the stress intensity factor vector, defined by the relation (4.98). At the right crack tip from equation (4.111) it is:

$$\mathbf{t}_2(x,0) = D_y^\circ \mathbf{k} + \frac{x}{\sqrt{x^2 - a^2}}(\mathbf{t}_2^\infty - D_y^\circ \mathbf{k}) \qquad x > a \qquad (4.129)$$

and therefore:

$$\mathbf{K}_{perm}(a) = \begin{bmatrix} \sqrt{\pi a}\,\sigma_{xy}^\infty \\ \sqrt{\pi a}\,\sigma_{yy}^\infty \\ \sqrt{\pi a}(D_y^\infty - D_y^\circ) \end{bmatrix} = \begin{bmatrix} K_{II} \\ K_I \\ K_D \end{bmatrix} \qquad (4.130)$$

Relation (4.128) permits to find a link among the three components of stress intensity factor:

$$K_D = -\frac{R_{31}K_{II} + R_{32}K_I}{R_{33}} \qquad (4.131)$$

4.3.3. The semipermeable crack

For the semipermeable crack model, the boundary conditions coincide with those for the permeable one. They are:

$$\begin{aligned} \sigma_{yy}^+(x,0) = \sigma_{yy}^-(x,0) = 0 \\ \sigma_{xy}^+(x,0) = \sigma_{xy}^-(x,0) = 0 \end{aligned} \qquad |x| < a \qquad (4.132)$$

$$D_y^+(x,0) = D_y^-(x,0) = D_y^\circ = -\varepsilon_c \frac{\Delta\varphi(x,0)}{\Delta V(x,0)} \qquad |x| < \infty \qquad (4.133)$$

$$E_x^+(x,0) = E_x^-(x,0)$$

where ε_c is the dielectric constant, or permittivity, of the medium contained inside the crack cavity. $\Delta\varphi(x,0)$ and $\Delta V(x,0)$ can be obtained from equation (4.114) that, combined with (4.93), allows to calculate the discontinuity:

$$\Delta\mathbf{U} = \begin{bmatrix} \Delta U \\ \Delta V \\ \Delta\varphi \end{bmatrix} = 2\sqrt{a^2 - x^2}\,\mathbf{RJ} \qquad (4.134)$$

One gets:

$$\frac{\Delta\varphi(x,0)}{\Delta V(x,0)} = \frac{R_{31}\sigma_{xy}^{\infty} + R_{32}\sigma_{yy}^{\infty} + R_{33}\left(D_{y}^{\infty} - D_{y}^{\circ}\right)}{R_{21}\sigma_{xy}^{\infty} + R_{22}\sigma_{yy}^{\infty} + R_{23}\left(D_{y}^{\infty} - D_{y}^{\circ}\right)} \qquad |x| < a \qquad (4.135)$$

Substituting the latter expression into the first of equations (4.133):

$$D_{y}^{\circ} = -\varepsilon_{c}\frac{R_{31}\sigma_{xy}^{\infty} + R_{32}\sigma_{yy}^{\infty} + R_{33}\left(D_{y}^{\infty} - D_{y}^{\circ}\right)}{R_{21}\sigma_{xy}^{\infty} + R_{22}\sigma_{yy}^{\infty} + R_{23}\left(D_{y}^{\infty} - D_{y}^{\circ}\right)} \qquad (4.136)$$

a quadratic equation dependent on the unknown quantity D_{y}° is found:

$$R_{23}(D_{y}^{\circ})^{2} + \left(\varepsilon_{c}R_{33} - [\mathbf{R}]_{2}\,\mathbf{t}_{2}^{\infty}\right)D_{y}^{\circ} - \varepsilon_{c}\,[\mathbf{R}]_{3}\,\mathbf{t}_{2}^{\infty} = 0 \qquad (4.137)$$

One must choose the solution to the quadratic equation that gives rise to a real root (the value of D_{y}° must be a real number). Furthermore, the solution has to respect the condition $\Delta V > 0$; in other words it must result:

$$D_{y}^{\circ} < \frac{[\mathbf{R}]_{2}\,\mathbf{t}_{2}^{\infty}}{R_{23}} \qquad (4.138)$$

Now, one may notice that from relation (4.133)-1, in case of a purely electric applied load (i.e. $\sigma_{xy}^{\infty} = \sigma_{yy}^{\infty} = 0$), an inconsistency would rise: the electric displacement results $D_{y}^{\circ} = -\varepsilon_{c}\dfrac{R_{33}}{R_{23}}$, independent on the electric field applied, and this is clearly not reasonable. This derives from having considered the crack as one-dimensional, while it actually has a thickness. The problem can be overpassed by considering the flaw to have an elliptical shape (with a small b/a ratio); the relation deriving from this hypothesis is:

$$D_{y}^{\circ} = \frac{\varepsilon_{c}R_{33}}{\varepsilon_{c}R_{33} + b/a}D_{y}^{\infty} \qquad (4.139)$$

valid for $\mathbf{t}_{2}^{\infty} = (0,0,D_{y}^{\infty})$. If $\varepsilon_{c} = 0$ (impermeable crack) equation (4.139) gives $D_{y}^{\circ} = 0$; if $\varepsilon_{c} = \infty$ (permeable crack) it gives $D_{y}^{\circ} = D_{y}^{\infty}$.

4.4   Representation of the solution in polar coordinates

Allow a polar coordinate system (r,θ) with origin in the crack tip $x = a$, as represented in Fig. 4.4.
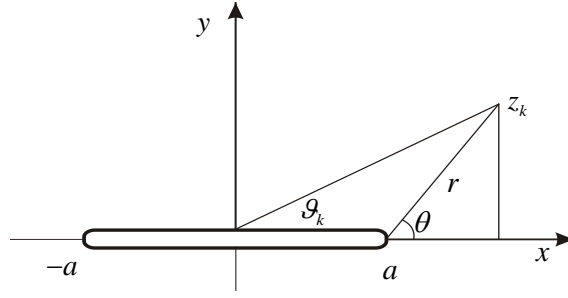
Fig. 4.4 – Relation between Cartesian and polar coordinates for a complex variable z

Operating a transformation from the complex coordinates defined in Section 4:

$$z_k = \xi_k + i\eta_k = x + \left(\frac{-p_k + iq_k}{p_k^2 + q_k^2}\right)y = x + \left(r_k + is_k\right)y \qquad k = 1,2,3 \qquad (4.140)$$

where:

$$r_k = \frac{-p_k}{p_k^2 + q_k^2} = \frac{-p_k}{\left|\lambda_k\right|^2}, \qquad s_k = \frac{q_k}{p_k^2 + q_k^2} = \frac{q_k}{\left|\lambda_k\right|^2}, \qquad (4.141)$$

to polar coordinates, one gets:

$$z_k = x + \left(r_k + is_k\right)y = \left(a + r\cos\theta\right) + \left(r_k + is_k\right)r\sin\theta =$$
$$= a\left\{1 + \frac{r}{a}\left[\cos\theta + r_k\sin\theta + is_k\sin\theta\right]\right\} \qquad k = 1,2,3 \qquad (4.142)$$

Allow the position:

$$\rho_k e^{i\vartheta_k} = \frac{r}{a}\left[\cos\theta + r_k\sin\theta + is_k\sin\theta\right] \qquad (4.143)$$

and consider the real and imaginary parts of the two complex number in equation (4.143) must be equal, in order to obtain the relations:

$$\rho_k\cos\vartheta_k = \frac{r}{a}\left[\cos\theta + r_k\sin\theta\right]$$
$$\rho_k\sin\vartheta_k = \frac{r}{a}s_k\sin\theta \qquad (4.144)$$

that, squared and summed, give:

$$\rho_k^2 = \left(\frac{r}{a}\right)^2\left[\cos^2\theta + r_k^2\sin^2\theta + 2r_k\cos\theta\sin\theta + s_k^2\sin^2\theta\right] =$$
$$= \left(\frac{r}{a}\right)^2\left[\cos^2\theta + r_k\sin 2\theta + \left(r_k^2 + s_k^2\right)\sin^2\theta\right] \qquad (4.145)$$

Now, posing:

$$\rho_k = \frac{r}{a}c_k(\theta) \qquad c_k(\theta) = \left[\cos^2\theta + r_k\sin 2\theta + \left(r_k^2 + s_k^2\right)\sin^2\theta\right]^{\frac{1}{2}} \qquad (4.146)$$

from equation (4.142) one can write:

$$z_k = a + rc_k(\theta)e^{i\vartheta_k} = a + \zeta_k \qquad k = 1,2,3 \qquad (4.147)$$

where:

$$\vartheta_k = \mathrm{tg}^{-1}\left(\frac{\sin\vartheta_k}{\cos\vartheta_k}\right) = \mathrm{tg}^{-1}\left(\frac{s_k\sin\theta}{\cos\theta + r_k\sin\theta}\right) \qquad (4.148)$$

and:

$$\zeta_k = rc_k(\theta)e^{i\vartheta_k} = z_k - a \qquad (4.149)$$

With the new variables, function $f(z_k)$ gets the aspect:

$$f(z_k) = \frac{z_k}{\sqrt{z_k^2 - a^2}} = \frac{a + \zeta_k}{\sqrt{\zeta_k}\sqrt{2a + \zeta_k}} = \frac{a + \zeta_k}{\sqrt{2a\zeta_k}\sqrt{1 + \dfrac{\zeta_k}{2a}}} \qquad (4.150)$$

The Taylor series of $\left(1 + \dfrac{\zeta_k}{2a}\right)^{-\frac{1}{2}}$ in the interval $\left|\dfrac{\zeta_k}{2a}\right| < 1$, up to the second term,

results:

$$\left(1 + \frac{\zeta_k}{2a}\right)^{-\frac{1}{2}} = 1 - \frac{1}{2}\left(\frac{\zeta_k}{2a}\right) + \dots \qquad (4.151)$$

thus:

$$f(z_k) = \frac{a + \zeta_k}{\sqrt{2a\zeta_k}}\left(1 - \frac{\zeta_k}{4a}\right) = \left(\sqrt{\frac{a}{2\zeta_k}} + \sqrt{\frac{\zeta_k}{2a}}\right)\left(1 - \frac{\zeta_k}{4a}\right) \qquad (4.152)$$

For $\left|\zeta_k/2a\right| \ll 1$, that is, in the vicinity of the crack tip, the following approximation is valid:

$$f(z_k) = \sqrt{\frac{a}{2\zeta_k}} - \frac{1}{4}\sqrt{\frac{\zeta_k}{2a}} + \sqrt{\frac{\zeta_k}{2a}} - \frac{1}{4}\sqrt{\frac{\zeta_k}{2a}}\frac{\zeta_k}{a} \cong$$

$$\cong \sqrt{\frac{a}{2\zeta_k}} = \sqrt{\frac{a}{2rc_k(\theta)}}e^{-i\frac{\vartheta_k}{2}} = \sqrt{\frac{a}{2rc_k(\theta)}}\left(\cos\frac{\vartheta_k}{2} - i\sin\frac{\vartheta_k}{2}\right) = f_k(r,\theta) \qquad (4.153)$$

The same reasoning can be applied to $h(z_k)$:

$$h(z_k) = \sqrt{z_k^2 - a^2} = \sqrt{2a\zeta_k}\sqrt{1 + \frac{\zeta_k}{2a}} \cong$$

$$\cong \sqrt{2a\zeta_k} = \sqrt{2arc_k(\theta)}e^{i\frac{\vartheta_k}{2}} = \sqrt{2arc_k(\theta)}\left(\cos\frac{\vartheta_k}{2} + i\sin\frac{\vartheta_k}{2}\right) = h_k(r,\theta) \qquad (4.154)$$

Substituting equations (4.153) and (4.154) respectively into the expressions of generalized stresses and displacements, one gets their representations at the crack tip.

For the impermeable crack case, considering $\mathbf{K}_{\mathrm{imp}}(a) = \sqrt{\pi a}\,\mathbf{t}_2^\infty$, one obtains for the stress vectors from equations (4.83) and (4.84):

$$\mathbf{t}_2 = \mathrm{Re}\left\{\mathbf{H}\left[\mathbf{diag}\left[\sqrt{\frac{a}{2rc_k(\theta)}}e^{-i\frac{\vartheta_k}{2}}\right]\right]\mathbf{H}^{-1}\right\}\mathbf{t}_2^\infty = \mathrm{Re}\left\{\mathbf{H}\left[\mathbf{diag}\left[\frac{e^{-i\frac{\vartheta_k}{2}}}{\sqrt{c_k(\theta)}}\right]\right]\mathbf{H}^{-1}\right\}\sqrt{\frac{a}{2r}}\mathbf{t}_2^\infty =$$

$$= \frac{1}{\sqrt{2\pi r}}\mathrm{Re}\left\{\mathbf{H}\left[\mathbf{diag}\left[\frac{e^{-i\frac{\vartheta_k}{2}}}{\sqrt{c_k(\theta)}}\right]\right]\mathbf{H}^{-1}\right\}\mathbf{K}_{\mathrm{imp}}(a)$$

$$(4.155)$$

$$\mathbf{t}_1 = \mathbf{t}_1^\infty - \mathrm{Re}\left[\mathbf{GH}^{-1}\right]\mathbf{t}_2^\infty + \mathrm{Re}\left\{\mathbf{G}\left[\mathbf{diag}\left[\frac{z_k}{\sqrt{z_k^2 - a^2}}\right]\right]\mathbf{H}^{-1}\right\}\mathbf{t}_2^\infty =$$

$$= \mathbf{t}_1^\infty - \mathrm{Re}\left[\mathbf{GH}^{-1}\right]\mathbf{t}_2^\infty + \mathrm{Re}\left\{\mathbf{G}\left[\mathbf{diag}\left[\sqrt{\frac{a}{2rc_k(\theta)}}e^{-i\frac{\vartheta_k}{2}}\right]\right]\mathbf{H}^{-1}\right\}\mathbf{t}_2^\infty$$

$$(4.156)$$

and for the generalized displacement vector, from equation (4.89):

$$\frac{\mathbf{U}}{a} = \frac{\mathbf{U}^\infty}{a} + \mathrm{Re}\left\{\mathbf{E}\,\mathbf{diag}\left[\sqrt{\frac{2r}{a}c_k(\theta)}e^{i\frac{\vartheta_k}{2}}\right]\mathbf{H}^{-1}\right\}\mathbf{t}_2^\infty - \mathrm{Re}\left\{\mathbf{E}\,\mathbf{diag}\left[1+\frac{r}{a}c_k(\theta)e^{i\vartheta_k}\right]\mathbf{H}^{-1}\right\}\mathbf{t}_2^\infty$$

$$(4.157)$$

that, neglecting a rigid displacement and considering that $\sqrt{r/a}$ predominates r/a when $r/a \ll 1$, can be approximated as:

$$\mathbf{U} = \mathrm{Re}\left\{\mathbf{E}\,\mathbf{diag}\left[\sqrt{2rac_k(\theta)}e^{i\frac{\vartheta_k}{2}}\right]\mathbf{H}^{-1}\right\}\mathbf{t}_2^\infty = \sqrt{\frac{2r}{\pi}}\mathrm{Re}\left\{\mathbf{E}\,\mathbf{diag}\left[\sqrt{c_k(\theta)}e^{i\frac{\vartheta_k}{2}}\right]\mathbf{H}^{-1}\right\}\mathbf{K}_{\mathrm{imp}}(a)$$

$$(4.158)$$

For the permeable and semipermeable crack cases, developments are formally equal, keeping present the different expression of the stress intensity factor vector (4.130). From relations (4.111) and (4.112):

$$\mathbf{t}_2 = D_y\mathbf{k} + \mathrm{Re}\left\{\mathbf{H}\left[\mathbf{diag}\left[\sqrt{\frac{a}{2rc_k(\theta)}}e^{-i\frac{\vartheta_k}{2}}\right]\right]\mathbf{H}^{-1}\right\}\mathbf{J} = D_y\mathbf{k} + \mathrm{Re}\left\{\mathbf{H}\left[\mathbf{diag}\left[\frac{e^{-i\frac{\vartheta_k}{2}}}{\sqrt{c_k(\theta)}}\right]\right]\mathbf{H}^{-1}\right\}\sqrt{\frac{a}{2r}}\mathbf{J} =$$

$$= D_y^{\circ}\mathbf{k} + \frac{1}{\sqrt{2\pi r}}\,\mathrm{Re}\left\{\mathbf{H}\left[\mathbf{diag}\left[\frac{e^{-i\frac{\vartheta_k}{2}}}{\sqrt{c_k(\theta)}}\right]\right]\mathbf{H}^{-1}\right\}\mathbf{K}_{\mathrm{perm}}(a) \qquad (4.159)$$

$$\mathbf{t}_1 = \mathbf{t}_1^{\infty} - \mathrm{Re}\left[\mathbf{GH}^{-1}\right]\mathbf{J} + \mathrm{Re}\left\{\mathbf{G}\left[\mathbf{diag}\left[\sqrt{\frac{a}{2rc_k(\theta)}}\,e^{-i\frac{\vartheta_k}{2}}\right]\right]\mathbf{H}^{-1}\right\}\mathbf{J} =$$

$$= \mathbf{t}_1^{\infty} - \mathrm{Re}\left[\mathbf{GH}^{-1}\right]\mathbf{J} + \mathrm{Re}\left\{\mathbf{G}\left[\mathbf{diag}\left[\frac{e^{-i\frac{\vartheta_k}{2}}}{\sqrt{c_k(\theta)}}\right]\right]\mathbf{H}^{-1}\right\}\sqrt{\frac{a}{2r}}\,\mathbf{J} =$$

$$= \mathbf{t}_1^{\infty} - \mathrm{Re}\left[\mathbf{GH}^{-1}\right]\mathbf{t}_2^{\infty} + \mathrm{Re}\left\{\mathbf{G}\left[\mathbf{diag}\left[\frac{e^{-i\frac{\vartheta_k}{2}}}{\sqrt{c_k(\theta)}}\right]\right]\mathbf{H}^{-1}\right\}\frac{\mathbf{K}_{\mathrm{perm}}(a)}{\sqrt{2\pi r}} \qquad (4.160)$$

and from relation (4.114):

$$\mathbf{U} = \sqrt{\frac{2r}{\pi}}\,\mathrm{Re}\left\{\mathbf{E}\,\mathbf{diag}\left[\sqrt{c_k(\theta)}\,e^{i\frac{\vartheta_k}{2}}\right]\mathbf{H}^{-1}\right\}\mathbf{K}_{\mathrm{perm}}(a) \qquad (4.161)$$

Note in the expressions of stress components that also non-singular terms are included: they affect only the collinear stress component σ_{xx}. In fact, the generalized stress vector $\mathbf{t}_2$ is proportional to the inverse of the square root of the distance r from the crack tip, while the generalized stress vector $\mathbf{t}_1$ is composed of a part dependent on the ratio $\sqrt{1/r}$, that is on the position of the point where stresses are calculated, as well as of the terms $\mathbf{t}_1^{\infty}$ (later in the text referred to as NST 1) and $-\mathrm{Re}\left[\mathbf{GH}^{-1}\right]\mathbf{t}_2^{\infty}$ (referred to as NST 2), which are constant given the remote loading and the material characteristics.

It is clear that, the closer to the crack tip one calculates the fields, i.e. the smaller r is, the bigger the importance of the term where r appears at the denominator (inverse square root singularity) will be compared to that of the other terms (non-singular terms). For this reason, in many previous works the influence of non-singular terms has been neglected, and the asymptotic term only has been used to represent the generalized stress vector $\mathbf{t}_1$:

$$\mathbf{t}_1 = \mathrm{Re}\left\{\mathbf{G}\left[\mathbf{diag}\left[\frac{e^{-i\frac{\vartheta_k}{2}}}{\sqrt{c_k(\theta)}}\right]\right]\mathbf{H}^{-1}\right\}\frac{\mathbf{K}(a)}{\sqrt{2\pi r}} \qquad (4.162)$$

Such an approximation holds only in the very proximity of the crack tip, and totally omits considering the influence of the stress collinear to the crack line. In other words, it neglects the biaxiality of the applied load [14-19]. We will examine further in this thesis (Chapter 5) the influence that non-singular terms exert on the fracture quantities and on the crack extension.

To avoid the stress singularity at the crack tip, stresses must be calculated at some small radial distance r from the end of the crack. Such a distance $0 < r \ll 1$ can be seen as "critical" for the material under study. This problem is bypassed in the asymptotic representation since all the involved quantities are proportional to the factor $\sqrt{a/2r}$, and thus it is not necessary to specify its value. On the contrary, the non-singular representation cannot prescind from the determination of the ratio r/a. In accordance with many related works (see [14-19] and, about the extension of the fracture process zone in ferroelectrics, Ricoeur and Kuna [20]), a characteristic dimensionless distance $r/a = 10^{-2}$ has been taken into account. In some of the numerical applications, results obtained for this distance value have been compared with others obtained for the ratio $r/a = 10^{-1}$.

References

[1]   Viola E., Boldrini C., Tornabene F., *Non singular term effect on the fracture quantities of a crack in a piezoelectric medium.* Engng. Fract. Mech. (2008); 75: 4542-4567.

[2]   Boldrini C., Viola E., *Crack energy density of a piezoelectric material under general electromechanical loading,* Theor. Appl. Fract. Mech. (2008); 49: 321-333.

[3]   Boldrini C., Tornabene F., Viola E., *Analytical formulation by means of complex potentials of crack models in a piezoelectric material,* Convegno Materiali e Metodi Innovativi nell'Ingegneria Strutturale, Catania, 4-6 Luglio 2007.

[4]   Piva A., *An alternative approach to elastodynamic crack problems in an orthotropic medium,* Quart. Appl. Maths. (1987); 45:97-104.

[5]   Piva A., Viola E. *Crack propagation in an orthotropic medium,* Engng. Fract. Mech. (1988); 29:535-548.

[6]   Viola E., Piva A., Radi E., *Crack propagation in an orthotropic medium under general loading,* Engng. Fract. Mech. (1989); 34:1155-1174.

[7]   Stroh A.N., *Dislocations and cracks in anisotropic elasticity,* Philos. Mag. (1958); 3: 625-646.

[8]   Ting T.C.T., *Anisotropic Elasticity, Theory and Applications,* Oxford University Press, N.Y. (1996).

[9]   Qin Q.H., *Fracture Mechanics of Piezoelectric Materials,* Wit Press, Southampton, 2001.

[10]   Muskhelishvili N.I., *Some basic problems of the mathematical theory of elasticity,* Noordhoof, Groningen (1952).

[11]   Lekhnitskii S.G., *Theory of Elasticity of an Anisotropic Body,* Mir Publishers, Moscow (1977).

[12]   Viola, E., Piva, A., Hasan, W.,. *Metodi analitici per la soluzione di problemi al contorno in elasticità piana. Parte II. Problemi di Hilbert e sue applicazioni.* Nota tecnica, DISTART, sez. Scienza delle Costruzioni, Facoltà di Ingegneria, Università di Bologna (1996).

[13]   Suo Z., Kuo C.M., Barnett D.M., Willis J.R., *Fracture mechanics for piezoelectric ceramics,* J. Mech. Phys. Solids (1992); 40: 739-765.

[14]   Carpinteri A., Di Tommaso A., Viola E., *Collinear stress effect on the crack branching phenomenon,* Matériaux et Constructions, RILEM (1979); 12:439-446.

[15]   Piva A., Viola E., *Biaxial load effects on a crack between dissimilar media,* Engng. Fract. Mech. (1980); 13:143-174.

[16]   Viola E., Piva A., *Fracture behaviour by two cracks around an elliptic rigid inclusion,* Engng. Fract. Mech. (1981); 15:303-325

[17]   Eftis J., Jones D.L., *Influence of load biaxiality on the fracture load of centre cracked sheets,* Int. J. Fract. (1982); 20:267-289.

[18]   Eftis J., Jones D.L., Liebowitz H., *Load biaxiality and fracture: synthesis and summary,* Engng. Fract. Mech. (1990); 36:537-574.

[19]   Carloni C., Piva A., Viola E., *An alternative complex variable formulation for an inclined crack in an orthotropic medium,* Engng. Fract. Mech. (2003); 70:2033-2058.

[20]   Ricoeur A., Kuna M., *A micromechanical model for the fracture process zone in ferroelectrics,* Comp. Mat. Science. (2003); 27:235-249.

CHAPTER 5

REPRESENTATION OF RESULTS – NUMERICAL

APPLICATIONS

5.1   Representations of stress and displacement fields

In this section graphic representations of the principal fracture quantities are shown, under various remote loading conditions and parameters. We will refer to PZT-4 and PZT-5H piezoelectric ceramics, whose elastic, piezoelectric and dielectric constants are reported in Table 5.1 and Table 5.2 respectively, and to the impermeable crack model. Furthermore, with a view to experiments, where it is easier to impose an electric field in the medium than an electric displacement field, the electric loading E_x^∞ and E_y^∞ instead of D_x^∞ and D_y^∞ will be considered. The relation between the two far-field electric loadings, for impermeable case, is as follows:

$$D_x^\infty = \frac{1}{c_{44}}\left\{e_{15}\sigma_{xy}^\infty + \varepsilon_{11}\mu E_x^\infty\right\} \tag{5.1}$$

$$D_y^\infty = \frac{1}{\Delta}\left\{\left(e_{31}c_{33} - e_{33}c_{13}\right)\sigma_{xx}^\infty + \left(e_{33}c_{11} - e_{31}c_{13}\right)\sigma_{yy}^\infty + \left[\left(e_{31}^2 c_{33} + e_{33}^2 c_{11} - 2e_{31}e_{33}c_{13}\right) + \varepsilon_{33}\Delta\right]E_y^\infty\right\} \tag{5.2}$$

where:

$$\mu = c_{44} + \frac{e_{15}^2}{\varepsilon_{11}} \tag{5.3}$$

and

$$\Delta = c_{11}c_{33} - c_{13}^2 \tag{5.4}$$
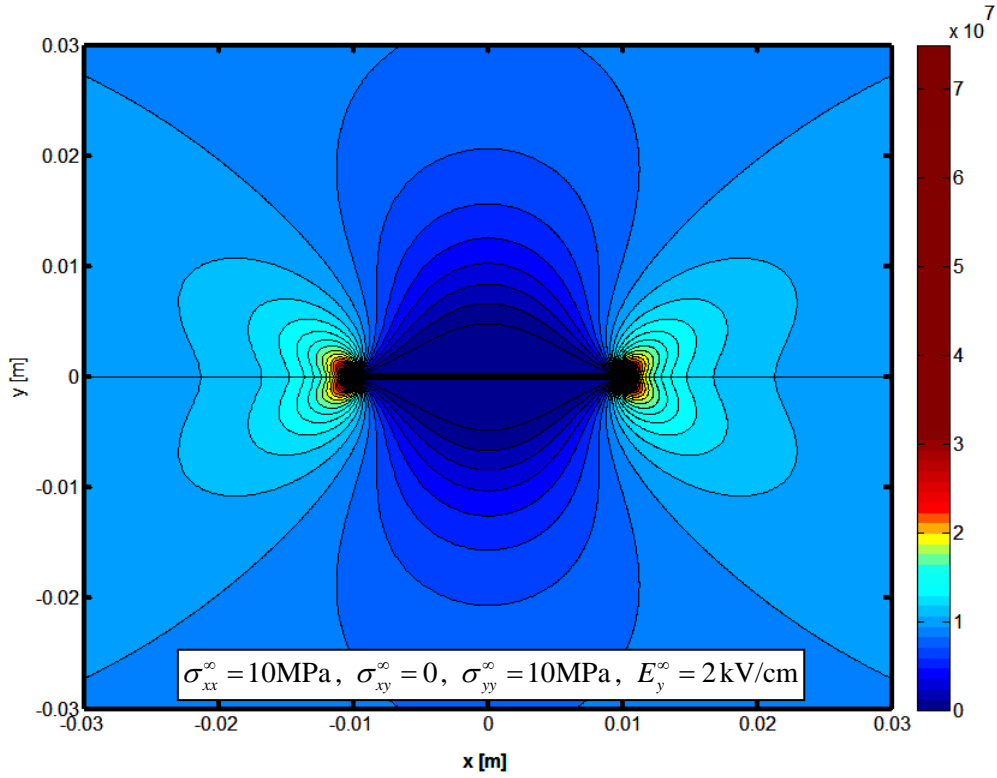
Fig. 5.1 – Field of the stress component σ_{yy} in the vicinity of the crack (values in Pa)
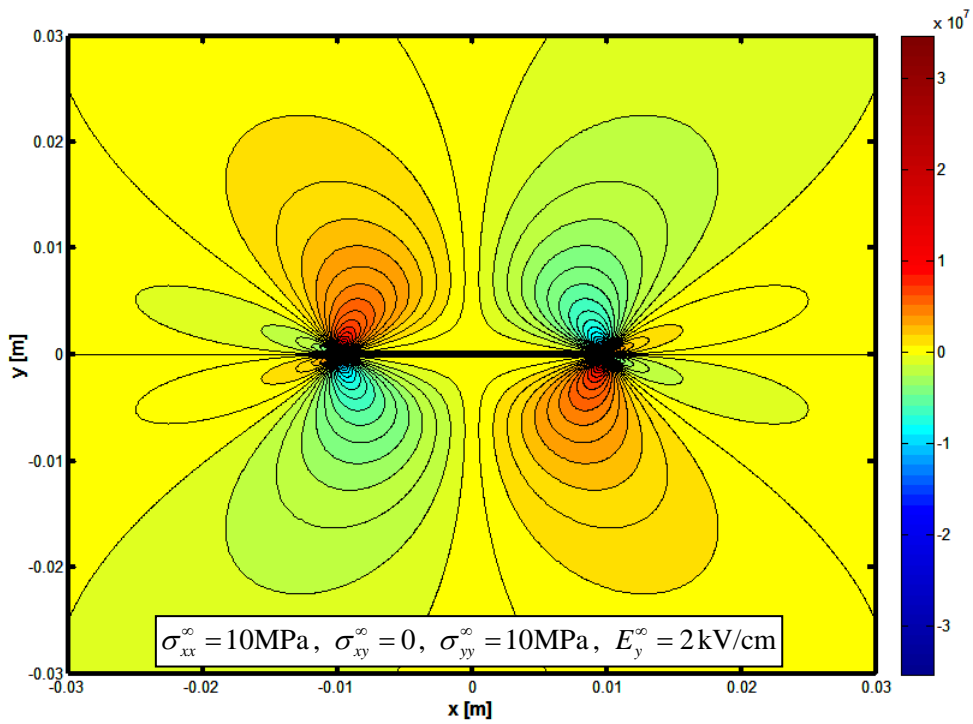
Fig. 5.2 – Field of the stress component σ_{xy} in the vicinity of the crack (values in Pa)

94
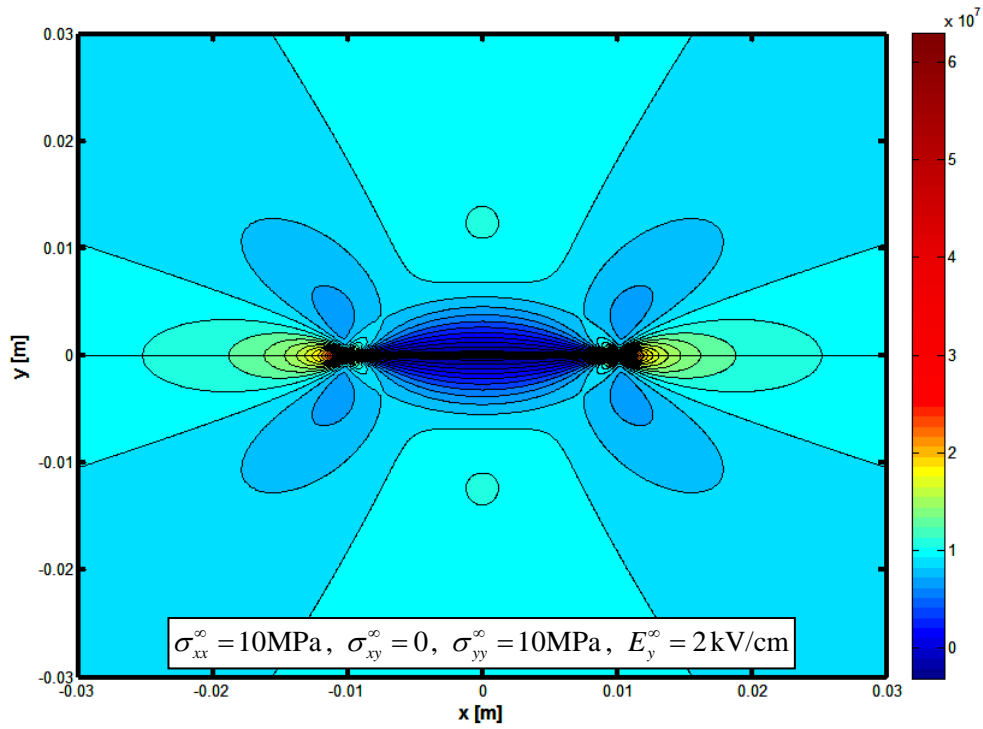
Fig. 5.3 – Field of the stress component σ_{xx} in the vicinity of the crack (values in Pa)
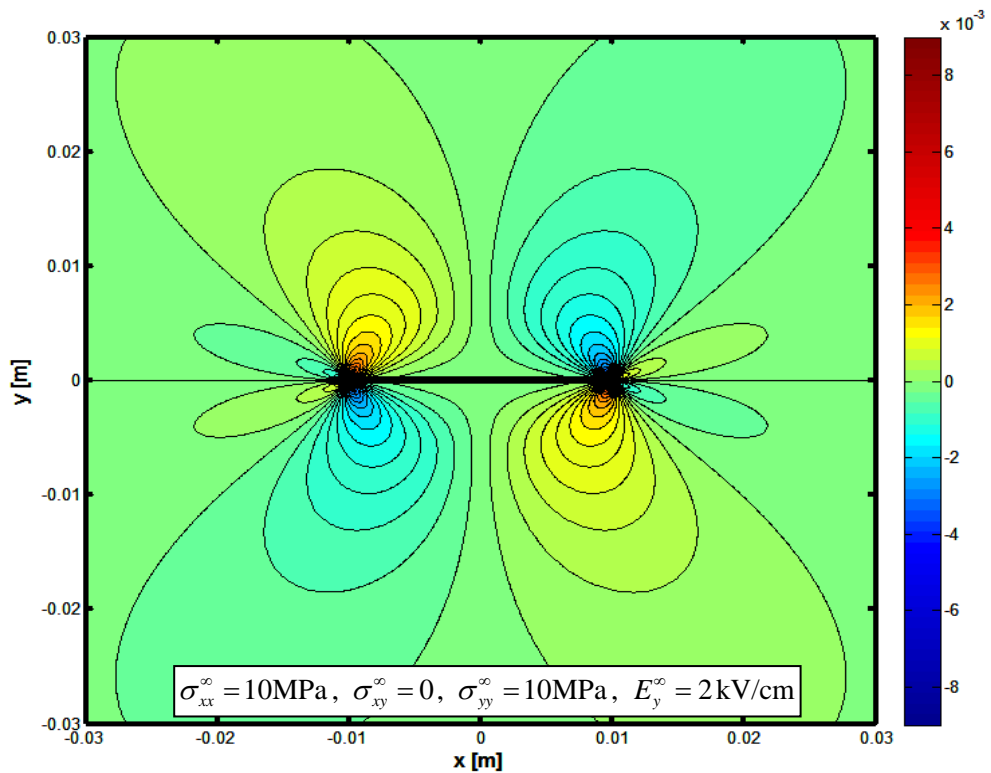
Fig. 5.4 – Field of the electric displacement component D_x in the vicinity of the crack (values in C/m²)
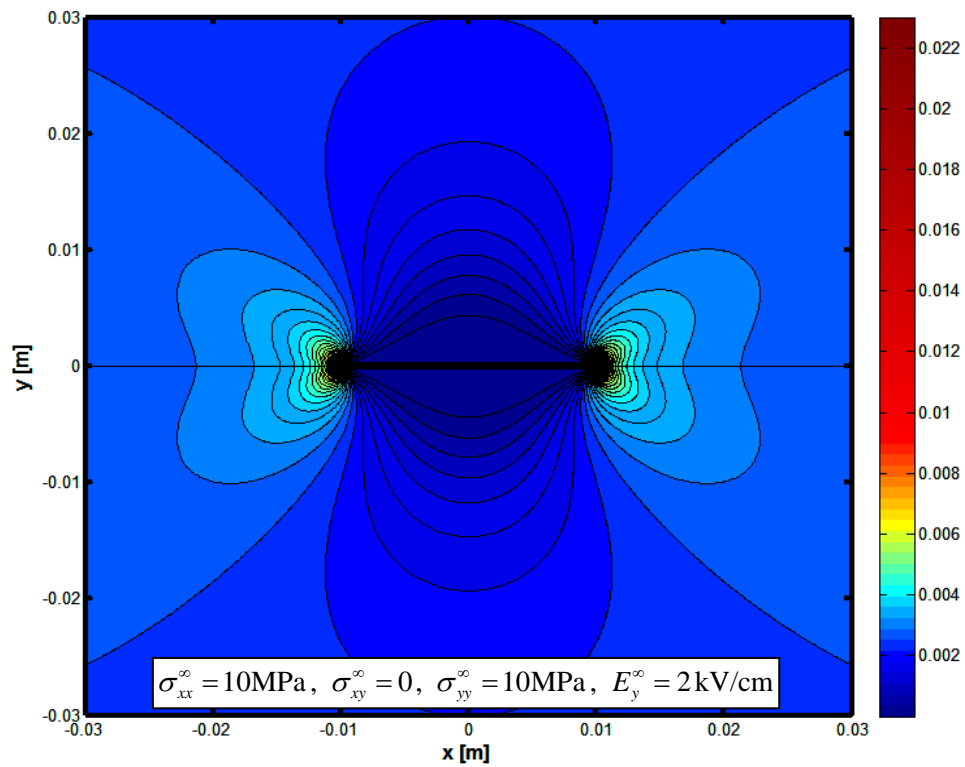
Fig. 5.5 – Field of the electric displacement component D_y in the vicinity of the crack (values in C/m²)
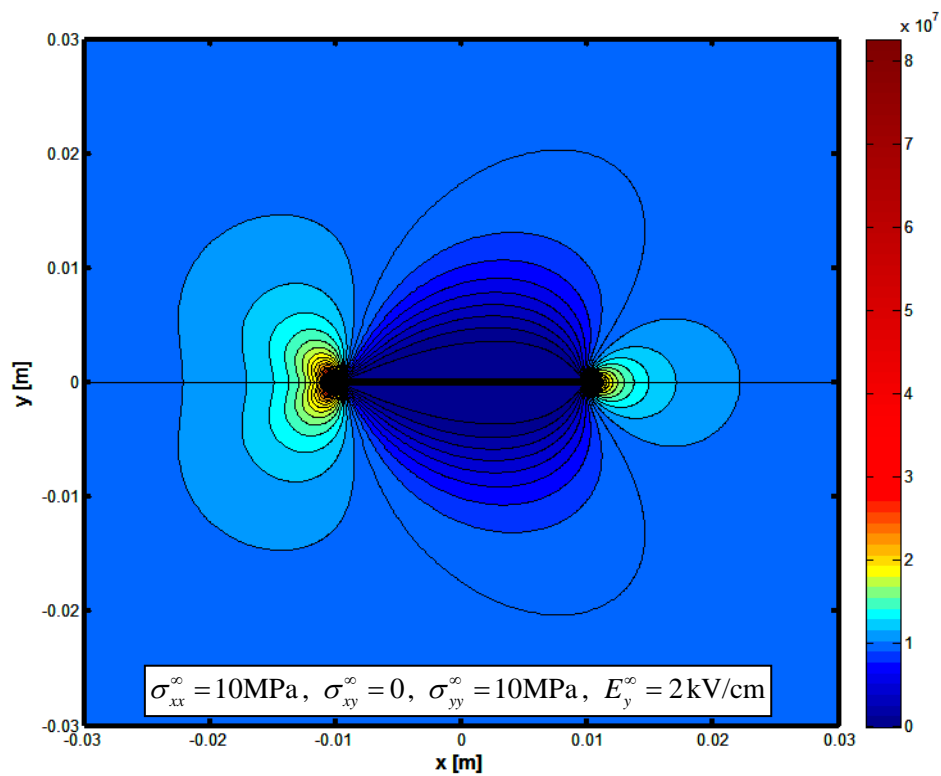
Fig. 5.6 – Field of the hoop stress $\sigma_{\theta\theta}$ in the vicinity of the crack (values in Pa)
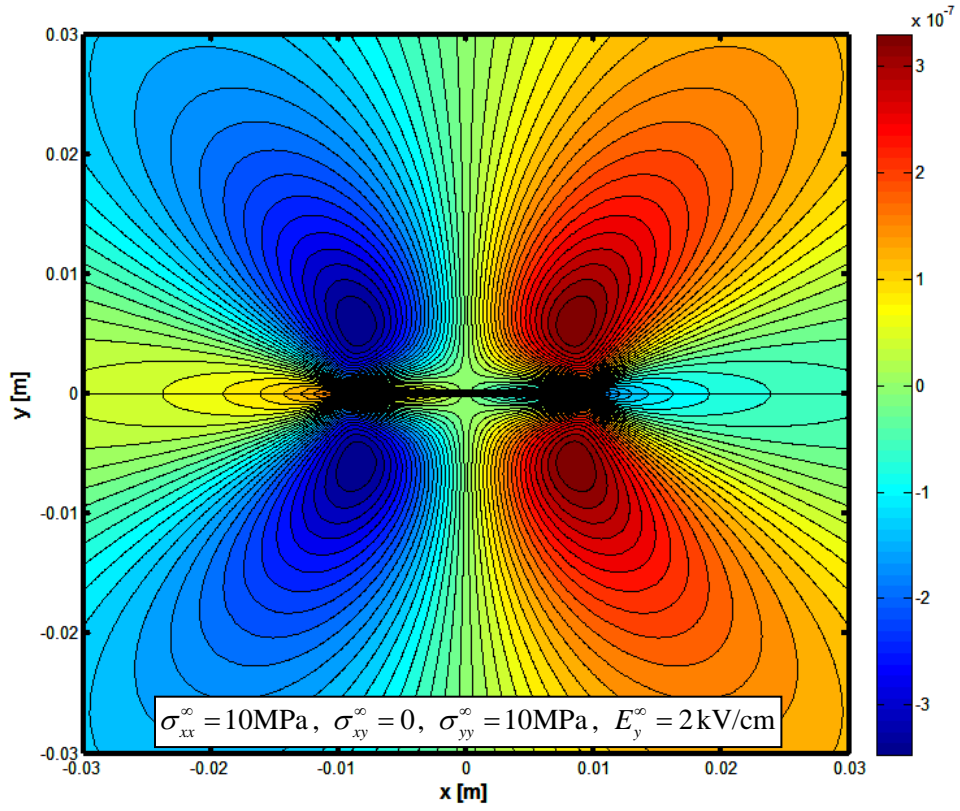
Fig. 5.7 – Field of the displacement u in the vicinity of the crack (values in m)
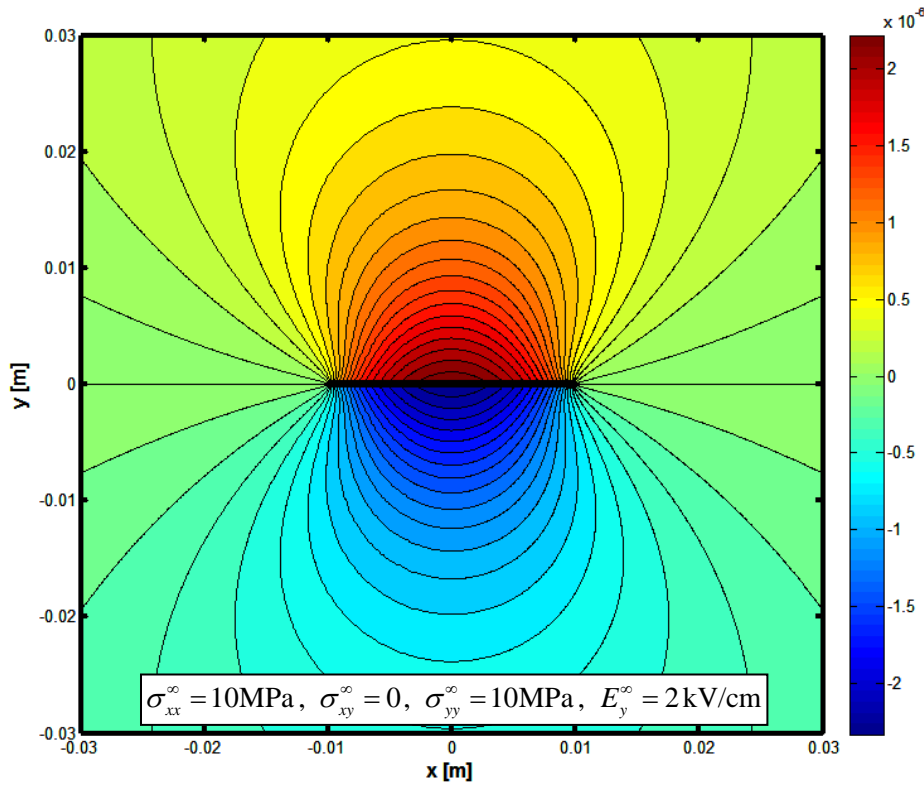
Fig. 5.8 – Field of the displacement v in the vicinity of the crack (values in m)
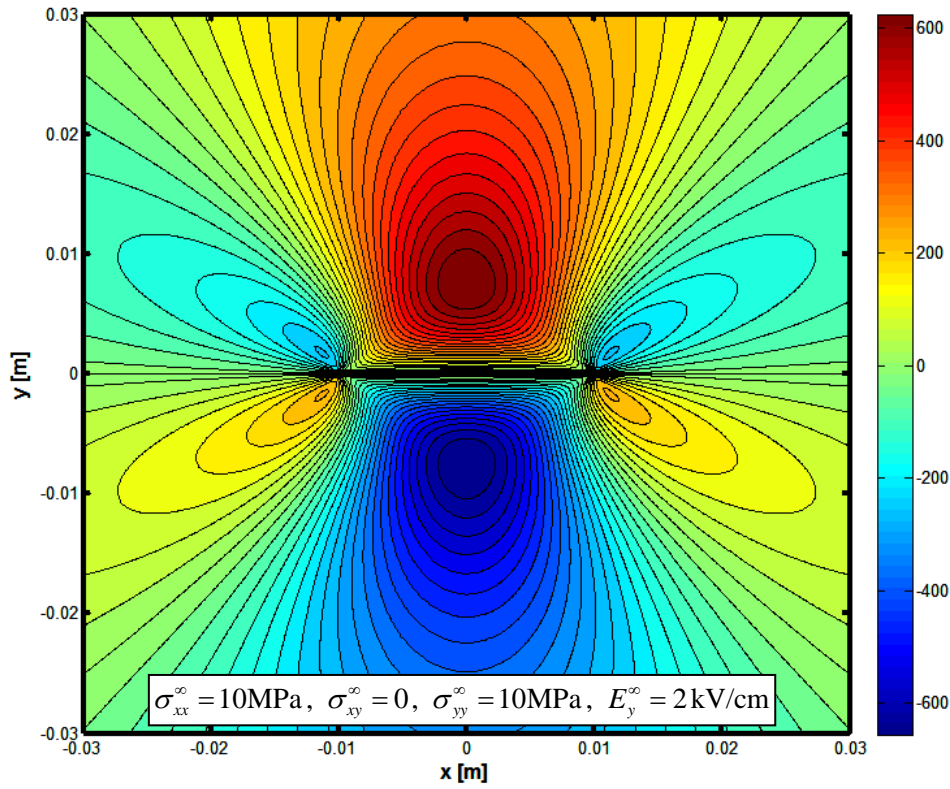
Fig. 5.9 – Field of the electric potential ϕ in the vicinity of the crack (values in V)

$\sigma_{xx}^{\infty} = 10\,\text{MPa}$, $\sigma_{xy}^{\infty} = 0$, $\sigma_{yy}^{\infty} = 10\,\text{MPa}$, $E_y^{\infty} = 2\,\text{kV/cm}$
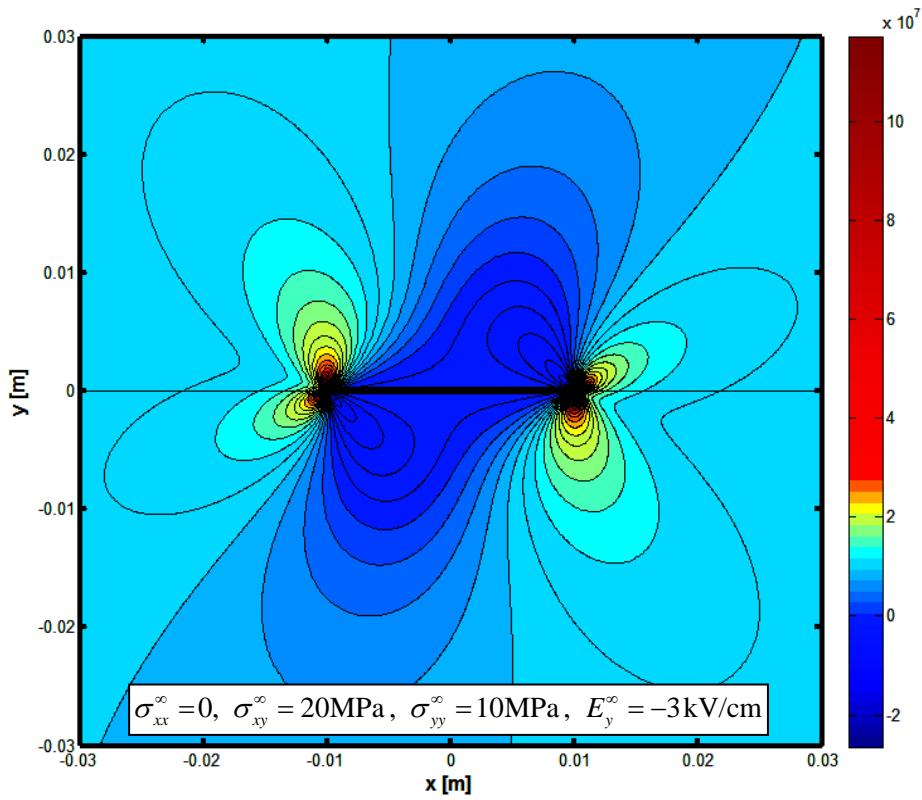
Fig. 5.10 – Stress component σ_{yy}, asymmetric loading conditions (values in Pa)

$\sigma_{xx}^{\infty} = 0$, $\sigma_{xy}^{\infty} = 20\,\text{MPa}$, $\sigma_{yy}^{\infty} = 10\,\text{MPa}$, $E_y^{\infty} = -3\,\text{kV/cm}$
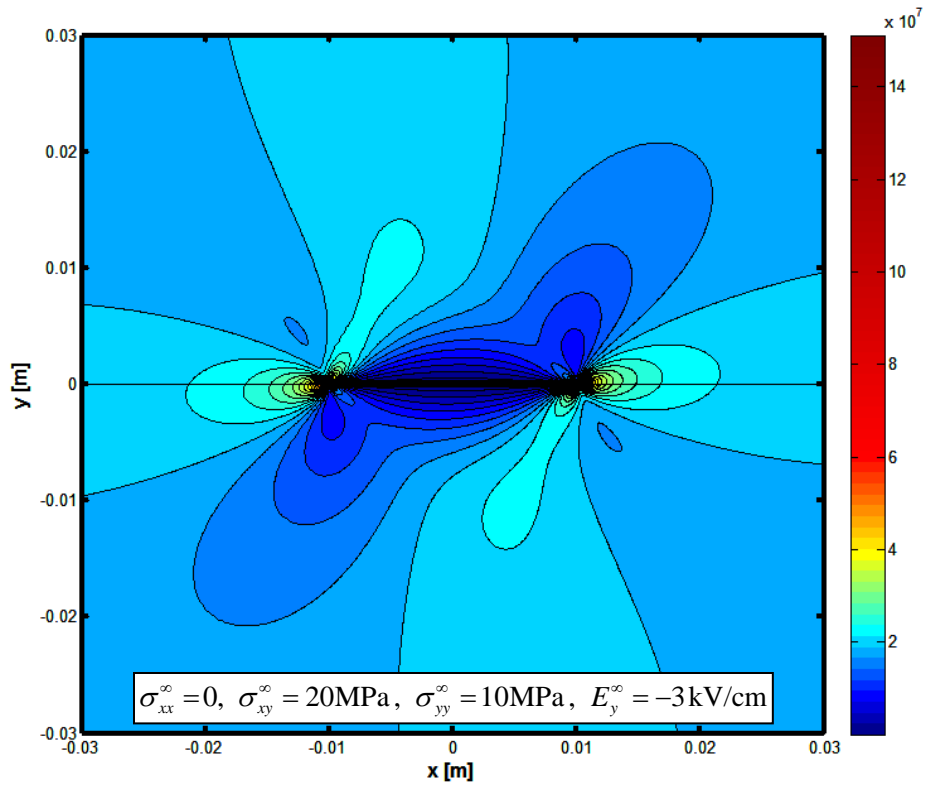
Fig. 5.11 – Stress component σ_{xy}, asymmetric loading conditions (values in Pa)
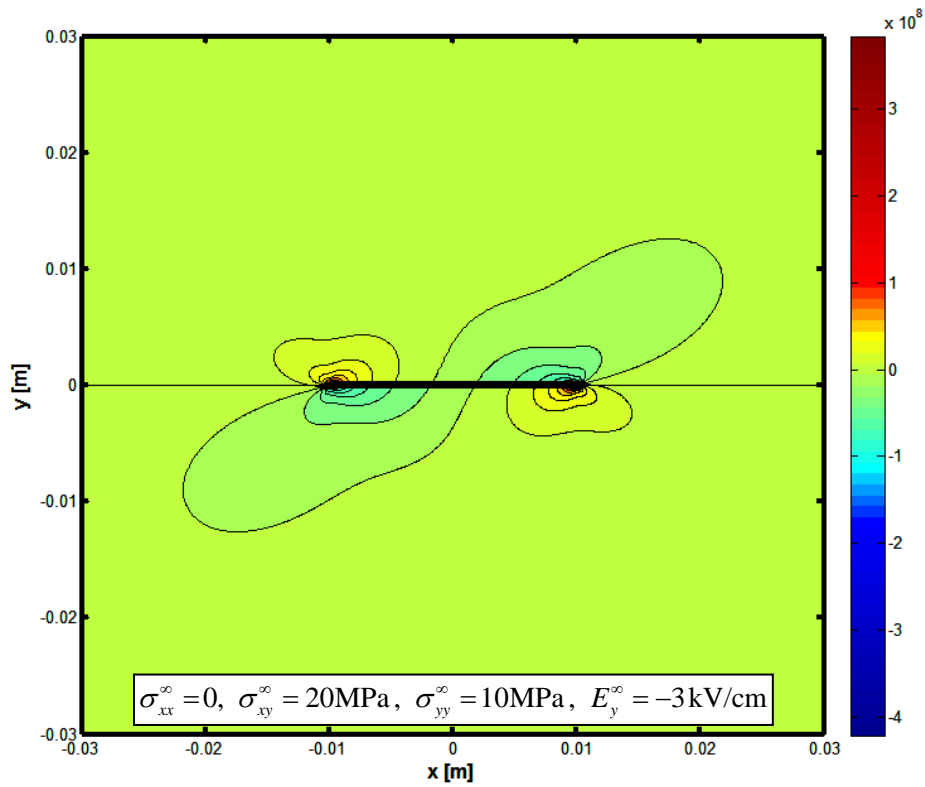
Fig. 5.12 – Stress component σ_{xx}, asymmetric loading conditions (values in Pa)
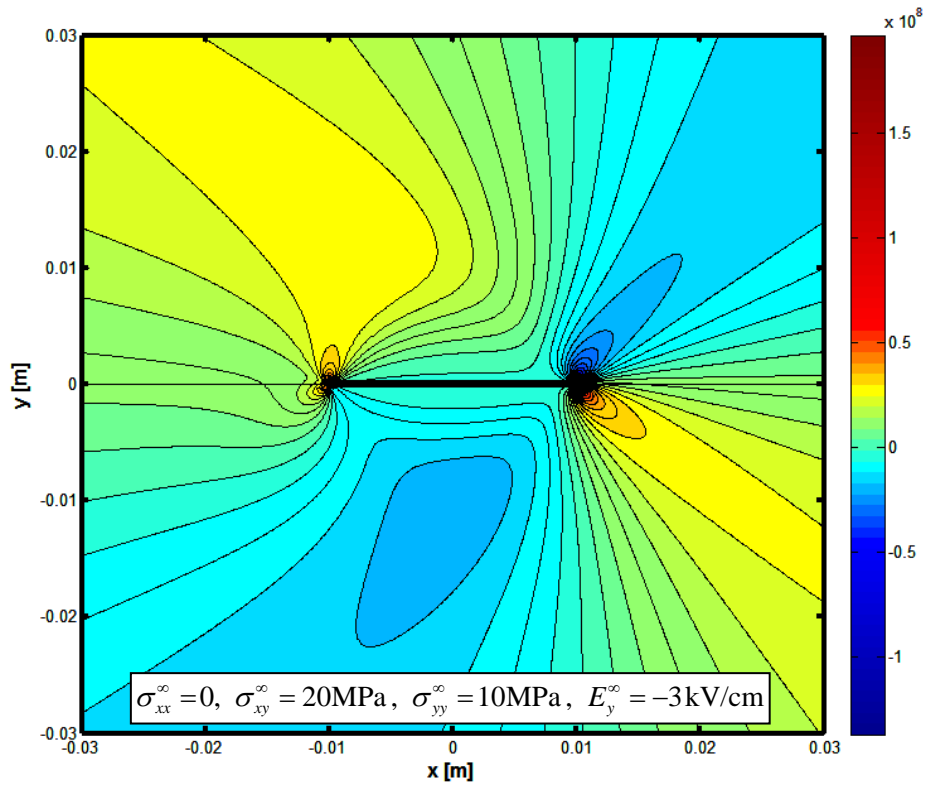
Fig. 5.13 – Field of the hoop stress $\sigma_{\theta\theta}$, asymmetric loading conditions (values in Pa)
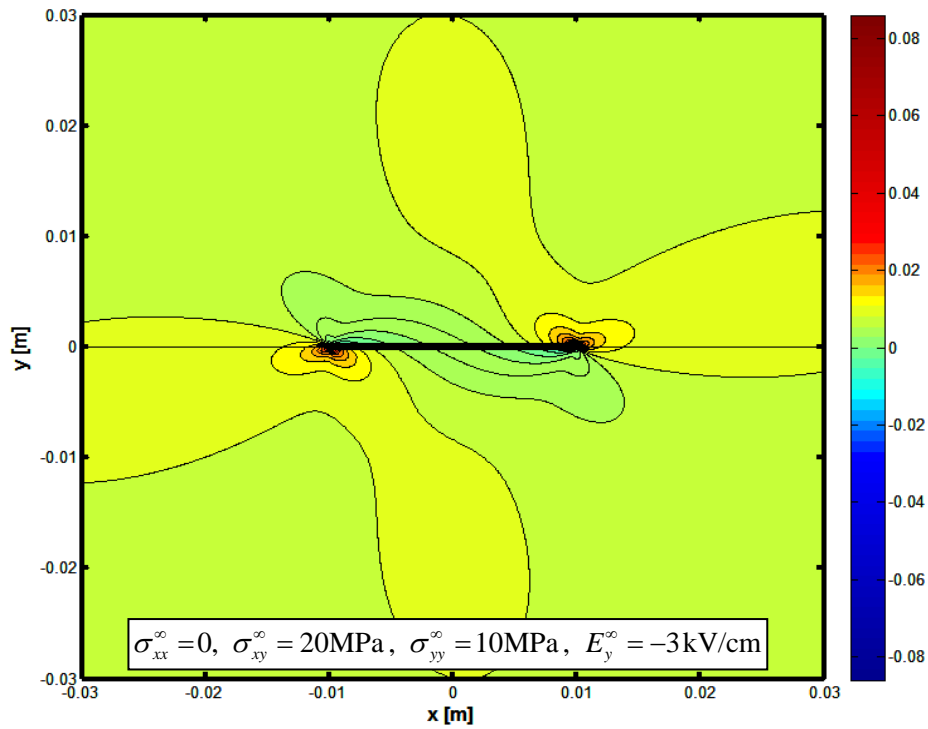
Fig. 5.14 – Field of the electric displacement D_x, asymmetric loading conditions (values in C/m²)

100
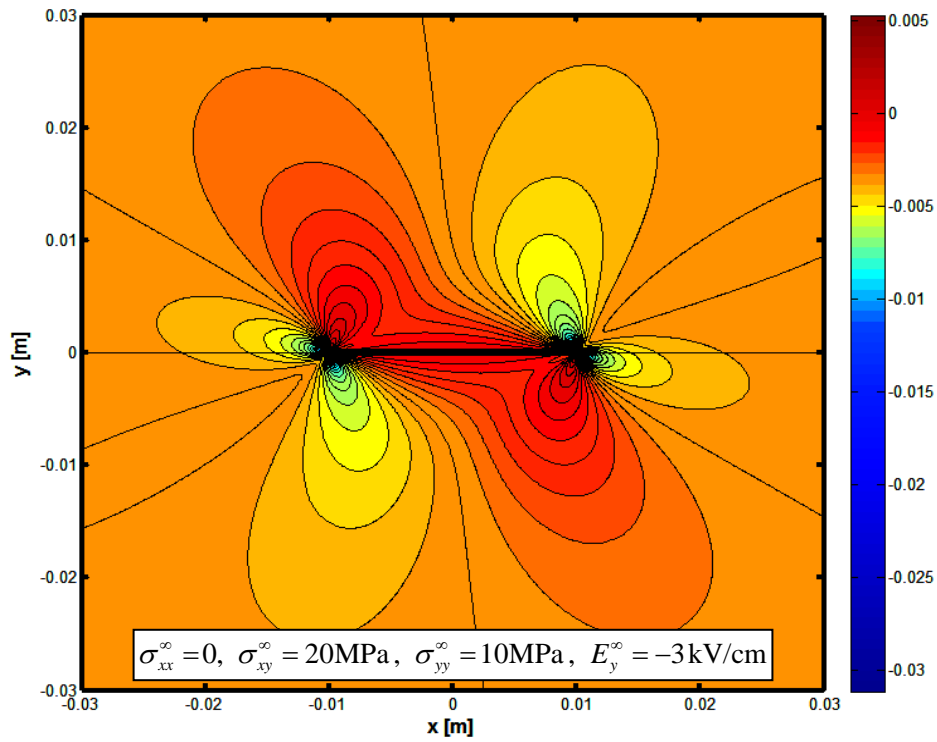
Fig. 5.15 – Field of the electric displacement D_y, asymmetric loading conditions (values in C/m²)
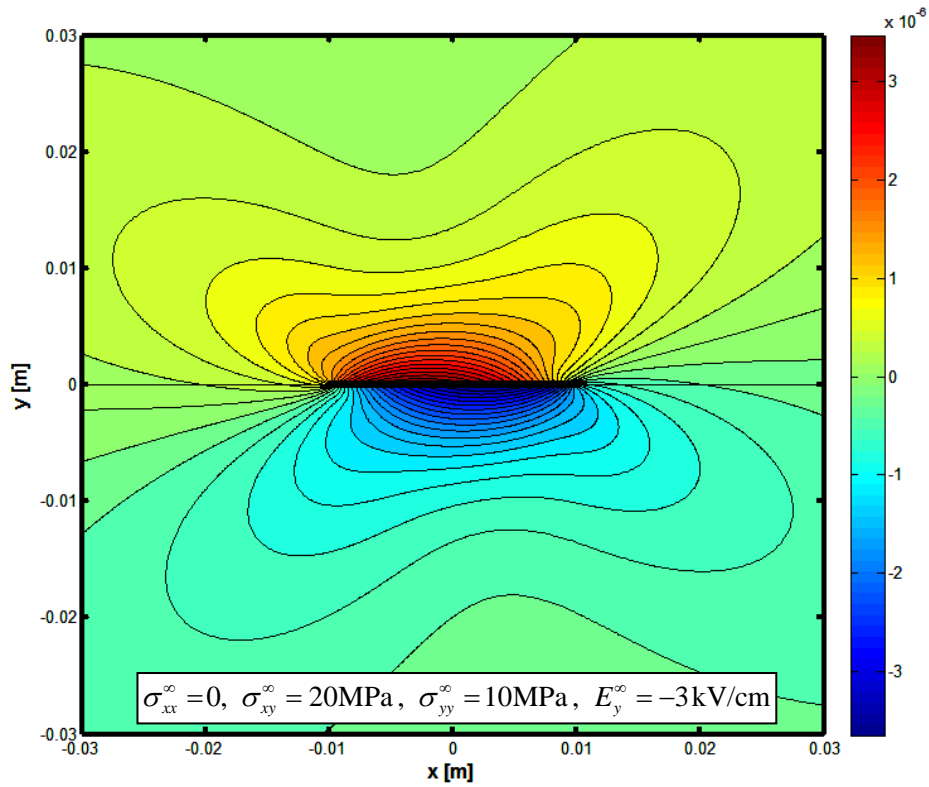
Fig. 5.16 – Field of the displacement u, asymmetric loading conditions (values in m)
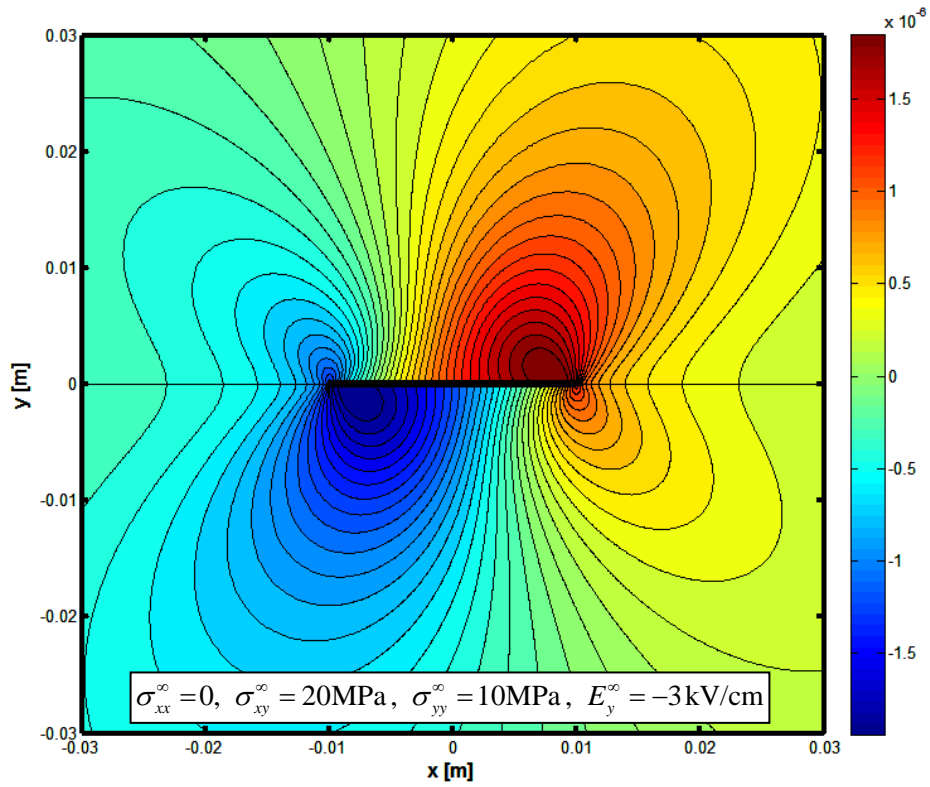
Fig. 5.17 – Field of the displacement v , asymmetric loading conditions (values in m)
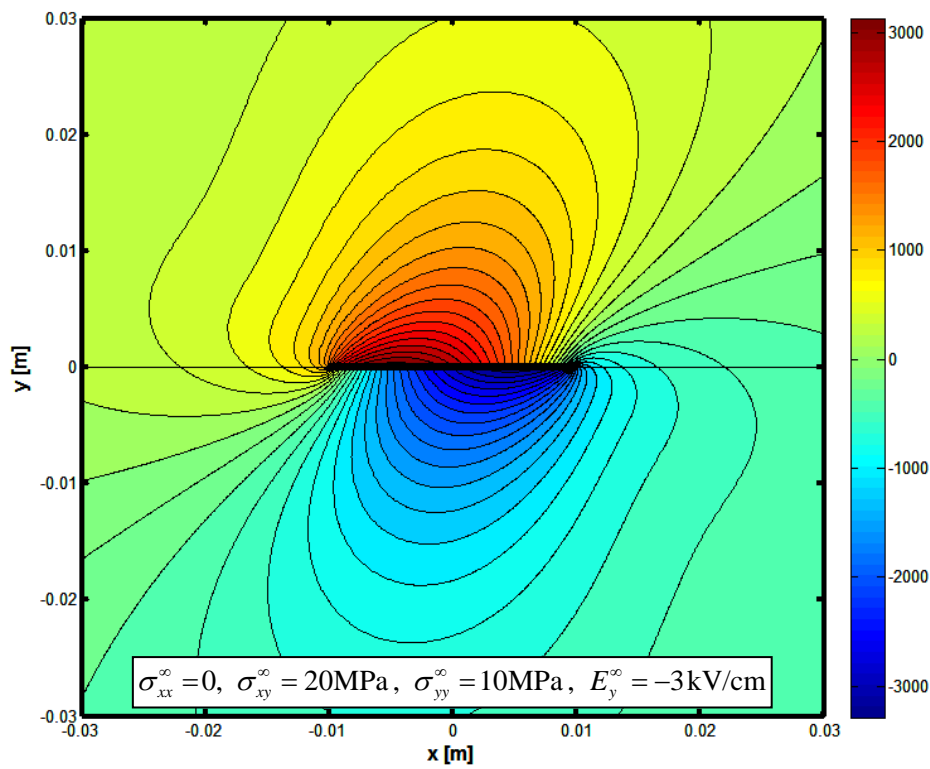
Fig. 5.18 – Field of electric potential ϕ , asymmetric loading conditions (values in V)

102

Both sets of figures (Fig. 5.1 – 5.9 for PZT-4 and 5.10 – 5.11 For PZT-5H) represent iso-stress and iso-displacement curves in the vicinity of the crack. It can be noted how in all figures depicting stress fields and electric displacement fields the presence of inverse square root singularities at the crack tips is qualitatively evident.

5.2 Influence of non-singular terms on the fracture behaviour

As far as the influence of load biaxiality and the effect of non-singular terms on the fracture response of cracked isotropic or orthotropic bodies is concerned several papers have been published: one can cite [1-5] among others. However, to the best of the author's knowledge, little work has been done so far to investigate the effect of the biaxial loading, and in particular of the collinear load which enters the so-called non-singular terms of the stress field formulation, on cracked piezoelectric media [6-7].

In the next sections of this thesis, by considering the presence of non-singular terms in the analytical solution, the influence of the remote load collinear to the crack on the stress and displacement fields, calculated at a given distance r from the tip, is examined thoroughly.

5.2.1. Stress components

We will examine in this section the effect on the electro-elastic solution of the choice of taking into account not only the asymptotic expressions of the principal fracture quantities, but also the non-singular terms, when they appear.

Expressions (4.156) and (4.160) outline the first stress vector $\mathbf{t}_1$ in the impermeable and permeable/semi-permeable cases respectively. One can note that the two non-singular terms NST1 and NST2 are discordant in sign; in fact, NST1 depends on $\mathbf{t}_1^\infty$ and contributes accordingly to the asymptotic term, while NST2 depends on $\mathbf{t}_2^\infty$ and contributes contrarily.

Figure 5.19 and 5.20, that refer to a piezoelectric ceramic PZT-4, show the contributions of the two non-singular terms separately, together, and compared to the asymptotic value, on the collinear stress field σ_{xx}, for two different values of the ratio r/a (10^{-2} and 10^{-1}). The two contributions taken separately have a bigger effect on the result than when evaluated together.
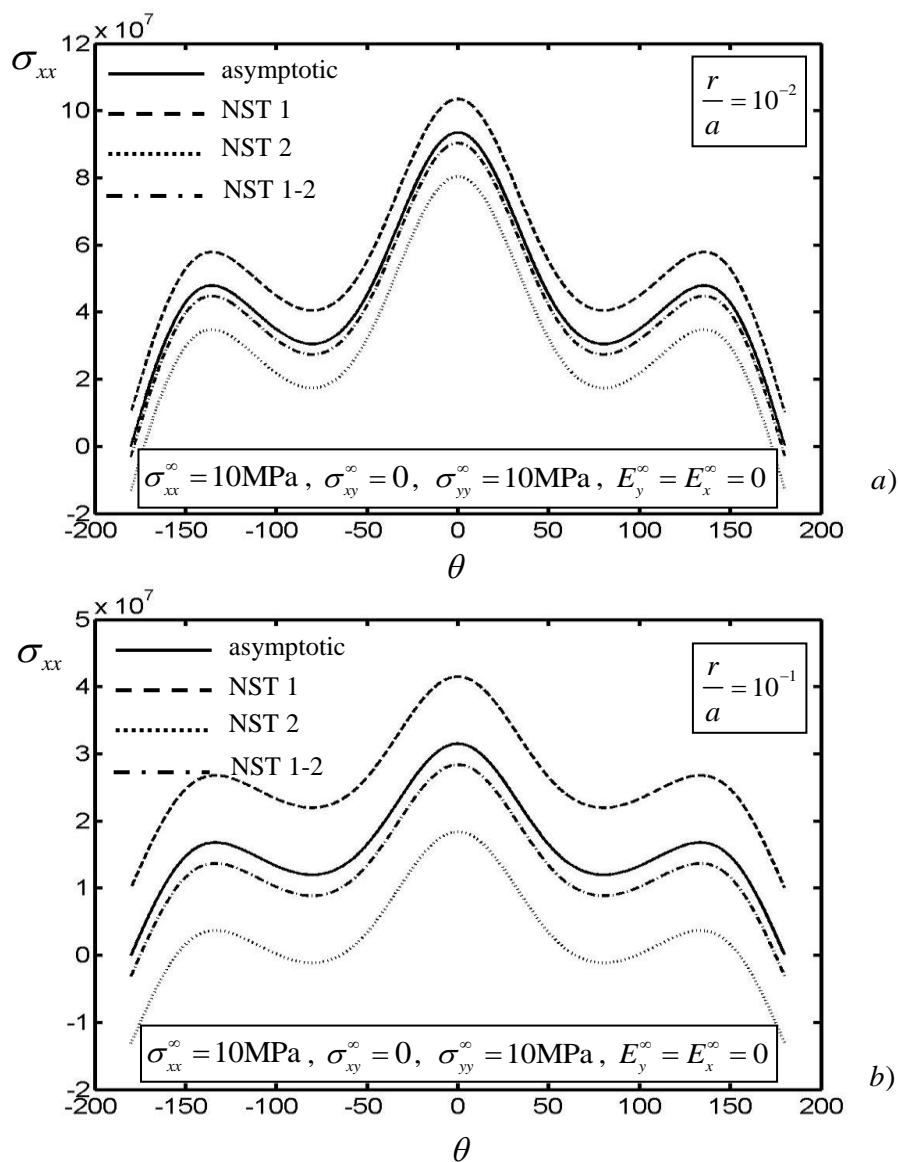
Fig. 5.19 – Asymptotic and non-singular trend of stress component σ_{xx} vs polar angle θ, for a ratio $r/a = 10^{-2}$ (a) and $r/a = 10^{-1}$ (b), in the impermeable crack case
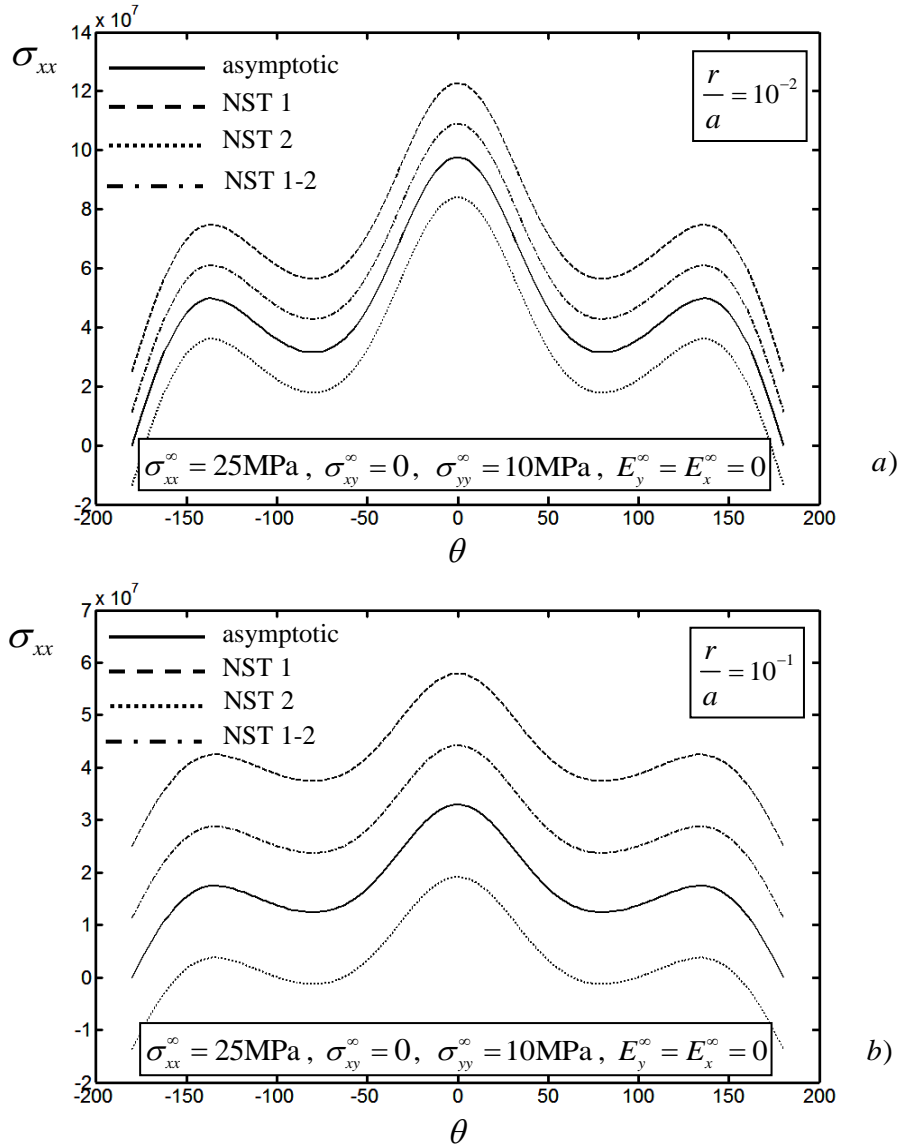
Fig. 5.20 – Asymptotic and non-singular trend of stress component σ_{xx} vs polar angle θ, for a ratio $r/a = 10^{-2}$ **(a) and** $r/a = 10^{-1}$ **(b), for a higher value of collinear load (impermeable)**

In the first loading condition ($\sigma_{xx}^{\infty} = 10\text{MPa}$, $\sigma_{xy}^{\infty} = 0$, $\sigma_{yy}^{\infty} = 10\text{MPa}$, $E_{y}^{\infty} = E_{x}^{\infty} = 0$), the non-singular results are slightly inferior to the asymptotic ones. In the second considered condition ($\sigma_{xx}^{\infty} = 25\text{MPa}$, $\sigma_{xy}^{\infty} = 0$, $\sigma_{yy}^{\infty} = 10\text{MPa}$, $E_{y}^{\infty} = E_{x}^{\infty} = 0$), the effect of NST1 becomes predominant on the effect of NST2, and the two contributions evaluated together produce an increase in the value of the results. One can say that when collinear loads are predominant the asymptotic solution will generally provide an underestimation of the results, and vice versa.

105

As it was expected, results are of lower value and the effect of non-singular terms is more noticeable for a higher ratio r/a. In other words, the error introduced by considering the asymptotic representation of σ_{xx} increases with the distance from the crack tip of the point where stresses are calculated.

When the remote loading is constituted of perpendicular and tangential loads, the asymptotic representation of σ_{xx} is always overestimating, as shown in Figures 5.21 (PZT-4), since only NST 2, taken with the sign discordant with that of the singular term, has an effect on the stress field of the considered stress component.
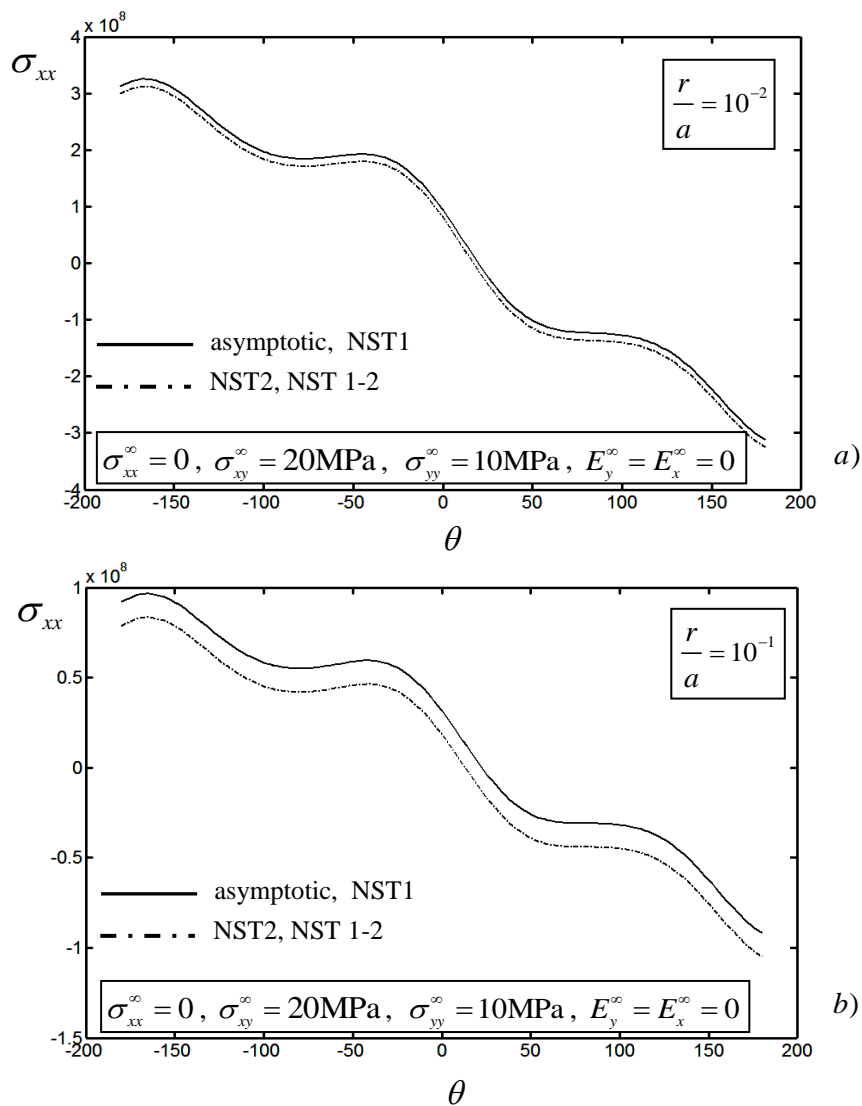
Fig. 5.21 – Asymptotic and non-singular trend of stress component σ_{xx} vs polar angle θ, for a ratio $r/a = 10^{-2}$ (a) and $r/a = 10^{-1}$ (b), asymmetric loading conditions (impermeable)
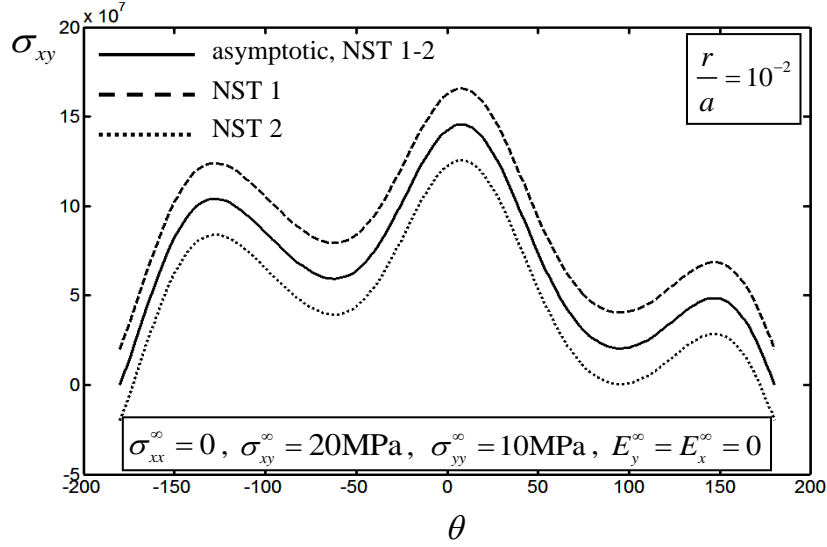
Fig. 5.22 – Asymptotic and non-singular trend of stress component σ_{xy} vs polar angle θ, for a ratio $r/a = 10^{-2}$, for asymmetric loading conditions (impermeable)

As a check, in Figure 5.22 the second component σ_{xy} of the stress vector $\mathbf{t}_1$ is depicted: the singular and non-singular representations correspond, as NST1 and NST2 nullify each other; as expected, the solution coincides to the one obtained by the first component of the stress vector $\mathbf{t}_2$.

Elastic constants $(10^{10}\ \mathrm{N/m^2})$	Piezoelectric constants $(\mathrm{C/m^2})$	Dielectric constants $(10^{-10}\ \mathrm{C/Vm})$
$c_{11} = 13.9$	$e_{13} = -6.98$	$\varepsilon_{11} = 60$
$c_{12} = 7.78$	$e_{33} = 13.8$	$\varepsilon_{33} = 54.7$
$c_{13} = 7.43$	$e_{15} = 13.4$	
$c_{33} = 11.3$		
$c_{44} = 2.56$		

Table 5.1 – Constants of PZT-4 piezoelectric ceramic

Elastic constants $(10^{10}\ \mathrm{N/m^2})$	Piezoelectric constants $(\mathrm{C/m^2})$	Dielectric constants $(10^{-10}\ \mathrm{C/Vm})$
$c_{11} = 12.6$	$e_{13} = -6.5$	$\varepsilon_{11} = 151$
$c_{12} = 5.5$	$e_{33} = 23.3$	$\varepsilon_{33} = 130$
$c_{13} = 5.3$	$e_{15} = 17$	
$c_{33} = 11.7$		
$c_{44} = 3.53$		

Table 5.2 – Constants of PZT-5H piezoelectric ceramic

5.2.2. Electric displacement

For a positive electric field applied at infinity in the x- direction, the singular solution underestimates the values of the electric displacement D_x, as illustrated in Figure 5.23, for both the impermeable and permeable crack models.
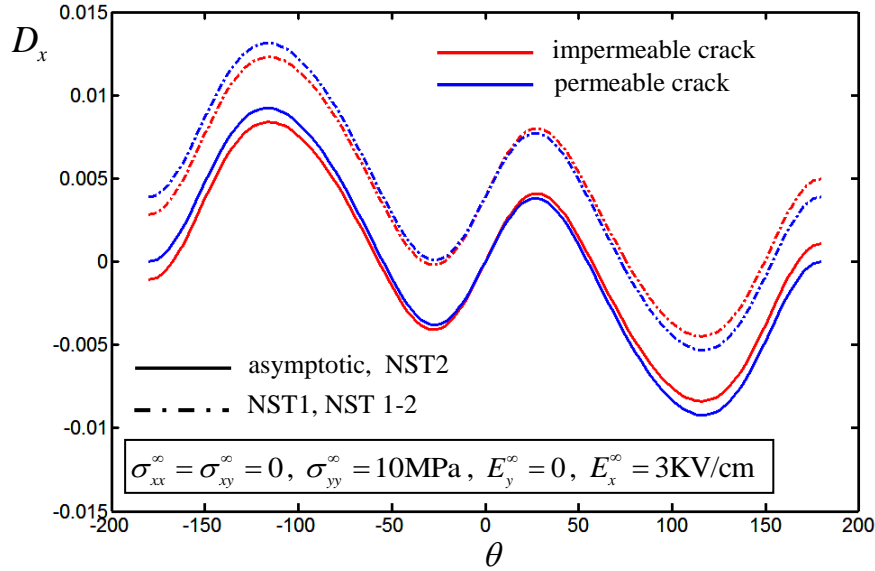
Fig. 5.23 – **Asymptotic and non-singular trend of electric displacement D_x vs polar angle θ, for a ratio $r/a = 10^{-2}$**

5.2.3. Hoop stress

The influence of non-singular terms will be investigated also on the circumferential stress $\sigma_{\theta\theta}$, defined by the relation:

$$\sigma_{\theta\theta} = \sigma_{xx} \sin^2 \theta + \sigma_{yy} \cos^2 \theta - \sigma_{xy} \sin 2\theta \qquad (5.5)$$

which will be later adopted as a fracture parameter as outlined in the maximum circumferential stress criterion, proposed by Erdogan and Sih [8].

The circumferential stress $\sigma_{\theta\theta}$, with the contributions of the two non-singular terms $\mathbf{t}_1^\infty$ (NST 1) and $-\mathrm{Re}\left[\mathbf{GH}^{-1}\right]\mathbf{t}_2^\infty$ (NST 2), is represented in Figure 5.24 for two different values of the ratio r/a (10^{-2} and 10^{-1}); the dissimilarity among the curves increases with the distance from the crack tip, and the considerations on the signs of the two contributions can be repeated.
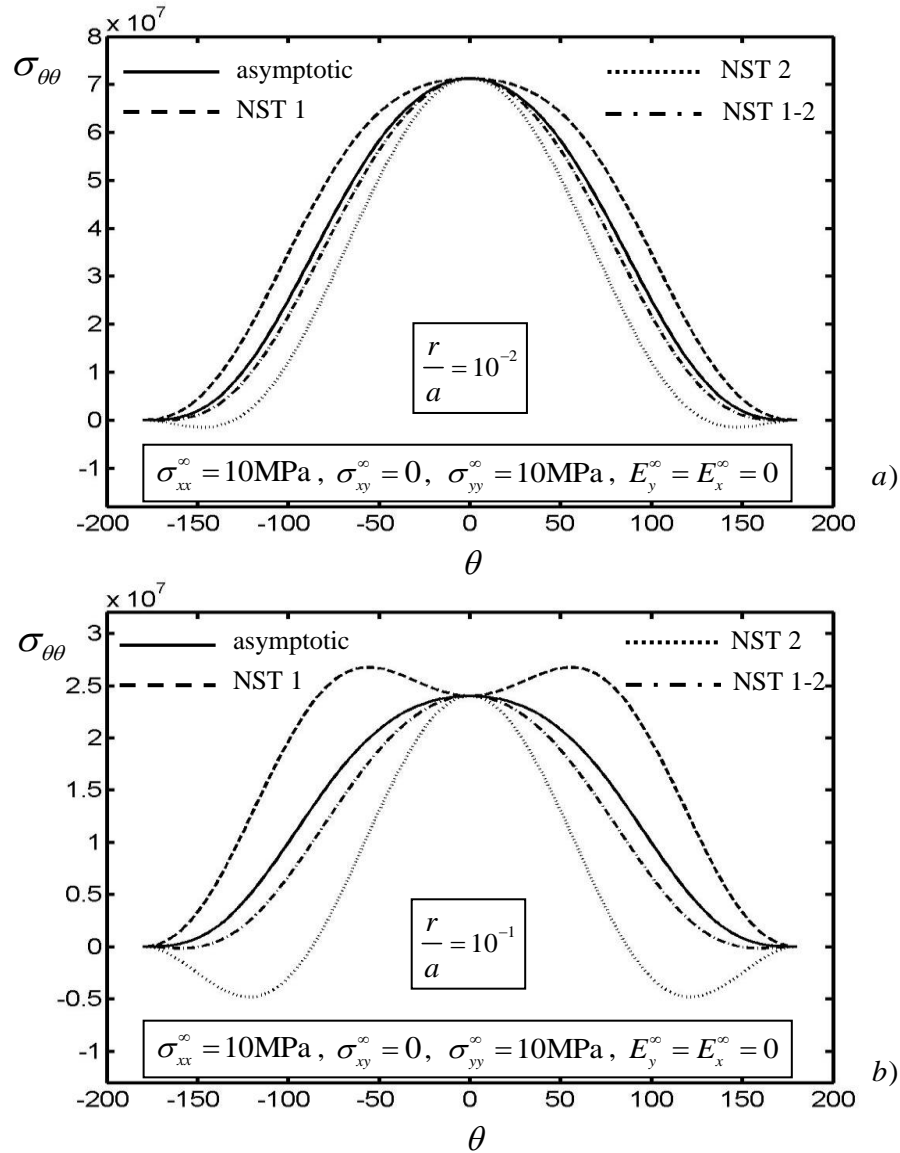
Fig. 5.24 – **Asymptotic trend of hoop stress** $\sigma_{\theta\theta}$ **vs polar angle** θ **compared with the trends comprehensive of non-singular term effects, for a ratio** $r/a = 10^{-2}$ **(a) and** $r/a = 10^{-1}$ **(b), in the permeable crack case**

5.3   Influence of load biaxiality

5.3.1. Stress components

We have seen how considering only the singular behaviour of a cracked mean equals to neglecting the biaxiality of applied loads. Now we will examine the effect that a far-field biaxial mechanical load exerts on the fracture quantities. To

do so, let us define two biaxial load parameters $s_1 = \sigma_{xx}^\infty / \sigma_{yy}^\infty$, ratio of collinear to perpendicular loads, and $s_2 = \sigma_{xy}^\infty / \sigma_{yy}^\infty$, ratio of tangential to perpendicular loads. The effect of the biaxial load parameter $s_1 = \sigma_{xx}^\infty / \sigma_{yy}^\infty$ on the stress component σ_{xx} is shown in Figures 5.25 and 5.26 for a PZT-4 ceramic for two different values of r/a.
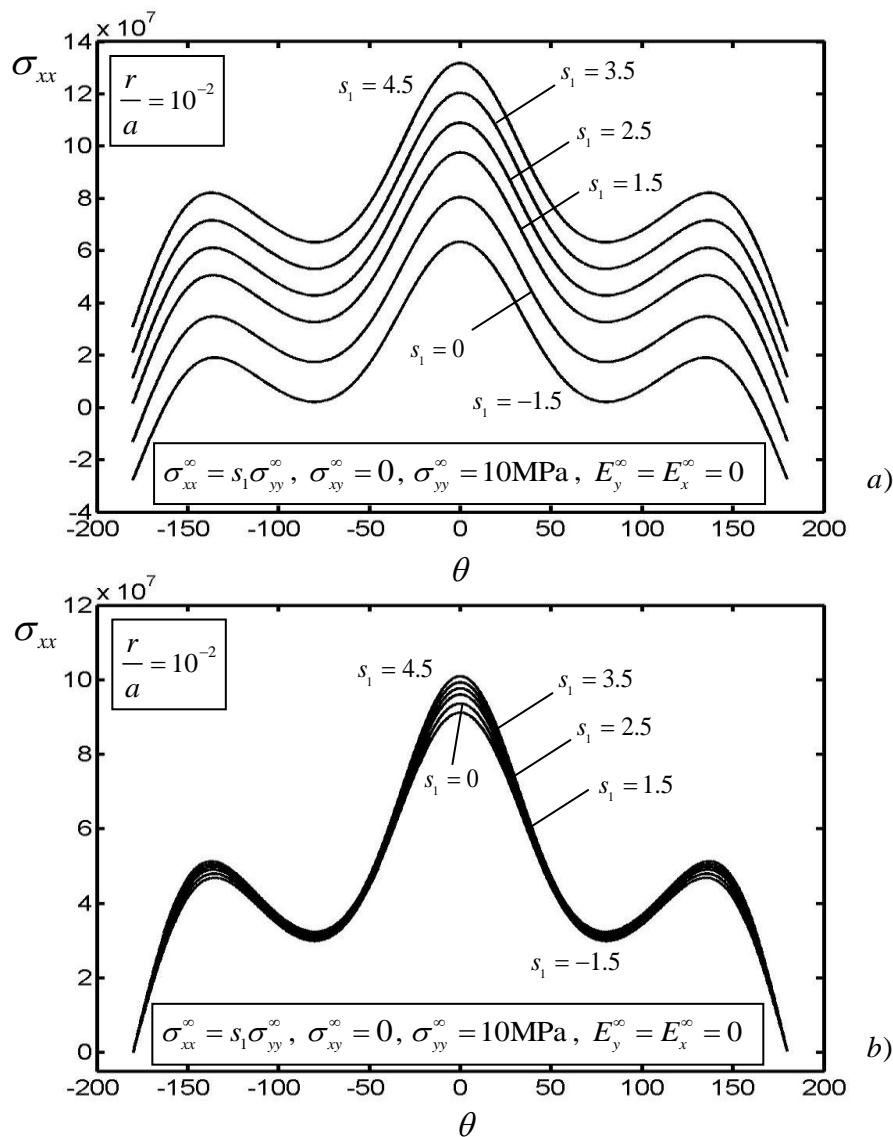
Fig. 5.25 – Stress component σ_{xx} vs polar angle θ for different values of biaxial load parameter s_1 and $r/a = 10^{-2}$, when the effect of non-singular terms is considered (a) and not considered (b)
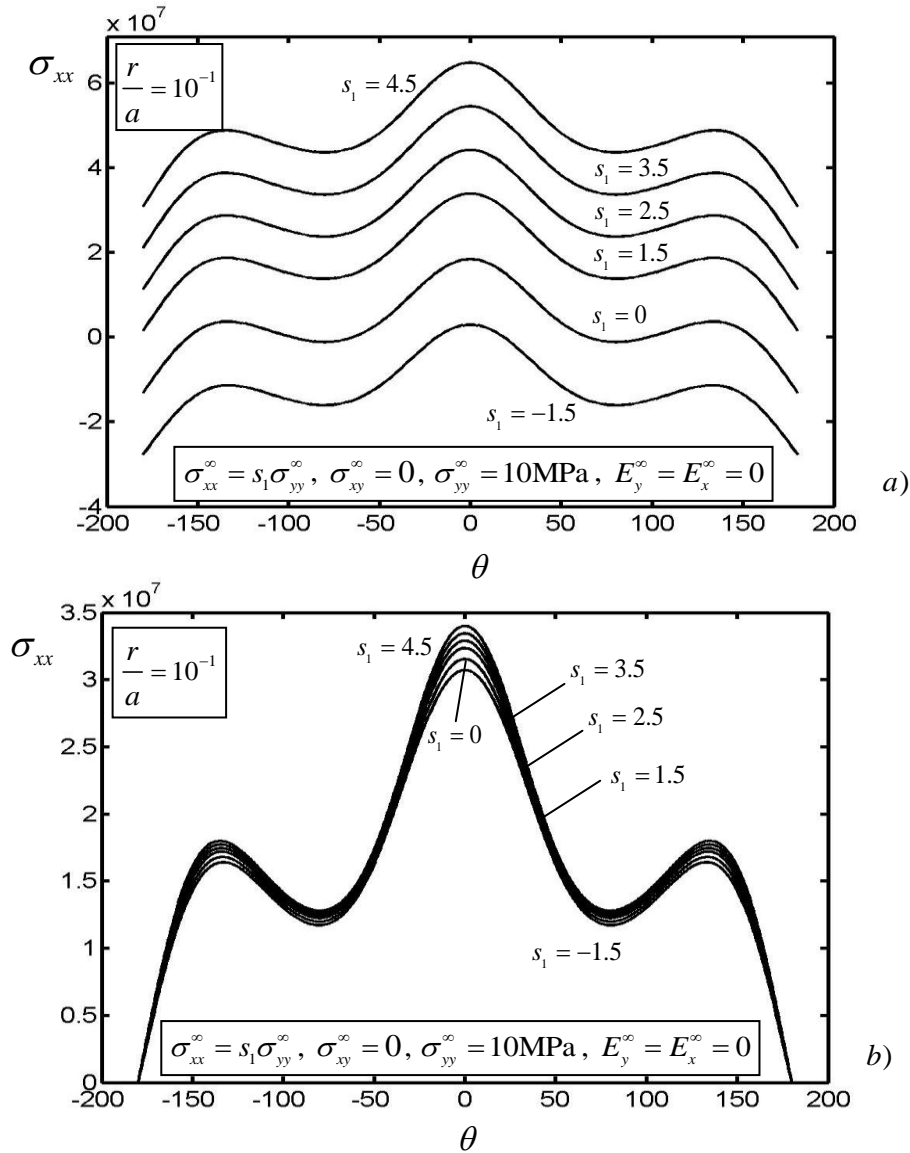
Fig. 5.26 – Stress component σ_{xx} **vs polar angle** θ **, for different values of biaxial load parameter** s_1 **and** $r/a = 10^{-1}$ **, when the effect of non-singular terms is considered (a) and not considered (b)**

It can be seen that asymptotic trends vary with s_1 much less than non-asymptotic ones, and that each time they underestimate or overestimate the value of σ_{xx} according to s_1, for the aforesaid considerations on the sign of the terms.

The slight dependence of the asymptotic solution on the collinear load derives from piezoelectric interaction, as one can verify by looking at the relation (5.2), where σ_{xx}^{∞} appears in the expression linking D_y^{∞} to E_y^{∞}.

111
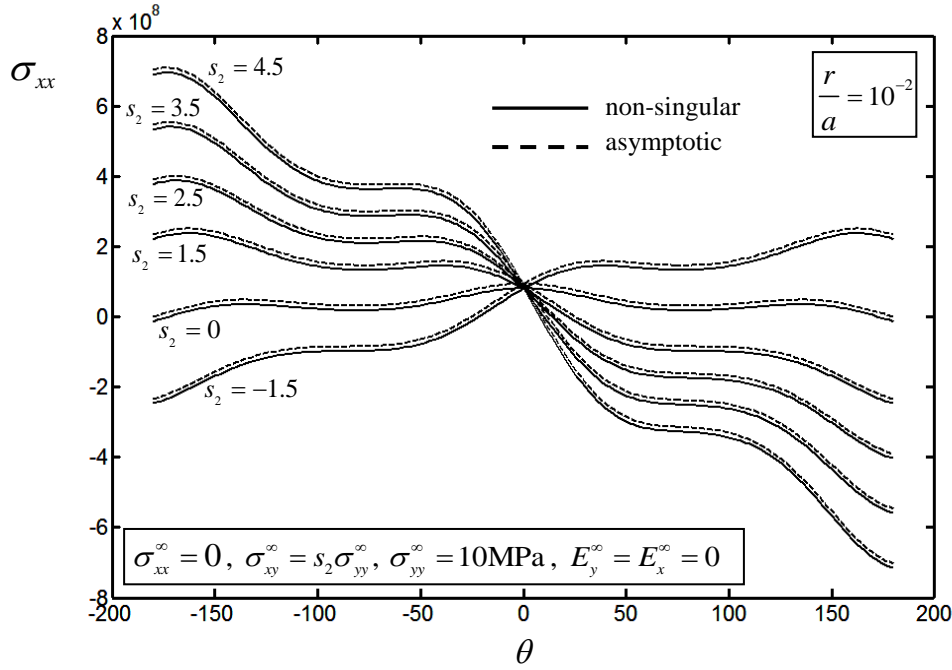
Fig. 5.27 – Stress component σ_{xx} vs polar angle θ, for different values of biaxial load parameter s_2

Figure 5.27 depicts the dependence on the biaxial load parameter $s_2 = \sigma_{xy}^\infty / \sigma_{yy}^\infty$ of the stress σ_{xx}: as already seen, the asymptotic representation of σ_{xx} is always slightly overestimating, and the difference between the two solutions is negligible for all values of s_2.

The next two figures (Fig. 5.28 and 5.29) illustrate the trends of stress components σ_{xy} and σ_{yy} for various values of the parameter s_2. The remote mechanical load σ_{xy}^∞ has been varied in direct ratio to σ_{yy}^∞ without any electric loading, and the graphs refer to a PZT-5H ceramic. One can observe that the tangential stress is an increasing function of s_2, with qualitatively similar trends.

An interesting feature of the curves depicting σ_{yy} is that they present three constant values, irrespectively of the applied tangential load: one corresponds to the direction collinear to the crack ($\theta = 0$), the other two being symmetric with respect to it. The same behaviour can be observed in other piezoelectric ceramic (PZT-4, PZT-7, PZT-7A, PZT-6B) used in our numerical applications, with subtle differences in the angle of the symmetric radial directions along which σ_{yy} results to depend only on the far-field applied perpendicular loading σ_{yy}^∞.

The dependence of σ_{xy} and σ_{yy} on the parameter s_1 in the presence of mechanical-only applied loads is practically negligible, and due to a slight piezoelectric interaction.
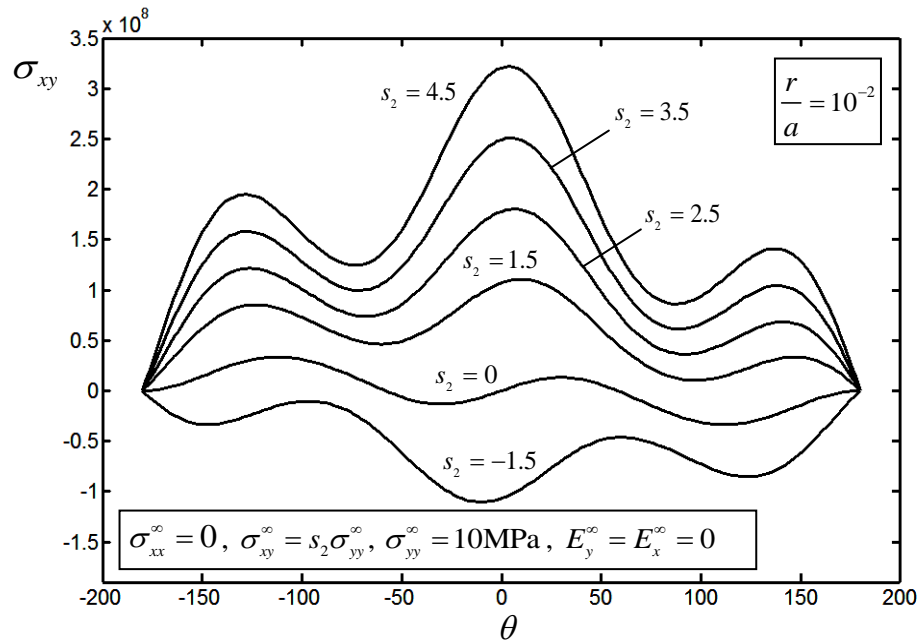
Fig. 5.28 – Remote tangential load effect on the stress component σ_{xy} vs angle θ at the crack tip in the impermeable crack case
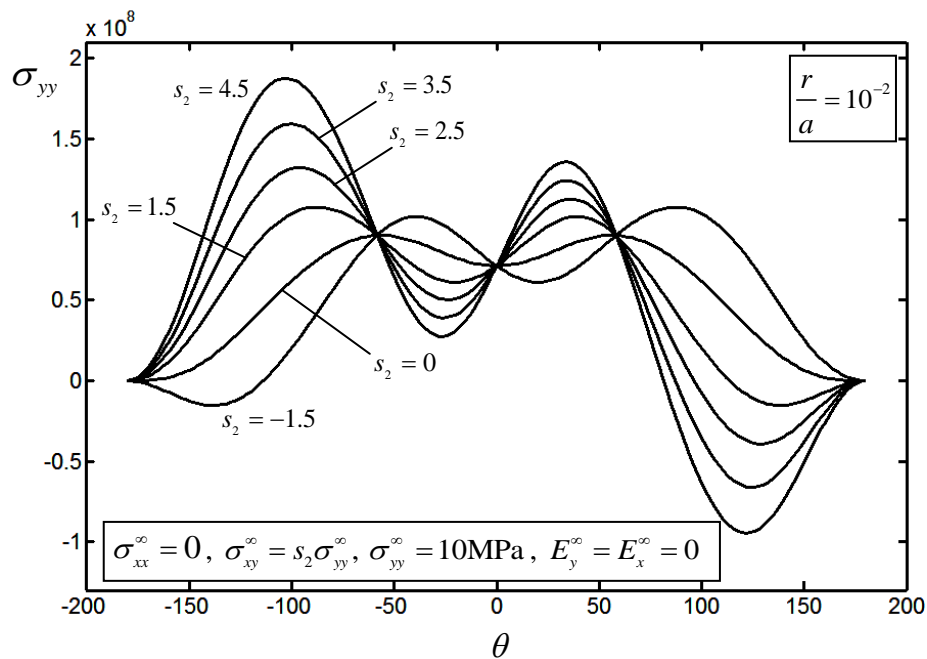
Fig. 5-29 – Remote tangential load effect on the stress component σ_{yy} vs angle θ at the crack tip in the impermeable crack case

5.3.2. Hoop stress

Figures 5.30 and 5.31 show the effect on the hoop stress of the biaxial load parameter $s_1 = \sigma_{xx}^\infty / \sigma_{yy}^\infty$. These graphs show that when asymptotic values are considered the trends of $\sigma_{\theta\theta}$ vs the polar angle are very similar to each other, and always present their maximum for $\theta = 0$.
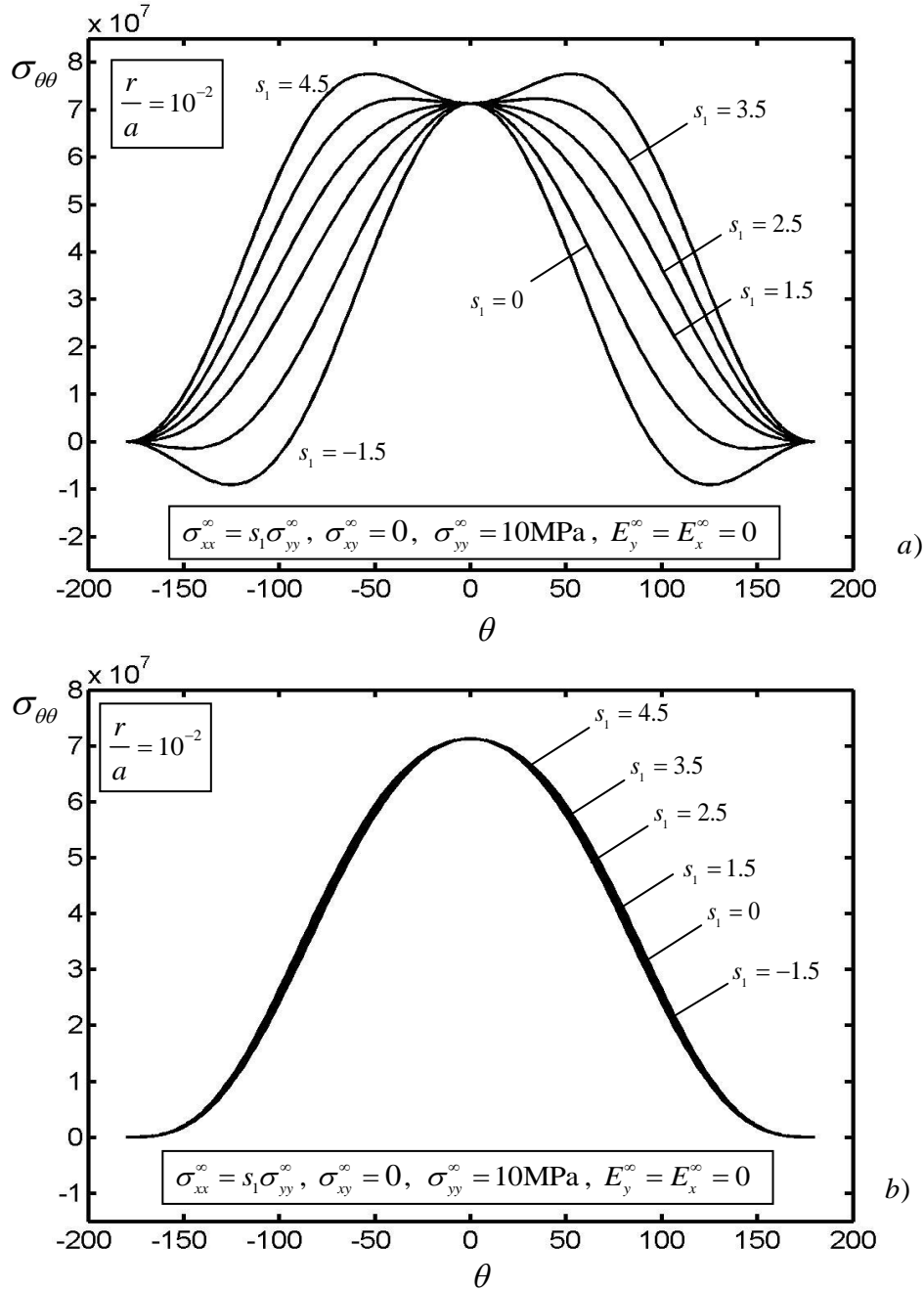
Fig. 5.30 – Biaxial load parameter s_1 effect on the hoop stress $\sigma_{\theta\theta}$ vs polar angle θ when the effect of non-singular terms is considered (a) and not considered (b), in the impermeable crack case (PZT-4)

On the contrary, when non-singular terms are considered, for high values of s_1 the maximum value of $\sigma_{\theta\theta}$ is not anymore found in correspondence of the crack axis direction, but its position varies depending on the entity and sign of biaxial load. The effect is more evident but qualitatively of the same kind when stresses are evaluated at a further distance from the tip of the crack.
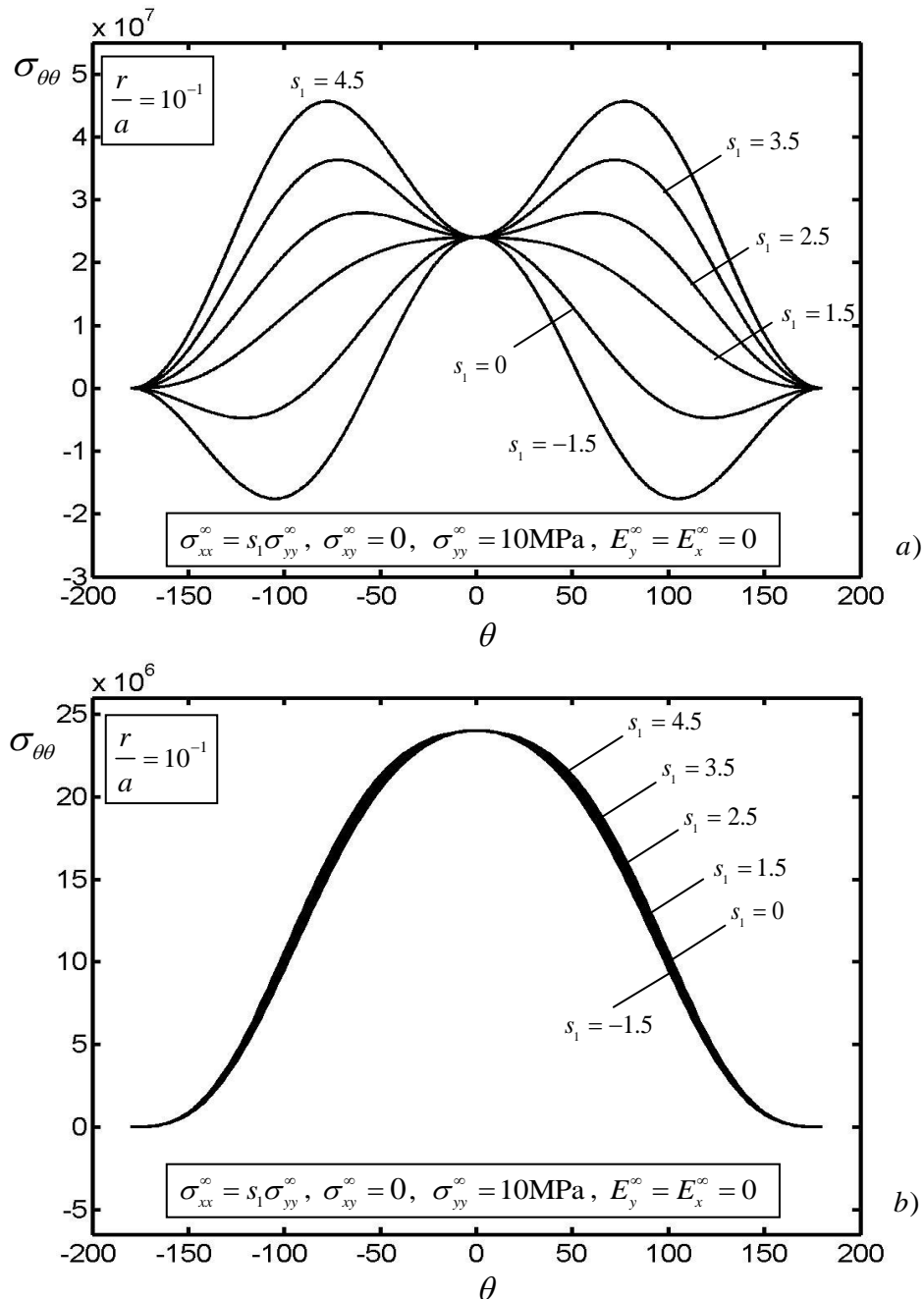
Fig. 5.31 – Biaxial load parameter s_1 effect on the hoop stress $\sigma_{\theta\theta}$ vs polar angle θ for $r/a = 10^{-1}$, when the effect of non-singular terms is considered (a) and not considered (b), in the impermeable crack case (PZT-4)
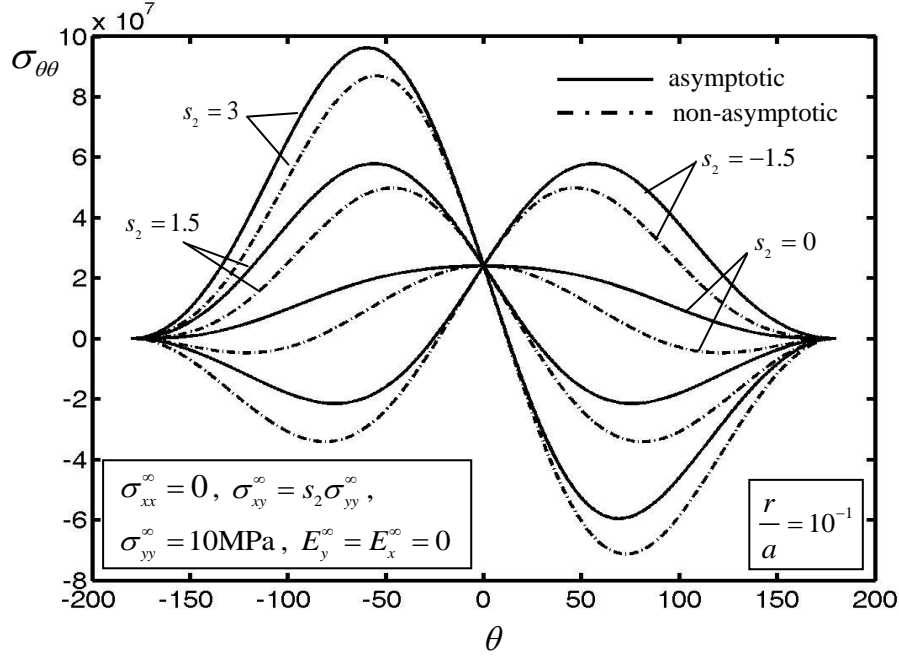
Fig. 5.32 –**Effect of the biaxial load parameter** s_2 **on the hoop stress** $\sigma_{\theta\theta}$ **vs polar angle** θ **in the impermeable crack case**

From Figure 5.32 it can be seen that the effect of the biaxial load parameter $s_2 = \sigma_{xy}^\infty / \sigma_{yy}^\infty$ on $\sigma_{\theta\theta}$ is more negligible but still present both for what concern the values and the position of the maxima.

5.3.3. Electric displacements

In this section the effect of variations of the biaxial loading parameters on the electric displacements in the x- and y-direction is represented, for a PZT-4 piezoelectric ceramic.

Figures 5.33 and 5.34 show the trends of the electric displacement component D_x for different values of $s_1 = \sigma_{xx}^\infty / \sigma_{yy}^\infty$ and $s_2 = \sigma_{xy}^\infty / \sigma_{yy}^\infty$, for the impermeable, semi-permeable and permeable crack models, in the case of mechanical-only remote applied loading.

One can see that asymptotic and non-asymptotic results coincide for every value of the applied collinear load (i.e. of the parameter s_1), while the same is not true when the parameter s_2 is considered.

116
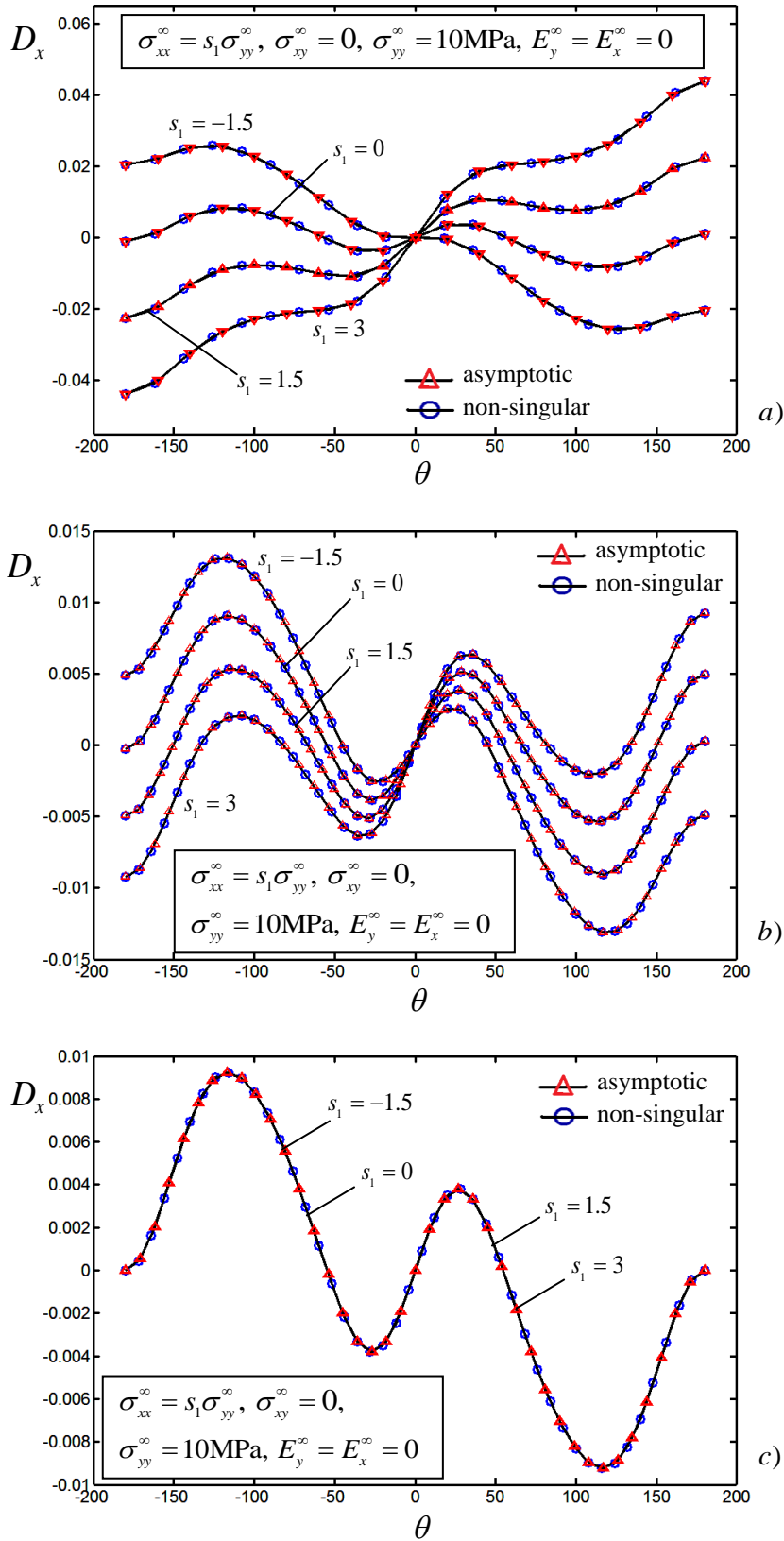
Fig. 5.33 −Effect of the biaxial load parameter s_1 on the electric displacement D_x vs polar angle θ in the impermeable (a), semi-permeable with $\varepsilon = 1$ (b) and permeable (c) crack models $\left(r/a = 10^{-2} \right)$
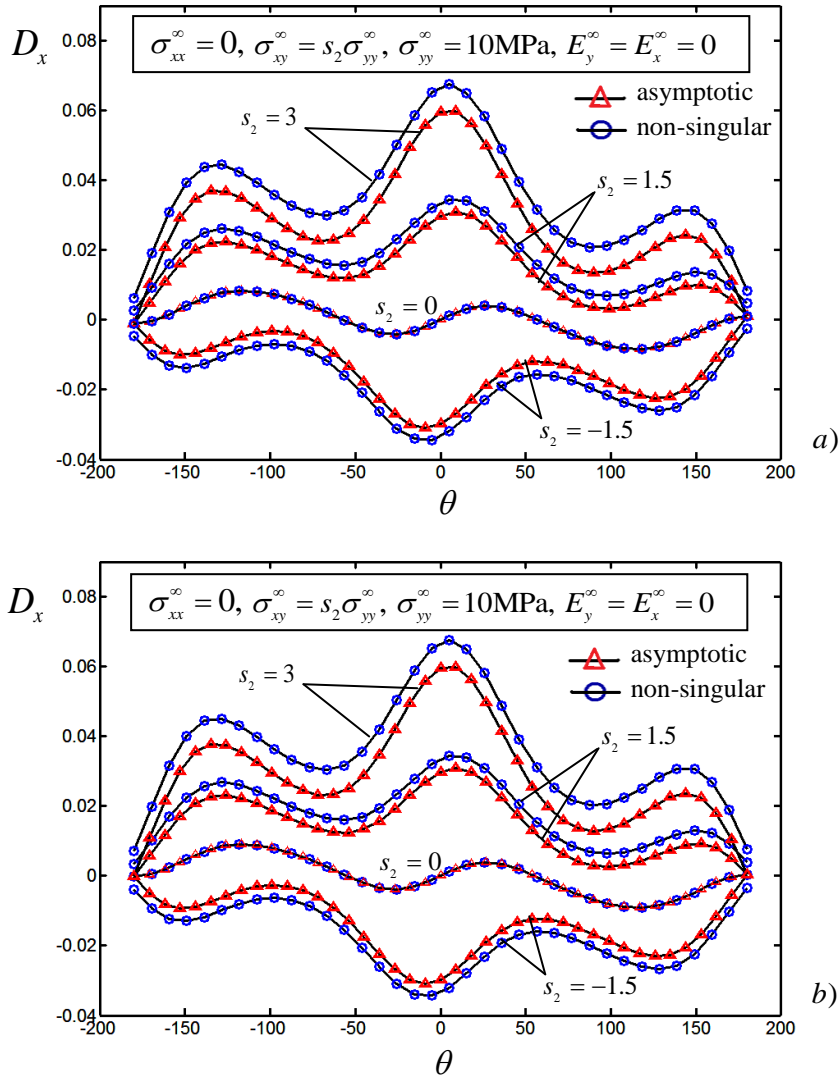
Fig. 5.34 –Effect of the biaxial load parameter s_1 on the electric displacement D_x vs polar angle θ in the impermeable (a) and permeable (b) crack models ($r/a = 10^{-2}$)

It should be noted that in the permeable case D_x is actually not affected at all from the collinear load. D_x results to be an increasing function of s_2, and the values of the collinear electric displacement differ only imperceptibly from the permeable to impermeable cases (and therefore to the semi-permeable).

The behaviour of the three crack models is qualitatively the same when only mechanical loads are applied, and the semi-permeable model is, as it was expected, middle way between the two extreme cases.
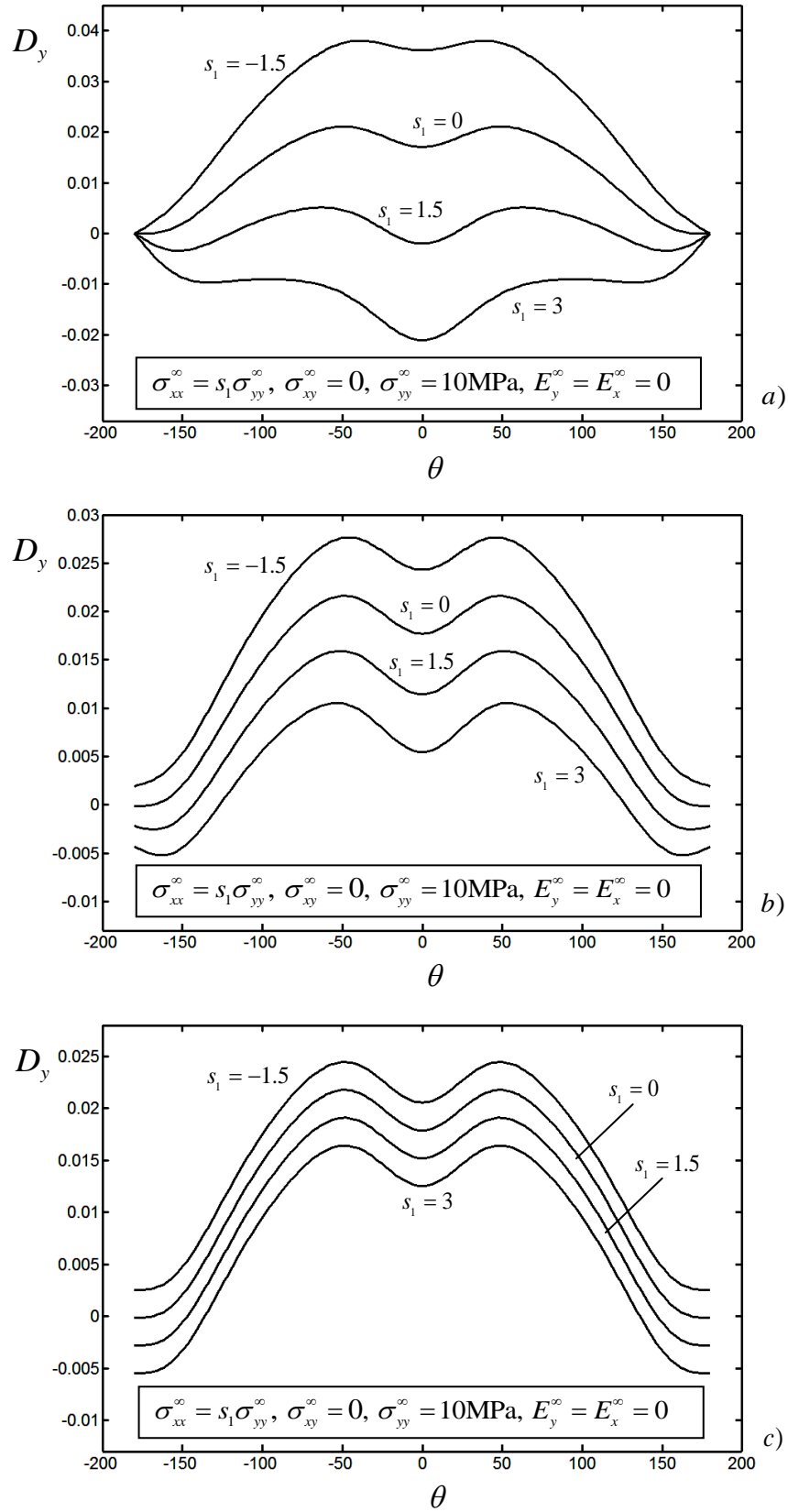
Fig. 5.35 –**Effect of the biaxial load parameter** s_1 **on the electric displacement** D_y **vs polar angle** θ **in the impermeable (a), semi-permeable with** $\varepsilon = 1$ **(b) and permeable (c) crack models** $\left(r/a = 10^{-2} \right)$
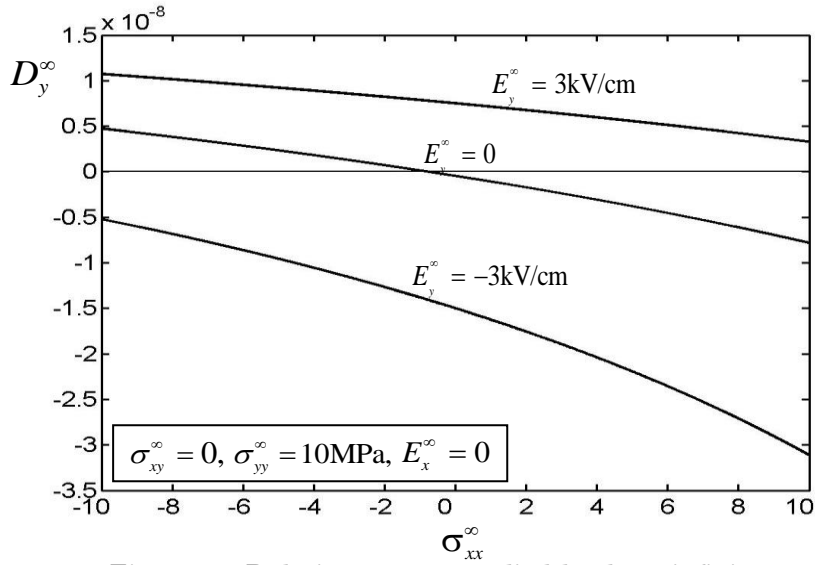
Fig. 5.36 –Relation among applied loads at infinity
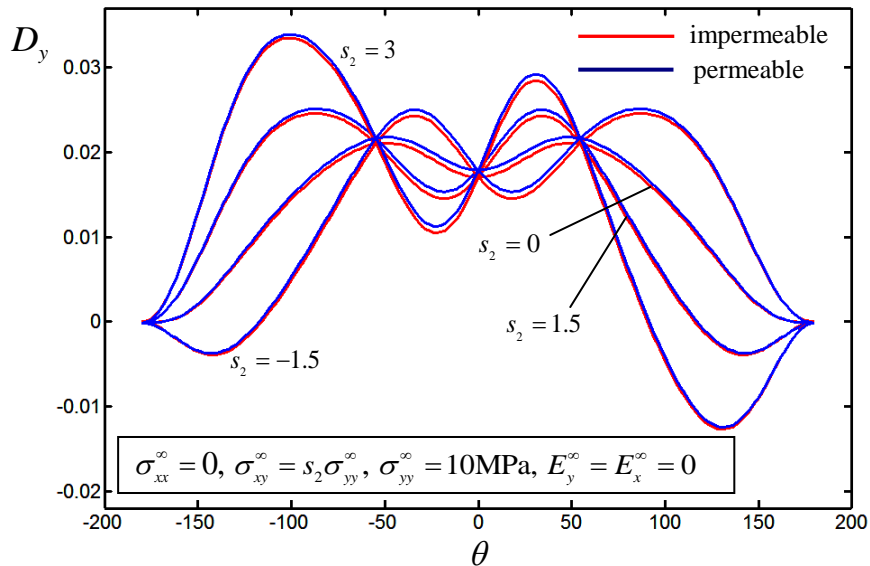
Fig. 5.37 –Effect of the biaxial load parameter s_2 on the electric displacement D_y vs polar angle θ in the impermeable and permeable cases $\left(r/a = 10^{-2} \right)$

Figures 5.35 illustrate the trends of the electric displacement component D_y for different values of $s_1 = \sigma_{xx}^\infty / \sigma_{yy}^\infty$, for impermeable, semi-permeable and permeable crack models (mechanical-only applied loading). D_y results to be a decreasing function of the applied collinear load, for every crack model. The dependency of electric displacements on σ_{xx}^∞ comes from relation (5.2), linking the remote

electric displacement to other applied loads: plotting D_y^∞ against collinear load at infinity, given other loads, one sees that the trend is decreasing (Fig. 5.36).

The trends of the electric displacement D_y for various values of biaxial loading parameter s_2 (Fig. 5.37) is qualitatively similar to those of the stress σ_{yy}, presenting three constant values, one corresponding to the direction collinear to the crack ($\theta = 0$), the other two being symmetric with respect to it. The difference between impermeable and permeable (and thus semi-permeable) behaviour is very limited when the remote loading is purely mechanical.

5.3.4. Elastic displacements

The elastic displacement fields of a PZT-3 ceramic are shown in Figure 5.38, for different loading combinations governed by the biaxial loading parameters s_2.

The two representations of u are similar in trend, although the asymptotic one overestimates the other.

It is inferred that the vertical displacement v is an increasing function of the parameter s_2 in the non-singular representation, while this is not true as far as the asymptotic solution is concerned.

5.4 Influence of the applied electric field and of the permittivity of the crack on the fracture quantities

5.4.1. Stress components

The stress components referred to a PZT-5H ceramic have been plotted in the presence of a biaxial load for different values of E_y^∞ in order to estimate the influence of the remote electric loading on the fracture quantities. Since the piezoelectric effect induces stresses of about one order of magnitude inferior to the mechanical effect, it is to be noted that the reference applied load has been reduced to an entity of 1 MPa, in order for the influence of the electric field to result evident.
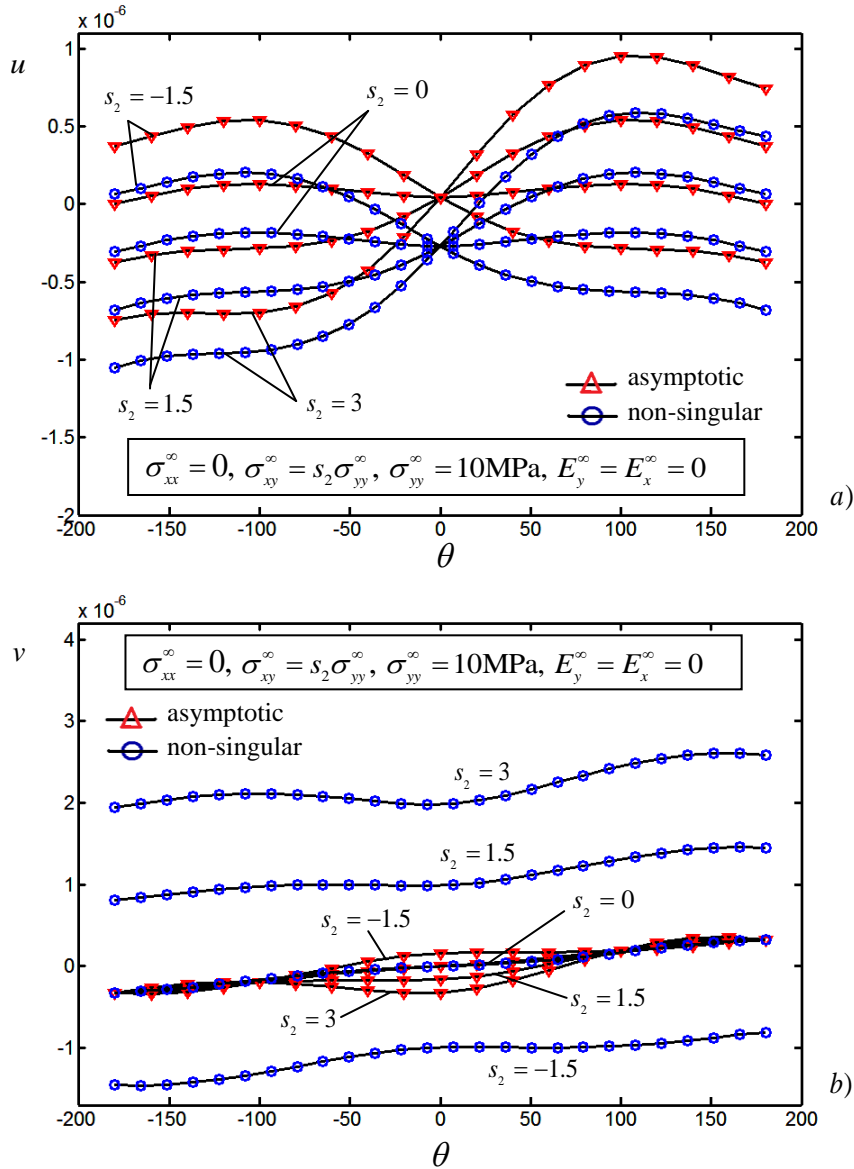
Fig. 5.38 –Effect of the biaxial load parameter s_2 **on the elastic displacements** u **(a) and** v **(b) vs polar angle** θ **asymptotic and non-singular representations** $\left(r/a = 10^{-2} \right)$

The four pairs of figures 5.39, 5.40, 5.41 and 5.42 refer to the three stress components and to the circumferential stress. The effect of the electric field on stresses is noticeable in the case of impermeable crack while is not present in the case of perfectly permeable crack.
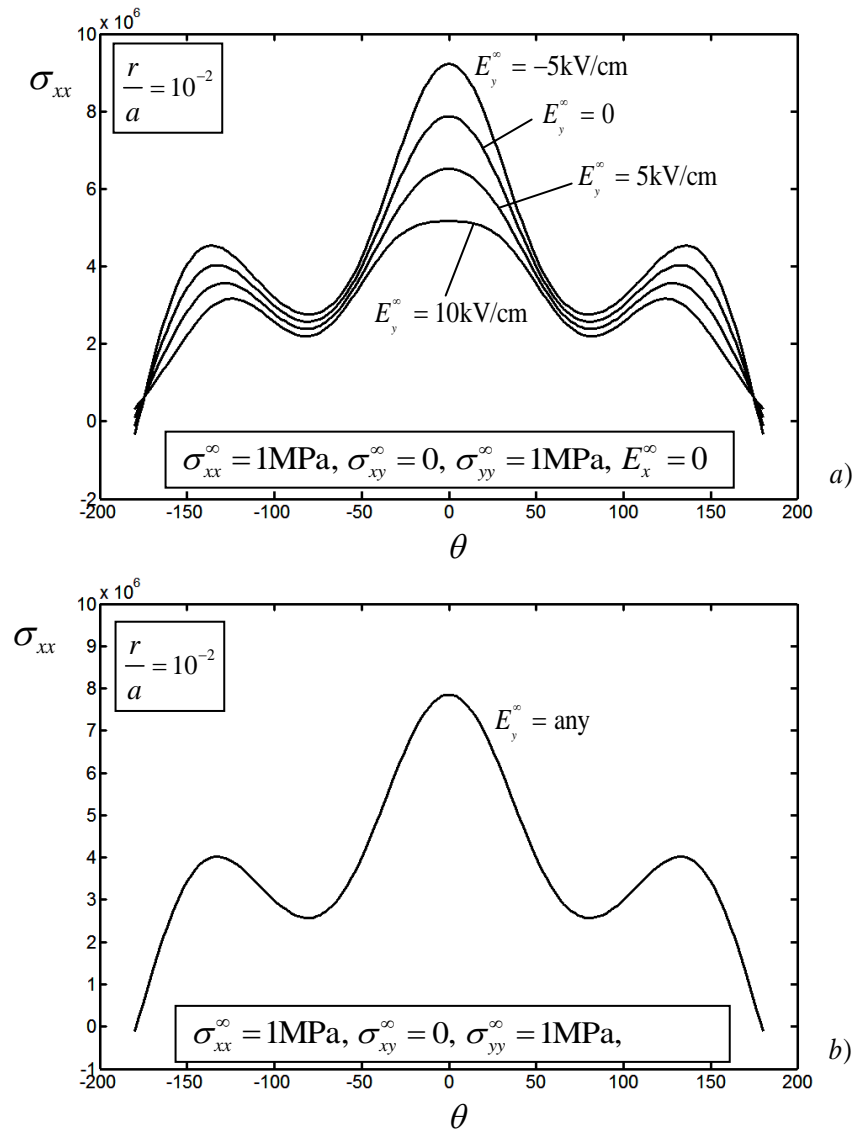
Fig. 5.39 – Effect of the applied electric field on the stress component σ_{xx} vs polar angle θ in the impermeable (a) and permeable (b) crack models

The effect of a positive field is to lower the amplitude of the curves for what concerns the collinear and tangential stresses, whereas the opposite result is produced on the perpendicular stress. The electric field does not modify the magnitude of the maximum value of circumferential stress.
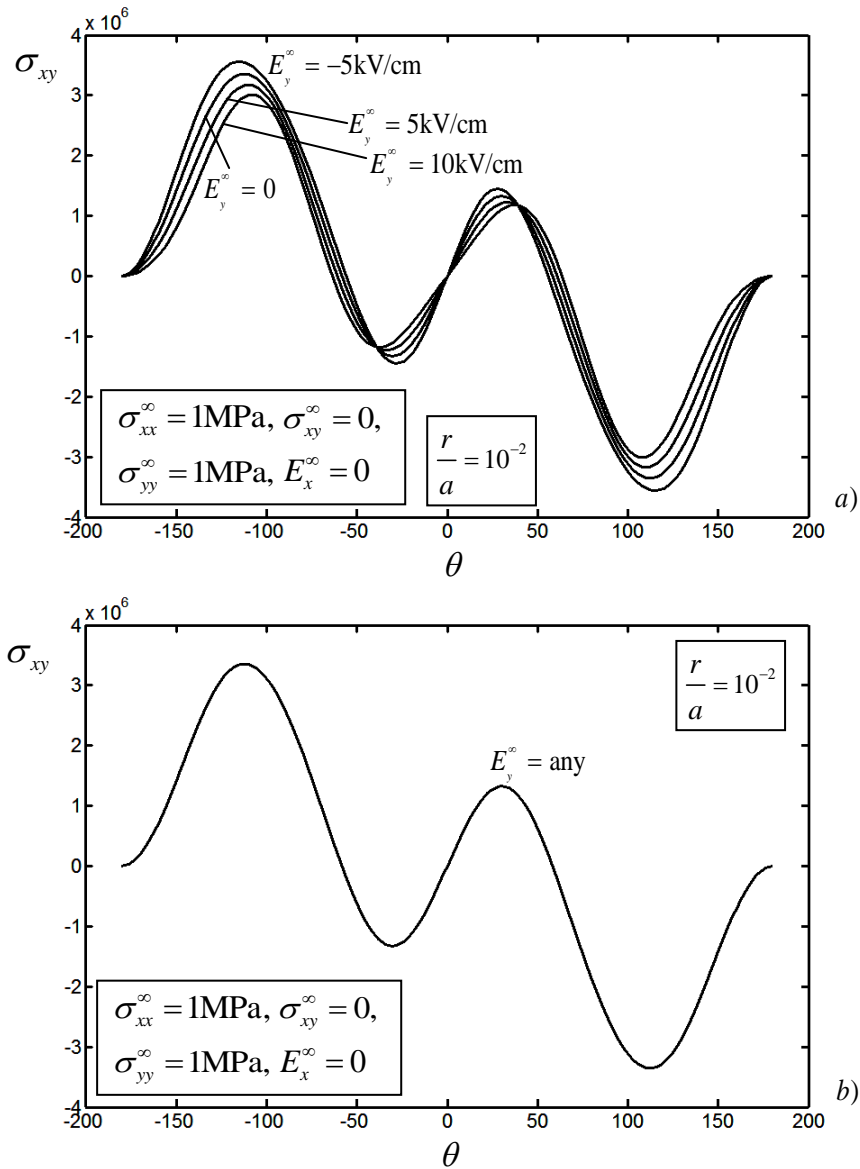
Fig. 5.40 –Effect of the applied electric field on the stress component σ_{xy} vs polar angle θ in the impermeable (a) and permeable (b) crack models

5.4.2.   Electric displacements

Figure 5.43 illustrate how the electric displacement curves are affected by the application of electric fields in the y-direction. One can state that there is no difference between the asymptotic and non-asymptotic representations, and that the effect of the applied electric field tends to vanish going from the impermeable, through the semipermeable, to the permeable crack model.
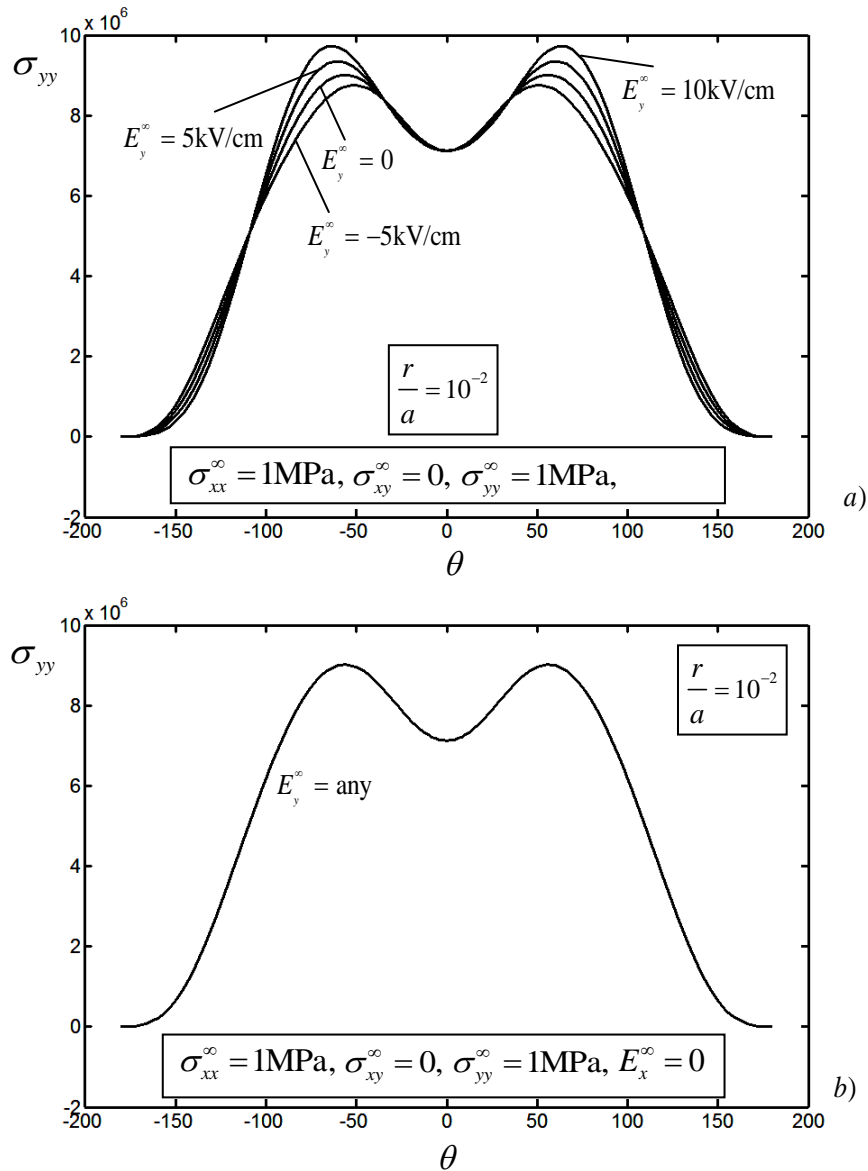
Fig. 5.41 – Effect of the applied electric field on the stress component σ_{yy} vs polar angle θ in the impermeable (a) and permeable (b) crack models

Figure 5.44 show the effect of an electric field applied in the x-direction, that is completely neglected in the asymptotic solution and affects only this electric displacement component.

The electric field applied in the x-direction has no influence on the component D_y. When the electric loading is applied in the y-direction, D_y increases with the field, whichever crack model is chosen. The different behaviors of impermeable, permeable and semi-permeable cracks are shown in Figure 5.45. It can be noted that the electric displacement in y in the impermeable case is always equal to

zero on the crack faces (that is, for $\theta = \pm\pi$), accordingly to the electric boundary conditions. Those conditions do not hold when other crack models are considered. The same behaviors of different crack models can be observed in Figure 5.46, which reports the entity of the electric displacement D_y at $\theta = 0$ and $\theta = -\pi$ plotted against the relative permittivity of the medium inside the crack (in logarithmic scale), for different values of applied electric field. It is inferred that D_y is an increasing function of the field for all crack models.
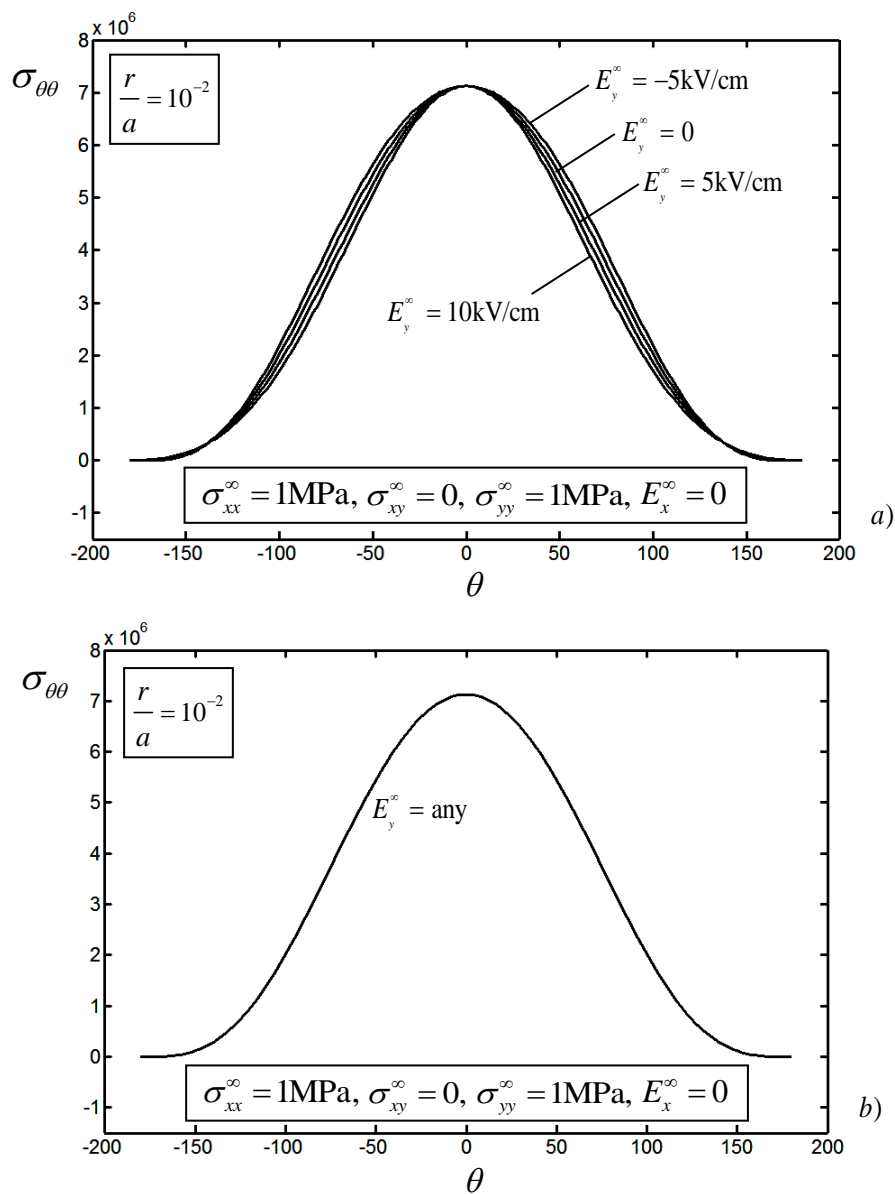
Fig. 5.42 –Effect of the applied electric field on the hoop stress $\sigma_{\theta\theta}$ vs polar angle θ in the impermeable (a) and permeable (b) crack models

126
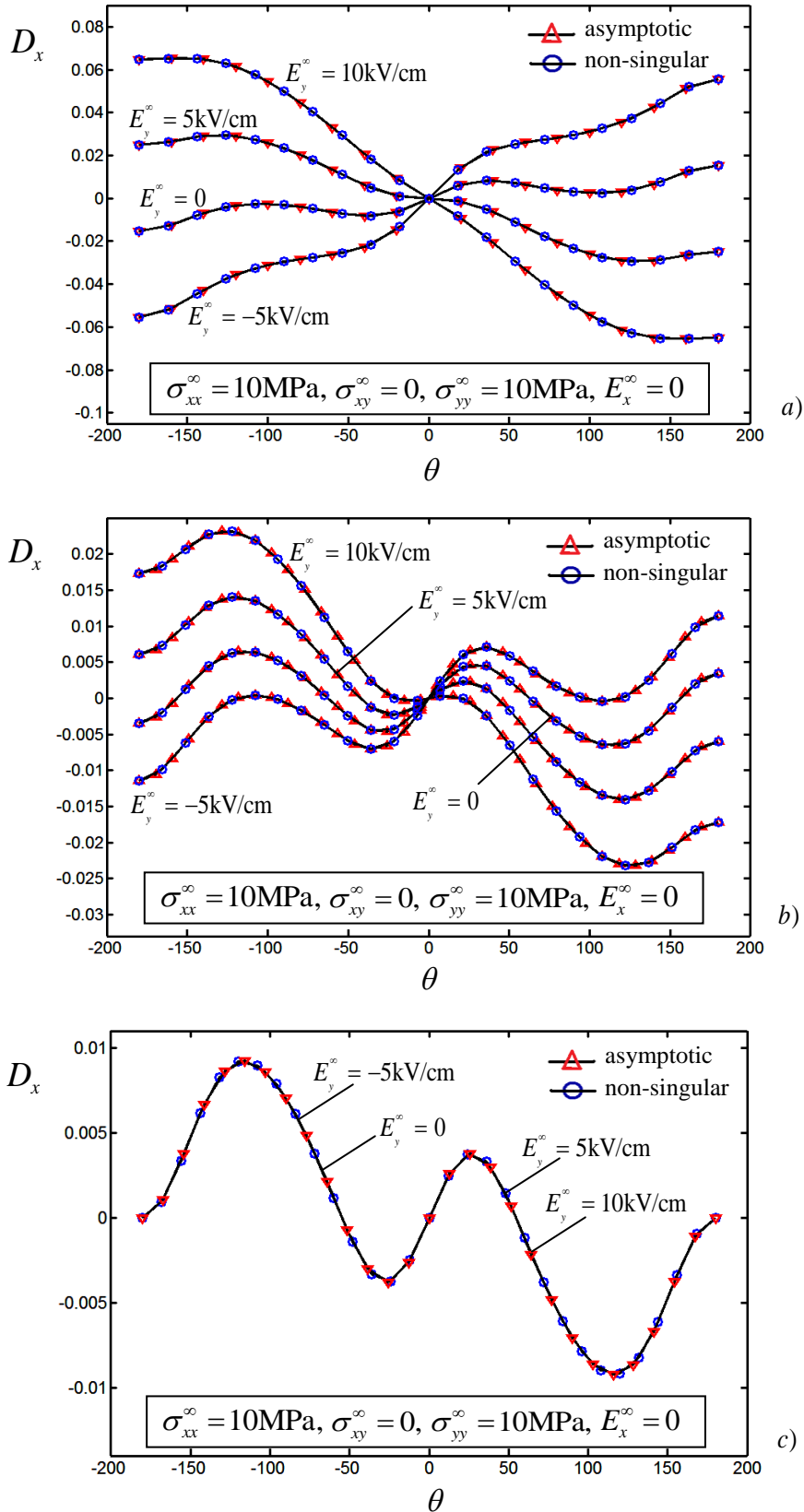
Fig. 5.43 –Effect of the applied electric field E_y on the electric displacement D_x vs polar angle θ in the impermeable (a), semi-permeable with $\varepsilon = 1$ (b) and permeable (c) crack models ($r/a = 10^{-2}$)
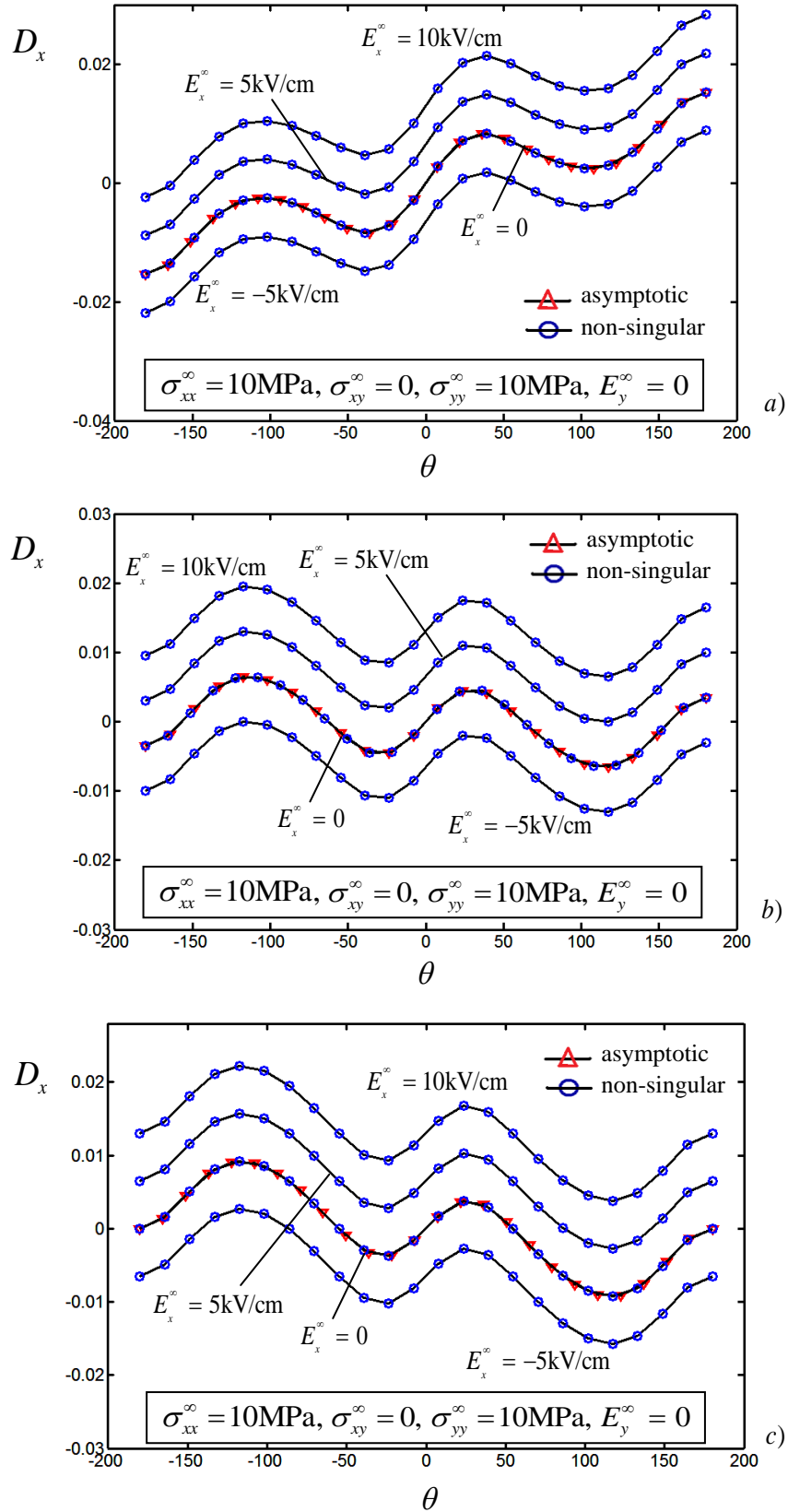
Fig. 5.44 – Effect of the applied electric field E_x on the electric displacement D_x vs polar angle θ in the impermeable (a), semi-permeable with $\varepsilon = 1$ (b) and permeable (c) crack models $(r/a = 10^{-2})$

128
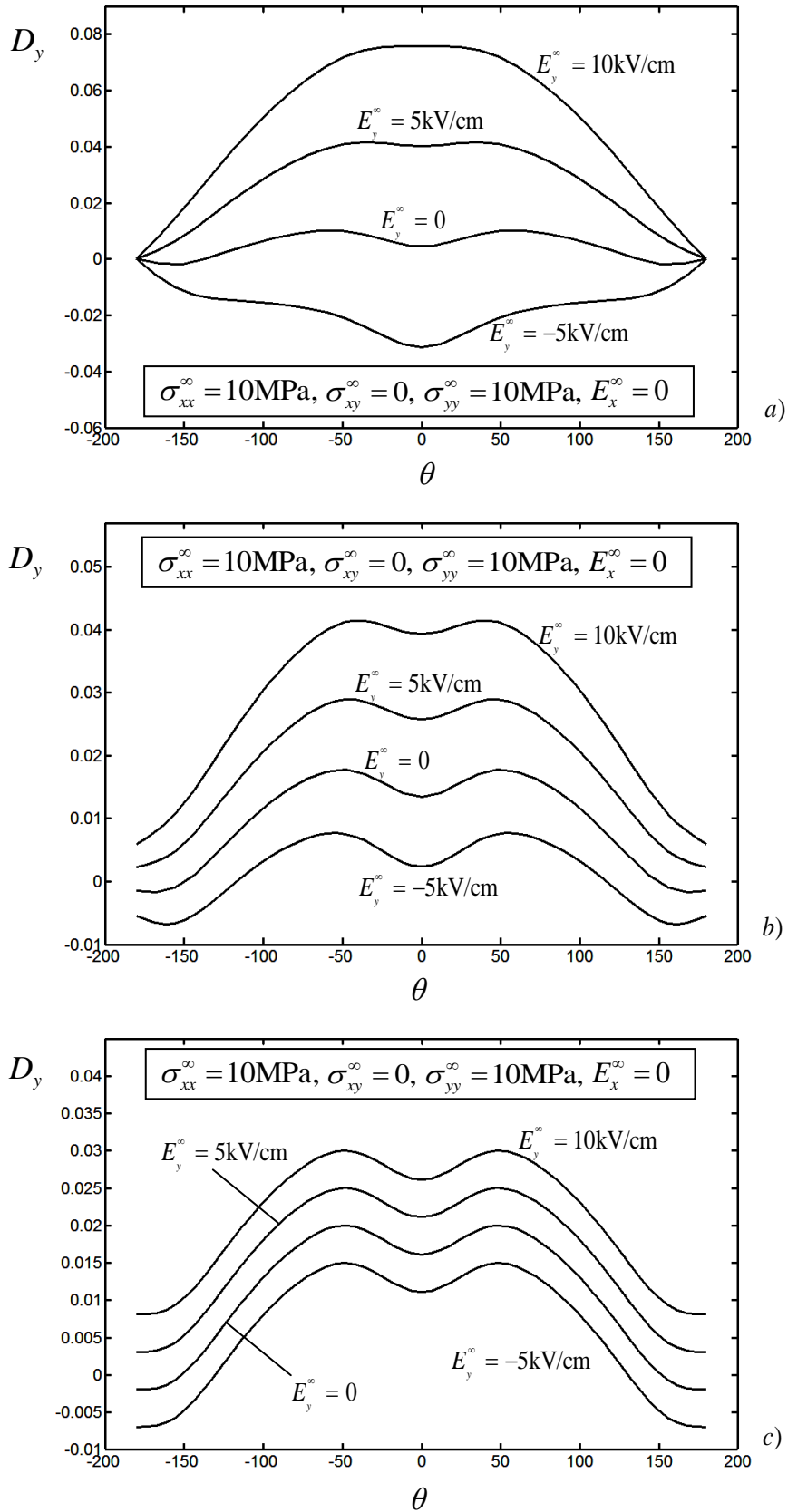
Fig. 5.45 –Effect of the applied electric field E_y on the electric displacement D_y vs polar angle θ in the impermeable (a), semi-permeable with $\varepsilon = 1$ (b) and permeable (c) crack models ($r/a = 10^{-2}$)
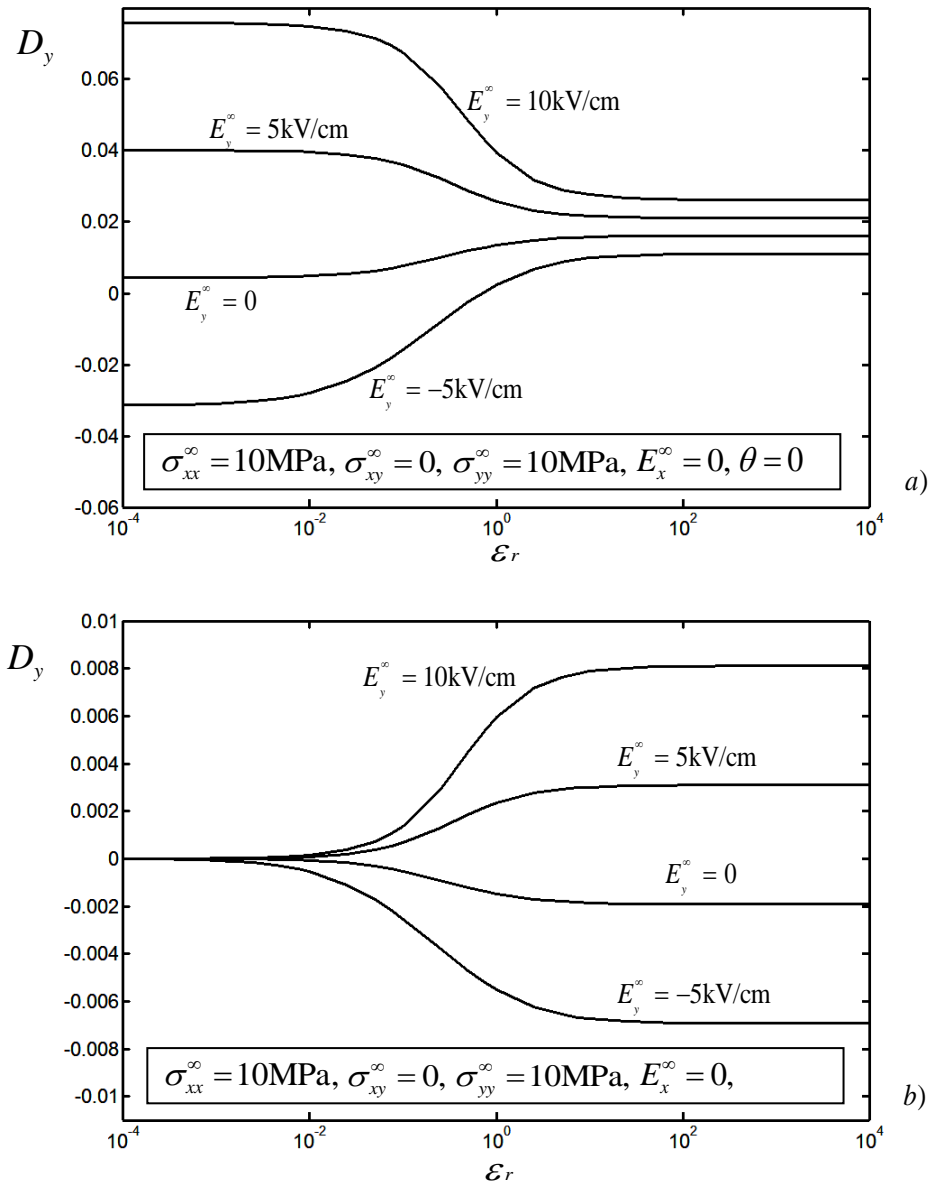
Fig. 5.46 –Influence of the permittivity of the medium inside the crack on the electric displacement D_y at $\theta = 0$ (a) and $\theta = -\pi$ (b), for different values of the applied electric field E_y $(r/a = 10^{-2})$ – **PZT-4**

5.5   **Application of two fracture criteria**

5.5.1.   *Maximum Circumferential Stress Criterion*

The maximum circumferential stress criterion, as proposed by Erdogan and Sih [8], is chosen here as the means to demonstrate how the inclusion of non-singular terms, that is, the consideration of load biaxiality, can alter the predicted direction of incipient crack branching.

This criterion utilizes as a fracture parameter the circumferential stress $\sigma_{\theta\theta}$, depicted in Fig. 5.47 and defined by the relation:

$$\sigma_{\theta\theta} = \sigma_{xx} \sin^2 \theta + \sigma_{yy} \cos^2 \theta - \sigma_{xy} \sin 2\theta \qquad (5.6)$$
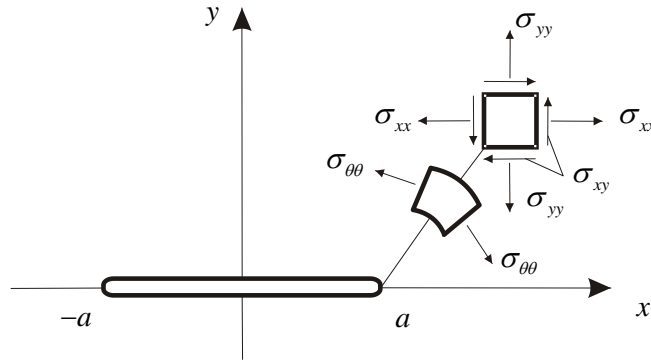
Fig. 5.47 – Relation between Cartesian stress components and circumferential stress

According to this criterion, crack extension will take place initially along the direction, identified by the polar angle θ, perpendicular to that one where the tensile stress attains maximum value, once this reaches a critical value, characteristic of the material under study.

Designating the polar angle that defines the direction of extension as θ_0, the following conditions must be satisfied for the circumferential stress to be maximized:

$$\sigma_\theta \big|_{\theta=\theta_0} > 0 \tag{5.7}$$

$$\frac{\partial}{\partial \theta}(\sigma_\theta)\big|_{\theta=\theta_0} = 0 \tag{5.8}$$

$$\frac{\partial^2}{\partial \theta^2}(\sigma_\theta)\big|_{\theta=\theta_0} < 0 \tag{5.9}$$

The crack extension begins as soon as the following situation is reached:

$$\sigma_\theta \big|_{\theta=\theta_0} = \sigma_{\theta cr} \tag{5.10}$$

The criterion is formulated in terms of stresses, and the material parameters do not appear. For this reason, the application of this criterion can be seen as questionable for piezoelectric materials, but it will be accepted as a simplified means to interpret the effect of far-field biaxial loading on crack branching.

We have already seen in the section where the influence of load biaxiality was analysed how the inclusion of non-singular terms in the expressions of stress components has the result of modifying the shape of the curves depicting the hoop stress, particularly for high values of applied collinear load (see Fig. 5.30 and 5.31). This effect acquires a great importance when the maximum hoop stress criterion is adopted to predict the crack extension angle.

When non-singular terms are considered, for high values of s_1 the maximum value of $\sigma_{\theta\theta}$ is not anymore found in correspondence of the crack axis direction, despite the symmetry of the loading condition.

This means that a prediction on the crack branching angle through the maximum hoop stress criterion based on the asymptotic solution of the electro-elastic problem would infer results disaccording with those got through the complete solution, if the collinear applied load was high compared to the other loads. These outcomes are in accordance with those obtained by some other authors, who carried out the analysis for isotropic and orthotropic cracked plates, finding significant biaxial loading effects on the direction of initial crack extension investigated through the maximum stress ratio theory [1-6,9].

For a better understanding of the influence of the collinear load on the stress field at the vicinity of the crack tip, the iso-stress curves referred to the hoop stress

$\sigma_{\theta\theta}$, obtained for the same material (piezoelectric ceramic PZT-4) and loading combination of Figures 5.30 and 5.31, and $s_1 = 4.5$, are mapped in Figure 5.48 for $r/a = 10^{-2}$ and Figure 5.49 for $r/a = 10^{-1}$.

Figure 5.50 illustrates the locus of the values of the polar angle θ which correspond to the different maximum values of the function of the circumferential stress $\sigma_{\theta\theta} = \sigma_{xx} \sin^2 \theta + \sigma_{yy} \cos^2 \theta - \sigma_{xy} \sin 2\theta$, in relation to the ratio $s_1 = \sigma_{xx}^{\infty} / \sigma_{yy}^{\infty}$ of the remote collinear load to the remote perpendicular load. The result is in agreement with Figures 5.30-5.31 and 5.48-5.49. In fact, one can see that the graph referring to the asymptotic solution is a straight line showing a constant angle $\theta = 0$ (since the loading combination is symmetric). On the contrary, the curves that take into account the effect of non-singular terms at two different distances from the crack tip, divert abruptly from the horizontal when the biaxial loading parameter s_1 reaches the value of about 3 (about 2 for $r/a = 10^{-1}$). This means that, for the material under analysis, when the collinear load is three or more times higher than the perpendicular one, the hypothetical incipient branching angle θ_0 is different from $\theta_0 = 0$. The same qualitative behaviour has been found in other piezoelectric ceramics taken into consideration in our numerical applications, with some differences in the values of loading parameter that trigger the deviation.

In Figure 5.51 the locus of the polar angle correspondent to the maximum hoop stress is plotted as a function of the biaxial loading parameter $s_2 = \sigma_{xy}^{\infty} / \sigma_{yy}^{\infty}$ of the remote tangential load to the remote perpendicular load. As already seen in Figure 5.32, the variance between asymptotic and non-asymptotic results is more modest, so the error introduced with the simplified solution is negligible at the vicinity of the crack tip. For a remote loading almost purely tangential (high s_2) the incipient branching angle tends to 70° (in accordance with what pointed out in the above cited work of Erdogan and Sih [8]).
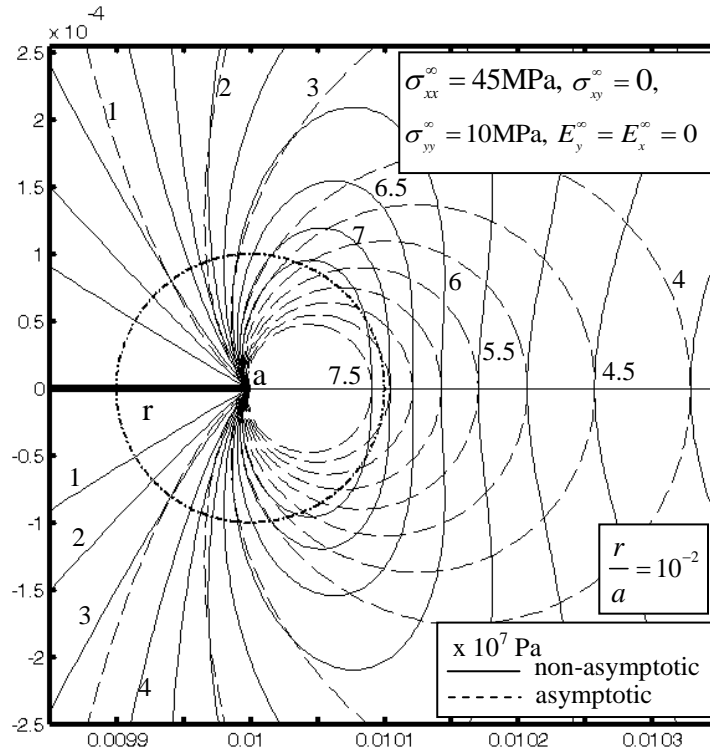
Fig. 5.48 – Iso-stress curves for hoop stress $\sigma_{\theta\theta}$ in the vicinity of the crack tip, when the solution is evaluated at $r/a = 10^{-2}$
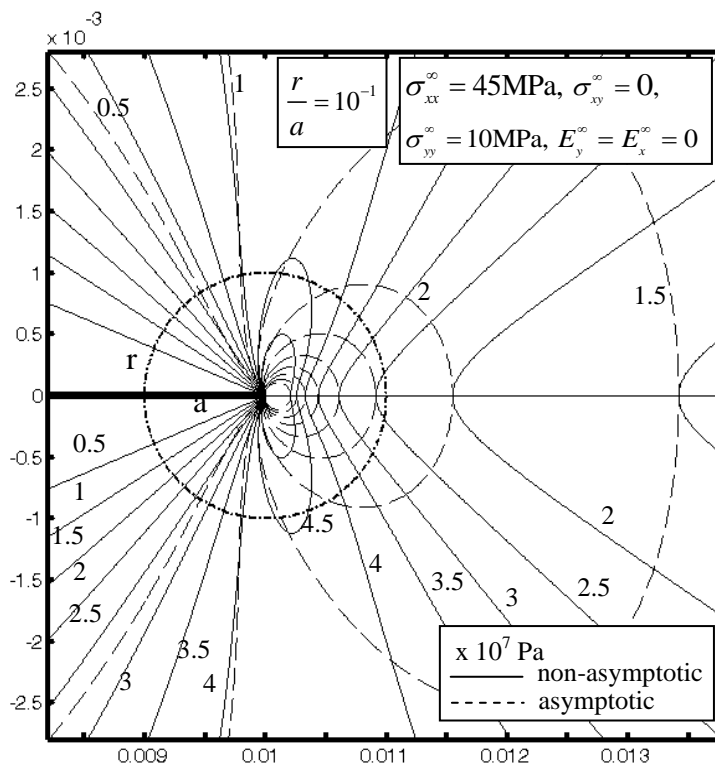
Fig. 5.49 – Iso-stress curves for hoop stress $\sigma_{\theta\theta}$ in the vicinity of the crack tip, when the solution is evaluated at $r/a = 10^{-1}$
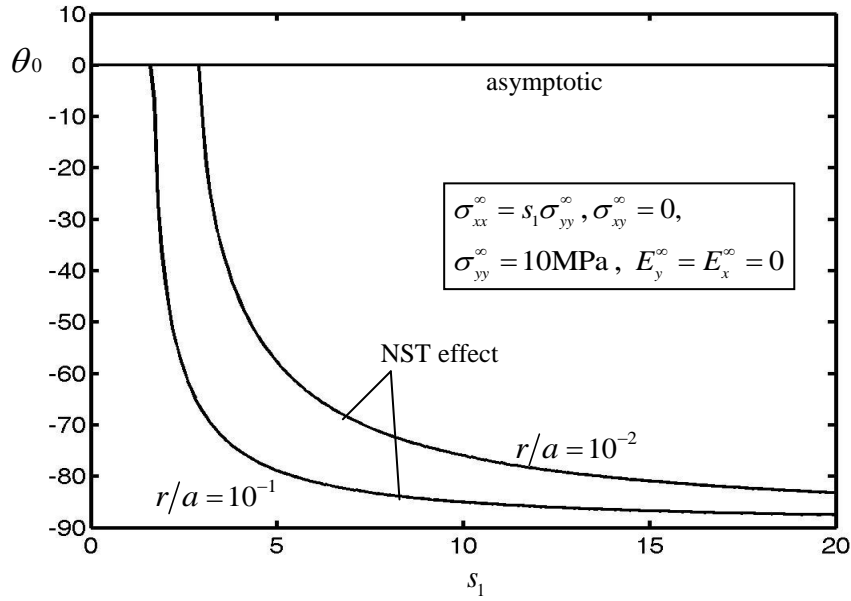
Fig. 5.50 – Locus of polar angles corresponding to the maximum values of hoop stress $\sigma_{\theta\theta}$, in relation to the biaxial loading parameter $s_1 = \sigma_{xx}^{\infty}/\sigma_{yy}^{\infty}$, in the asymptotic and non-singular representations
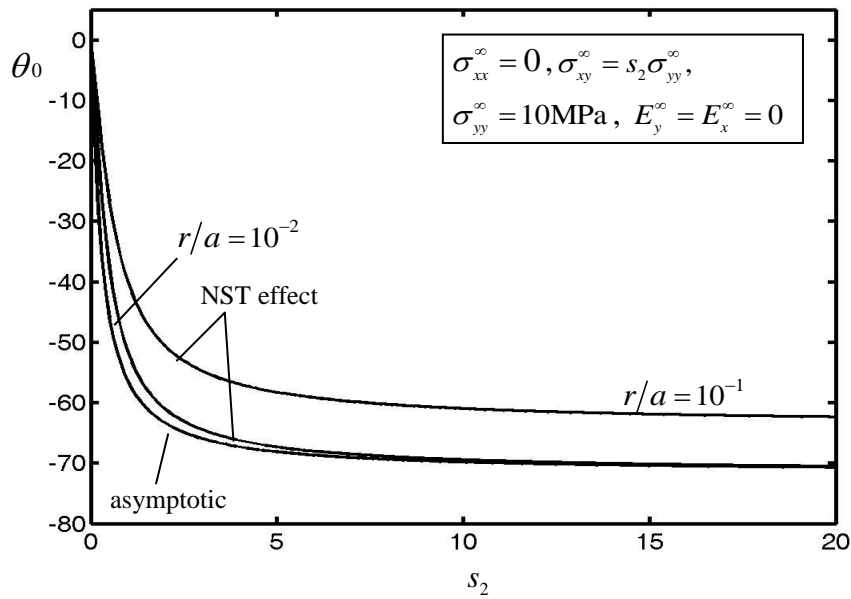
Fig. 5.51 – Locus of polar angles corresponding to the maximum values of hoop stress $\sigma_{\theta\theta}$, in relation to the biaxial loading parameters $s_2 = \sigma_{xy}^{\infty}/\sigma_{yy}^{\infty}$, in the asymptotic and non-singular representations

The results of this analysis show that the influence of non-singular terms is in general not negligible, as the omission of the non-singular stresses means

neglecting the biaxiality of the applied load and its effects. It appears evident that a local failure criterion is dependent on a parameter related to the biaxial load as well.

5.5.2.   *Minimum Crack Energy Density Criterion*

More than thirty years ago, the volume energy density was proposed by Sih [10-11] as a fracture criterion, and the energy density factor S as the fundamental parameter in this theory. According to this theory, the stationary value of S corresponding to the maximum of minimum values is assumed to coincide with the direction of crack initiation, and crack extension occurs when S_{min} reaches a critical magnitude S_c that can be seen as an intrinsic material characteristic. Lately, a number of works have suggested the extension of this criterion to the piezoelectric case: one can cite [12-24]. We will as well adopt this criterion to analytically study the fracture behaviour of a cracked piezoelectric ceramic.

Similarly to the linear elastic case [10-11], the energy density for a linear piezoelectric material in the unit volume element $\mathrm{d}V$ of a general three-dimensional system can be defined as:

$$\frac{\mathrm{d}W}{\mathrm{d}V} = \frac{1}{2}\sigma_{ij}\varepsilon_{ij} + \frac{1}{2}D_i E_i \tag{5.11}$$

and has the physical meaning of the work done during electromechanical deformation.

The increment of energy $\mathrm{d}W$ becomes increasingly high as the considered unit volume approaches a defect, because the local stress and strain can be many times greater than the global average. The two terms on the right side are generally referred to in the literature as the mechanical and the electrical portions of the energy stored in $\mathrm{d}V$:

$$\left(\frac{\mathrm{d}W}{\mathrm{d}V}\right)_M = \frac{1}{2}\sigma_{ij}\varepsilon_{ij}, \qquad \left(\frac{\mathrm{d}W}{\mathrm{d}V}\right)_E = \frac{1}{2}D_i E_i \tag{5.12}$$

However, it should be noted that the electrical-mechanical interaction is present in both terms, as one can verify with the substitution in (5.11) of the constitutive relations:

$$\begin{aligned}
\left(\frac{\mathrm{d}W}{\mathrm{d}V}\right)_M &= \frac{1}{2}\gamma_{ij}c_{ijks}\gamma_{ks} - \frac{1}{2}\gamma_{ij}e_{sij}E_s \\
\left(\frac{\mathrm{d}W}{\mathrm{d}V}\right)_E &= \frac{1}{2}\gamma_{ij}e_{sij}E_s - \frac{1}{2}E_i\varepsilon_{ij}E_j
\end{aligned}
\tag{5.13}$$

or the inverse constitutive relations:

$$\begin{aligned}
\left(\frac{\mathrm{d}W}{\mathrm{d}V}\right)_M &= \frac{1}{2}\sigma_{ij}H_{ijks}\sigma_{ks} - \frac{1}{2}\sigma_{ij}g_{sij}D_s \\
\left(\frac{\mathrm{d}W}{\mathrm{d}V}\right)_E &= \frac{1}{2}\sigma_{ij}g_{sij}D_s - \frac{1}{2}D_i\beta_{ij}D_j
\end{aligned}
\tag{5.14}$$

What is meant by mechanical and electrical energy is indeed ambiguous because the unique coupling effect peculiar of piezoelectric materials renders the separation of the two phenomena not possible. Thus, the neglect of one or the other does not imply that the mechanical or the electrical part is actually excluded from the analysis.

The right-hand terms of equations (5.14) can be obtained from the formulations of the stress fields (4.159) and (4.160) to yield an expression involving energy singular and non-singular terms such that:

$$\frac{\mathrm{d}W}{\mathrm{d}V} = \frac{S_s}{r} + S_{ns}(r) \tag{5.15}$$

where r is the angular distance from the crack tip. One can define the energy density factor S as a function of the applied mechanical and electrical loads and of the considered polar coordinates r and θ, as:

$$S = S_s + rS_{ns}(r) = r\frac{\mathrm{d}W}{\mathrm{d}V} \tag{5.16}$$

According to the energy density fracture criterion, at the crack tip the location of the maximum of S relative minimum values corresponds to the radial direction of potential extension of an existing damage. Crack initiation is triggered when the quantity $(\mathrm{d}W/\mathrm{d}V)_{\min}$ reaches a critical value $(\mathrm{d}W/\mathrm{d}V)_c$, characteristic of the material under study, while rapid (unstable) crack extension leading to failure

takes place when both $\left(\mathrm{d}W/\mathrm{d}V\right)_{\min}$ and the crack growth increment r_{c} become critical:

$$S_{\mathrm{c}} = r_{\mathrm{c}} \left(\frac{\mathrm{d}W}{\mathrm{d}V} \right)_{\mathrm{c}} \tag{5.17}$$

As already mentioned, the energy density criterion does not require an "a priori" knowledge of the direction of incipient crack branching, which is instead predicted by minimizing the function. The necessary and sufficient conditions for identifying the angle θ_0 where the S factor is minimum are:

$$\left. \frac{\partial S}{\partial \theta} \right|_{\theta = \theta_0} = 0 \tag{5.18}$$

$$\left. \frac{\partial^2 S}{\partial \theta^2} \right|_{\theta = \theta_0} > 0 \tag{5.19}$$

Since in the formulation of the energy density (5.15) non-singular terms are retained, the S factor is also dependent on the radius, and an appropriate value r should be determined experimentally for the material considered in the analysis. We considered in our study a crack semilength $a = 1\mathrm{cm}$ and a characteristic distance $r = 10^{-1}\,\mathrm{mm}$ (such that $r/a = 10^{-2}$).

Many authors [12-24] consider the energy density criterion to be preferred rather than the traditional Griffith's Energy Release Rate approach when analysing piezoelectric fracture, because of a better agreement of theoretical results with some empirical outcomes.

Griffith's theory uses the Energy Release Rate, or the energy dissipated during fracture per unit of newly created fracture surface area, as the parameter governing the fracture behaviour. This quantity is central in Fracture Mechanics, because the energy that must be supplied to a crack tip for it to propagate must be balanced by the amount of energy dissipated due to the formation of new surfaces and to other dissipative processes such as plasticity. Griffith's Energy Release Rate failure criterion states that a damage will grow when the local energy stored is greater than, or equal to, the amount necessary for the creation of a unit area (or length of crack for bi-dimensional problems), which is a critical

value G_c. G_c is called fracture energy and is considered to be a material property, independent of the applied loads and the geometry of the body.

It is possible to calculate the Energy Release Rate G for crack branching (ERR), for example from the specific energy flux at the tip $x = a$ (Freund, 1972 [25]). The formula gives:

$$G = \frac{\pi}{4}\Big[\mathbf{t}_2^T(r,0)\mathbf{U}(r,\pi)\Big] \tag{5.20}$$

This theory was widely used in fracture mechanics of brittle elastic materials as a main crisis criterion. In an attempt to define such a criterion, able to predict the critical load that triggers crack extension and the system response to different conditions, for piezoelectric materials, the energy release rate concept has been extended to these materials and widely used as a main fracture parameter for many years. However, as pointed out in several works [26-28], this criterion contradicts available experimental results, failing to predict the effect of applied electric field. In particular, the influence of applied electric field on the crack growth enhancement and retardation cannot be correctly assessed when the energy release rate approach is used.

During experimental tests conducted on cracked piezoelectric bodies, it was observed [29] that a positive electric field tends to open the crack and reduce the critical load while a negative field increases it. Theoretical results obtained following the ERR theory, instead, imply that crack initiation and extension are always impeded by the presence of an electric field, regardless of its direction [24, 30-32].

In fact, as displayed in Figure 5.52 for a PZT-4 ceramic, when mechanical load is applied only in the direction perpendicular to the crack (red curve), the addition of any electric loading, has the consequence of diminishing the value of G associated to the impermeable model, regardless of its sign. This implies that if prior to the application of the field the energy content of the system was about the critical threshold, after it would be less; in other words, as the absolute value

of applied E_y^∞ is increased, a propagating crack would tend to arrest or fracture crisis would be diverted. These theoretical results contradict experimental observations, which showed that crack growth is enhanced by the application of an electric field parallel to the material polarization (positive) and retarded by a field in the opposite direction [26,27]. The same figure depicts also the influence of biaxial (collinear) load applied at infinity. The effect of a positive s_1 is to right-shift the ERR curve with no appreciable variation of its value, and vice versa, but the trends remain unchanged.

In presence of a tangential remote loading (Figure 5.53), the ERR in an increasing function of the applied load irrespectively of its sign, but again the application of an electric field has the effect of diminishing the value of G, in disagreement with experimental tests.

In order to bypass this discrepancy, some researchers (Park and Sun [26-27]) proposed to use only the mechanical part of the energy release rate as a fracture parameter, but many others objected that this approach is physically inconsistent (see for example Zhang et al. [28] and McMeeking [33]).
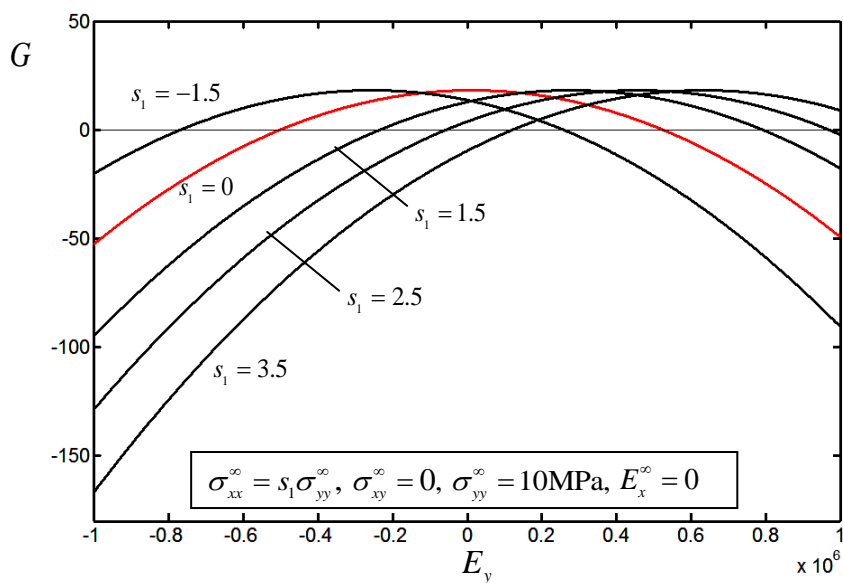
Fig 5.52 – Effect of the applied electric field and of the biaxial load parameter s_1 on the trends of the Energy Release Rate curves (impermeable case)
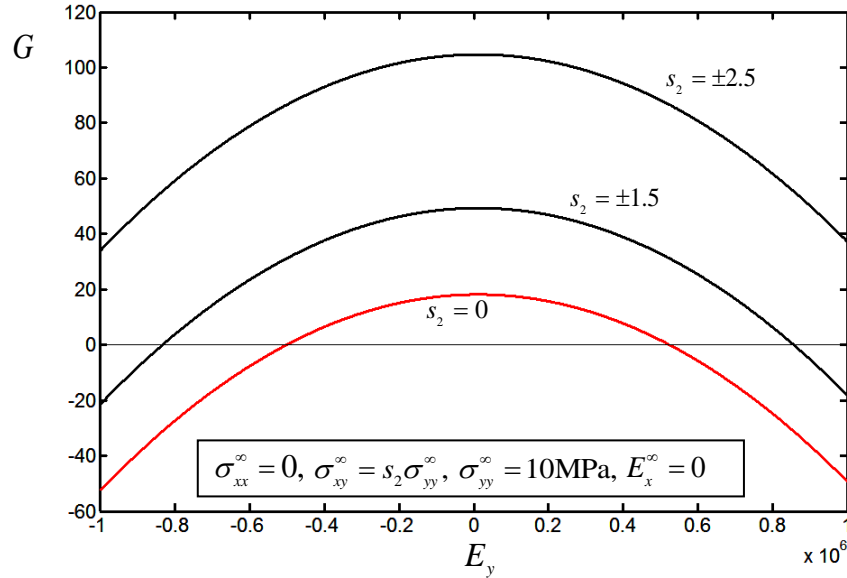
Fig 5.53 – Effect of the applied electric field and of the biaxial load parameter s_2 on the trends of the Energy Release Rate curves (impermeable case)

Lately, a number of works have suggested the extension of the Minimum Crack Energy Density criterion to the piezoelectric case, in substitution of the Maximum Energy Release Rate: one can cite [12-24]. We will see that the theoretical results of this approach are not in opposition with experimental observations.

In the graphs of Fig 5.54 the effect of the applied electric field E_y^∞ on the minimum energy density factor $S_{\min}$ is plotted together with the Energy Release Rate. One can see that for all the models this energetic quantity increases monotonically with positive E_y^∞ and decreases for negative applied field, presenting a minimum in the impermeable case for $E_y^\infty = 2.5\,\mathrm{KV/cm}$, in accordance with what pointed out also by Sih in [14]. These outcomes qualitatively agree with the results of the experiments carried out by some authors [29]. If the applied mechanical load is biaxial ($\sigma_{yy}^\infty, \sigma_{xx}^\infty$) all the curves related appear shifted to the right, and those related to S result also increased in value (Figure 5.55). The trends of G in the permeable case are always represented by horizontal lines, since with this hypothesis the remote electric load has no influence on the energy release rate. It is important to underline that the energy density factor S is

141

always a positive quantity. On the contrary, the energy release rate G becomes negative for applied electric field high enough (positive or negative). All the numerical applications in this paper are referred to a PZT-4 piezoelectric ceramic.
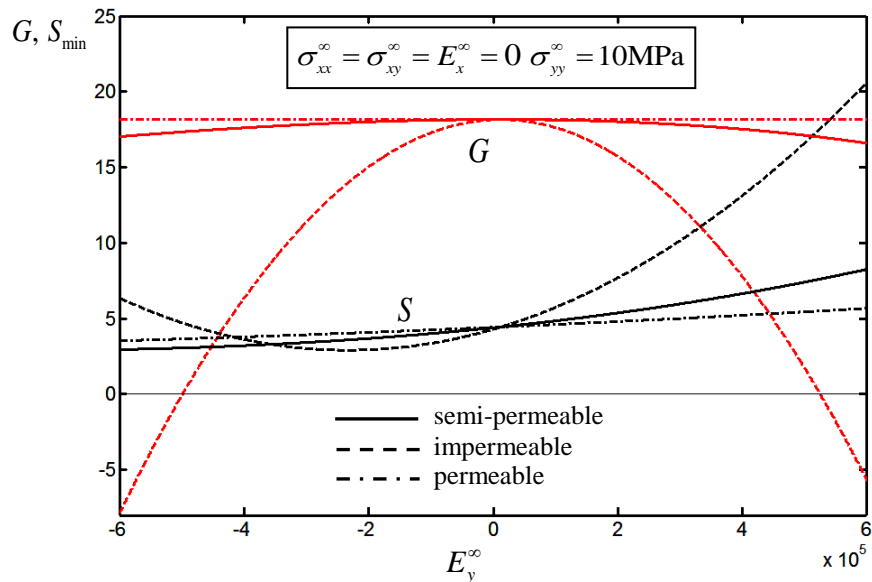
Fig. 5.54 –Applied electric field influence on the Energy Density Factor and Energy Release Rate, for the three crack models $(r/a = 10^{-2})$
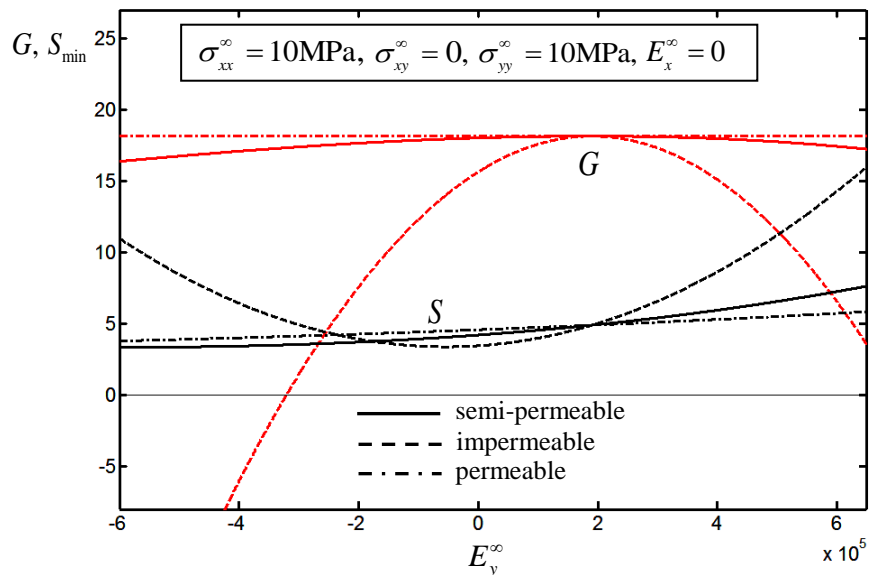
Fig. 5.55 –Applied electric field influence on the Energy Density Factor and Energy Release Rate, for the three crack models, with biaxial mechanical load $(r/a = 10^{-2})$
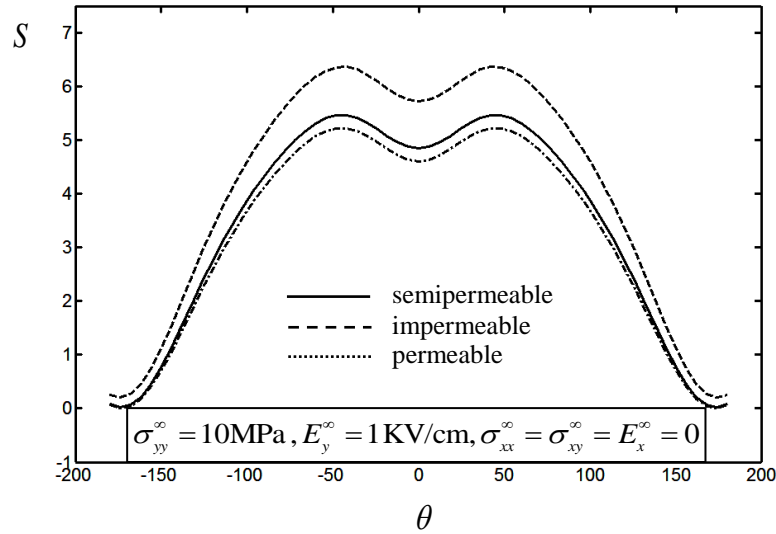
Fig. 5.56 – Influence of the permittivity of the crack on the Energy Density Factor vs polar angle
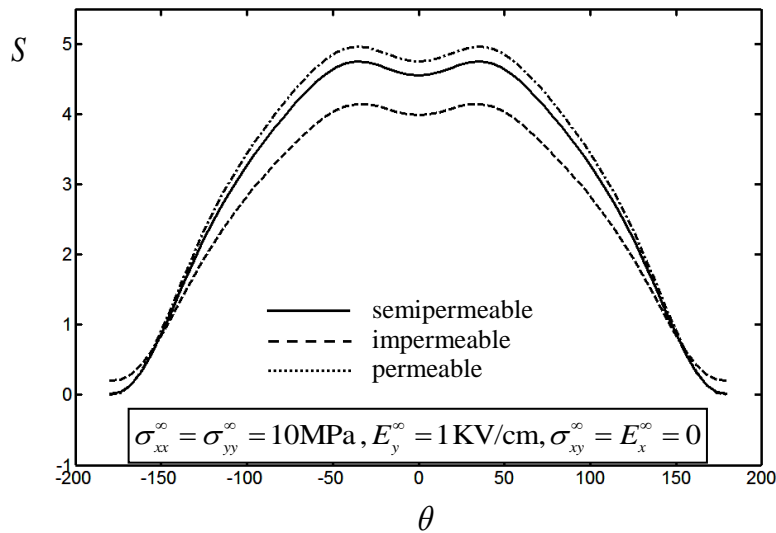
Fig. 5.57 – Influence of the permittivity of the crack on the Energy Density Factor vs polar angle, biaxial load

Figure 5.56 depicts the influence of the considered electric boundary conditions on the energy density factor plotted as a function of the polar angle θ, for a mixed opening-electric mode. It can be seen that S of the impermeable crack is larger than that of the permeable crack, the semipermeable one (with air filling the cavity) laying in between. Under these conditions the energy density factor takes the minimum value $S_{\min}$ at $\theta = 0$.
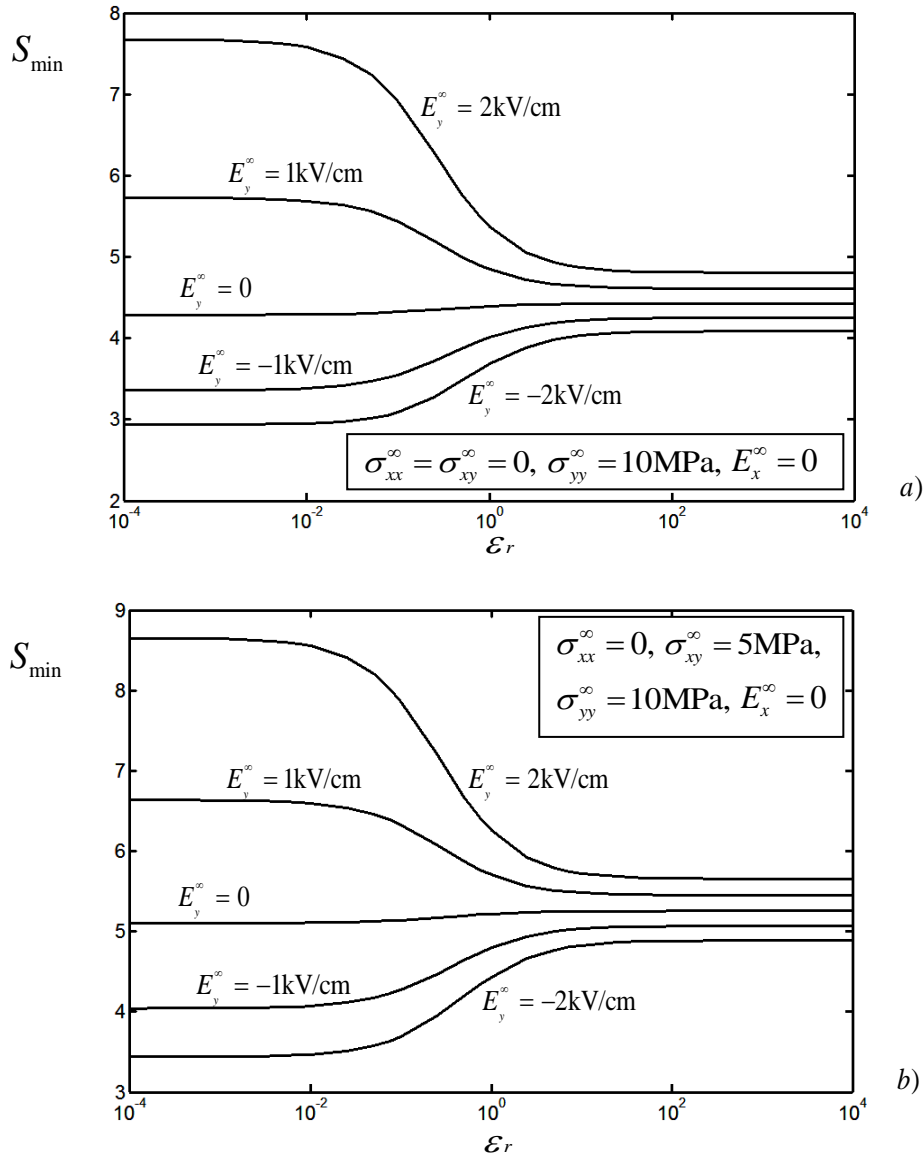
Fig. 5.58 – Crack permeability influence on the Energy Density Factor for different mixed mode loading conditions

In Figure 5.57 a collinear load has been added to the previous remote loading condition: the order of relative entities of the energy density referring to the three crack models is reversed, according with Fig. 5.54 and 5.55.

More generally one can affirm that, for the material and loading conditions under study, when a positive electric field is applied at infinity, the actual value of S_{min} is less than that obtained in the approximation of impermeable crack, and larger than the one obtained in the case of perfectly permeable crack, and the opposite

occurs when $E_y^\infty < 0$ is applied. A collinear applied load can have the effect of modifying these values. This is shown in Figure 5.58 a-b which plot S_{min} versus the relative permittivity of the medium inside the crack considered in logarithmic scale ($\varepsilon_r = 10^{-4}$ and $\varepsilon_r = 10^4$ correspond to the impermeable and permeable boundary conditions, $\varepsilon_r = 1$ identifies a crack filled with air or vacuum) with monoaxial and biaxial load.

It should be highlighted that, as underlined in [18, 19], the piezoelectric fracture load is underestimated by the assumption of impermeable crack subjected to positive field and vice versa, for the examined values of applied electric loading.

Figures 5.59, 5.60 and 5.61 represent the curves of the energy density factor for different loading combinations, governed by the loading parameters $s_1 = \sigma_{xx}^\infty / \sigma_{yy}^\infty$, $s_2 = \sigma_{xy}^\infty / \sigma_{yy}^\infty$ and $s_E = E_y^\infty / \sigma_{yy}^\infty \left[m^2/C \right]$.
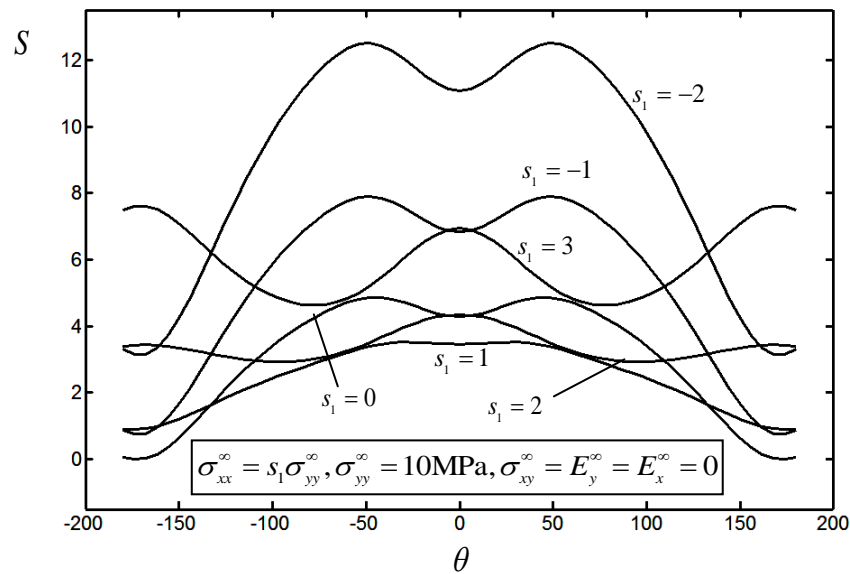
Fig. 5.59 – Influence of the biaxial load parameter $s_1 = \sigma_{xx}^\infty / \sigma_{yy}^\infty$ on the normalized Energy Density Factor vs polar angle in the impermeable case $(r/a = 10^{-2})$
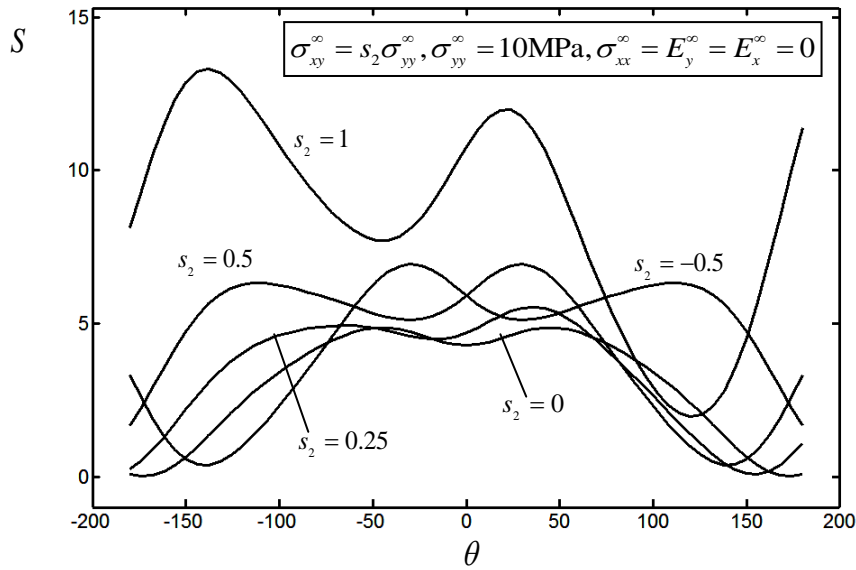
Fig. 5.60 – Influence of the biaxial load parameter $s_2 = \sigma_{xy}^\infty / \sigma_{yy}^\infty$ on the normalized Energy Density Factor vs polar angle in the impermeable case $(r/a = 10^{-2})$
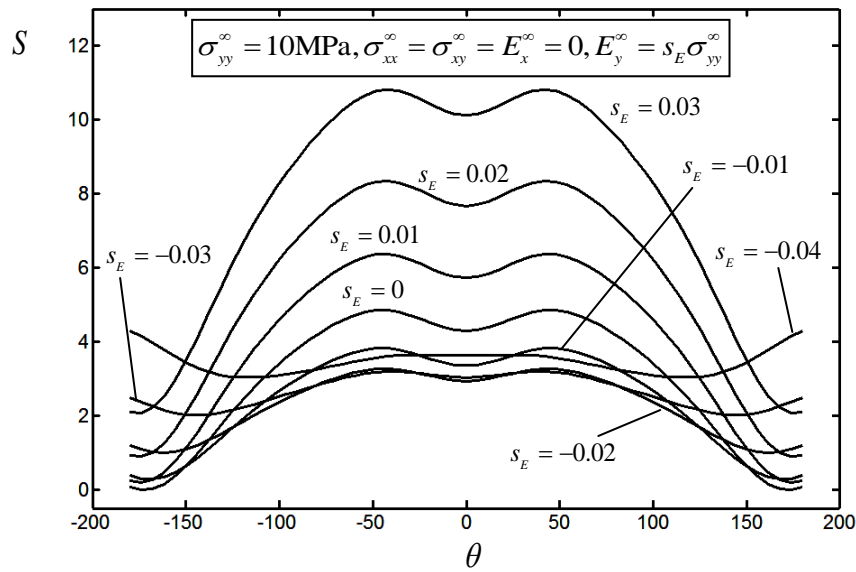
Fig. 5.61 – Influence of the electric load parameter $s_E = E_y^\infty / \sigma_{yy}^\infty$ on the normalized Energy Density Factor vs polar angle in the impermeable case $(r/a = 10^{-2})$

The value of S^* and the position of the maximum of relative minimum are, generally speaking, very sensitive to the biaxial load and to the electric field applied. Some interesting considerations can be drawn from these figures. In particular, Figure 5.60 shows that the maximum of the minimum values increases

146

with the shear mechanical load (regardless of its sign), whereas from Figure 5.59 one can note that to an increase in s_1 initially corresponds a decrease in the energy density factor and vice versa.

The effect of a positive applied electric field (Figure 5.61) is always to augment the value of S^* while the application of a negative E_y^∞ causes initially a decrease of the energy density, that then starts to rise again for sufficiently low electric field values. The same effect was shown in Figure 5.54.

Another important issue arising from the analysis of Figure 5.59-5.61 is that the biaxial or mixed mode load can influence the position of S_{min}, thus determining, at least theoretically, a deviation in the crack branching direction. This happens for any applied tangential load and for sufficiently high applied collinear loads and low (negative) electric loads.

In Figure 5.62, as an example, the influence of tangential loading on the angle θ_0 of incipient crack branching is estimated, as predicted by the crack energy density criterion (CED). The above angle is compared to that one obtained by means of another direction-sensitive approach, namely, the maximum circumferential stress criterion (MCS), as proposed in [8].

As Figure 5.62 depicts, the two theories are quite in agreement, showing similar curves and asymptotic trends in the range of -70° to -75° (Erdogan and Sih predicted a branching angle of about -70° for pure tangential load).
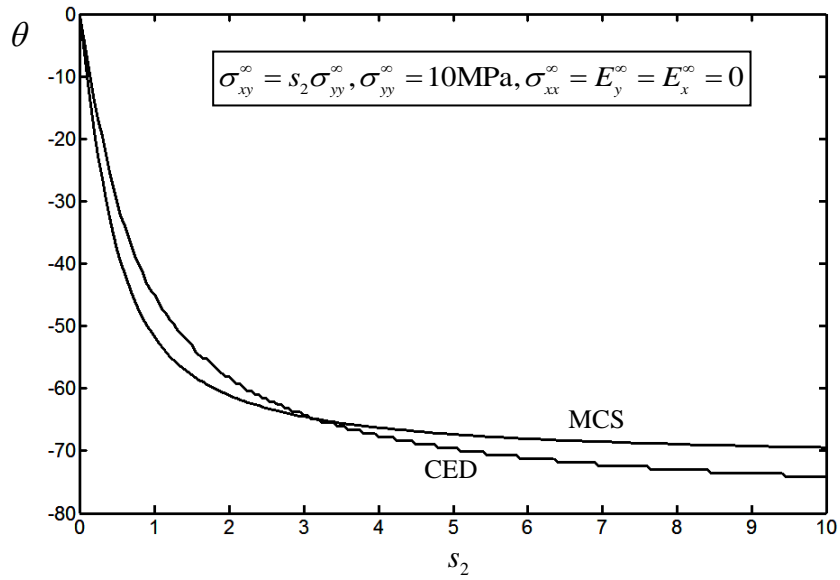
Fig. 5.62 – Prediction of the incipient branching angle through the Crack Energy Density criterion (CED) and the Maximum Circumferential Stress criterion (MCS), in relation to the biaxial loading parameter $s_2 = \sigma_{xy}^{\infty} / \sigma_{yy}^{\infty}$, impermeable case ($r/a = 10^{-2}$)

Conclusions

In this thesis the closed-form solution of the static crack problem in a piezoelectric medium arbitrarily loaded at infinity was yielded through a simple analytical method. Our approach can be regarded as alternative to other formalisms generally used for deriving the complex variable formulation of the electro-elastic fields.

The effect of the application of an electric field, of the considered electric boundary conditions and of the permittivity of the medium inside the crack have been discussed thoroughly.

The influence of biaxial load has been analyzed, observing that non-singular terms significantly affect the stress component collinear to the crack, as well as the electric and elastic displacements and the circumferential stress. Inclusion of non-singular stress terms along with the maximum circumferential stress or the minimum energy density criteria results in marked differences in the predicted direction of crack extension. In particular, the incipient branching angle is found to draw away from the crack axis as the load parallel to the crack increases, despite the symmetry of the loading condition. The results of the analysis show that the influence of non-singular terms is in general not negligible, and that the omission of the non-singular stresses means neglecting the biaxiality of the applied load. It appears evident that a local failure criterion is dependent on a parameter related to the biaxial load as well. Moreover, the critical conditions of stress and electric quantities have been evaluated at a small and specified radial distance from the crack tip; such distance should be a material property, as pointed out in many works [e.g. 1-2, 5-7, 9], but it is still under discussion.

Further analytical and experimental work is needed for defining a reliable fracture criterion that may predict the failure of piezoelectric structures and devices subjected to biaxial electro-mechanical loading.

References

[1]   Eftis J., Jones D.L., Liebowitz H., *Load biaxiality and fracture: synthesis and summary*, Engng. Fract. Mech. (1990); 36:537-574.

[2]   Viola E., *Non-singular stresses effects on two interacting equal collinear cracks*, Engng. Fract. Mech. (1983); 18:801-814.

[3]   Ma H., Zhao L.G., Chen Y.H., *Non-singular terms for multiple cracks in anisotropic elastic solids*, Theor. Appl. Fract. Mech. (1997); 27:129-134.

[4]   Lim W.K., Choi S.Y., Sankar B.V., *Biaxial load effects on crack extension in anisotropic solids*, Engng. Fract. Mech. (2001); 68:403-416.

[5]   Nobile L., Piva A., Viola E., *On the inclined crack problem in an orthotropic medium under biaxial loading*, Engng. Fract. Mech. (2004); 71:529-546.

[6]   Viola E., Boldrini C., Tornabene F., *Non singular term effect on the fracture quantities of a crack in a piezoelectric medium.* Engng. Fract. Mech. (2008); 75: 4542-4567.

[7]   Boldrini C., Viola E., *Crack energy density of a piezoelectric material under general electromechanical loading,* Theor. Appl. Fract. Mech. (2008); 49: 321-333.

[8]   Erdogan F., Sih G.C., *On the crack extension in plates under plane loading and transverse shear*, J. Basic Engng. (1963); 85:519-527.

[9]   Carpinteri A., Di Tommaso A., Viola E., *Collinear stress effect on the crack branching phenomenon*, Matériaux et Constructions, RILEM (1979); 12:439-446.

[10] Sih G.C., *Some basic problems in fracture mechanics and new concepts*, J. Engng. Fract. Mech. (1973); 5: 365-377.

[11] Sih G.C., *Mechanics of Fracture*, Vols. I-VII. Martinus Nijhoff, Netherlands, 1973-1982.

[12] Sih G.C., Zuo J.Z., *Multiscale behavior of crack initiation and growth in piezoelectric ceramics*, Theor. Appl. Fract. Mech. (2000); 34: 123-141.

[13] Zuo J.Z., Sih G.C., *Energy density theory formulation and interpretation of cracking behaviour for piezoelectric ceramics*, Theor. Appl. Fract. Mech. (2000); 34: 17-33.

[14] Sih G.C., *A field model interpretation of crack initiation and growth behaviour in ferroelectric ceramics: change of poling direction and boundary condition*, Theor. Appl. Fract. Mech. (2002); 38: 1-14.

[15] Sih G.C., Chen E.P., *Dilatational and distortional behaviour of cracks in magnetoelectro-elastic materials*, Theor. Appl. Fract. Mech. (2003); 40: 1-21.

[16] Shen S., Nishioka T., *Fracture of piezoelectric materials: energy density criterion*, Theor. Appl. Fract. Mech. (2000); 33: 57-65.

[17] Wang B.L., Noda N., *Mixed mode crack initiation in piezoelectric ceramic strip*, Theor. Appl. Fract. Mech. (2000); 34: 35-47.

[18] Soh A.K., Fang D.N., Lee K.L., *Fracture analysis of piezoelectric materials with defects using energy density theory*, Int. J. Solids Struct. (2001); 38: 8331-8344.

[19] Lee K.L., Soh A.K., Fang D.N., Liu J.X., *Fracture behaviour of inclined elliptical cavities subjected to mixed-mode I and II electro-mechanical loading*, Theor. Appl. Fract. Mech. (2004); 41: 125-135.

[20] Chue C.H., Weng S.M., *Fracture analysis of piezoelectric materials with an arbitrarily oriented crack using energy density theory*, Comp. Struct. (2005); 83: 1251-1265.

[21] Nam B.G., Watanabe K., *Crack energy density and energy release rate for piezoelectric material*, Int. J. Solids Struct. (2007); 44: 3904-3919.

[22] Nam B.G., Watanabe K., *Effect of electric boundary conditions on crack energy density and its derivatives for piezoelectric material*, Engng. Fract. Mech. (2008); 75: 207-222.

[23] Nam B.G., Liu R., Tsuchida S., Watanabe K., *Applicability of crack energy density to fracture strength evaluation of piezoelectric ceramics*, Mat. Sci. Eng. A. (2007) 343-347.

[24] Boldrini C., Viola E., *Crack energy density of a piezoelectric material under general electromechanical loading,* Theor. Appl. Fract. Mech. (2008); 49: 321-333.

[25] Freund L.B., *Energy flux into the tip of an extending crack in an elastic solid*, J. Elasticity (1972); 2: 341-349.

[26] Park S.B., Sun C.T., *Effect of electric field on fracture of piezoelectric ceramics*, Int. J. Fract. (1995); 70: 203-216.

[27] Park S.B., Sun C.T., *Fracture criteria for piezoelectric ceramics*, J. Am. Ceram. Soc. (1995); 78: 1475-1480.

[28] Zhang T.Y., Qian C.F., Tong P., *Linear electro-elastic analysis of a cavity or a crack in a piezoelectric material*, Int. J. Solids Struct. (1998); 35: 2121-2149.

[29] Tobin A.G., Pak Y.E., *Effect of electric fields on fracture behaviour of PZT ceramics*, in Smart Materials (Edited by VK Vardan) Proc. SPIE (1993) 1916:76-86.

[30] Suo Z., Kuo C.M., Barnett D.M., Willis J.R., *Fracture mechanics for piezoelectric ceramics,* J. Mech. Phys. Solids (1992); 40: 739-765.

[31] Pak Y.E., *Linear electro-elastic fracture mechanics of piezoelectric materials*, Int. J. Fract. (1992); 54: 79-100.

[32] Pak Y.E., *Crack extension force in a piezoelectric material.* J. Appl. Mech. (1990); 57: 647-653.

[33] McMeeking R.M., *Crack tip energy release rate for a piezoelectric compact tension specimen*, Engng. Fract. Mech. (1999); 64: 217-244.

APPENDIX A

MATHEMATICAL DEFINITIONS, THEOREMS AND HILBERT PROBLEM

A.1   Positive sense of description of a curve

Consider a region R^+ having one or more non-intersecting contours $C_0,...,C_n$ as its boundary. The positive sense of description of each contour is conventionally taken to be that for which the region R^+ lies to the left, as indicated in Figure A1.
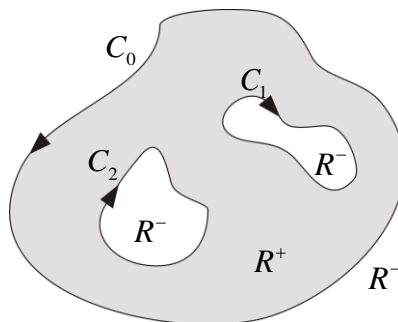
Fig. A1 – Convention on the positive sense of description of contours

A.2   Cauchy's theorem

Given a function $f(z)$ analytic in the region R and continuous on its contour C, then:

$$\oint_C f(z)dz = 0 \qquad\qquad (A.1)$$

A.3 Cauchy integrals

Let D^+ be a simply connected region bounded by the contour $C = C(\sigma)$, positive anticlockwise, and denote the open region exterior to D^+ by D^- (Figure A2).
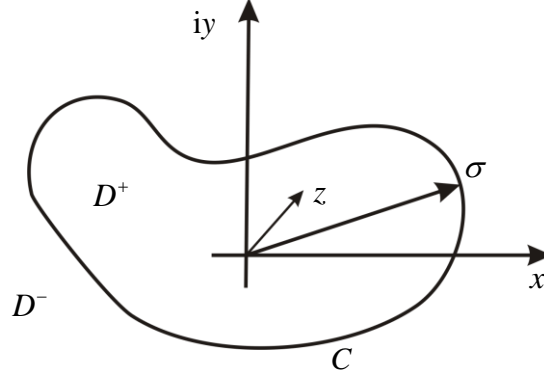
Fig. A2 – Simply connected region bounded by $C = C(\sigma)$

If $f(z)$ is a complex function holomorphic (analytical) in D^+ and continuous on C, the following equalities hold:

$$\frac{1}{2\pi i}\oint_C \frac{f(\sigma)d\sigma}{\sigma - \zeta} = f(\zeta) \qquad\qquad \zeta \in D^+ \qquad\qquad (A.2)$$

$$\frac{1}{2\pi i}\oint_C \frac{f(\sigma)d\sigma}{\sigma - \zeta} = 0 \qquad\qquad \zeta \in D^- \qquad\qquad (A.3)$$

If $f(z)$ is a complex function holomorphic (analytical) in $D^- \cup \{\infty\}$ and continuous on C, the following equalities hold:

$$\frac{1}{2\pi i}\oint_C \frac{f(\sigma)d\sigma}{\sigma - \zeta} = f(\infty) \qquad\qquad \zeta \in D^+ \qquad\qquad (A.4)$$

$$\frac{1}{2\pi i}\oint_C \frac{f(\sigma)d\sigma}{\sigma - \zeta} = f(\infty) - f(\zeta) \qquad \zeta \in D^- \qquad\qquad (A.5)$$

Relations (A.2)-(A.5) are termed Cauchy integrals.

A.4 Hölder condition

A function $f(t)$ defined on a curve L (open or closed) is said to satisfy a Hölder condition on L if for any two points $t_1, t_2 \in L$ the following holds:

$$\left| f(t_2) - f(t_1) \right| \le A \left| t_2 - t_1 \right|^{\mu}, \qquad 0 \le \mu \le 1. \tag{A.6}$$

The positive constants A and μ are termed respectively Hölder costant and index.

If a function satisfies the Hölder condition on a curve L then it is continuous on L and it can be indicated with $f(t) \in H^{\mu}(L)$ o $f(t) \in H(L)$.

A.5 Sectionally continuous and sectionally holomorphic functions

Assume L to be a curve with a given direction in the complex plane. About any point $\zeta \in L$ (different from the end points) it is possible to define a neighbourhood:

$$D_{\zeta} - L = \left\{ z, z \notin L; 0 < \left| z - \zeta \right| < \delta \right\} \tag{A.7}$$

and the respective right $\Omega_{\zeta}^{-} = (D_{\zeta} - L)^{-}$ and left neighbourhoods $\Omega_{\zeta}^{+} = (D_{\zeta} - L)^{+}$.
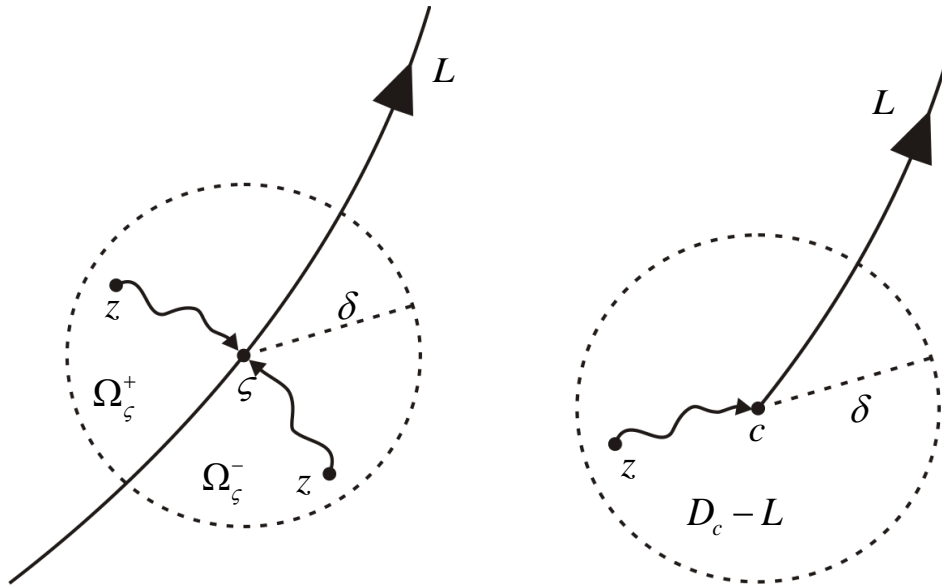
Fig. A3 – Sectionally continuous functions

A complex function $F(z)$ continuous in any neighbourhood $D_{\zeta} - L$ of L, defined as:

$$F(z) = \begin{cases} F^{+}(z), & z \in \Omega_{\zeta}^{+} \\ F^{-}(z), & z \in \Omega_{\zeta}^{-} \end{cases} \tag{A.8}$$

155

and for which:

$$\forall \zeta \in L, \ \exists \begin{cases} \lim_{z \to \zeta} F^+(z) = F^+(\zeta) \\ \lim_{z \to \zeta} F^-(z) = F^-(\zeta) \end{cases} \tag{A.9}$$

is said to be sectionally continuous.

The values $F^+(\zeta)$ and $F^-(\zeta)$ are termed left and right limits of $F(z)$ on L. It is demonstrable that these limits are continuous functions and consequently the discontinuity $g(\zeta) = F^+(\zeta) - F^-(\zeta)$ is as well a continuous function. In other words a function is sectionally continuous in a neighbourhood of L if it is continuous in the neighbourhood and if its right and left limits exist at all interior points of L. At the end points of a curve it is as well possible to define a neighbourhood:

$$D_c - L = \left\{ z, z \notin L; 0 < |z - c| < \delta \right\} \tag{A.10}$$

and the function $F(z)$ is said to be continuous in $\zeta = c$ if:

$$\Omega_\zeta^- \quad \lim_{\substack{z \to c \\ z \in D_c - L}} F(z) = F(c) = F^+(c) = F^-(c) \tag{A.11}$$

A function $F(z)$ is said to be sectionally holomorphic in a region R cut along an arc L if:

1. it is holomorphic for all $z \in R - L$,

2. it is sectionally continuous in the neighbourhood of L,

3. it is such that at an end c of the arc L:

$$|F(z)| \leq \frac{A}{|z - c|^\alpha}, \quad A > 0, \quad 0 \leq \alpha \leq 1. \tag{A.12}$$

A.6 Index of a function

Let L be a simple contour and $G(\zeta)$ a function continuous on L. The index of the function $G(\zeta)$ is defined as:

$$\chi = \text{Ind} \, G(\zeta) \equiv \frac{\left[\arg G(\zeta) \right]_L}{2\pi}, \tag{A.13}$$

where $\left[\arg G(\zeta) \right]_L$ is the variation $\arg G(\zeta)$ undergoes when ζ circulates positively around the contour. Since one has:

156

$$\log G(\zeta) = \log|G(\zeta)| + i(\arg G(\zeta) + 2k\pi), \qquad k \in Z \qquad (A.14)$$

and $|G(\zeta)|$ gets back to its initial value after a whole circulation, one can write:

$$\left[\log G(\zeta)\right]_L = i\left[\arg G(\zeta)\right]_L, \qquad (A.15)$$

$$\chi = \frac{1}{2\pi i}\left[\log G(\zeta)\right]_L = \frac{1}{2\pi i}\int_L d\left[\log G(\zeta)\right] \qquad (A.16)$$

Due to its continuity, the variation of the argument of $G(\zeta)$ along a whole circulation is a multiple of 2π.

A.7 Classes of finite order functions

A function $f(z)$ is said to be of order k in a point $z = z_0$ if, in a neighbourhood of such point, it can be represented by the Laurent expansion:

$$f(z) = \frac{a_{-k}}{(z-z_0)^k} + \frac{a_{-k+1}}{(z-z_0)^{k-1}} + \ldots + a_0 + a_1(z-z_0) + \ldots, \qquad a_{-k} \neq 0; \quad (A.17)$$

that is if $f(z)$ has in z_0 a pole of k-order if $k > 0$, a zero of $(-k)$-order if $k < 0$, or is analytic in z_0 if $k = 0$.

A function $f(z)$ is said to be of order k at infinity if in a neighbourhood of $z = \infty$ it can be represented by the Laurent expansion:

$$f(z) = a_k z^k + a_{k-1} z^{k-1} + \ldots, \qquad a_k \neq 0; \qquad (A.18)$$

if $k > 0$, $z = \infty$ is a pole of order k, if $k < 0$ $z = \infty$ is a zero of order $(-k)$, if $k = 0$ it is $f(\infty) = a_0$.

The following classes of functions are defined:

A_0^∞: Class of analytic functions of zero order and finite at infinity ($f(\infty) = a_0 \neq 0$).

A_{-1}^∞: Class of analytic functions of zero order and null at infinity ($f(\infty) = 0$).

$A_{-r}^\infty, r \geq 2$: Class of analytic functions of (-r) order at infinity, which have at infinity a zero of order r.

$A_n^\infty, n > 0$: Class of analytic functions of order n at infinity. These functions have at infinity a pole of order n and in a neighbourhood of $z = \infty$ can be represented in the form:

$$f(z) = P_n(z) + \sum_{k \geq n}^{\infty} \frac{a_k}{z^k} \tag{A.19}$$

where $P_n(z) = a_n z^n + a_{n-1} z^{n-1} + \dots + a_1 z + a_0$, with $a_n \neq 0$.

A.8 Formule di Sokhotski-Plemelj

The problem is to study the existence of Cauchy's integral limit values on a curve L:

$$F(z) = \frac{1}{2\pi i} \int_L \frac{f(t)dt}{t - z} , \qquad z \notin L \tag{A.20}$$

when z tends to a point on the contour of integration.

It is possible to demonstrate that if $f(t)$ satisfies the Hölder condition (i.e. $f(t) \in H(L)$), the left and right limit values, defined as:

$$
\begin{aligned}
F^+(\zeta) &= \frac{1}{2\pi i} \lim_{\substack{z \to \zeta \\ z \in D^+}} \int_L \frac{f(t)dt}{t - z} , \qquad \zeta \in L \\
F^-(\zeta) &= \frac{1}{2\pi i} \lim_{\substack{z \to \zeta \\ z \in D^-}} \int_L \frac{f(t)dt}{t - z} , \qquad \zeta \in L
\end{aligned}
\tag{A.21}
$$

exist and the following relations hold:

$$F^+(\zeta) - F^-(\zeta) = f(\zeta) , \tag{A.22}$$

$$F^+(\zeta) + F^-(\zeta) = \frac{1}{\pi i} \int_L \frac{f(t)dt}{t - \zeta} , \tag{A.23}$$

or:

$$F^+(\zeta) = \frac{f(\zeta)}{2} + \frac{1}{2\pi i} \int_L \frac{f(t)dt}{t - \zeta} , \tag{A.24}$$

$$F^-(\zeta) = -\frac{f(\zeta)}{2} + \frac{1}{2\pi i} \int_L \frac{f(t)dt}{t - \zeta} . \tag{A.25}$$

Relations (A.22) e (A.23) are said Sokhotski-Plemelj formulae; they still hold if applied to the union of two or more curves.

A.9 Hilbert problem on a closed contour

Let L be a regular closed contour in C and D^+ and D^- the inner and outer regions. The Hilbert problem for L consists in determining the sectionally analytic function $\Phi(z)$, $z \in C^\infty$, of finite order at infinity, that satisfies the boundary condition:

$$\Phi^+(\zeta) - G(\zeta)\Phi^-(\zeta) = 0, \qquad \zeta \in L \qquad \text{(homogeneous problem)} \qquad \text{(A.26)}$$

or the boundary condition:

$$\Phi^+(\zeta) - G(\zeta)\Phi^-(\zeta) = g(\zeta), \qquad \zeta \in L \qquad \text{(non-homogeneous problem)} \qquad \text{(A.27)}$$

$G(\zeta), g(\zeta)$ are functions of the complex variable $\zeta \in L$, hölderian on L, and $G(\zeta) \neq 0$.

A.9.1 Plemelj problem

Let us initially consider the Plemelj problem, obtained from (A.27) by posing $G(\zeta) = 1$.

One must seek the sectionally analytic function $\Phi(z)$ knowing its discontinuity $g(\zeta)$ on the closed curve:

$$\Phi^+(\zeta) - \Phi^-(\zeta) = g(\zeta), \qquad \zeta \in L \qquad \text{(A.28)}$$

Since $g(\zeta)$ satisfies the Hölder condition on L, from Sokhotski-Plemelj formulae we have that the function:

$$F(z) = \frac{1}{2\pi i} \int_L \frac{g(t)dt}{t-z}, \qquad z \notin L \qquad \text{(A.29)}$$

satisfies the condition (A.28):

$$F^+(\zeta) - F^-(\zeta) = g(\zeta), \qquad \zeta \in L. \qquad \text{(A.30)}$$

Subtracting (A.30) from (A.28) one gets:

$$\Phi^+(\zeta) - F^+(\zeta) = \Phi^-(\zeta) - F^-(\zeta), \qquad \zeta \in L \qquad \text{(A.31)}$$

that shows that the function

$$H(z) = \Phi(z) - F(z) \qquad \text{(A.32)}$$

is analytic on C.

The order of $H(z)$ at infinity must equal the order of $\Phi(z)$, thus if $\Phi(z) \in A_n^\infty$ one can write:

$$H(z) = P_m(z), \qquad \forall z \in C^\infty, \tag{A.33}$$

where P_m is an arbitrary polynomial of rank $m \leq n$, and the general solution of the Hilbert problem takes the form:

$$\Phi(z) = \frac{1}{2\pi i} \int_L \frac{g(t)dt}{t - z} + P_m(z) , \qquad z \notin L \tag{A.34}$$

where the coefficients $a_0, ..., a_m$ are $m+1$ complex constants.

A.9.2 The homogeneous Hilbert problem

Let us now solve the homogeneous problem (A.26):

$$\Phi^+(\zeta) - G(\zeta)\Phi^-(\zeta) = 0, \qquad \zeta \in L.$$

It is necessary to distinguish various cases depending on the value of the index χ of the function $G(\zeta)$ on L.

i) $\chi = 0$

In this case the function $\log G(\zeta)$ is monodrome (single-valued function). Consider the logarithm of (A.26):

$$\log \Phi^+(\zeta) - \log \Phi^-(\zeta) = \log G(\zeta), \qquad \zeta \in L, \tag{A.35}$$

that can be written as:

$$\left[\log \Phi(\zeta)\right]^+ - \left[\log \Phi(\zeta)\right]^- = \log G(\zeta), \qquad \zeta \in L. \tag{A.36}$$

Since the logarithm of an analytic function is itself analytic, we found the formulation of a Plemelj problem for the sectionally analytic function $\Gamma(z) = \log\left[\Phi(z)\right]$.

By taking $\Gamma(\infty) = 0$ we get the solution in the form:

$$\Gamma(z) = \frac{1}{2\pi i} \int_L \frac{\log\left[G(t)\right]dt}{t - z} , \qquad z \notin L, \tag{A.37}$$

and thus

$$X(z) = e^{\Gamma(z)} = \exp\left[\frac{1}{2\pi i} \int_L \frac{\log\left[G(t)\right]dt}{t - z}\right], \tag{A.38}$$

satisfies the Hilbert problem (A.26) when $\chi = 0$, and it is such that $X(\infty) = 1$. If it is required that $\Phi(z) \in A_0^\infty$, one can observe that $X(z)$ satisfies the condition:

$$X^+(\zeta) = G(\zeta)X^-(\zeta), \qquad \zeta \in L, \tag{A.39}$$

and thus from (A.26) and (A.39) one gets:

$$\frac{\Phi^+(\zeta)}{X^+(\zeta)} = \frac{\Phi^-(\zeta)}{X^-(\zeta)}, \qquad \zeta \in L \tag{A.40}$$

The function

$$F(z) = \frac{\Phi(\zeta)}{X(\zeta)} \tag{A.41}$$

is such that $F(z) = c$ (complex constant), so the required solution is:

$$\Phi(z) = cX(z). \tag{A.42}$$

If the condition $\Phi(\infty) = 0$ is required, it results $c = 0$ and the solution is $\Phi(z) = 0$; if on the other hand $\Phi(z) \in A_m^\infty, m > 0$, from (A.41) it derives $F(z) = P_m(z)$ and

$$\Phi(z) = P_m(z)X(z) \tag{A.43}$$

ii) $\chi > 0$

In this case the function $\log G(\zeta)$ is polidrome (multiple-valued). Let us consider a point $z_0 \in D^+$, the function:

$$h(\zeta) = (\zeta - z_0)^\chi, \qquad \zeta \in L, \qquad \chi > 0 \tag{A.44}$$

has index χ on L, and thus the function:

$$G_0(\zeta) = \frac{G(\zeta)}{h(\zeta)} = (\zeta - z_0)^{-\chi} G(\zeta), \qquad \zeta \in L, \tag{A.45}$$

has index 0.

We can write the problem in the form:

$$\Phi^+(\zeta) = G_0(\zeta)(\zeta - z_0)^\chi \Phi^-(\zeta), \qquad \zeta \in L \tag{A.46}$$

and defining a new sectionally analytic function

$$\Psi(z) = \begin{cases} \Phi(z) & z \in D^+ \\ (z - z_0)^\chi \Phi(z), & z \in D^- \end{cases} \tag{A.47}$$

the problem becomes homogeneous of index zero for $\Psi(z)$:

$$\Psi^+(\zeta) = G_0(\zeta)\Psi^-(\zeta), \qquad \zeta \in L. \tag{A.48}$$

If the solution $\Phi(z) \in A_0^\infty$, $\Psi(z)$ must be of order χ at infinity, and posing:

$$X_0(z) = \exp\left[\frac{1}{2\pi i}\int_L \frac{\log[G_0(t)]dt}{t-z}\right], \qquad z \notin L \tag{A.49}$$

the solution becomes:

$$\Psi(z) = P_\chi(z)X_0(z) \tag{A.50}$$

where P_χ is a polynomial of rank χ.

For $\Phi(z)$ one obtains:

$$\Phi(z) = \begin{cases} \Psi(z) \\ (z-z_0)^{-\chi}\Psi(z) \end{cases} = P_\chi(z)\begin{cases} X_0(z) \\ (z-z_0)^{-\chi}X_0(z) \end{cases} = P_\chi(z)\begin{cases} e^{\Gamma(z)} & , \ z \in D^+ \\ (z-z_0)^{-\chi}e^{\Gamma(z)} & , \ z \in D^- \end{cases}$$

$$\tag{A.51}$$

where $\Gamma(z) = \dfrac{1}{2\pi i}\displaystyle\int_L \dfrac{\log[G_0(t)]dt}{t-z} = \dfrac{1}{2\pi i}\displaystyle\int_L \dfrac{\log[(t-z_0)G(t)]dt}{t-z}$.

In compact form one can write:

$$\Phi(z) = P_\chi(z)X(z) \tag{A.52}$$

with:

$$X(z) = \begin{cases} X^+(z) = e^{\Gamma(z)} & , \ z \in D^+ \\ X^-(z) = (z-z_0)^{-\chi}e^{\Gamma(z)} & , \ z \in D^- \end{cases}. \tag{A.53}$$

iii) $\chi < 0$

In this case the function $\Psi(z)$ has in $z = \infty$ a zero of order $-\chi$, and the problem has the null solution only.

Function (A.53) is termed the canonical or fundamental function of the homogeneous problem, and satisfies the following:

-   $X^+(\zeta) = G(\zeta)X^-(\zeta), \qquad \zeta \in L$,

-   $X(z) \neq 0, \ \forall z \in C$,

-   $X(z) \in A_{-\chi}^\infty$.

A.9.3 The non-homogeneous Hilbert problem

The non-homogeneous Hilbert problem is:

$$\Phi^+(\zeta) - G(\zeta)\Phi^-(\zeta) = g(\zeta), \qquad \zeta \in L \tag{A.54}$$

From the characteristics of the canonical function:

$$G(\zeta) = \frac{X^+(\zeta)}{X^-(\zeta)}, \qquad \zeta \in L \tag{A.55}$$

thence:

$$\frac{\Phi^+(\zeta)}{X^+(\zeta)} - \frac{\Phi^-(\zeta)}{X^-(\zeta)} = \frac{g(\zeta)}{X^+(\zeta)}, \qquad \zeta \in L, \tag{A.56}$$

and defining the function

$$F(z) = \frac{\Phi(\zeta)}{X(\zeta)} \tag{A.57}$$

(A.56) becomes:

$$F^+(\zeta) - F^-(\zeta) = \frac{g(\zeta)}{X^+(\zeta)}, \qquad \zeta \in L \tag{A.58}$$

which is a Plemelj problem for $F(z)$.

The solution is always in the form:

$$\Phi(z) = X(z)F(z) = \frac{X(z)}{2\pi i} \int_L \frac{g(t)dt}{X^{+(t)}(t-z)} + X(z)P_\chi(z) \tag{A.59}$$

where $P_\chi(z)$ is a polynomial of rank $\leq \chi$ which depends on the order of $\Phi(z)$.

A.10   Hilbert problem for an open boundary

Let us consider an open boundary $L = ab$, the problem consists in the determination of a sectionally analytic function $\Phi(z)$, $z \in C^\infty - L$, of finite order at infinity, such as:

$$\Phi^+(\zeta) - G(\zeta)\Phi^-(\zeta) = g(\zeta), \qquad \zeta \in L, \ \zeta \neq (a,b), \tag{A.60}$$

with $\{G(\zeta), g(\zeta)\} \in H(L)$, $G(\zeta) \neq 0$, $\forall \zeta \in L$.

We will consider the case $G(\zeta) = k = \text{cost.}, k \in C$.

The discussion can be extended to the case that the boundary L consists of N disconnected arches: $L = \bigcup_{k=1}^{N} L_k$, $L_k = a_k b_k$.

A.10.1 Hilbert problem for an open contour

The solution must satisfy the relation:

$$\Phi^+(\zeta) = k\Phi^-(\zeta), \qquad \zeta \in L, \ \ \zeta \neq (a,b), \ \ k \in C. \tag{A.61}$$

One can write:

$$\log k = \log|k| + i\vartheta, \qquad \vartheta = \arg k, \quad 0 \leq \vartheta \leq 2\pi \tag{A.62}$$

and calculate the integral:

$$\Gamma(z) = \frac{1}{2\pi i} \int_L \frac{\log k}{t - z} dt, \qquad z \notin L. \tag{A.63}$$

It results:

$$\Gamma(z) = \frac{\log k}{2\pi i} \int_L \frac{dt}{t - z} = \gamma \log\left(\frac{z-b}{z-a}\right), \qquad \gamma = \frac{\log k}{2\pi i}. \tag{A.64}$$

The complex number γ can be formulated as:

$$\gamma = \alpha + i\beta, \quad \alpha = \frac{\vartheta}{2\pi}, \quad \beta = -\frac{\log|k|}{2\pi} \tag{A.65}$$

with $0 \leq \alpha < 1, \ -\infty < \beta < \infty$.

Using Sokhotski-Plemelj formulae (A.22) and (A.23) the two limit values of the function on L can be calculated:

$$\Gamma^+(\zeta) = i\pi\gamma + \gamma \int_L \frac{dt}{t - \zeta}, \qquad \zeta \in L, \tag{A.66}$$

$$\Gamma^-(\zeta) = -i\pi\gamma + \gamma \int_L \frac{dt}{t - \zeta}, \qquad \zeta \in L. \tag{A.67}$$

Eliminating the logarithm, one can pass to the function $X(z)$, whose limits are:

$$X^+(\zeta) = \exp\left[\Gamma^+(\zeta)\right] = \exp\left[i\pi\gamma + \gamma \int_L \frac{dt}{t - \zeta}\right], \qquad \zeta \in L, \tag{A.68}$$

$$X^-(\zeta) = \exp\left[\Gamma^-(\zeta)\right] = \exp\left[-i\pi\gamma + \gamma \int_L \frac{dt}{t - \zeta}\right], \qquad \zeta \in L, \tag{A.69}$$

and for which the following relation holds:

$$\frac{X^+(\zeta)}{X^-(\zeta)} = \exp\left[2\pi i\gamma\right] = \exp(\log k) = k, \qquad \zeta \in L \tag{A.70}$$

which is the condition (A.61). The function

$$X(z) = \left(\frac{z-b}{z-a}\right)^\alpha \left(\frac{z-b}{z-a}\right)^{i\beta} \tag{A.71}$$

lacks the requirement of being sectionally analytic on the contour, not verifying the condition (A.12):

$$|F(z)| \leq \frac{A}{|z-c|^{\alpha}}, \qquad A > 0, \quad 0 \leq \alpha \leq 1$$

at both ending points.

Various classes of particular solutions to the problem exist:

1. Class $h_2 \equiv h(a,b)$ of functions limited in both ending points of the arch;

2. Class $h_1(a) \circ h_1(b)$ of functions limited in $z = a\,(b)$ and having an integrable singularity at the other ending point (the aforesaid function $X(z)$ belongs to this class);

3. Class h_0 of functions having integrable singularities at both ending points.

i) Procedure for obtaining a solution of class h_2

One can define the function:

$$X_2(z) = (z-a)^p (z-b)^q X(z) \tag{A.72}$$

where $X(z)$ is the function defined in (A.71), and the two integers p and q are such that:

$$\begin{aligned} 0 < p - \alpha < 1, \\ 0 < q + \alpha < 1. \end{aligned} \tag{A.73}$$

Since $0 < \alpha < 1$, it is clear that conditions (A.73) hold only for $p = 1$ and $q = 0$, thus, (A.72) takes the form:

$$X_2(z) = \left(\frac{z-b}{z-a}\right)^{i\beta} (z-b)^{\alpha}(z-a)^{1-\alpha} = (z-b)^{\gamma}(z-a)^{1-\gamma}, \tag{A.74}$$

and it is demonstrable that it satisfies all the requirements for being a class h_2 canonical solution.

The behaviour at infinity can be understood from its Laurent expansion in the neighbourhood of $z = \infty$. It is:

$$X_2(z) = z\left[1 - \frac{\gamma(b-a)+a}{z} + O\left(\frac{1}{|z^2|}\right)\right], \tag{A.75}$$

and so one can infer that X_2 has at infinity a first order pole.

165

ii) Procedure for obtaining a solution of class h_1

One can define the function:

$$X_1^{a,b}(z) = (z-a)^p (z-b)^q X(z) \tag{A.76}$$

where $X(z)$ is the function defined in $(A.71)$, and the two integers p and q are such that:

$$\begin{array}{l} 0 < p-\alpha < 1 \\ -1 < q+\alpha < 0 \end{array}, \quad \text{for class } h_1(a), \tag{A.77}$$

$$\begin{array}{l} -1 < p-\alpha < 0 \\ 0 < q+\alpha < 1 \end{array}, \quad \text{for class } h_1(b). \tag{A.78}$$

Since $0 < \alpha < 1$, from (A.77) it results $p = 1, q = -1$, whereas from (A.78) one gets $p = q = 0$. Thus, the canonical functions are respectively:

$$X_1^a(z) = \left(\frac{z-b}{z-a}\right)^{i\beta} (z-b)^{\alpha-1}(z-a)^{1-\alpha} = (z-b)^{\gamma-1}(z-a)^{1-\gamma} \tag{A.79}$$

$$X_1^b(z) = (z-b)^\gamma (z-a)^{-\gamma} \tag{A.80}$$

It is easy verifying that $\in A_0^\infty$.

iii) Procedure for obtaining a solution of class h_0

Integers p and q are defined as:

$$\begin{array}{l} -1 < p-\alpha < 1 \\ -1 < q+\alpha < 0 \end{array}, \tag{A.81}$$

so it derives $p = 0, q = -1$, the particular canonical function becomes:

$$X_0(z) = \left(\frac{z-b}{z-a}\right)^{i\beta} (z-b)^{\alpha-1}(z-a)^{-\alpha} = (z-b)^{\gamma-1}(z-a)^{-\gamma} \tag{A.82}$$

and one can verify that $X_0(z) \in A_{-1}^\infty$, that is, it has a first order zero at infinity.

A.10.2.   Homogeneous problem general solution for an open contour

Given a generic particolar canonical function $X(z)$ of problem *(A.61)*, one gets:

$$X^+(\zeta) = kX^-(\zeta), \quad \zeta \in L. \tag{A.83}$$

Combining (A.*61)* and (A.*83)*:

$$\frac{\Phi^+(\zeta)}{X^+(\zeta)} = \frac{\Phi^-(\zeta)}{X^-(\zeta)}, \quad \zeta \in L \tag{A.84}$$

one can define the function:

$$\Psi(z) = \frac{\Phi(z)}{X(z)}, \tag{A.85}$$

for which:

$$\Psi^+(\zeta) = \Psi^-(\zeta), \qquad \zeta \in L, \tag{A.86}$$

that therefore results to be analytical in C (or in C^∞ if it is finite at infinity).
For Liouville's generalized theorem, $\Psi(z)$ can be represented by a polynomial of
appropriate rank:

$$\Psi(z) = P_k(z) \tag{A.87}$$

and the homogeneous Hilbert problem general solution becomes:

$$\Phi(z) = X(z)P_k(z) \tag{A.88}$$

The polynomial rank depends on the class $\Phi(z)$ belongs to: for example, if
$\Phi(z) \in A_n^\infty$, $n > 1$, the polynomial rank will be equal to $n-1$, n, $n+1$, respectively,
if $\Phi(z)$ belongs to h_2, h_1 or h_0 class. In particular, if $\Phi(z) \in A_{-1}^\infty$, the only possible
solution is of h_0 class, and the polynomial becomes a constant (differently, $P_k(z)$
should have negative rank).

A.10.3. Non-homogeneous problem general solution for an open contour

Given a generic canonical function $X(z)$ one has:

$$k = \frac{X^+(\zeta)}{X^-(\zeta)}, \qquad \zeta \in L \tag{A.89}$$

and, substituting into (A.60), one obtains:

$$\frac{\Phi^+(\zeta)}{X^+(\zeta)} - \frac{\Phi^-(\zeta)}{X^-(\zeta)} = \frac{g(\zeta)}{X^+(\zeta)}, \qquad \zeta \in L, \tag{A.90}$$

which, with $h(\zeta) = \dfrac{g(\zeta)}{X^+(\zeta)}$, is a Plemelj problem for the function $\Psi(z) = \dfrac{\Phi(z)}{X(z)}$:

$$\Psi^+(\zeta) - \Psi^-(\zeta) = h(\zeta), \qquad \zeta \in L. \tag{A.91}$$

The Plemelj problem solution is:

$$\Psi(z) = \frac{1}{2\pi i} \int_L \frac{h(t)dt}{t - z} + P(z) \tag{A.92}$$

and so the Hilbert problem solution is:

$$\Phi(z) = \frac{X(z)}{2\pi i} \int_L \frac{g(t)dt}{X^+(t)(t-z)} + X(z)P(z) \tag{A.93}$$

The canonical function $X(z)$ takes the form correspondent to the required class.

A.11 Hilbert problem for a segment on the real axis

Let us suppose the function has singularities in both ending points of the segment, and therefore belongs to class h_0. The canonical function is:

$$X_0(z) = (z-b)^{\gamma-1}(z-a)^{-\gamma} \tag{A.94}$$

with $\gamma = \alpha + i\beta$, $\alpha = \dfrac{\vartheta}{2\pi} = \dfrac{1}{2}$ and $\beta = -\dfrac{\log|k|}{2\pi} = -\dfrac{\log 1}{2\pi} = 0$, so:

$$X_0(z) = \frac{1}{\sqrt{(z-b)(z-a)}} \tag{A.95}$$

Let us indicate with $L^+ = \{z^+; z^+ = x+i0^+, a < x < b\}$ the upper edge of the segment and with $L^- = \{z^-; z^- = x+i0^-, a < x < b\}$ the lower edge. Posing:

$$\begin{aligned} z-a &= \rho_1 e^{i\vartheta_1} \\ z-b &= \rho_2 e^{i\vartheta_2} \end{aligned} \tag{A.96}$$

(A.95) becomes:

$$X_0(z) = \frac{1}{\sqrt{\rho_1\rho_2}} e^{-i\left(\frac{\vartheta_1+\vartheta_2}{2}\right)} \tag{A.97}$$

The limit values for $z \to z^+$, $z \to z^-$ can be respectively obtained for $\vartheta_1 = 0$, $\vartheta_2 = \pi$ and for $\vartheta_1 = 2\pi$, $\vartheta_2 = \pi$, resulting:

$$X_0^+(z) = \frac{1}{\sqrt{\rho_1\rho_2}} e^{-i\frac{\pi}{2}} = -\frac{i}{\sqrt{\rho_1\rho_2}} = -\frac{i}{\sqrt{(x-a)(b-x)}} \qquad a < x < b \tag{A.98}$$

$$X_0^-(z) = \frac{1}{\sqrt{\rho_1\rho_2}} e^{i\frac{\pi}{2}} = -\frac{i}{\sqrt{\rho_1\rho_2}} = \frac{i}{\sqrt{(x-a)(b-x)}} = -X_0^+(z) \qquad a < x < b \tag{A.99}$$

168
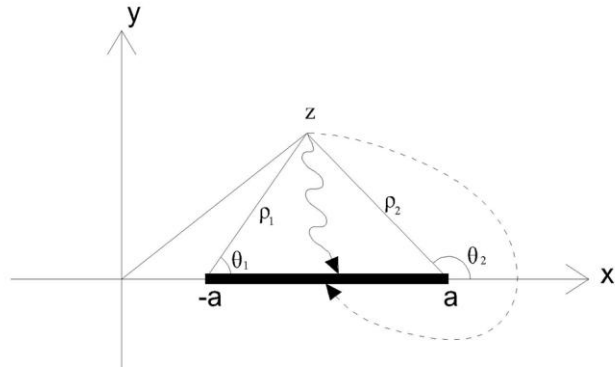
Fig. A4 – Hilbert problem for a segment on the real axis

APPENDIX B

MATRIX D IN EXPLICIT FORM

The explicit form of the fundamental matrix governing the electroelastic problem is given in this Appendix. The shape of the matrix as obtained in Chapter 4 is:

$$\mathbf{D} = \begin{bmatrix} \mathbf{A}^{-1}\left(\mathbf{B}+\mathbf{B}^{T}\right) & \mathbf{A}^{-1}\mathbf{C} \\ \mathbf{-1} & \mathbf{0} \end{bmatrix} \tag{B.1}$$

where:

$$\mathbf{A} = \begin{bmatrix} c_{11} & 0 & 0 \\ 0 & c_{44} & e_{15} \\ 0 & e_{15} & -\varepsilon_{11} \end{bmatrix}, \quad \mathbf{B} = \begin{bmatrix} 0 & c_{13} & e_{31} \\ c_{44} & 0 & 0 \\ e_{15} & 0 & 0 \end{bmatrix}, \quad \mathbf{C} = \begin{bmatrix} c_{44} & 0 & 0 \\ 0 & c_{33} & e_{33} \\ 0 & e_{33} & -\varepsilon_{33} \end{bmatrix} \tag{B.2}$$

We calculate the inverse of matrix $\mathbf{A}$:

$$\mathbf{A}^{-1} = \begin{bmatrix} c_{11} & 0 & 0 \\ 0 & c_{44} & e_{15} \\ 0 & e_{15} & -\varepsilon_{11} \end{bmatrix}^{-1} == \frac{1}{-c_{11}\left(c_{44}\varepsilon_{11}+e_{15}^2\right)} \begin{bmatrix} -\left(c_{44}\varepsilon_{11}+e_{15}^2\right) & 0 & 0 \\ 0 & -c_{11}\varepsilon_{11} & -c_{11}e_{15} \\ 0 & -c_{11}e_{15} & c_{11}c_{44} \end{bmatrix} =$$

$$= \begin{bmatrix} \dfrac{1}{c_{11}} & 0 & 0 \\ 0 & \dfrac{\varepsilon_{11}}{\left(c_{44}\varepsilon_{11}+e_{15}^2\right)} & \dfrac{e_{15}}{\left(c_{44}\varepsilon_{11}+e_{15}^2\right)} \\ 0 & \dfrac{e_{15}}{\left(c_{44}\varepsilon_{11}+e_{15}^2\right)} & -\dfrac{c_{44}}{\left(c_{44}\varepsilon_{11}+e_{15}^2\right)} \end{bmatrix} = \begin{bmatrix} \dfrac{1}{c_{11}} & 0 & 0 \\ 0 & \dfrac{\varepsilon_{11}}{\mu\varepsilon_{11}} & \dfrac{e_{15}}{\mu\varepsilon_{11}} \\ 0 & \dfrac{e_{15}}{\mu\varepsilon_{11}} & -\dfrac{c_{44}}{\mu\varepsilon_{11}} \end{bmatrix} \tag{B.3}$$

with $\mu = c_{44} + \dfrac{e_{15}^2}{\varepsilon_{11}}$.

Now the submatrices are obtained:

$$\mathbf{A}^{-1}\left(\mathbf{B}+\mathbf{B}^{T}\right)=\begin{bmatrix}\dfrac{1}{c_{11}} & 0 & 0 \\[2mm] 0 & \dfrac{\varepsilon_{11}}{\mu\varepsilon_{11}} & \dfrac{e_{15}}{\mu\varepsilon_{11}} \\[2mm] 0 & \dfrac{e_{15}}{\mu\varepsilon_{11}} & -\dfrac{c_{44}}{\mu\varepsilon_{11}}\end{bmatrix}\begin{bmatrix}0 & \left(c_{13}+c_{44}\right) & \left(e_{15}+e_{31}\right) \\[2mm] \left(c_{13}+c_{44}\right) & 0 & 0 \\[2mm] \left(e_{15}+e_{31}\right) & 0 & 0\end{bmatrix}=$$

$$=\begin{bmatrix}0 & \dfrac{c_{p}}{c_{11}} & \dfrac{e_{p}}{c_{11}} \\[3mm] \dfrac{c_{p}\varepsilon_{11}+e_{p}e_{15}}{\mu\varepsilon_{11}} & 0 & 0 \\[3mm] \dfrac{c_{p}e_{15}-e_{p}c_{44}}{\mu\varepsilon_{11}} & 0 & 0\end{bmatrix}$$

(B.4)

where $c_{p}=c_{13}+c_{44}$ and $e_{p}=e_{15}+e_{31}$, and:

$$\mathbf{A}^{-1}\mathbf{C}=\begin{bmatrix}\dfrac{1}{c_{11}} & 0 & 0 \\[2mm] 0 & \dfrac{\varepsilon_{11}}{\mu\varepsilon_{11}} & \dfrac{e_{15}}{\mu\varepsilon_{11}} \\[2mm] 0 & \dfrac{e_{15}}{\mu\varepsilon_{11}} & -\dfrac{c_{44}}{\mu\varepsilon_{11}}\end{bmatrix}\begin{bmatrix}c_{44} & 0 & 0 \\[2mm] 0 & c_{33} & e_{33} \\[2mm] 0 & e_{33} & -\varepsilon_{33}\end{bmatrix}=\begin{bmatrix}\dfrac{c_{44}}{c_{11}} & 0 & 0 \\[3mm] 0 & \dfrac{\varepsilon_{11}c_{33}+e_{15}e_{33}}{\mu\varepsilon_{11}} & \dfrac{\varepsilon_{11}e_{33}-e_{15}\varepsilon_{33}}{\mu\varepsilon_{11}} \\[3mm] 0 & \dfrac{e_{15}c_{33}-c_{44}e_{33}}{\mu\varepsilon_{11}} & \dfrac{e_{15}e_{33}+c_{44}\varepsilon_{33}}{\mu\varepsilon_{11}}\end{bmatrix}$$

(B.5)

Now $\mathbf{D}$ can be built:

$$\mathbf{D}=\begin{bmatrix}0 & \dfrac{c_{p}}{c_{11}} & \dfrac{e_{p}}{c_{11}} & \dfrac{c_{44}}{c_{11}} & 0 & 0 \\[3mm] \dfrac{c_{p}\varepsilon_{11}+e_{p}e_{15}}{\mu\varepsilon_{11}} & 0 & 0 & 0 & \dfrac{\varepsilon_{11}c_{33}+e_{15}e_{33}}{\mu\varepsilon_{11}} & \dfrac{\varepsilon_{11}e_{33}-e_{15}\varepsilon_{33}}{\mu\varepsilon_{11}} \\[3mm] \dfrac{c_{p}e_{15}-e_{p}c_{44}}{\mu\varepsilon_{11}} & 0 & 0 & 0 & \dfrac{e_{15}c_{33}-c_{44}e_{33}}{\mu\varepsilon_{11}} & \dfrac{e_{15}e_{33}+c_{44}\varepsilon_{33}}{\mu\varepsilon_{11}} \\[3mm] -1 & 0 & 0 & 0 & 0 & 0 \\[2mm] 0 & -1 & 0 & 0 & 0 & 0 \\[2mm] 0 & 0 & -1 & 0 & 0 & 0\end{bmatrix}$$

(B.6)

FOREWORD

This annex describes some of the outcomes of an experimental project to which the PhD candidate collaborated between 2008 and 2009 during her stay as a Visiting Researcher at The City College of New York, Department of Mechanical Engineering. The official title of the project, that started in 2006 and is currently still ongoing, is COMPOSITE STRUCTURAL DAMAGE SELF-SENSING VIA ELECTRICAL RESISTIVITY MEASUREMENT - PHASE IIA-3, and the sponsor is the National Science Foundation (NSF) through Global Contour Ltd., Rockwell, TX.

The aim of the project is to test a new technique of composite structural self-diagnostic (CSSD), based on electrical and mechanical properties of composite materials, for detecting the presence or extension of interlaminar damage in laminated composites.

Principal investigators are Prof. F. Delale and Prof. B. Liaw from The City College of New York, and Dr. J.C. Chung from Global Contour. The PhD candidate took part in every step of the research, from the preparation of the specimens with electrodes and strain gauges, to the machine testing, and processing of the data.

All the experiments have been carried out at the Laboratory of Solid Mechanics and Materials of The City College of New York.

STRUCTURAL SELF-SENSING FOR DAMAGE IN COMPOSITE MATERIALS

1. Introduction

Damages in composite materials can be detected using several techniques.

In this work, we will highlight a new technique, composite structural self-diagnostic (CSSD), based on electrical and mechanical properties of composite materials, which can detect the presence or extension of damage.

The Phase II project currently in progress aims to capitalize on the Phase I success of innovative self-sensing of composite structural damage and strain utilizing the electrical conductivity (resistivity) of carbon (graphite)-reinforced composite materials for structural health monitoring (SHM) of composite structures. The on-going Phase II technology is for full-scale development (FSD) of composite structural self-diagnostic (CSSD) system/technique. The technology is concentrated on the development of system hardware/software and implementation procedures, such as microchip-based Nodal Electrical Resistivity Acquisition Circuitry ($NERAC^{TM}$), composite structural self-monitoring computer hardware and software, and data acquisition technique and diagnostic procedures for field implementation.

The CSSD technology developed up to date is well described in the Phase I final report [1], and the CSSD self-sensing system/technique full-scale development (FSD) approach is detailed out in Global Contour's NSF Phase II proposal [2]. Following is a brief recap of the composite self-sensing technology development status for readers' convenience.

Most in-service structures, such as aircraft, rotorcraft, ground vehicles and civil structures, require periodic inspection/maintenance to monitor their structural

integrity so that their life expectancy can be prolonged and more importantly, catastrophic failure can be prevented. However, schedule-driven time-based maintenance (TBM) can be time-consuming, labor-intensive and expensive. More significantly, this type of non-continuous monitoring may miss the window of opportunity for catastrophic prevention if a certain incipient warning sign was undetected between the inspection/maintenance schedules due to human error.

To overcome this problem, various scientifically advanced techniques have been proposed for continuous, automated structural health monitoring, so-called condition-based maintenance (CBM) during the past decade [5-7]. Practically, newly developed CBM require the use of third-party embedded sensors, such as MEMS, PZTs, fiber optic sensors, etc., which tend to compromise the structural integrity of the hosting structural component.

Carbon fiber composites are basically piezoresistive and electrically conductive. Thus, the material characteristics provide damage and strain self-sensing capabilities. Self-sensing means the material itself functions as sensor, and thereby, eliminates cumbersome third-party sensor embedding, which presents technical barriers to the aircraft manufacturers as well as economic burden to airlines.

The basic principle is that damage such as fiber breakage or delamination between laminae causes a decrease of the electrical conductivity in the affected region, leading to a resistance change measured using electrode pairs. In self-sensing, electrical contacts (electrodes) play an extremely important role in electrical resistance signal acquisition from flight critical composite aircraft structures. The electrodes must be functionally effective, durable and protected from flight environmental hazards. The development of such an electrode material, installation/maintenance processes is proposed for this Phase IIA project.

The use of change in electrical resistance for monitoring fracture process can be dated back to decades ago (e.g., [3]). Due to carbon fiber's inherent nature of piezoresistivity and electrical conductivity ($\rho = 2*10^{-5} \Omega\text{m}$), this technique has been applied by many researchers for the study of carbon-based composites. Chung and

her associates [4-16] have conducted extensive research in the area of self-sensing/self-monitoring/self-diagnosing of carbon-based composites. The matrices of these composites were made of carbon [5], polymers [6-12], cement [13,14] or concrete [15,16] whereas the reinforcements were either short (discontinuous) or long continuous carbon fibers. In addition to standard tensile loading, they have also studied the effect of temperature [7-9,16] and fatigue [12]. Both two- and four-probe methods were applied in their studies. Other notable studies in this area are listed in References [17-47].

Phase II research and development work is focused on technology FSD and necessary CSSD system/technique for commercialization preparation. The technology FSD work will involve largely self-sensing methods development and system hardware/software development for field applicable self-sensing technology implementation. The composite material to be used for phase II work is IM7-G/8552, which is commonly used for high performance aircrafts such as Boeing 7E7 passenger jet and Lockheed-Martin F-35 Joint Strike Fighter.

The goal of CSSD technology is to prevent the catastrophic failures of aircraft and rotorcraft by predicting impending failures of flight-critical composite structural components without application of third-party embedded sensors such as MEMS, PZT and fiber optic sensors. The application of the CSSD technology also reduces the maintenance cost of the aircraft and rotorcraft due to automated structural health monitoring and diagnostic feature.

2.   Project Objectives and Tasks

The objective of the proposed Phase IIA-3 project is to develop a piezoresistivity-based self-sensing technique for fatigue-induced delamination detection in carbon fiber composites. Once proven successfully, it is expected that the developed technique can be used widely for the flight-ready prognostics of aerospace vehicles. Under Global Contour's SBIR Phase II, both four-probe and two-probe methods are being investigated. Four-probe method data acquisition is performed in such a fashion that AC or DC current is supplied with two outer probes, and voltage is measured with two inner probes. In reality, it is an electric potential measurement technique. If the current density is uniform in the material the resistance of the composite is obtained independently of the resistance caused by imperfect bonding. On the other hand, the two-probe method uses the same probes to supply current and measure voltage at the same time. The two-probe technique is a rather direct resistivity measurement technique, and it is easily affected by contact resistivity. However, if the contact resistivity is alleviated, it presents user-friendlier features for diversified applications than the four-probe technique. Under Phase IIA-3 project, the following research work has been and is currently performed to develop field-applicable electrical resistivity data acquisition and damage assessment-quantification techniques for composite structural self-diagnostic system:

1. Explore commercially available, performance-efficient and environmentally durable (low to high temperatures) point electrodes suitable for carbon fiber composite self-sensing applications.
2. Study available procedures for electrode installation by secondary adhesive bonding and the protection coating application process of electrode utilizing a Mil-Spec or commercial process.

180

3. Install discrete electrodes (called perimetric point electrodes) and acquire base-line electrical resistivity data on ASTM-Standard recommended Double-Cantilever-Beam (DCB) type and End-Notched-Flexure (ENF) type composite specimens [1-4]. Both types of specimens are made of 24-layer carbon fiber-based aerospace-grade composites with 6"L x 1"W in dimension. As recommended, the DCB specimens will have a 3" pre-crack generated by a Teflon-insert whereas the END specimens will have a 2" pre-crack, also produced by a Teflon insert.

4. Induce delamination damage due to monotonic loading in the composite specimen, and acquire the electrical resistivity data for the damaged condition. The *in situ* delamination damage will also be confirmed by optical and acoustic emission (A/E) methods.

5. The by-product of the tests will be the experimental data of Mode I and II interlaminar fracture toughness of the composite. These data will be generated using procedures described by ASTM Standard and the composite research community [1-4]. They will be very useful for the aerospace industry.

6. Induce delamination damage due to fatigue loading in the composite specimen, and acquire the electrical resistivity data for the damaged condition. Again, the *in situ* delamination damage will also be confirmed by optical and A/E methods.

7. Develop a damage mechanics-based theoretical model (analytical and/or finite element analysis technique) to study mechanical properties and electrical resistance changes.

8. Verify experimental results with the proposed damage-mechanics based theoretical model for micro-to-mesoscopic analyses; especially damage pattern identification (i.e., delamination or other types of damage) through the proposed perimetric point electrode technique.

The composite material used in Phase IIA and IIA-2 projects was Hexcel IM7-G carbon fibers reinforced 8552 epoxy (IM7/8552) unidirectional prepregs with 24 plies in a quasi-isotropic lay-up configuration, i.e., $[0°/+45°/90°/-45°]_{3S}$ autoclave-cured at 350°, fabricated by Global Contour's subcontractor, Sawyer Composites in Fort-Worth, TX. The IM7 carbon fiber is commonly used for high performance aerospace vehicles such as high performance aircraft such as Lockheed-Martin F-22 Raptor, F-35 Joint Strike Fighter, etc. Phase IIA-2 effort concentrated mainly on the effect of quasi-static loading; whereas this proposal will emphasize fatigue loading produced by an MTS Universal Testing System. Fatigue-induced composite delamination has always been a major concern in the component design of many aerospace vehicles.

The major technological break-through will be the exploration of commercially available electrode material and installation/protection processes suitable for practical aircraft composite structural self-sensing on damage and strain. In self-sensing, the perimetric electrodes play an extremely important role in electrical resistance signal acquisition from flight critical composite aircraft structures. The electrodes must be functionally effective, durable and protected from flight environmental hazards.

In addition to the MTS monotonic and fatigue loading tests, the feasibility study will also be verified by commercially available general-purpose finite element codes (e.g., ABAQUS). Once successful, the product may be applicable for aerospace composite structures and other industrial infrastructures for assessing damage. Non-destructive and non-invasive damage-detection via the multifunctional material property-based self-sensing technique will be particularly useful for hard-to-find defects, such as composite delamination and cracks concealed underneath the lap joint of a rivet connection.

The proposing institution is the City College of the City University of New York (CUNY City College). Success of the proposed project will nurture NSF CREST research involvement of the advanced technology research and development through collaboration between Global Contour Ltd. (SBIR Phase IIB grantee) and the

CREST Center for Mesoscopic Modeling and Simulation (CMMS) of CUNY City College.

The previous 2006 Phase IIA-2 project was a second pilot project attempted by the Office of Industrial Innovation (OII/ENG) and Human Resource Development (HRD/EHR) of NSF. Global Contour-CUNY CREST team was one of four grantees that participated in the pilot project, and demonstrated successful accomplishment.

Phase IIA-3 project activity will accelerate the subject technology FSD, and will advance the scientific and technological knowledge base in relation to damage self-sensing of carbon fiber polymer-matrix composites. Specifically, the proposed activity will bring the technology developed in Phase II project to a level that will allow field-testing and subsequent commercialization. Phase IIA-3 project will complement the activity of the composite self-sensing SBIR FSD by addressing (i) practical point electrode application, (ii) damage identification by involving the electrical resistivity acquisition, and (iii) applicability of the carbon fiber composite self-sensing technique to the detection of composite delamination caused by monotonic or fatigue loading. Even though they are central to the implementation of the self-sensing technology in practical structures, the afore-mentioned three issues are yet to be addressed fully.

Furthermore, the theoretical modeling aspect of the work will help provide fundamental understanding of the self-sensing behavior. Finally, in addition to technical support from Global Contour Ltd, the proposed activity will make use of the mathematical modeling and materials testing expertise of the Phase IIA and IIA-2 investigators from CUNY City College.

3. Project Progress

3a)   DCB and ENF Composite Specimen Preparation

Although the project started officially on October 1, 2007, a 12"(L)x12"(W)x3/8"(T) composite panel needed to be machined into DCB and ENF specimens was received from Dr. Jaycee Chung of Global Contour Ltd in February 2008. The delay was mainly due to careful selection of proper composite material to ensure its quality to be what the project needed and to minimize its cost to fit the budget.

Per Dr. Chung's suggestion, the panel was sent for machining into specimens using electrical discharge machining (EDM) by Advantage EDM, NJ. The choice of the high-precision EDM is due to its minimal material removal. This is important when machining the pre-crack in a DCB or ENF specimen. However, the EDM technique could not work for this composite panel since it does not contain enough electrical conductivity required for EDM to work.

We next switched to the second best choice for minimal material removal, the water-jet cutting. The company chosen was Wet Jet Precision, Inc., UT. The composite panel was machined into various sizes of DCB, ENF and tensile strip specimens for the proposed tests. The machining process consisted of:

1. Cutting the composite panel into specimens as shown in Figure 1.
2. Machining the specimens obtained in Step 1 according to the drawing details shown in Figure 2.
3. For DCB, attaching the piano hinges for machine testing (Figure 3).

As shown in Fig. 2, at the end of the machining process, the total of:

- 8 specimens @ 1''x6" (with the initial thickness of 3/8") with a 2" long pre-crack introduced by water Jet
- 10 specimens @ 6"x1" (with the initial thickness of 3/8") with a 3" long pre-crack introduced by water Jet

184

- 4 specimens @ 8"x1" in the longitudinal direction with 3/16" thickness
- 4 specimens @ 1"x10" in the vertical direction with 3/16" thickness

were obtained.

2 specimens @1"*10" in the vertical direction: they will each be cut into 2 **through** the thickness to make the thickness 3/16"

12"

12"

3/8"

8 specimens @1''*6'' in the vertical direction: 4 will be machined to introduce a 2''long crack (with water Jet) **through** the thickness and the remaining 4 will have a 3'' long crack

2 specimens @8"*1" in the longitudinal direction: they will each be cut into 2 **through** the thickness to make the thickness 3/16"

10 specimens @6''*1'' in the longitudinal direction: 5 will be machined to introduce a 2''long crack (with water Jet) **through** the thickness and the remaining 5 will have a 3'' long crack

Fig. 1 - Plan for machining the composite panel.

2"

6"

6"

3"

1"

3/8"

3/8"

1"
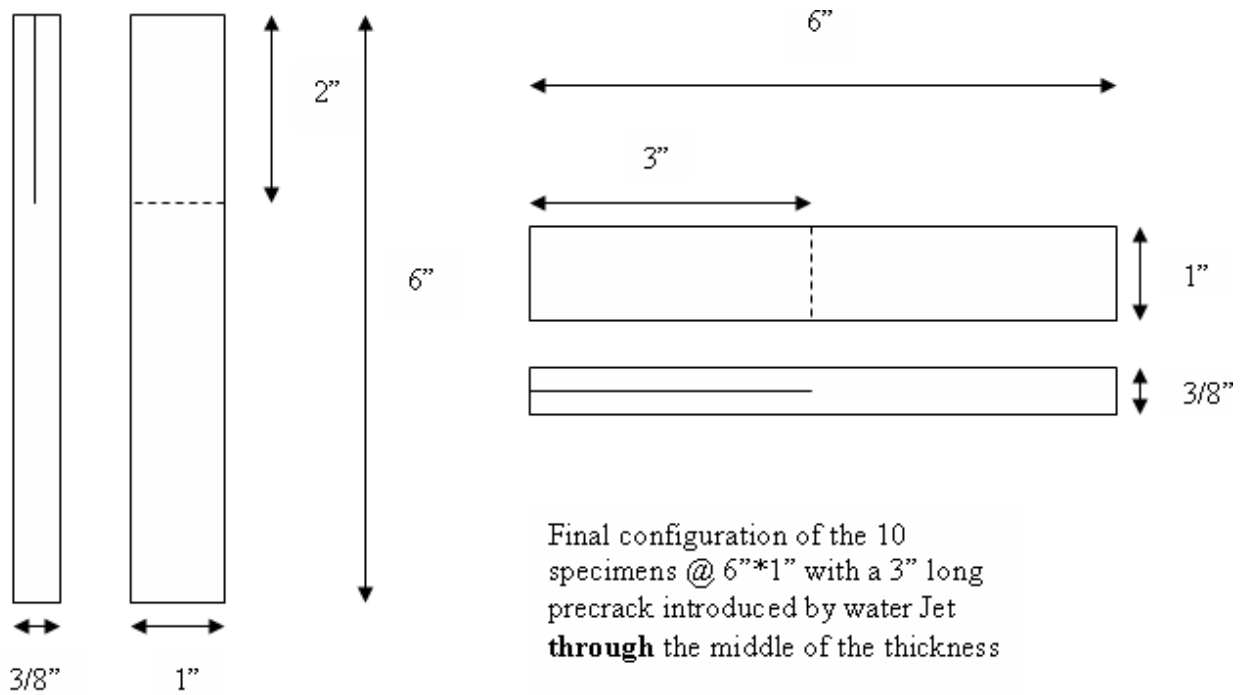
Final configuration of 8 specimens @1''*6" with a 2" long precrack introduced by water Jet **through** the middle of the thickness

Final configuration of the 10 specimens @ 6"*1" with a 3" long precrack introduced by water Jet **through** the middle of the thickness

Fig. 2 - Specimens configuration

Piano hinge

P

h

W

a_0

a

P

L
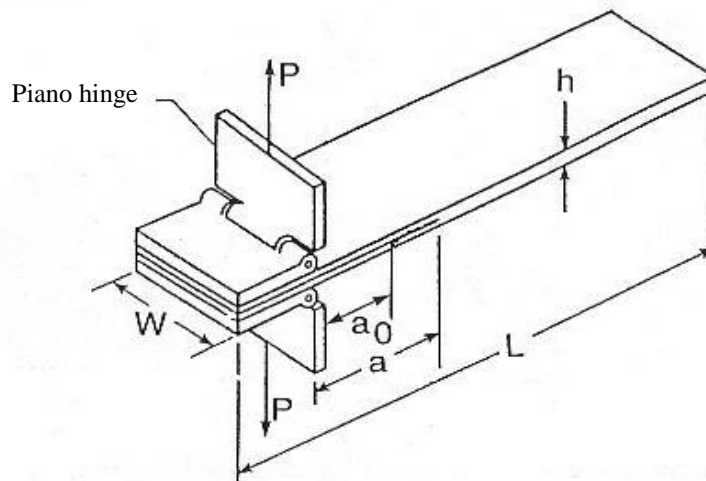
Fig. 3 – Model of a Double Cantilevered Beam (DCB) specimen

Preliminary static and fatigue debonding detection tests were carried out on DCB specimens made of two bonded aluminum 6061-T6 layers. A Teflon insert was placed between the two aluminum layers to simulate a 75-mm-long pre-crack; whereas the remaining length was bonded using 3M DP-810 adhesive.

3b-i) Quasi-Static DCB Tests

The force-displacement curve of the bonded aluminum DCB test is shown in Figure 4. Per ASTM D5528-01 Standard [43-46], a loading rate of 0.02 in/min (or 0.5 mm/min) for the cross-head speed of the MTS machine was used. Whenever crack advancement due to delamination was detected, the machine was unloaded with a cross-head speed of 0.1 in/min (*or* −2.5 mm/min). These unloading steps are necessary for evaluating Mode I interlaminar fracture toughness G_I. The resulting 12-cycle of displacement vs time record is shown in Figure 5.

The force and displacement data were used to calculate the Mode I interlaminar fracture toughness G_I. Figure 6 shows the Mode I interlaminar fracture toughness G_I data calculated by three different methods: (1) BT: beam theory, (2) MBT: modified beam theory, and (3) CC: compliance calibration Method (refer to ASTM D 5528 Standards for the different calculation methods for the Mode I interlaminar fracture toughness)

Results computed by these three methods give a G_I estimated to be around 3000 J/m^2 for the modified beam theory (MBT) and the compliance calibration (CC) methods and 2000 J/m^2 for the Beam theory (BT).
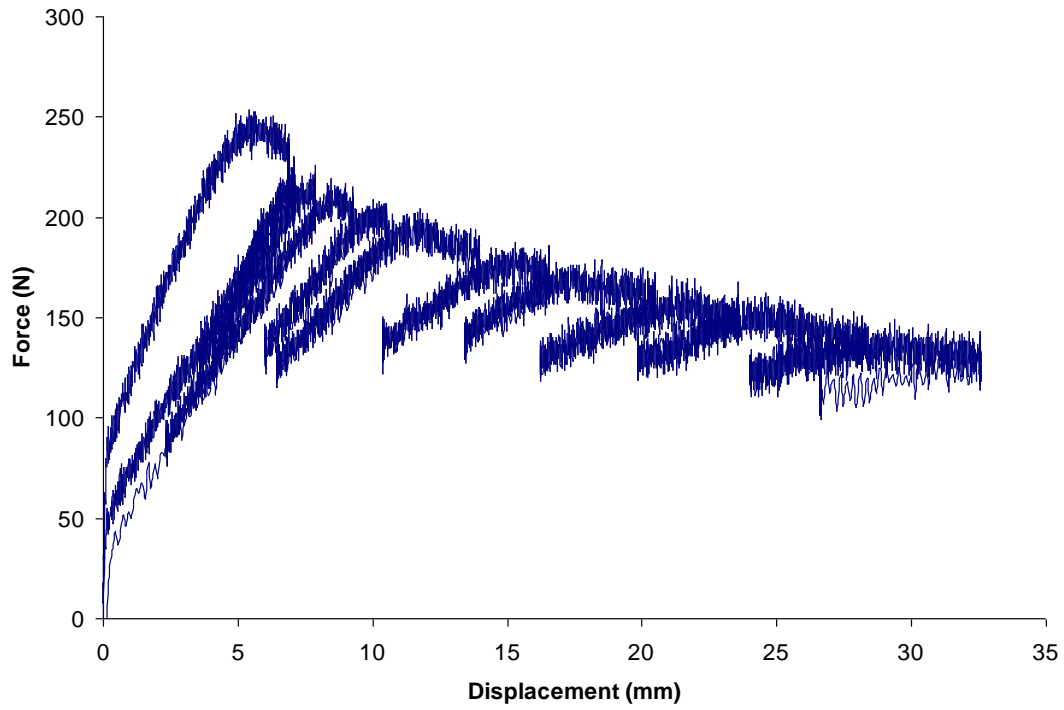
Fig. 4 - MTS force-displacement record of the interlaminar Mode I fracture test of the bonded aluminum DCB specimen.
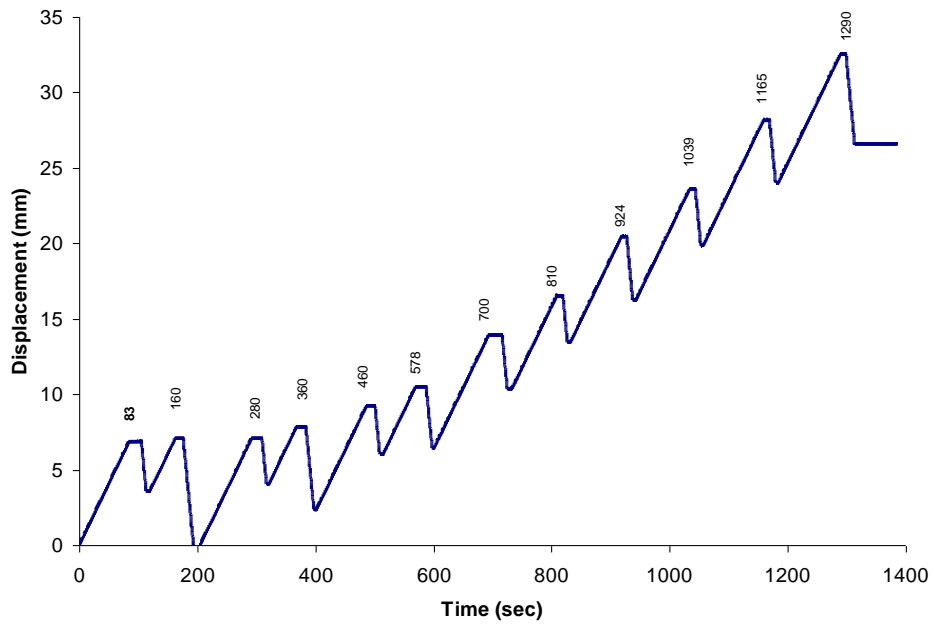
Fig. 5 - MTS cross-head displacement *vs* time record showing 12 loading-unloading cycles during the interlaminar Mode I fracture test of the bonded aluminum DCB specimen.
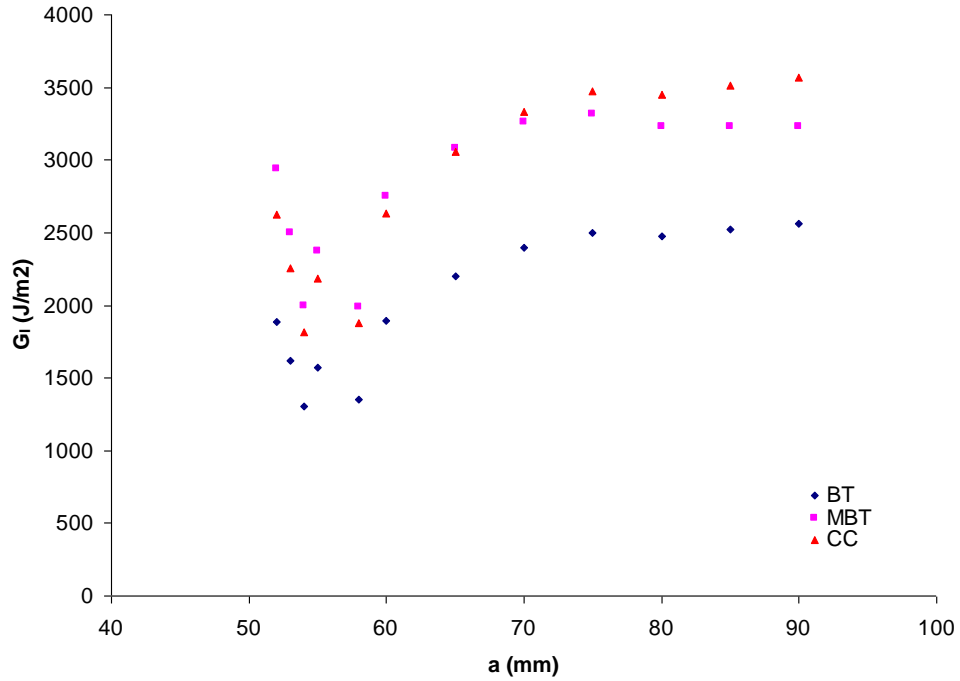
Fig. 6 - Interlaminar Mode I fracture toughness of bonded aluminum DCB specimen computed by three different methods: (1) BT: beam theory, (2) MBT: modified beam theory, and (3) CC: compliance calibration Method.

3b-ii) Fatigue DCB Tests

The fatigue load of 0.5 in maximum amplitude and 1Hz frequency was applied for 900 cycles and then increased to 0.75 in maximum amplitude and 1Hz for 1000 cycles. A part of the applied load is shown in Figure 7. Finally, using ASTM 6115-97 standard, the G-N curve was plotted in Figure 8.
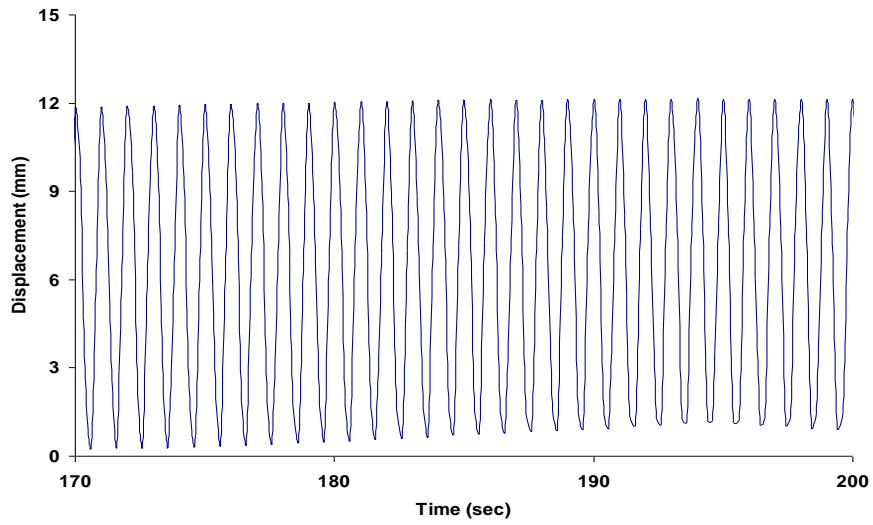
Fig. 7 - A segment of the MTS cross-head displacement *vs* time record showing the fatigue load applied to the bonded aluminum DCB specimen.
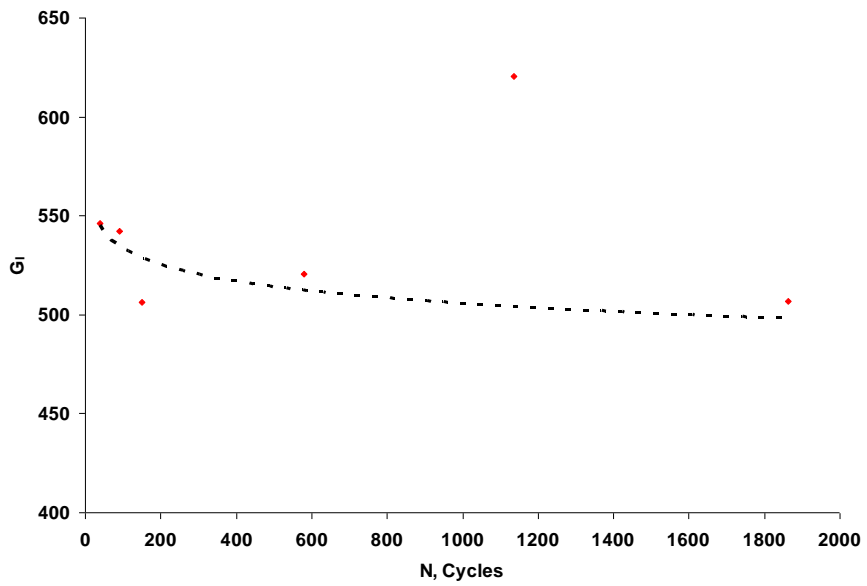
Fig. 8 - G-N curve for the fatigue test on the bonded aluminum DCB specimen.

<u>3c)</u>   <u>Preliminary ENF fatigue tests</u>

As in the preliminary DCB tests, preliminary fatigue tests were carried out on two specimens, each made of two bonded aluminum 6061-T6 strips. Again a Teflon insert was placed between the two aluminum strips to simulate the 50-mm long pre-crack while the remaining length was adhered using 3M DP-810 adhesive. The loading pattern is shown in the table below:

Table 1 - ENF-Fatigue test specifications

	Frequency (Hz)	Amplitude (inches)	No. of cycles
Test 1	1	0.1	300
	1	0.2	700
	1	0.3	850
	1	0.4	1100
Test 2	1	0.2	500
	1	0.3	1000
	1	0.4	3693
	1	0.5	349

The force and displacement data were used to calculate the Mode II interlaminar fracture toughness G_{II}. As far as Mode II (ENF) tests are concerned, there are no current international standards available to obtain G_{II}, therefore, Bernoulli-Euler beam theory was used. Figure 9 shows the Mode II interlaminar fracture toughness G_{II} data calculated using the direct beam theory (DBT) from the two tests. From the figure, the interlaminar mode II fracture toughness value for both the ENF specimen is estimated about 4600 J/m2, which is consistent with the prevailing handbook values.
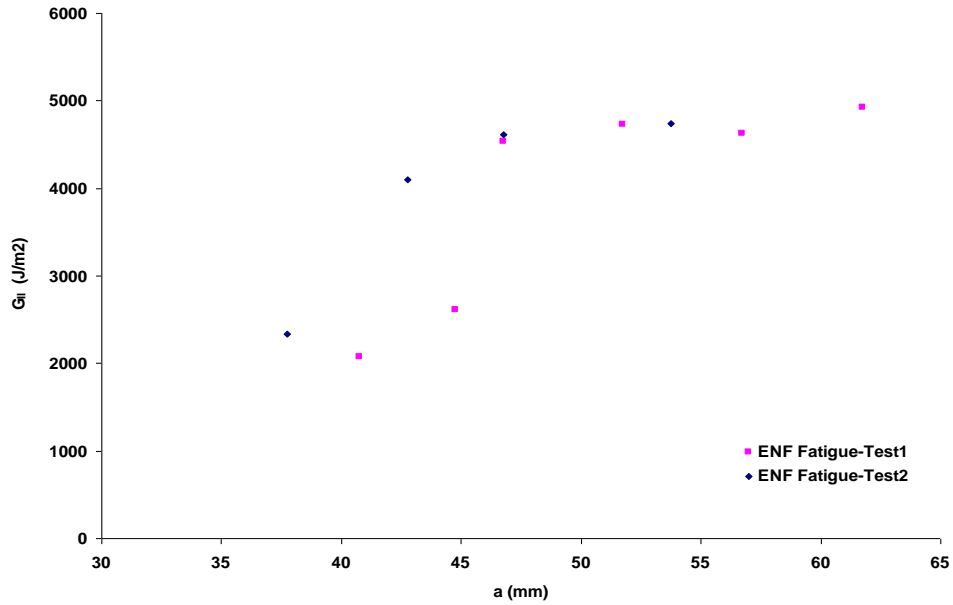
Fig. 9 - Interlaminar Mode II fracture toughness of bonded aluminum ENF specimen computed by direct beam theory

3d)   DCB tests on composite specimens

3d-i) Quasi-Static DCB Tests

Three DCB composite specimens were tested for quasi-static interlaminar fracture. The same test procedure, as per ASTM D5528-01 Standard, was followed.

The three composite specimens are named DCB-1, DCB-2 and DCB-3. Figure 10 shows one of these composite specimens mounted in an MTS 810 22-kip universal testing system through a pair of high-strength steel piano hinges.

As seen in the photo, four techniques were used for Mode I delamination detection: (1) the ASTM recommended optical method, (2) one Physical Acoustics Corporation acoustic emission (A/E) sensor glued to the specimen at the free end of the DCB specimen, (3) four strain gauges for strain measurement, and (4) the innovative piezoresistivity-based self-sensing technique. Figure 11 illustrates the layout of this DCB composite specimen with both 2- and 4-probe electrode positions.

Mechanical load was then applied from the MTS 810 testing machine through the steel piano hinges to the DCB composite specimen. Per ASTM D5528-01 Standard, a loading rate of 0.02 in/min (*or* 0.5 mm/min) for the cross-head speed of the MTS machine was used. Whenever crack advancement due to delamination was detected, the machine was unloaded with a cross-head speed of −0.1 in/min (*or* −2.5 mm/min). The resulting 11-cycle of displacement vs time record is shown in Figure 12. Figure 13 shows the force-displacement curve recorded by the MTS system during the interlaminar fracture tests of the DCB-3 composite specimen. Figure 14 shows the top view of the DCB specimen with 2- and 4-probe electrode locations as well as the 2 strain gauges. Figure 15 shows two *in situ* fractographs depicting delamination crack propagation in the DCB-3 composite specimen at $\Delta a = 12$ mm and 20 mm, respectively.
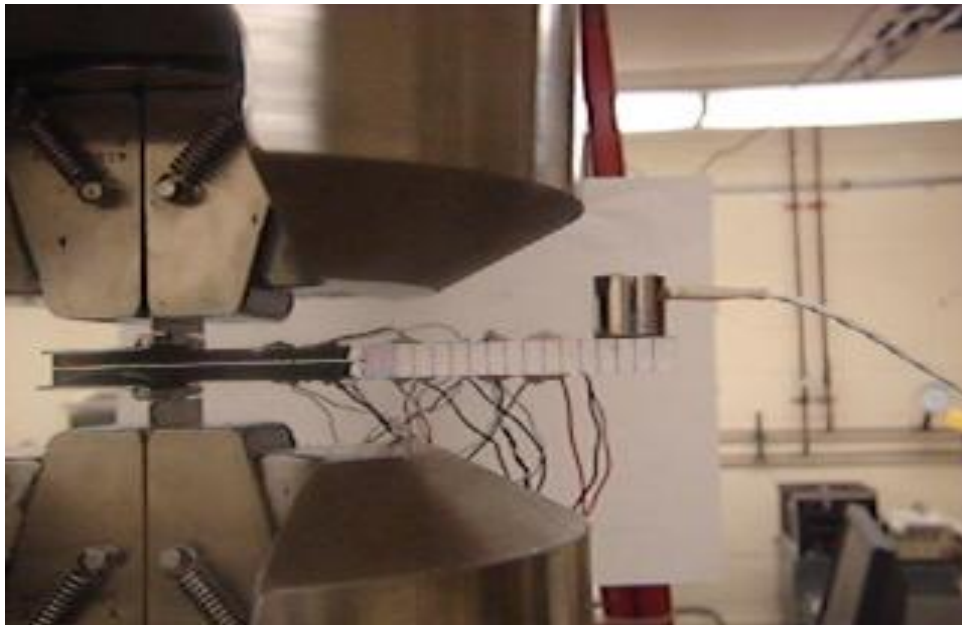
Fig. 10 - The DCB-3 composite specimen mounted in an MTS universal testing system through a pair of piano hinges. The specimen was painted with markers for optical detection; glued with one A/E sensor for sound detection; and installed with 2- and 4-probe electrodes for resistance detection of delamination.
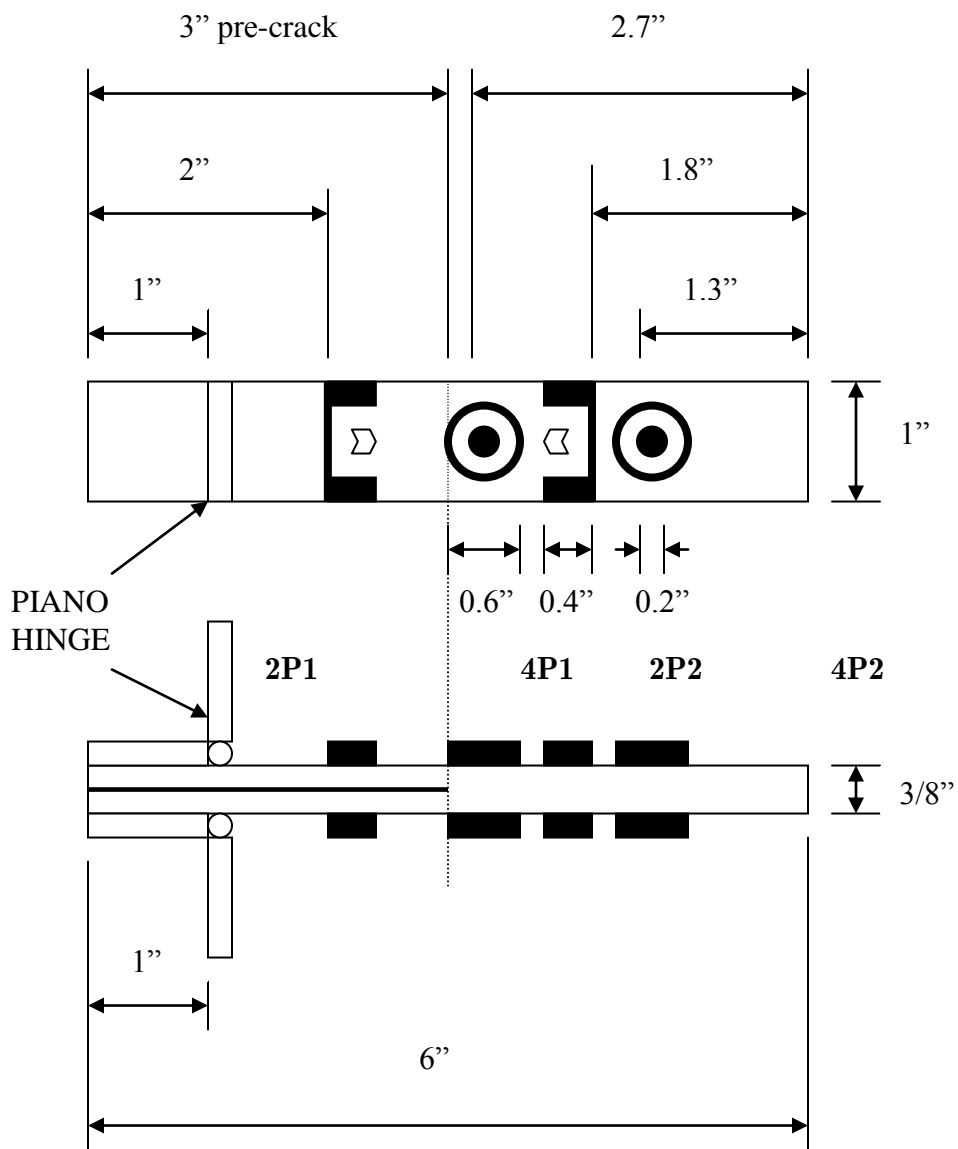
Fig. 11 - Layout of the DCB composite specimen with 2- and 4-probe electrode positions.

Note: ⟨ indicates a strain gauge and 2P, 4P represent the 2-and 4-probe electrode locations respectively.
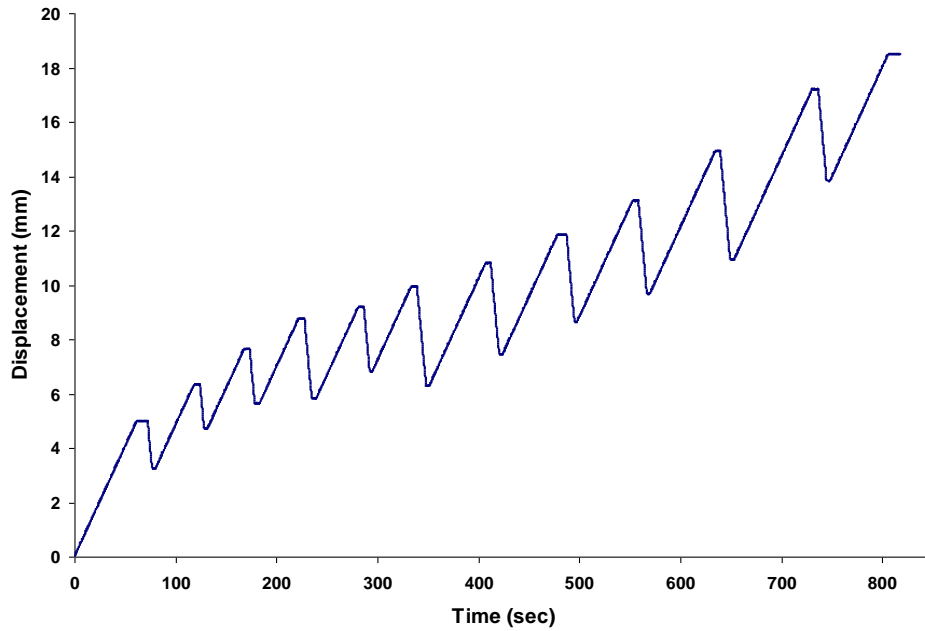
Fig. 12 - MTS cross-head displacement *vs* time record showing 11 loading-unloading cycles during the interlaminar Mode I fracture test of the DCB-3 composite specimen.
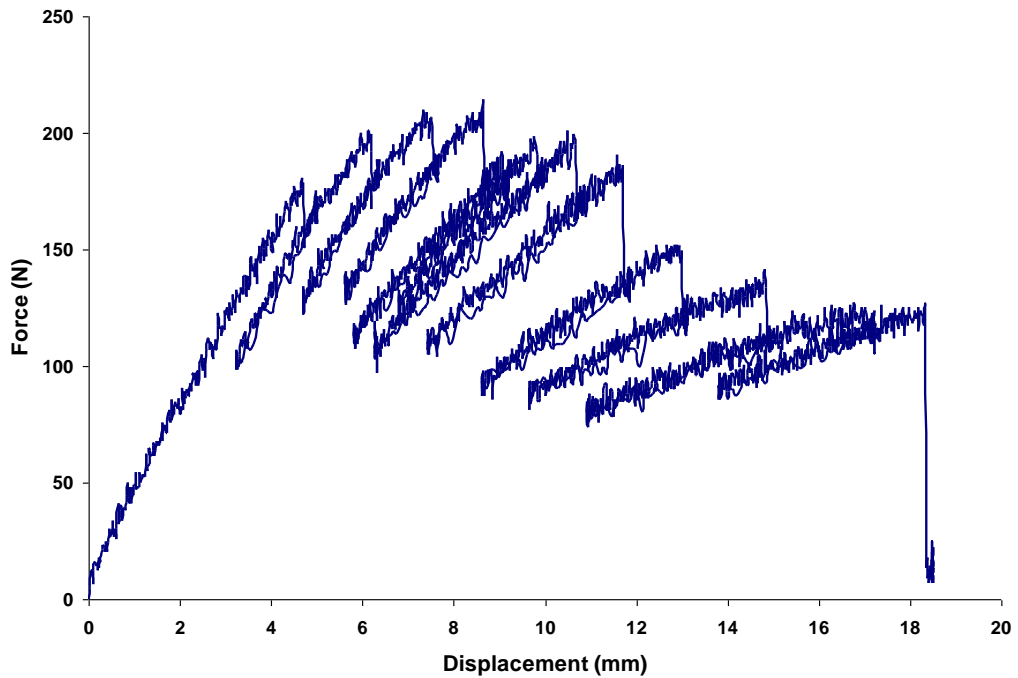
Fig. 13 - MTS force-displacement record of the interlaminar Mode I fracture test of the DCB-3 composite specimen.
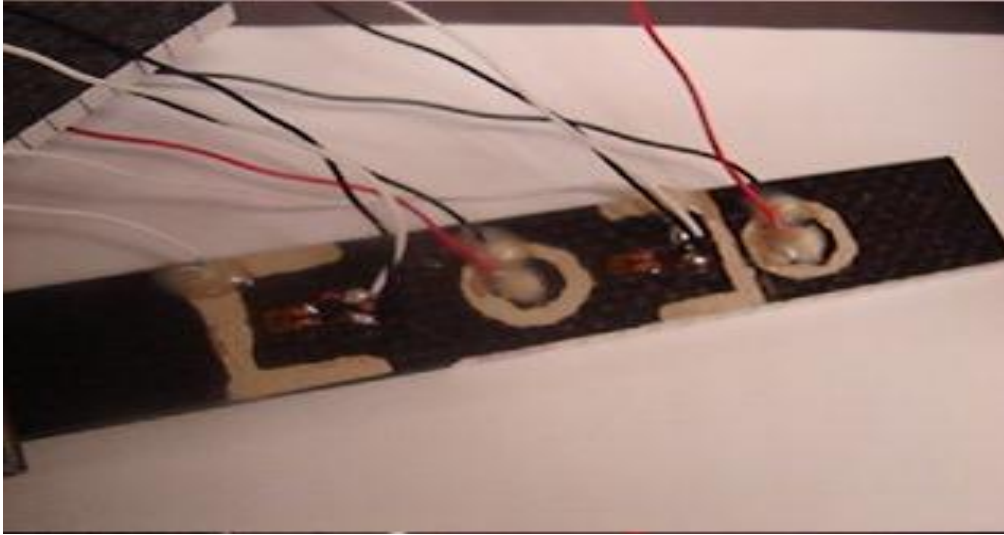
Fig. 14 - Top view of the DCB-3 specimen with 2- and 4-probe electrode locations as well as the 2 strain gauges
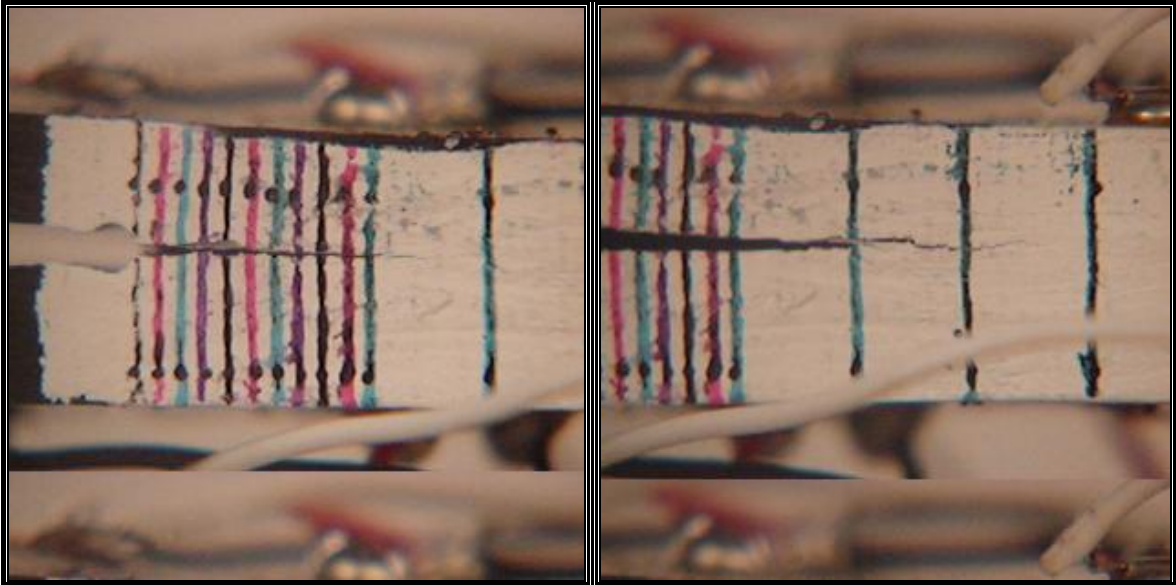
(a) $\Delta a = 12$ mm   (b) $\Delta a = 20$ mm

Fig. 15 - *In situ* fractographs depicting delamination crack propagation in the DCB-3 composite specimen.

As mentioned earlier, A/E signals and self-sensing piezoresistivity changes using 2- and 4-probes were also recorded. Figure 16 shows excellent agreement between the A/E cumulative counts from the A/E sensors *vs* the above-mentioned MTS cross-head displacement record (see Figure 12 above) of the DCB interlaminar fracture test. The increases in A/E cumulative count during the loading phases and flat during the unloading phases indicate that the industry-proven A/E technique "heard" with keen sensitivity the advancement of the delamination crack during the loading phases and became "deaf" when the crack stopped to propagate during the unloading phases.
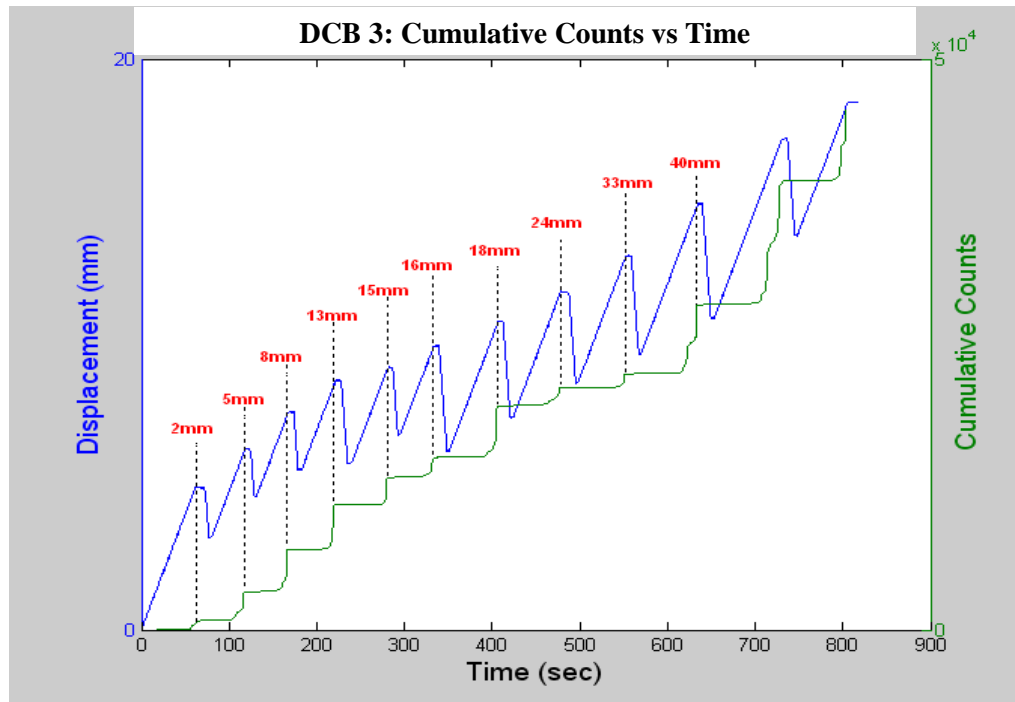
Fig. 16 - Excellent agreement between the A/E cumulative count *vs* MTS cross-head displacement records of the interlaminar Mode I fracture test of the DCB-3 composite specimen.
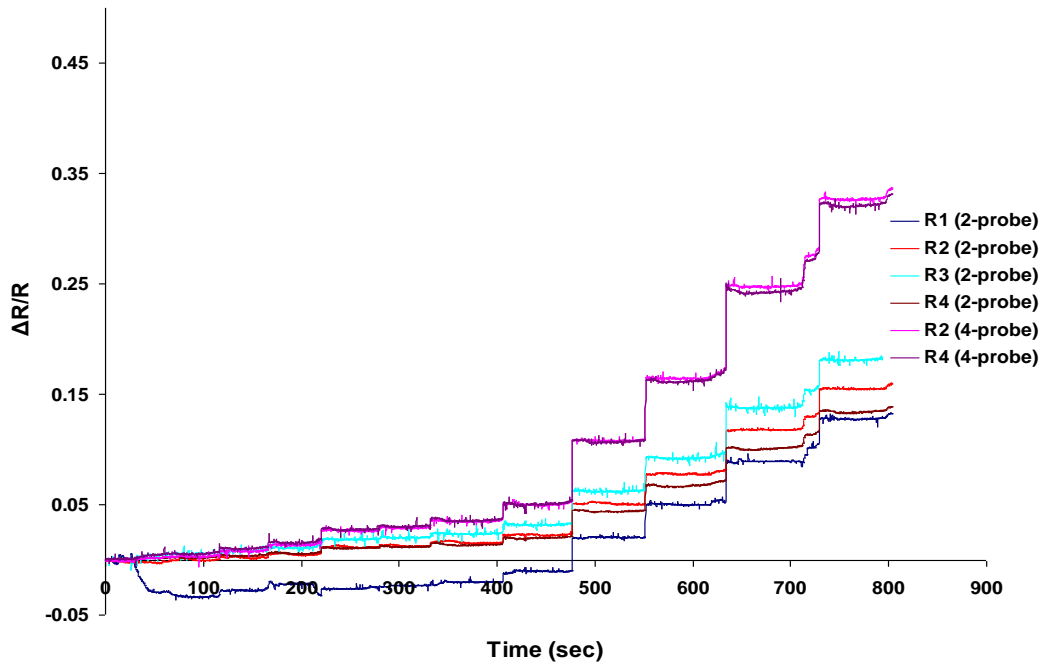
Fig. 17 - Self-sensing resistance records from two sets of 2-probe electrodes (called R_1 and R_2, respectively) vs the two sets of 4-probe electrodes (called R_2 and R_4, respectively) of the same DCB interlaminar fracture test of the DCB-3 composite specimen
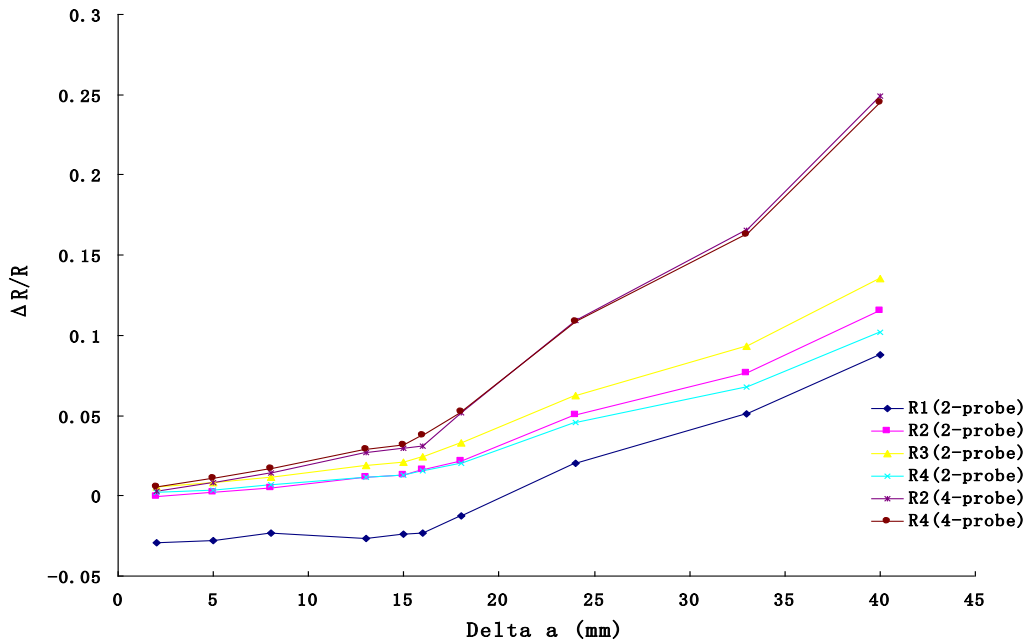
Fig. 18 - Detection of delamination crack extension Δa by 2- and 4-probe self-sensing techniques

As far as the self-sensing technique is concerned, Figure 17 depicts good agreement between the self-sensing resistance records from two sets of 2-probe electrodes (called R_1 and R_2, respectively) *vs* the two sets of 4-probe electrodes (called R_2 and R_4, respectively) of the same DCB interlaminar fracture test of the DCB-3 composite specimen. The 2-probe resistance measurement technique was also applied to the same 4-probe locations, and the results are also shown (called R_2 (2-probe) and R_4 (2-probe) respectively). As shown in Figure 17, the resistance measurements of these 2- and 4-probe electrodes increased suddenly when delamination occurred during the loading phase, and remained relatively constant during the unloading phases; indicating that the proposed self-sensing technique is very promising for the detection of delamination in composites.

Figure 18 shows the detection of delamination crack extension Δa by the 2- and 4-probe self-sensing techniques.

Finally, the force-displacement-crack length data were also used to estimate the Mode I interlaminar fracture toughness G_I of the composite specimens. As shown in Figure 19, the result is an almost perfect Γ-shaped R-curve. These Mode I interlaminar fracture toughness G_I data were calculated by two different methods: (1) BT: beam theory and (2) CC: compliance calibration Method. As depicted in Figure 19, results computed by these two methods are very agreeable with a G_I estimated to be around 12000-14000 J/m^2 for both DCB 1 and DCB 2 specimens, whereas results from the DCB 3 specimen present lower values, around 2000 J/m^2 , which may be due to specimen impurities.
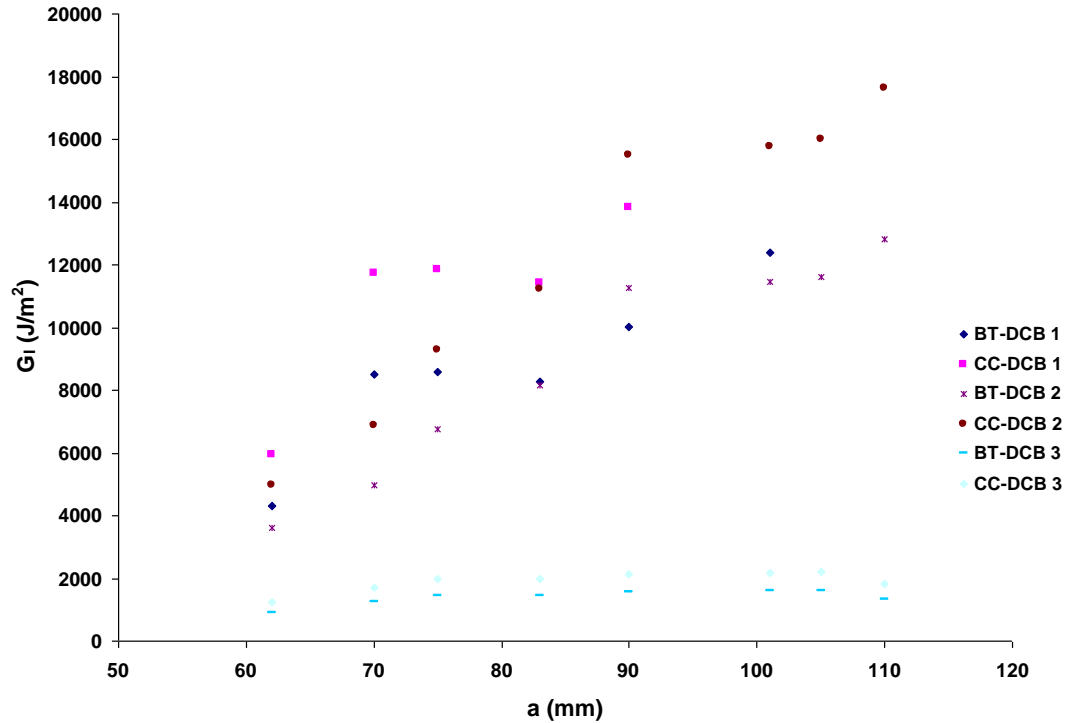
Fig. 19 - Interlaminar Mode I fracture toughness of the three composite specimens computed by two different methods: (1) BT: beam theory and (2) CC: compliance calibration Method.

3d-2) Composite DCB interlaminar fatigue tests

The DCB composite specimens were also tested for interlaminar fatigue fracture. As in the case of the quasi-static DCB interlaminar fracture test, four techniques were used for delamination detection: (1) the optical method, (2) one Physical Acoustics Corporation acoustic emission (A/E) sensor glued to the specimen at the free end of the DCB specimen, (3) four strain gauges for strain measurement, and (4) the innovative piezoresistivity-based self-sensing technique. As in quasi-static tests, the first composite DCB specimen (called Fatigue 1) was soldered with both 2- and 4-probe electrode, as shown in Fig. 11, and was tested for interlaminar fatigue fracture.

200

It should be noted that the resistances R1 and R3 represent the 2-probes resistances at locations 2P1 and 2P2, respectively; whereas the resistances R2 and R4 represent the 4-probes resistances at locations 4P1 and 4P2, respectively.

Mechanical load was applied from the MTS 810 testing machine through the steel piano hinges to the DCB composite specimen. The test was displacement controlled, with an average displacement of 56.5% of the initial crack detection displacement i.e. the displacement when $a = a_0$ (which is thereafter referred to as the reference displacement δ_{ref}) from the quasi-static DCB test. Table 2 shows the test sequence and parameters for the fatigue test. In the table, a_{start} and a_{final} represent the initial and final crack length, respectively; while f is the fatigue load frequency and N is the number of fatigue cycles applied.

Table 2 - DCB fatigue test sequence and parameters for the composite "Fatigue 1"

Fatigue Test Sequence	$\delta_{ave} / \delta_{ref}$	$\delta_{max} / \delta_{ref}$	a_{start} (mm)	a_{final} (mm)	N (cycles)	f (Hz)
I	56.5%	75%	0	0	2233	1
II	56.5%	75%	3	7	15598	1
III	56.5%	75%	7	7	18615	1
IV	56.5%	75%	7	7	20120	1
V	56.5%	80%	7	7	9998	1
VI	56.5%	80%	7	7	12092	1
VII	56.5%	85%	7	8	11268	1
VIII	56.5%	90%	8	15	28794	1
IX	56.5%	95%	15	20	22092	1
X	56.5%	95%	20	20	13009	1
XI	56.5%	100%	20	21	3866	1
XII	56.5%	100%	21	23	19312	1
XIII	56.5%	105%	23	24	3967	1

As far as the self-sensing technique is concerned, Fig. 20 depicts good sensitivity for the self-sensing resistance records from the 4-probe electrodes (called R2 and R4,

respectively). The values of the resistance change from the 4-probe electrodes highlight the success of the 4-probe electrodes in detecting the crack propagation. The 2-probe electrodes (called R1 and R3, respectively) of the same DCB interlaminar fracture fatigue test did not show enough sensitivity. Consequently the resistance change picked up by the very probes was very small. Figure 21 shows poor resistance records from the 2-probe electrodes.

During the testing, the initial resistance was measured every time we changed the load level; due to humidity and other outer conditions, the specimen resistance changed during the course of the test. For that reason, we used the resistance measured at the beginning of every load level change as the reference for resistance change calculations. Figures 22 and 23 show the resistance change by the 2- and 4-probe electrodes respectively. Figure 24 shows the detection of delamination crack extension Δa by the 2- and 4-probe self-sensing techniques. As mentioned, optical method was also used to detect the crack propagation. Figure 25 shows two *in situ* fractographs depicting delamination crack propagation in the DCB composite specimen at $\Delta a = 8$ and $\Delta a = 21$mm, respectively.

After the first fatigue test, we decided to change the layout of the specimen and carried out the second DCB fatigue test on a composite specimen call Fatigue 2 (see Fig. 26). Note that in the layout, 2P and 4P represent the 2- and 4-probe electrode locations, respectively. The resistances R1 and R3 represent the 2-probes resistances at locations 2P1 and 2P2, respectively; whereas the resistances R2 and R4 represent the 4-probes resistances at locations 4P1 and 4P2, respectively.

Again, the test was displacement-controlled with an average displacement of 75% of the initial crack detection displacement (referred to as the reference displacement δ_{ref}) from the quasi-static DCB tests. Table 3 shows the test sequence and parameters for the fatigue test on the DCB composite specimen Fatigue 2.
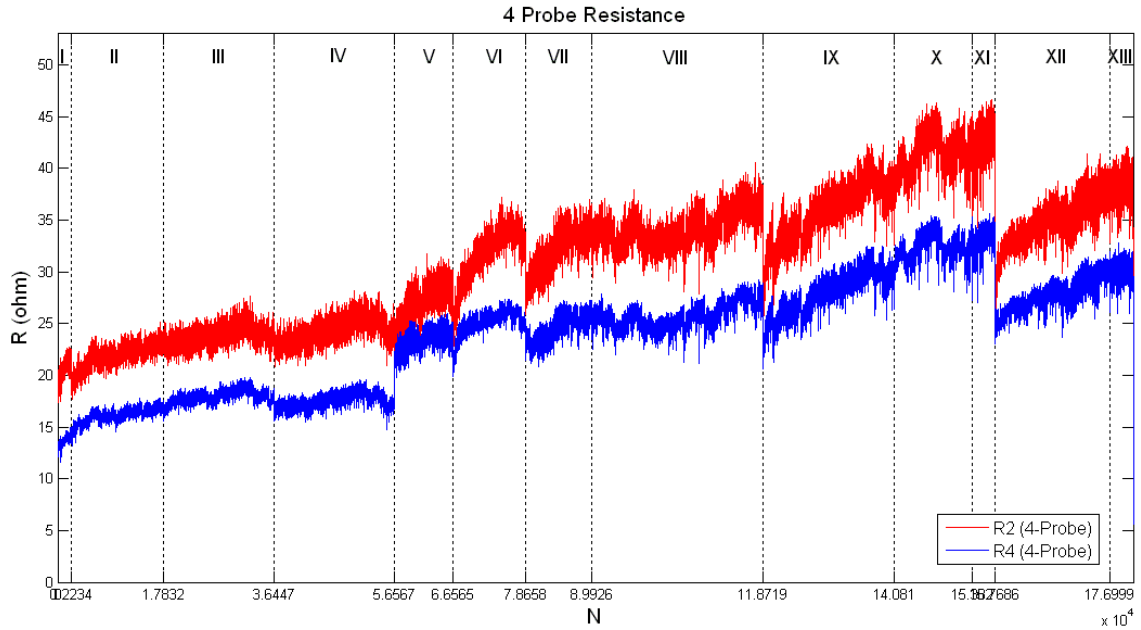
Fig. 20 - Resistance (4-probe electrodes) vs. N for the DCB composite specimen: Fatigue 1
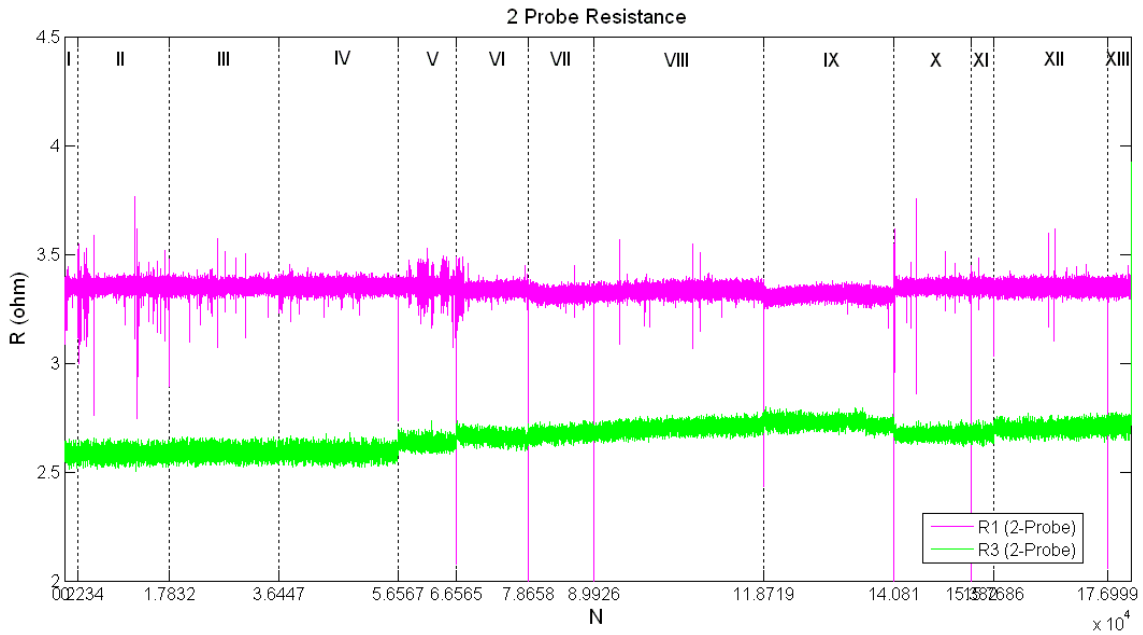
Fig. 21 - Resistance (2-probe electrodes) vs. N for the DCB composite specimen: Fatigue 1
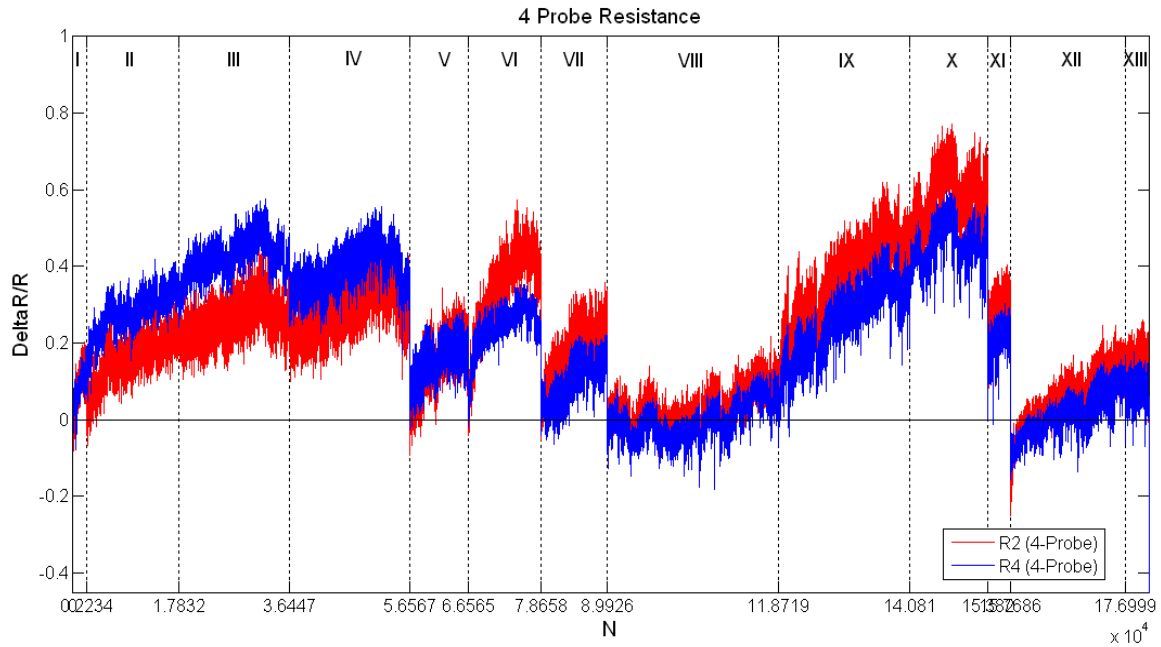
Fig. 22 - $\Delta R/R$ (4-probe electrodes) vs. N for the DCB composite specimen: Fatigue 1
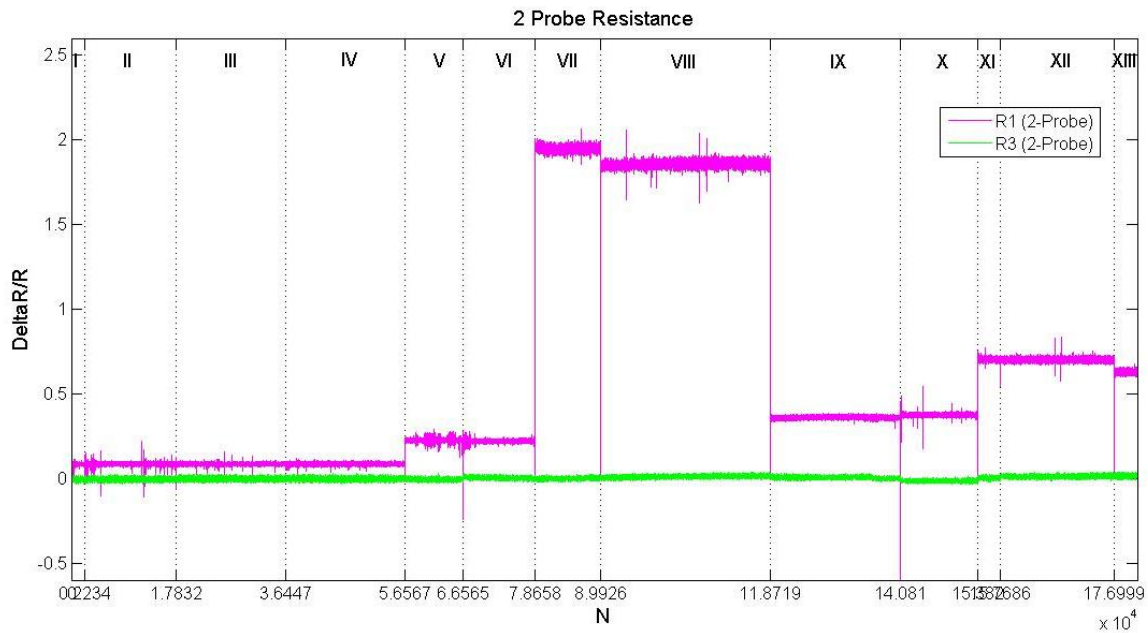
Fig. 23 - $\Delta R/R$ (2-probe electrodes) vs. N for the DCB composite specimen: Fatigue 1

204
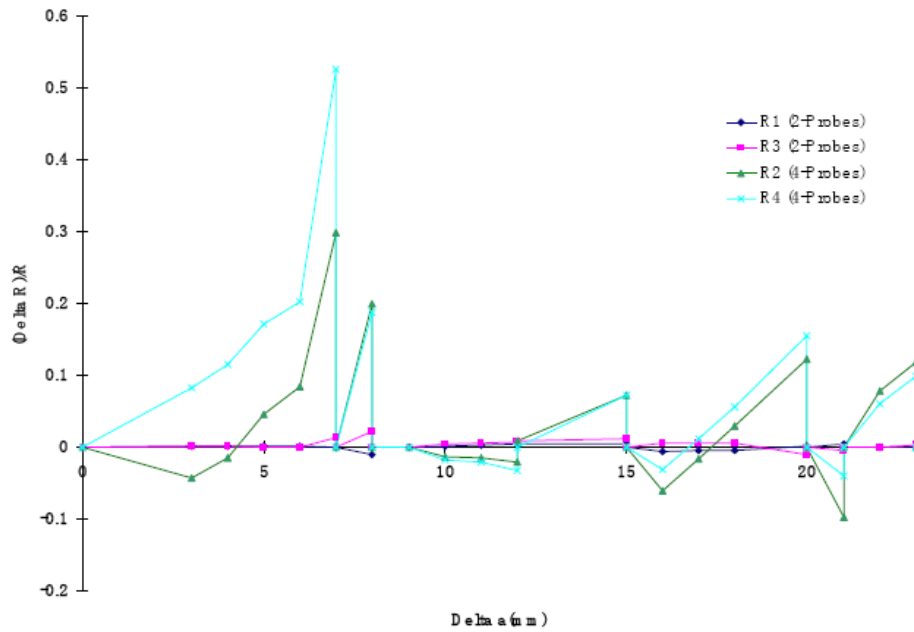
Fig. 24 - $\Delta R/R$ vs. Δa for the DCB composite specimen: Fatigue 1
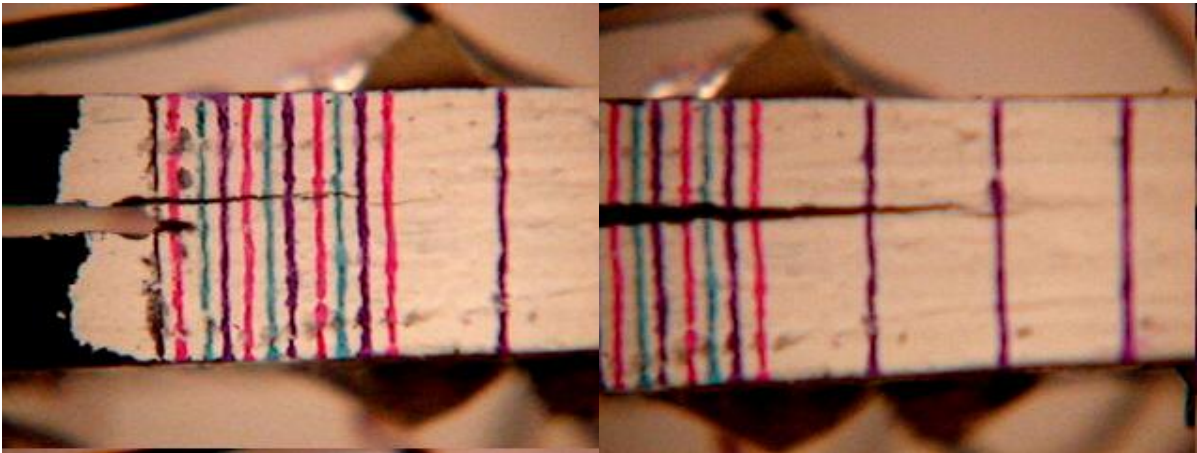
Fig. 25 - *In situ* fractographs depicting delamination crack propagation in the fatigue test for the DCB composite specimen: Fatigue 1
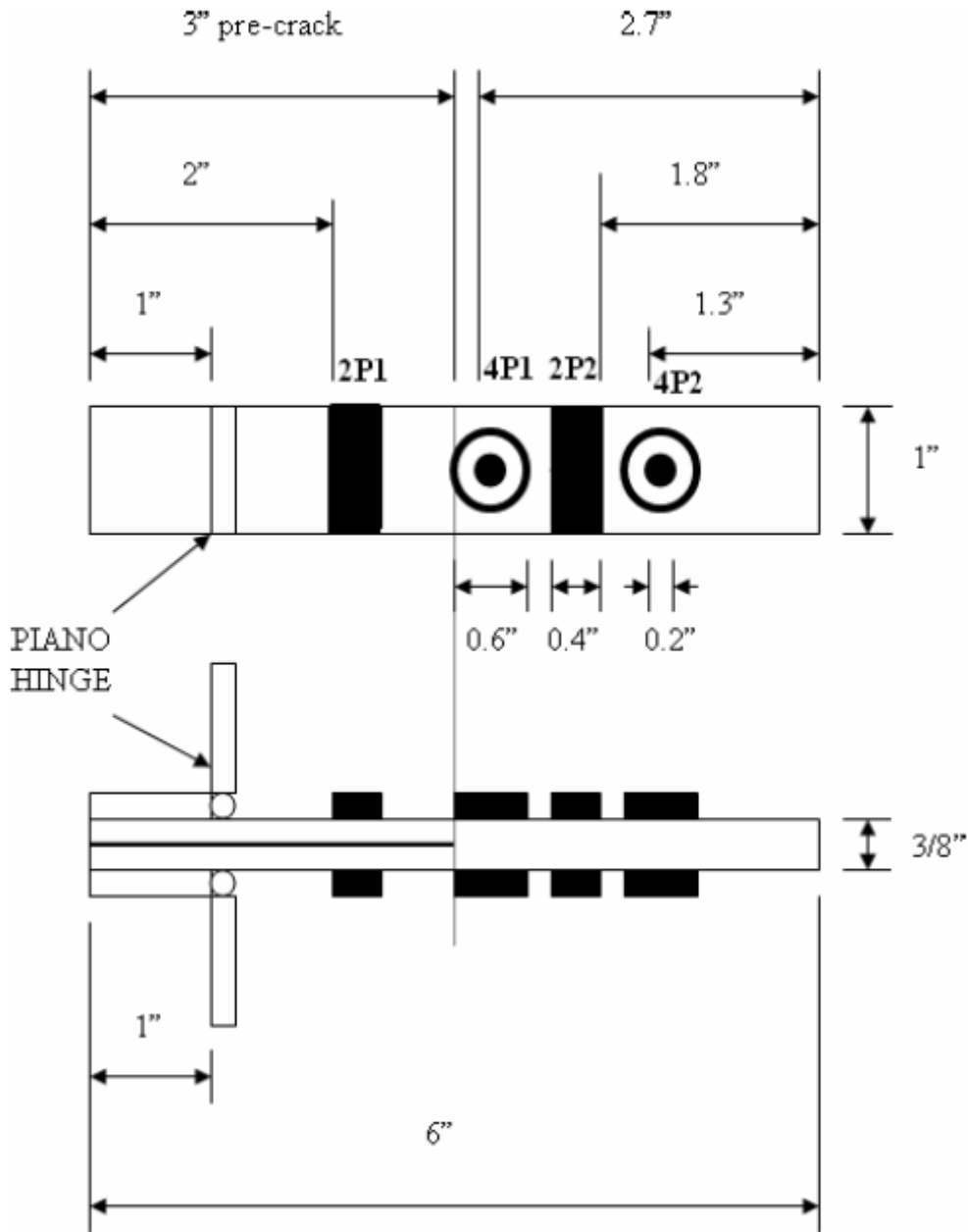
Fig. 26 - Layout of the DCB composite specimen Fatigue 2 with 2- and 4-probe electrode positions

Once again, as far as the self-sensing technique is concerned, Fig. 27 illustrates good sensitivity for the self-sensing resistance records from the 4-probe electrodes (called R2 and R4, respectively). The 2-probe electrodes (called R1 and R3, respectively) of the same DCB interlaminar fracture fatigue test did not show enough sensitivity;

206

Figure 28 shows poor resistance records from the 2-probe electrodes. The values of the resistance change from the 4-probe electrodes highlights the success of the 4-probe electrodes in detecting the crack propagation during the fatigue test for the DCB composite specimen Fatigue 2 whereas the 2-probe technique did show poor sensitivity. Figures 29 and 30 show the detection of delamination crack extension Δa by the 2- and 4-probe self-sensing techniques on the DCB composite specimen Fatigue 2, respectively.

Table 3- DCB fatigue test sequence and parameters for the composite specimen "Fatigue 2"

Fatigue Test Sequence	$\delta_{ave}/\delta_{ref}$	$\delta_{max}/\delta_{ref}$	a_{start} (mm)	a_{final} (mm)	N (cycles)	f (Hz)
I	75%	90%	0	0	7200	1
II	75%	90%	0	0	14400	2
III	75%	90%	0	3	21600	3
IV	75%	90%	3	5	43200	3
V	75%	95%	5	7	43200	3
VI	75%	95%	7	7	21600	3
VII	75%	105%	7	14	32400	3
VIII	75%	105%	14	17	43200	3
IX	75%	115%	17	22	43200	3
X	75%	125%	22	26	43200	3
XI	75%	135%	26	30	32400	3
XII	75%	145%	30	35	32400	3
XIII	75%	155%	35	38	32400	3
XIV	85%	165%	38	45	43200	3
XV	95%	175%	45	76.2	750	3
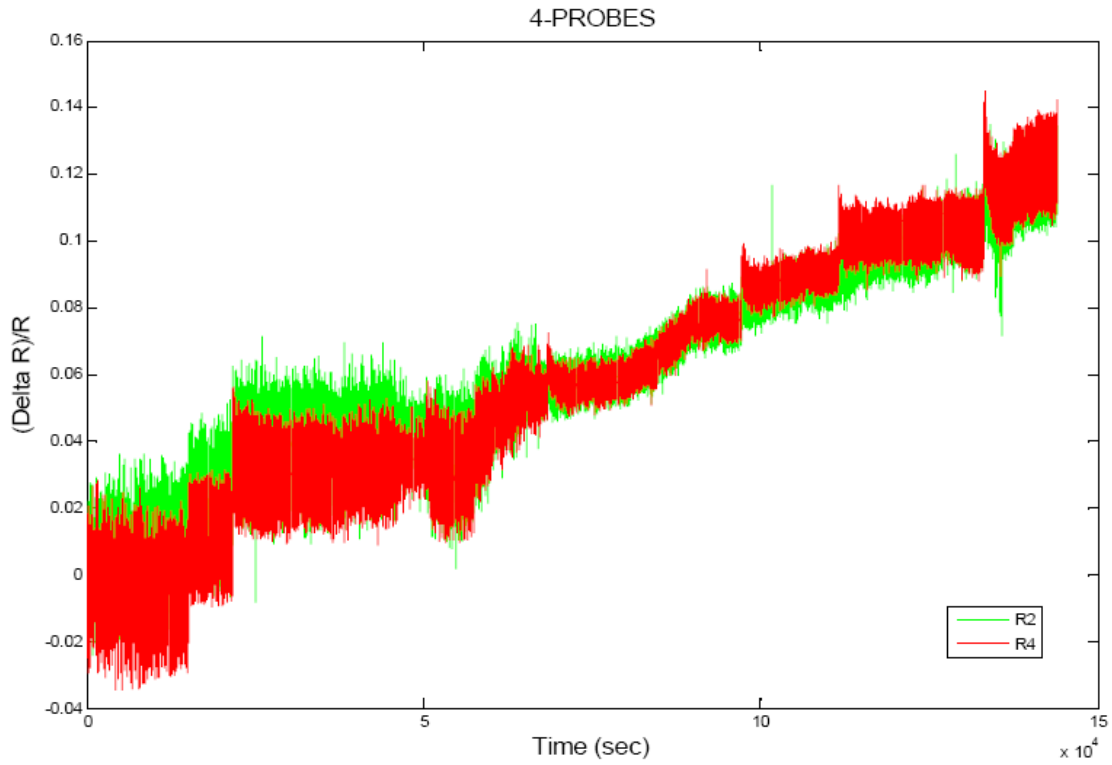
Fig. 27 - $\Delta R/R$ (4-probe electrodes) vs. time for the DCB composite specimen Fatigue 2
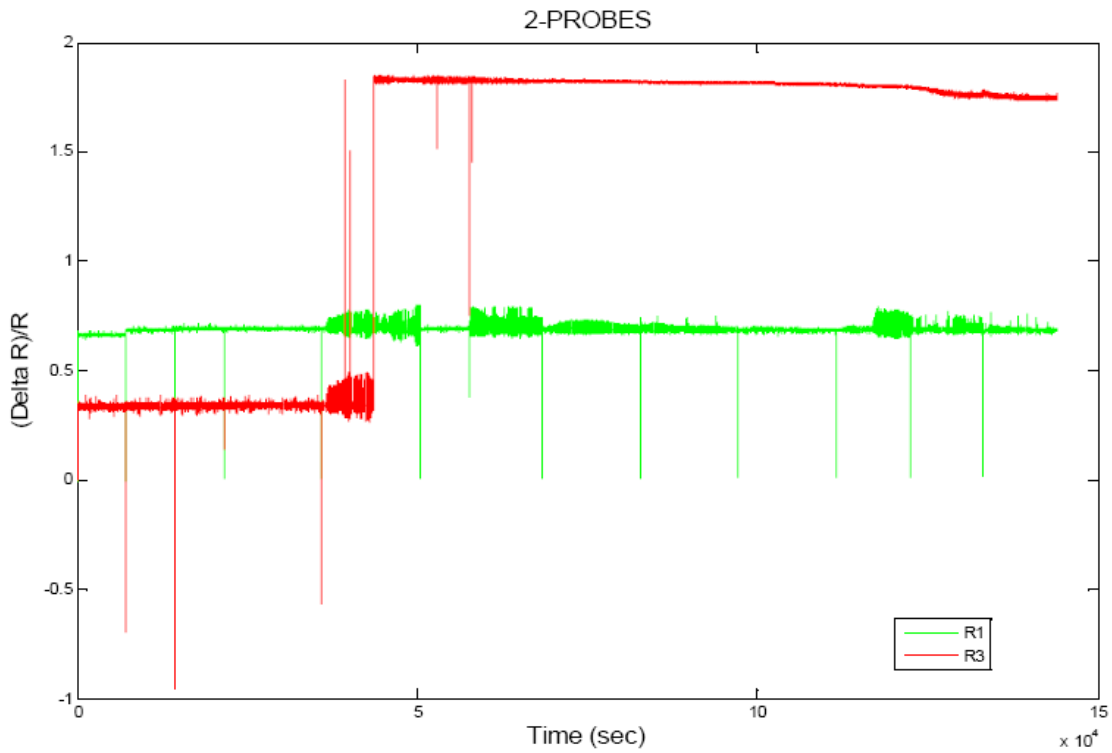
Fig. 28 - $\Delta R/R$ (2-probe electrodes) vs. time for the DCB composite specimen Fatigue 2

208
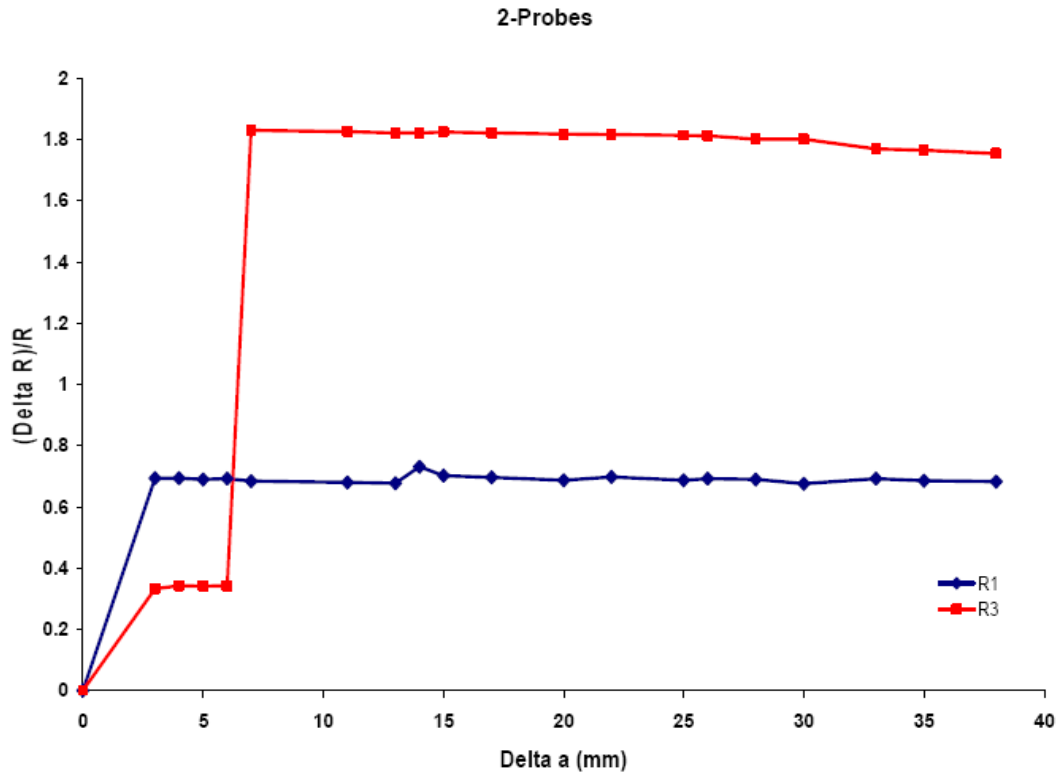
Fig. 29 - $\Delta R/R$ **(2-probe electrodes) vs.** Δa **for the DCB composite specimen Fatigue 2**
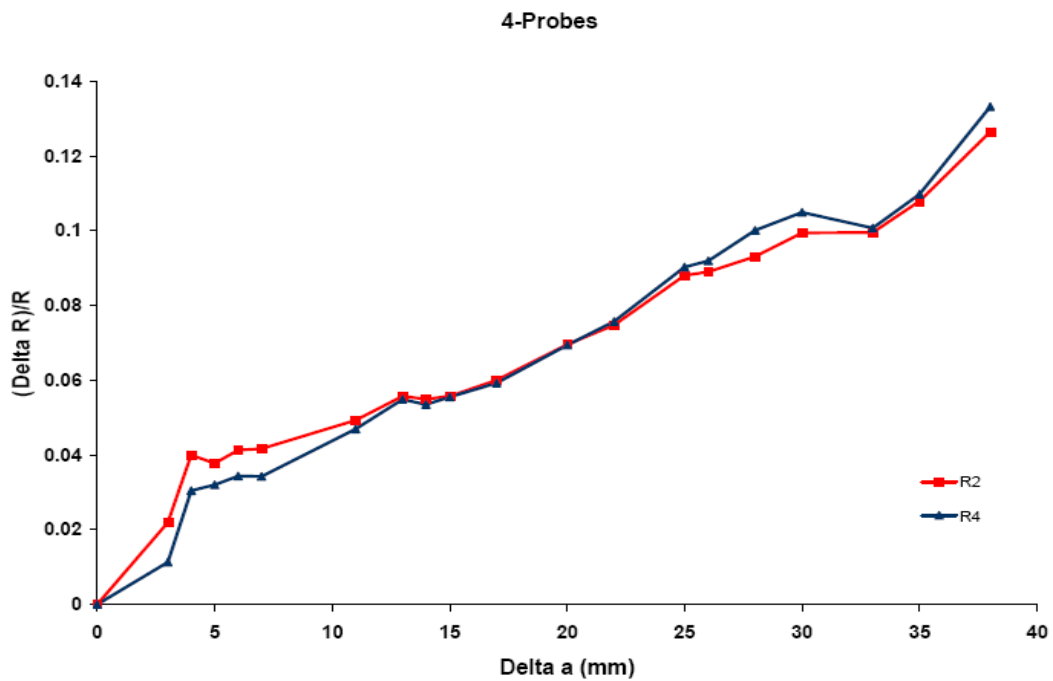
Fig. 30 - $\Delta R/R$ **(4-probe electrodes) vs.** Δa **for the DCB composite specimen Fatigue 2**

4. Summary

In summary, since the inception of this research project, which is in collaboration between CCNY and Global Contour Ltd., progress has been made with the following accomplishments:

- Preliminary DCB quasi-static tests of aluminum 6061-T6 strips bonded by 3M DP-810 adhesive were conducted following the ASTM D5528-01 Standard.

- The familiar Γ-shaped R-curve was obtained for the above tests with a Mode I interlaminar fracture toughness G_I estimated to be around 3000 J/m^2.

- Preliminary DCB fatigue tests of aluminum 6061-T6 strips bonded by 3M DP-810 adhesive were conducted to ensure the feasibility of the proposed technique.

- Preliminary ENF quasi-static and fatigue tests of aluminum 6061-T6 strips bonded by 3M DP-810 adhesive were conducted.

- The familiar Γ-shaped R-curve was obtained for the above tests with a Mode II interlaminar fracture toughness G_{II} estimated to be around 4,600 J/m^2.

- Mode I interlaminar fracture tests of the DCB composite specimens.

- The familiar Γ-shaped R-curve was obtained for the above tests with a Mode I interlaminar fracture toughness G_I estimated to be around 12000 - 14000 J/m^2 for two of the specimens.

- Two Mode I interlaminar fatigue tests of the DCB composite specimens had been tested. The results show that 4-probe technique is more promising than the 2-probe technique for composite self-sensing applications.

5. **Future Tasks**

- Mode I interlaminar fatigue tests of the third DCB composite specimens.

- Mode II interlaminar fracture tests of the ENF composite specimens.

- Mode II interlaminar fatigue tests of the ENF composite specimens.

References

[1]   Global Contour Ltd., NSF SBIR Phase I Report to NSF (2003).

[2]   Global Contour Ltd., NSF SBIR Phase II Proposal to NSF (2004).

[3]   Kobayashi, A.S., Emery, A.F. and Liaw, B.M. Dynamic fracture toughnesses of reaction bonded silicon nitride. *Journal of the American Ceramic Society*, **66**(2): 151-155, 1983.

[4]   Chung, D.D.L. Self-monitoring structural materials. Reports: A Review Journal, *Materials Science and Engineering*, **R22**: 57-78, 1998.

[5]   Wang, S. and Chung, D.D.L. Self-monitoring of strain and damage by a carbon-carbon composite. *Carbon*, **35**(5): 621-630, 1997.

[6]   Chung, D.D.L. and Wang, S. Self-monitoring of damage and strain in carbon fiber polymer-matrix structural composites by electrical resistance measurement. Polymers and Polymer *Composites*, **11**(7): 515-525, 2003.

[7]   Chung, D.D.L. Thermal analysis of carbon fiber polymer-matrix composites by electrical resistance measurement. *Thermochimica Acta*, **364**: 121-132, 2000.

[8]   Mei, Z. and Chung, D.D.L. Thermal stress-induced thermoplastic composite debonding, studied by contact electrical resistance measurement. *International Journal of Adhesion and Adhesives*, **20**: 135-139, 2000.

[9]   Mei, Z. and Chung, D.D.L. Thermal history of carbon-fiber polymer-matrix composite, evaluated by electrical resistance measurement. *Thermochimica Acta*, **369**: 87-93, 2001.

[10]   Wang, S. and Chung, D.D.L. Apparent negative electrical resistance in carbon fiber composites. *Composites: Part B*, **30**: 579-590, 1999.

[11]   Wang, S., Mei, Z. and Chung, D.D.L. Interlaminar damage in carbon fiber polymer-matrix composites, studied by electrical resistance measurement. *International Journal of Adhesion and Adhesives*, **21**: 465-471, 2001.

[12] Wang, X. and Chung, D.D.L. Self-monitoring of fatigue damage and dynamic strain in carbon fiber polymer-matrix composite. *Composites: Part B*, **29B**: 63-73, 1998.

[13] Wang, X. and Chung, D.D.L. Short carbon fiber reinforced epoxy coating as a piezoresistive strain sensor for cement motar. *Sensors and Actuators A*, **71**: 208-212, 1998.

[14] Wen, S. and Chung, D.D.L. Piezoresistivity in continuous carbon fiber cement-matrix composite. *Cement and Concrete Research*, **29**: 445–449, 1999.

[15] Chen, P.-W. and Chung, D.D.L. Concrete as a new strain/stress sensor. *Composites: Part B*, **27B**: 13-23, 1996.

[16] Mei, Z. and Chung, D.D.L. Effects of temperature and stress on the interface between concrete and its carbon fiber epoxy-matrix composite retrofit, studied by electrical resistance measurement. *Cement and Concrete Research*, **30**: 799-802, 2000.

[17] Abry, J.C., Bocharda, S., Chateauminois, A., Salvia, M. and Giraud, G. In situ detection of damage in CFRP laminates by electrical resistance measurements. *Composites Science and Technology*, **59**: 925-935, 1999.

[18] Abry, J.C., Choi, Y.K., Chateauminois, A. Dalloz, B., Giraud, G. and Salvia, M. In-situ monitoring of damage in CFRP laminates by means of AC and DC measurements. *Composites Science and Technology*, **61**: 855-864, 2001.

[19] Angelidis, N., Wei, C.Y. and Irving, P.E. The electrical resistance response of continuous carbon fibre composite laminates to mechanical strain. *Composites: Part A*, **35**, 1135–1147, 2004.

[20] Beloshenko, V.A., Varyukhin, V.N. and Voznyak, Y.V. Electrical properties of carbon-containing epoxy compositions under shape memory effect realization. *Composites: Part A*, **36**: 65–70, 2005.

[21] Ceysson, O., Salvia, M. and Vincent, L. Damage mechanisms characterization of carbon fibre/epoxy composite laminates by both electrical resistance

measurements and acoustic emission analysis, *Scripta Materialia*, **34**(8): 1273-1280, 1996.

[22] Hirano, S., Kishimoto, A. and Miyayama, M. Conductive coating on structural ceramics for strain detection utilizing electrical measurements. *Journal of the European Ceramic Society*, **19**: 2087-2095, 1999.

[23] Joseph, C. and C. Viney. Electrical resistance curing of carbon-fibre/epoxy composites. *Composites Science and Technology*, **60**: 315-319, 2000.

[24] Kaddour, A.S., Al-Salehi, F.A.R., Al-Hassani, S.T.S. and Hinton, M.J., Electrical resistance measurement technique for detecting failure in CFRP materials at high strain rates. *Composites Science and Technology*, **51**: 377-385, 1994.

[25] Kister, G., Wang, L., Ralph, B. and Fernando, G.F. Self-sensing E-glass fibres. *Optical Materials*, **21**: 713–727, 2003.

[26] Knite, M., Teteris, V. and Kiploka A. The effect of plasticizing agent on strain-induced change of electric resistivity of carbon–polyisoprene nano-composites. *Materials Science and Engineering C*, **23**: 787–790, 2003.

[27] Knite, M., Teteris, V., Kiploka, A. and Kaupuzs, J. Polyisoprene-carbon black nanocomposites as tensile strain and pressure sensor materials. *Sensors and Actuators A*, **110**: 142–149, 2004.

[28] Lei, H., Pitt, W.G., McGrath, L.K. and Ho, C.K. Resistivity measurements of carbon-polymer composites in chemical sensors: impact of carbon concentration and geometry. *Sensors and Actuators B*, **101**: 122–132, 2004.

[29] Muto, N., Arai, Y., Shin S.G., Matsubara, H., Yanagida, H., Sugita, M. and Nakatsuji, T. Hybrid composites with self-diagnosing function for preventing fatal fracture. *Composites Science and Technology*, **61**: 875-873, 2001.

[30] Park, J.B., Okabe, T., Takeda, N. and Curtin, W.A. Electromechanical modeling of unidirectional CFRP composites under tensile loading condition, *Composites: Part A*, **33**: 267-275, 2002.

[31] Park, J.-M., Kong, J.-W., Kim, D.-S. and Lee, J.-R. Non-destructive damage sensing and cure monitoring of carbon fiber/epoxyacrylate composites with UV and thermal curing using electro-micromechanical techniques. *Composites Science and Technology.* (in press).

[32] Reza, F., Yamamuro, J.A. and Batson, G.B. Electrical resistance change in compact tension specimens of carbon fiber cement composites. *Cement and Concrete Composites*, **26**: 873-881, 2004.

[33] Psarras, G.C., Parthenios, J., Bollas, D. and Galiotis, C. Stress and temperature self-sensing fibres. *Chemical Physics Letters* **367**: 270–277, 2003.

[34] Schuler, R., Joshi, S. and Schulte, K. Damage detection in CFRP by electrical conductivity mapping. *Composites Science and Technology*, **61**: 921-930, 2001.

[35] Schwartz, G., Cerveny, S. and A.J. Marzocca, A numerical simulation of the electrical resistivity of carbon black filled rubber. *Polymer*, **41**: 6589–6595, 2000.

[36] Seo, D.-C. and Lee, J.-J. Damage detection of CFRP laminates using electrical resistance measurement and neural network. *Composite Structures*, **47**: 525-530, 1999.

[37] Sodano, H.A., Park, G. and Inman, D.J. An investigation into the performance of macro-fiber composites for sensing and structural vibration applications. *Mechanical Systems and Signal Processing*, **18**: 683–697, 2004.

[38] Taya, M., Kim, W.J. and Ono, K. Piezoresistivity of a short fiber/elastomer matrix composite. *Mechanics of Materials*, **28**: 53–59, 1998.

[39] Todoroki, A. The effect of number of electrodes and diagnostic tool for monitoring the delamination of CFRP laminates by changes in electrical resistance. *Composites Science and Technology.* **61**: 1871-1880, 2001.

[40] Todoroki, A., Tanaka, M. and Y. Shimamura. Electrical resistance change method for monitoring delaminations of CFRP laminates: effect of spacing between electrodes. *Composites Science and Technology.* (in press)

[41] Xia, Z., Okabe, T., Park, J.B., Curtin, W.A. and Takeda, N. Quantitative damage detection in CFRP composites: coupled mechanical and electrical models. *Composites Science and Technology*, **63**: 1411–1422, 2003.

[42] Xiao, J., Li, Y. and Fan, W.X. A laminate theory of piezoresistance for composite laminates, *Composites Science and Technology* **59**: 1369-1373, 1999.

[43] ASTM D5528-01 Standard Test Method for Mode I Interlaminar Fracture Toughness of Unidirectional Fiber-Reinforced Polymer Matrix Composites.

[44] Carlsson, L.F., Adams, D.F., Pipes, R.B., *Experimental Characterization of Advanced Composite Materials*, 3rd ed., CRC Press, Boca Raton, FL, 2002.

[45] Pipes, R.B., Blakes, R.A., Jr., Gillespie, J.W., Jr. and Carlsson, L.F., Test Methods, *Delaware Composites Design Encyclopedia*, Vol. 6, Technomic Publishing, Lancaster, PA, 1990.

[46] Adams, D.F., *Test Methods for Composite Materials*, Seminar Notes, Technomic Publishing, Lancaster, PA.

[47] Ngabonziza Y., Boldrini C., Li J., Liaw B., Delale F., Chung J.C., 2009. Electrical resistance method for self-sensing damage in carbon fiber-reinforced composites under fatigue loading, *3rd International Conference on Integrity, Reliability and Failure*, Porto/Portugal, 20-24 July 2009